Conditional Expected Returns on Individual Stocks with and without Intertemporal Hedging*

Fousseni Chabi-Yo[†] Da-Hea Kim[‡] Gang Li[§]

July 1, 2026

Abstract

We derive tractable lower and upper bounds on the conditional expected excess return of an individual stock in a dynamic multi-period economy with portfolio rebalancing. The bounds depend on higher-order risk-neutral joint moments of market and stock returns and are implementable ex ante using index and single-name option prices. Our framework nests a no-intertemporal-hedging benchmark, isolating and quantifying the role of hedging motives. Empirically, the bounds are economically tight and outperform leading one-period benchmarks in out-of-sample forecasts of stock returns. The significant gap between hedging and non-hedging bounds highlights the role of intertemporal hedging in expected returns on individual stocks.

JEL Classification: G11, G12

Keywords: conditional expected return, intertemporal hedging, option-implied moments, higher-order risk preferences, cross-sectional stock returns

*We are grateful to Gurdip Bakshi, Xiaohui Gao Bakshi, Andrei Gonçalves, Amit Goyal, Bing Han, Yoontae Jeon, Ron Kaniel, Jun Pan, Tobias Sichert, David Schreindorfer, Jiang Wang, Paul Whalen, Qi Xu, as well as seminar participants at University of Massachusetts Amherst, Chinese University of Hong Kong, China Derivatives Youth Forum (2025), SKKU-USF Workshop (2026), NTU-TRIA Derivatives Workshop (2026), AsiaFA (2026) for many helpful comments.

[†]Isenberg School of Management, University of Massachusetts Amherst, fchabiyo@isenberg.umass.edu

[‡]SKK Business School, Sungkyunkwan University, daheakim@skku.edu

[§]CUHK Business School, The Chinese University of Hong Kong, gang.li@cuhk.edu.hk

1 Introduction

Expected returns on individual stocks are fundamental to asset pricing, capital allocation, and portfolio choice. Given this central role, a growing literature has sought reliable and implementable proxies. Recent advances, such as Martin and Wagner (2019), Kadan and Tang (2020), and Chabi-Yo, Dim, and Vilkov (2023), show that option prices can be used to bound or approximate expected returns, highlighting the value of forward-looking information embedded in option markets. These approaches, however, rest on simplifying assumptions,[1] most notably their confinement to a static, one-period setting. While analytically convenient, this restriction abstracts from time-varying economic conditions and portfolio rebalancing incentives, yielding only a partial characterization of equilibrium risk premia.

We address this limitation by introducing a dynamic multi-period economy in which investors rebalance portfolios as state variables evolve over time. Merton (1973) shows that expected excess returns compensate investors not only for contemporaneous market risk but also for exposure to innovations in state variables that shift future investment opportunities, because investors hedge these opportunity-set risks by tilting portfolios toward assets that perform well in adverse states. Subsequent work emphasizes the importance of such intertemporal hedging motives in economies with time-varying state variables (e.g., Brennan, Schwartz, and Lagnado, 1997; Campbell and Viceira, 1999; Wachter, 2002, 2013; Campbell, Chan, and Viceira, 2003; Liu, 2007). We build on this insight to derive option-implied bounds on stock-level equity premia in a multi-period setting with intertemporal

[1]Specifically, Martin and Wagner (2019) rely on a log-utility benchmark; Kadan and Tang (2020) approximate marginal utility using a first-order expansion; and Chabi-Yo, Dim, and Vilkov (2023) depend on realized betas for parameter calibration, despite employing higher-order expansions of the inverse marginal utility to move beyond the first-order simplification.

hedging.

Our framework has several advantages. First, it does not impose a parametric functional form for investors' utility. Under no-arbitrage and mild regularity conditions on inverse marginal utility, the stochastic discount factor (SDF) can be characterized in terms of market returns using a Taylor expansion of inverse marginal utility and economically motivated sign restrictions that require the product of risk prices and factor exposures to be positive. Preferences enter the framework through ratios of utility derivatives evaluated locally at the expansion point, rather than through a globally specified utility function. This local formulation allows the model to accommodate a broad class of preference specifications beyond constant relative risk aversion (CRRA), constant absolute risk aversion (CARA), or Epstein-Zin recursive utility, while avoiding the tight cross-restrictions on higher-order risk attitudes that these parametric specifications typically impose.

Second, our framework delivers tractable lower and upper bounds on conditional expected returns for individual stocks using only option prices, without relying on historical realized returns or accounting-based measures. The bounds depend on higher-order risk-neutral joint moments between market and stock returns: the lower bound uses untruncated moments, while the upper bound uses truncated, tail-sensitive moments. We obtain implementable approximations by representing the risk-neutral conditional expectation of stock returns given market returns with a flexible polynomial basis and matching its coefficients to higher-order risk-neutral moments of the stock and market marginal distributions. Because the inputs come from current index and single-name option prices, our bounds are forward-looking and implementable in real time.

Third, our framework nests the benchmark economy without intertemporal hedging, allowing us to quantify the incremental role of hedging motives. In the one-period benchmark, the SDF is determined entirely by the current market return and its higher-order terms. In the multi-period setting, it additionally depends on risk-neutral moments of future market returns and their interactions, capturing forward-looking opportunity-set risk. This nesting delivers a direct within-framework comparison of equity premia with and without hedging, enabling us to assess how the pure effect of hedging varies over time and across stocks.

In our framework, the hedging component depends jointly on stocks' exposure to future investment-opportunity risks and the preference loadings that price those exposures. The dynamic SDF introduces priced future-opportunity factors, so the stock-level bounds depend on stocks' risk-neutral covariances with these factors. When a stock performs poorly in states in which option prices signal greater future market risk, our local preference restrictions imply positive compensation for this adverse exposure. This compensation is the mechanism through which intertemporal hedging raises the expected-return bounds in our setting.

We test the framework on S&P 500 stocks at forecast horizons from one month to one year. In the static one-period setting, the average annualized lower (upper) bound ranges from 8% (17%) at the one-month horizon to 9% (16%) at the one-year horizon. The bounds are informative about future returns: a long–short strategy formed on bound quintiles earns annualized returns of 10% to 15%, depending on the horizon. Even in the static setting, our bounds improve out-of-sample forecast accuracy relative to the benchmarks of Martin and Wagner (2019), Kadan and Tang (2020), and Chabi-Yo, Dim, and Vilkov (2023), likely reflecting the greater flexibility of our framework.

We then extend the analysis to a dynamic multi-period setting with intertemporal hedging. Empirically, incorporating hedging raises the bounds, with stronger effects as the gap between the investment horizon and the forecast horizon widens. For example, at the one-month forecast horizon, increasing the investment horizon from three months to two years raises the average annualized lower bound from 9% to 15%, corresponding to an increase from 13% to 88% relative to the static counterpart of 8%. The hedging bounds, particularly the lower bound, continue to provide meaningful information about future returns and deliver notable improvements in tightness, pricing consistency, and forecast accuracy relative to existing benchmarks and their static counterparts.

Figure 1 plots time series of the hedging lower and upper bounds and their static counterparts for Apple and JP Morgan at the one-month forecast horizon. The hedging bounds generally lie above their static counterparts, with the gap widening during stress episodes such as the global financial crisis. Within each hedging bound, the share attributable to intertemporal hedging is sizable, time-varying, and often exceeds one-half of the total bound. Overall, the figure indicates that ignoring intertemporal hedging can materially understate both the level and the time variation of expected returns.

[Insert Figure 1 around here]

Having shown that the bounds are economically meaningful and informative about future returns, we next decompose the intertemporal hedging component and examine its drivers. We attribute hedging contributions to terms linked to forward conditional variance, skewness, and kurtosis of future market returns. Variance- and skewness-related components dominate, while kurtosis becomes relatively more important at longer forecast horizons. We also relate hedging contributions to betas with respect to cash-flow news, discount-rate news, and volatility news following Campbell et al. (2018). Although these betas are significantly associated with hedging contributions, they explain only a small fraction of the variation, suggesting that our option-implied hedging component captures intertemporal risks beyond the conventional news decomposition.

To reconcile our finding that intertemporal hedging raises expected returns with standard theoretical benchmarks, we examine the CRRA case within our framework. Under CRRA utility, a single risk-aversion coefficient determines the global utility function and all higher-order preference measures. This restriction has substantive implications: by pinning down the preference loadings on the intertemporal hedging terms, CRRA leads to a negative hedging component in our setting. We derive a closed-form option-based expression for expected excess returns under CRRA utility, both with and without hedging, and empirically confirm that the CRRA-implied hedging component is consistently negative. We also find that the resulting expected-return proxy underperforms our bounds across pricing consistency and forecast accuracy. This comparison highlights that the sign of the hedging component is not determined by the presence of intertemporal hedging alone, but depends on how preferences price stock exposure to future investment-opportunity risks. Our local preference specification, disciplined by economically motivated sign restrictions and calibrated utility-derivative ratios, allows the hedging component to be positive. This mechanism is consistent with Chabi-Yo, Gourier, and Langlois (2025), who show that, under empirically plausible conditions and without imposing a global utility function, a multi-period market premium can exceed the corresponding one-period premium when bad states combine low returns with higher future risk.

This paper builds on Chabi-Yo, Gourier, and Langlois (2025) but differs in both the object of interest and the theoretical contribution. Their analysis focuses on the market portfolio and quantifies the role of intertemporal hedging in expected market returns using market-level risk-neutral quantities. We instead study expected returns on individual stocks. Extending the framework to the cross-section is nontrivial because individual stock returns are not fully spanned by aggregate market fluctuations, and expected stock returns depend on how individual payoffs comove with market risks under the risk-neutral measure. To capture this dependence, we extend the stochastic-discount-factor expansion to fourth order and derive stock-level bounds using higher-order stock–market risk-neutral cross-moments. We also provide an implementable procedure to recover these cross-moments from index and single-name option prices. Thus, whereas Chabi-Yo, Gourier, and Langlois (2025) study intertemporal hedging in aggregate market premia, we make its role in the cross-section empirically tractable.

We contribute to the literature that uses option prices to infer equity premia. For the market portfolio, Martin (2017), Schneider and Trojani (2019), Chabi-Yo and Loudis (2020), and Tetlock, McCoy, and Shah (2024) develop option-based measures of conditional equity premia. Related studies use option prices to characterize forward-looking risk exposures and the pricing of higher-moment risks, including option-implied beta, market skewness risk, and co-skewness and co-kurtosis risk prices (Chang et al., 2012; Chang, Christoffersen, and Jacobs, 2013; Christoffersen et al., 2021).[2] At the individual-stock level, Martin and Wagner (2019) and Kadan and Tang (2020) develop variance-based bounds on expected returns, and Chabi-Yo, Dim, and Vilkov (2023) generalize these bounds beyond variance to the entire risk-neutral distribution. Unlike these stock-level studies, which identify expected returns in a single-period setting, we extend option-implied identification to a multi-period setting with intertemporal hedging and quantify its implications for risk premia.

Our study also connects to the intertemporal asset pricing literature. Samuelson (1969) and Merton (1969, 1971) develop dynamic consumption–portfolio choice under uncertainty, and Merton (1973) formalizes the ICAPM, linking expected returns to state variables that govern investment opportunities. Subsequent work derives portfolio implications under time-

[2] More recently, Fournier, Jacobs, and Orłowski (2024) develop a factor model for index option returns and estimate state-dependent risk premia associated with market, variance, tail, and higher-moment factors.

varying expected returns, interest rates, and volatility, typically under CRRA, CARA, or Epstein–Zin preferences (e.g., Kim and Omberg, 1996; Campbell and Viceira, 1999; Wachter, 2002; Brennan and Xia, 2002; Chacko and Viceira, 2005). More recent studies emphasize disaster risk and volatility as key drivers of risk premia (Wachter 2013; Tsai and Wachter 2015; Campbell et al. 2018; Seo and Wachter 2019). We build on this tradition by bringing option-implied identification to a multi-period setting and allowing intertemporal risks to operate through higher moments (skewness and kurtosis), not only volatility.

For the cross-section of stock returns, this literature uses the Campbell–Shiller decomposition (Campbell and Shiller, 1988) to separate cash-flow news and discount-rate news. Campbell and Vuolteenaho (2004) link higher premia to cash-flow "bad beta" relative to discount-rate "good beta," while Campbell, Polk, and Vuolteenaho (2010) and Campbell, Giglio, and Polk (2013) connect these channels to value–growth differences and recessions. Chabi-Yo, Gonçalves, and Loudis (2025) translate ICAPM state variables into tradable factors priced in the cross-section. We complement this line of work by making intertemporal hedging empirically tractable at the individual-stock level using option prices, allowing its role to be assessed over time and across firms.

The remainder of the paper is organized as follows. Section 2 develops the theoretical framework and derives lower and upper bounds on conditional expected returns for individual stocks in both one-period and multi-period settings. Section 3 details the construction of the empirical counterparts of the bounds from option price data. Section 4 presents the empirical analysis, evaluating their predictive performance against existing benchmarks. Section 5 discusses preference restrictions through the CRRA benchmark and the behavior of the implied SDF. Section 6 concludes.

2 Theory on Individual Stocks

Consider a static economy over the interval from time t to T_1 and let $R_{i,t\to T_1}$ denote the return on the risky asset over this period. We define the excess return on the stock i as $\mathcal{R}_{i,t\to T_1} = R_{i,t\to T_1} - R_{f,t\to T_1}$ and the excess market return as $\mathcal{R}_{M,t\to T_1} = R_{M,t\to T_1} - R_{f,t\to T_1}$. Under the no-arbitrage condition, it follows that

$$\mathbb{E}_t\left(\mathcal{R}_{i,t\to T_1}\right) = \mathbb{COV}_t^*\left(\frac{\mathbb{E}_t m_{t\to T_1}}{m_{t\to T_1}}, \mathcal{R}_{i,t\to T_1}\right), \tag{2.1}$$

where $m_{t\to T_1}$ is the Stochastic Discount Factor (SDF) from time t to time T_1. $\mathbb{COV}_t^*(\cdot,\cdot)$ denotes the conditional covariance under the risk-neutral measure. Throughout, a superscript $*$ indicates quantities evaluated under the risk-neutral measure. In the following sections, we characterize the SDF without imposing a parametric functional form on utility. We then use both the SDF and Eq.(2.1) to derive bounds on the expected excess returns of individual stocks.

2.1 Expected Excess Return without Intertemporal Hedging

We assume that the representative agent maximizes expected utility $u\,[.]$ at time t

$$\max_{\omega_t} \mathbb{E}_t u\left[W_{t\to T_1}\right]$$

subject to

$$W_{t\to T_1} = W_t\left(R_{f,t\to T_1} + \omega_t^\top\left(\mathbf{R}_{t\to T_1} - R_{f,t\to T_1}\mathbf{1}\right)\right),$$

where $\mathbf{R}_{t\to T_1}$ is a vector of returns of risky assets. Since there is no rebalancing between the dates t and T_1, intertemporal hedging motives are absent. The SDF implied by the first-order conditions is proportional to $u^{'}\left[W_t R_{M,t\to T_1}\right]$, where $R_{M,t\to T_1}$ is used as a proxy for the return on aggregate wealth.

The inverse SDF is proportional to the inverse marginal utility and can be written as:

$$\frac{\mathbb{E}_t m_{t\to T_1}}{m_{t\to T_1}} = \frac{\upsilon_{t\to T_1}}{\mathbb{E}_t^* \upsilon_{t\to T_1}} \tag{2.2}$$

with

$$\upsilon_{t\to T_1} = \frac{u^{'}\left[W_t R_{f,t\to T_1}\right]}{u^{'}\left[W_t R_{M,t\to T_1}\right]}. \tag{2.3}$$

Notice that $\upsilon_{t\to T_1} > 0$. Therefore, $\mathbb{E}_t^* \upsilon_{t\to T_1} > 0$. We next specify preference parameters:

$$\begin{array}{rclrcl} \tau_t & = & -\frac{u^{'}\left[W_t R_{f,t\to T_1}\right]}{W_t R_{f,t\to T_1} u^{''}\left[W_t R_{f,t\to T_1}\right]}, & \kappa_t & = & \frac{1}{3!}\frac{u^{''''}\left[W_t R_{f,t\to T_1}\right]\left(u^{'}\left[W_t R_{f,t\to T_1}\right]\right)^2}{\left(u^{''}\left[W_t R_{f,t\to T_1}\right]\right)^3}, \\ \rho_t & = & \frac{1}{2}\frac{u^{'''}\left[W_t R_{f,t\to T_1}\right] u^{'}\left[W_t R_{f,t\to T_1}\right]}{\left(u^{''}\left[W_t R_{f,t\to T_1}\right]\right)^2}, & \xi_t & = & \frac{1}{4!}\frac{u^{'''''}\left[W_t R_{f,t\to T_1}\right]\left(u^{'}\left[W_t R_{f,t\to T_1}\right]\right)^3}{\left(u^{''}\left[W_t R_{f,t\to T_1}\right]\right)^4}. \end{array} \tag{2.4}$$

Our framework does not impose a parametric functional form for utility. It only requires regularity conditions that permit a local expansion of utility around the deterministic benchmark wealth $W_t R_{f,t\to T_1}$. Hence, the approach is functional-form-free but not preference-free: τ_t, ρ_t, κ_t, and ξ_t are local preference measures evaluated at $W_t R_{f,t\to T_1}$ and known at time t. These parameters need not coincide with the corresponding measures evaluated at the state-contingent terminal wealth $W_t R_{M,t\to T_1}$ and therefore do not identify a global utility function.[3] The only excluded case is logarithmic utility, under which the inverse SDF coincides with the market return, implying $\tau_t = \rho_t = \kappa_t = \xi_t = 1$ and eliminating the higher-order preference channels that our bounds are designed to capture.

[3]A global utility specification would impose additional restrictions by linking local preference measures across wealth realizations. In particular, constant local risk aversion does not imply CRRA utility: $1/\tau_t$ is evaluated only at the risk-free benchmark $W_t R_{f,t\to T_1}$, whereas CRRA requires relative risk aversion to be constant across all wealth realizations.

The parameter τ_t denotes risk tolerance, with $1/\tau_t$ corresponding to relative risk aversion. The skewness preference ρ_t scales the third derivative of utility and captures the agent's prudence, namely the tendency to increase precautionary savings in response to risk in future income (Kimball, 1990). When $\rho_t > 1$, the agent is prudent and increases savings when facing income risk (Gollier, 2001). The parameter κ_t measures normalized kurtosis aversion, capturing sensitivity to fourth-moment risk in wealth. Although less studied than ρ_t (prudence), κ_t enters third-order Taylor expansions of inverse marginal utility and captures temperance, i.e., the agent's aversion to combining independent risks. Temperance is widely used in asset allocation, stochastic dominance, and higher-order risk premium models. Finally, ξ_t captures the fifth derivative of utility and reflects a higher-order "hyper-temperance," i.e., sensitivity to even finer features of risk, such as variation in how risks interact (e.g., interactions between skewness and kurtosis risks). Recent evidence shows that higher-order risk preferences such as prudence and temperance are strongly related to financial choices, and that relying on risk tolerance alone can lead to misleading inferences (Schneider and Sutter, 2026).

Under no-arbitrage conditions and assuming that regularity conditions on $\upsilon_{t\to T_1}$ are satisfied, we show in Online Appendix OA.1 that the inverse of the one-period SDF is given by (2.2), where a $\mathcal{K}^{\text{th}}$ order Taylor expansion-series of $\upsilon_{t\to T_1}$ around $\mathcal{R}_{M,t\to T_1} = 0$ yields

$$\upsilon_{t\to T_1} = 1 + \sum_{j=1}^{\mathcal{K}} \frac{a_{j,t}}{R^j_{f,t\to T_1}} \mathcal{R}^j_{M,t\to T_1}. \tag{2.5}$$

Specifically, the first four coefficients are

$$a_{1,t} = \frac{1}{\tau_t}, \quad a_{2,t} = \frac{1-\rho_t}{\tau_t^2}, \quad a_{3,t} = \frac{1-2\rho_t+\kappa_t}{\tau_t^3}, \quad a_{4,t} = \frac{1-3\rho_t+\rho_t^2+2\kappa_t-\xi_t}{\tau_t^4}. \tag{2.6}$$

For interpretation, applying the Carr and Madan (2001) spanning formula to $\mathcal{R}^j_{M,t\to T_1}$,

$j > 1$, we show in Online Appendix (OA.2.1) that the inverse SDF (2.2) can be expressed as a portfolio payoff from holding the market return and a continuum of call and put options maturing at T_1.

To sign $a_{j,t}$ and thus derive the implied restrictions on the preference parameters $1/\tau_t$, ρ_t, κ_t and ξ_t, we appeal to economic theory. Specifically, theory implies that

$$\underbrace{\frac{a_{j,t}}{\mathcal{R}^j_{f,t\to T_1}\mathbb{E}^*_t \upsilon_{t\to T_1}}}_{\text{Price of Risk}} \times \underbrace{\mathbb{COV}^*_t\left(\mathcal{R}^j_{M,t\to T_1}, \mathcal{R}_{M,t\to T_1}\right)}_{\text{Quantity of Risk}} > 0. \tag{2.7}$$

To see why this inequality holds, set $i = M$ in (2.1) and substitute (2.5) into (2.1), which yields a sum of risk premium terms. We rely on the following intuition: if the quantity of risk is positive, investors require a premium to hold an asset with positive exposure to the j-th factor, so the product of the quantity and the price of risk is positive. If the quantity of risk is negative, the asset has negative exposure to the j-th factor; investors still require compensation, implying a negative price of risk so that the premium remains positive. Hence, we posit that each risk premium, defined as the price of risk times exposure to the priced factor, is positive.

Given that $\upsilon_{t\to T_1} > 0$, it follows that $\mathbb{E}^*_t \upsilon_{t\to T_1} > 0$. Empirically, the moment conditions $\mathbb{E}^*_t \mathcal{R}^{2(j+1)}_{M,t\to T_1} \geq 0$ and $\mathbb{E}^*_t \mathcal{R}^{2j+1}_{M,t\to T_1} \leq 0$ are supported by the data. As a result, inequality (2.7) implies that $a_{2j+1,t} \geq 0$ and $a_{2j,t} \leq 0$, respectively. The sign of $a_{j,t}$ imposes the following restrictions on the parameters:

$$\frac{1}{\tau_t} > 0,\ \rho_t > 1,\ \kappa_t > 2\rho_t - 1,\ \xi_t > (1 - 2\rho_t + \kappa_t) - \rho_t\,(1-\rho_t) + \kappa_t. \tag{2.8}$$

The restrictions in (2.8) discipline the admissible ranges of the local preference parameters but leave their magnitudes to be specified in the empirical implementation. They also help explain why we do not impose CRRA in the main framework. CRRA ties all higher-order preference measures to a single risk-aversion coefficient and imposes a global restriction on marginal utility across wealth realizations. This restriction can conflict with the sign pattern implied by (2.7) for empirically plausible levels of risk aversion. We therefore work with local preference parameters subject to (2.8), describe their empirical calibration in Section 3.2, and study the CRRA case separately in Section 5.1 as a benchmark.

Next, replacing the inverse SDF (2.2) in (2.1) produces a sum of risk premia of the form

$$\underbrace{\frac{a_{j,t}}{\mathcal{R}^{j}_{f,t\to T_1}\mathbb{E}^{*}_{t}\upsilon_{t\to T_1}}}_{\text{Price of Risk}} \times \underbrace{\mathbb{COV}^{*}_{t}\left(\mathcal{R}^{j}_{M,t\to T_1}, \mathcal{R}_{i,t\to T_1}\right)}_{\text{Quantity of Risk}} > 0. \tag{2.9}$$

This term represents exposure to the risk factor $\mathcal{R}^{j}_{M,t\to T_1}$. Consistent with economic theory, we assume that investors require a positive premium to hold a stock with positive exposure to this factor. This assumption is also broadly supported by the data. Online Appendix Table OA.1 shows that the quantity of risk is predominantly positive for odd-order factors ($j = 1, 3$) and predominantly negative for even-order factors ($j = 2, 4$), consistent with the sign pattern implied by Eq. (2.9). Nevertheless, Eq. (2.9) may be violated for a given firm at a particular point in time. We interpret such violations as measurement error in Eq. (2.9); in that case, it is natural to use 0 as a lower bound for this expression. Next, we provide lower and upper bounds on the expected excess return.

Proposition 2.1. *Assume that (2.7) and (2.9) hold. Under no-arbitrage conditions, for any*

$\mathcal{K}$ >0, *the expected excess return on stock i admits a lower bound:*

$$\mathbb{E}_t\left[\mathcal{R}_{i,t\to T_1}\right] \geq \frac{\sum_{j=1}^{\mathcal{K}} \frac{a_{j,t}\mathcal{M}_{i,M,t}^{*(j)}}{R_{f,t\to T_1}^{j}}}{1+\sum_{j=1}^{\mathcal{K}} \frac{a_{j,t}}{R_{f,t\to T_1}^{j}}\mathbb{E}_t^{*}\mathcal{R}_{M,t\to T_1}^{j}}, \tag{2.10}$$

where

$$\mathcal{M}_{i,M,t}^{*(j)} = \mathbb{E}_t^{*}\left[\mathcal{R}_{M,t\to T_1}^{j}\mathcal{R}_{i,t\to T_1}\right]. \tag{2.11}$$

Furthermore, up to the $\mathcal{K}^{th}$-order expansion of the inverse marginal utility, for any threshold $k_0 \leq R_{f,t\to T_1}$, the expected excess return on stock i satisfies the upper bound:

$$\mathbb{E}_t\left[\mathcal{R}_{i,t\to T_1}\right] \leq \frac{\mathcal{M}_{i,M,t}^{*(0)}\left[k_0\right]+\sum_{j=1}^{\mathcal{K}} \frac{a_{j,t}}{R_{f,t\to T_1}^{j}}\mathcal{M}_{i,M,t}^{*(j)}\left[k_0\right]}{1+\sum_{j=1}^{\mathcal{K}} \frac{a_{j,t}}{R_{f,t\to T_1}^{j}}\mathbb{E}_t^{*}\mathcal{R}_{M,t\to T_1}^{j}}, \tag{2.12}$$

where

$$\mathcal{M}_{i,M,t}^{*(j)}\left[k_0\right] = \mathbb{E}_t^{*}\left[\mathcal{R}_{M,t\to T_1}^{j}\mathcal{R}_{i,t\to T_1}1_{R_{i,t\to T_1}\geq k_0}\right]. \tag{2.13}$$

Proof. See Online Appendix OA.1. □

Proposition 2.1 establishes static lower and upper bounds on the expected excess return of an individual stock for a given value of $\mathcal{K}$. Both bounds depend on risk-neutral quantities and the preference coefficients $a_{j,t}$ defined in (2.6). The key implementation challenge is that the bounds require risk-neutral cross-moments between the individual stock payoff and powers of the market return.[4] Because there are no traded derivatives written directly on

[4]This feature distinguishes the individual-stock problem from market-level option-implied expected-return formulas, such as Chabi-Yo and Loudis (2020), where the relevant objects are marginal risk-neutral moments of the market return. At the stock level, the bounds involve cross-moments between stock payoffs and market return factors, which are not directly spanned by standard index or single-name options.

the joint payoff of the market and an individual stock, these cross-moments are not directly observable.

To obtain implementable approximations, we consider the conditional risk-neutral expectations $\mathbb{E}_t^*\left[\mathcal{R}_{i,t\to T_1} \mid \mathcal{R}_{M,t\to T_1}\right]$ and $\mathbb{E}_t^*\left[\mathcal{R}_{i,t\to T_1} 1_{R_{i,t\to T_1}\geq k_0} \mid \mathcal{R}_{M,t\to T_1}\right]$, which are generally unknown functions of the market excess return $\mathcal{R}_{M,t\to T_1}$. We first consider the untruncated payoff. Let

$$g_{i,t}\left[r\right] = \mathbb{E}_t^*\left[\mathcal{R}_{i,t\to T_1} \,|\, \mathcal{R}_{M,t\to T_1} = r\right] \tag{2.14}$$

denote the conditional expectation of the individual stock excess return given the market excess return under the risk-neutral measure. Assume that $g_{i,t}\left[\cdot\right]$ is continuous on a compact support. By the Stone–Weierstrass theorem, for any $\delta > 0$, there exists a polynomial

$$g_{\mathcal{N},i,t}\left[r\right] = \sum_{k=1}^{\mathcal{N}} \underline{\gamma}_{i,k,t} r^k \tag{2.15}$$

such that

$$\sup_r \left|g_{i,t}(r) - g_{\mathcal{N},i,t}(r)\right| < \delta. \tag{2.16}$$

Accordingly, we approximate the conditional expectation by

$$g_{\mathcal{N},i,t}\left[\mathcal{R}_{M,t\to T_1}\right] = \sum_{k=1}^{\mathcal{N}} \underline{\gamma}_{i,k,t} \mathcal{R}^k_{M,t\to T_1}. \tag{2.17}$$

Equation (2.17) is a finite-dimensional approximation to the conditional expectation rather than a parametric specification. Since polynomials are dense in the space of continuous functions on compact sets, the approximation error can be made arbitrarily small by increasing the number of basis functions. Using the defining property of conditional expectations, the stock return admits the decomposition

$$\mathcal{R}_{i,t\to T_1} = g_{i,t}\left[\mathcal{R}_{M,t\to T_1}\right] - \mathbb{E}_t^* g_{i,t}\left[\mathcal{R}_{M,t\to T_1}\right] + \varepsilon_{i,t\to T_1}^*, \tag{2.18}$$

where

$$\mathbb{E}_t^*\left[\varepsilon_{i,t\to T_1}^* | g_{i,t}\left[\mathcal{R}_{M,t\to T_1}\right]\right] = 0.$$

The residual $\varepsilon_{i,t\to T_1}^*$ is defined under the risk-neutral measure, so the orthogonality conditions need not hold under the physical measure. Taking the qth risk-neutral moment of the exact decomposition gives

$$\mathbb{E}_t^*\mathcal{R}_{i,t\to T_1}^q = \mathbb{E}_t^*\left(g_{i,t}\left[\mathcal{R}_{i,t\to T_1}\right]\right)^q + \sum_{j=1}^{q}\binom{q}{j}\mathbb{E}_t^*\left[\left(g_{i,t}\left[\mathcal{R}_{i,t\to T_1}\right]\right)^{q-j}\left(\varepsilon_{i,t\to T_1}^*\right)^j\right]. \tag{2.19}$$

The first interaction term $\mathbb{E}_t^*\left[\left(g_{i,t}\left[\mathcal{R}_{i,t\to T_1}\right]\right)^{q-1}\varepsilon_{i,t\to T_1}^*\right]$ vanishes by the property of conditional expectations. The remaining higher-order interaction terms, however, cannot be identified from option prices alone. We therefore impose the identifying restrictions

$$\sum_{j=2}^{q}\binom{q}{j}\mathbb{E}_t^*\left[\left(g_{i,t}\left[\mathcal{R}_{i,t\to T_1}\right]\right)^{q-j}\left(\varepsilon_{i,t\to T_1}^*\right)^j\right] = 0, \qquad q = q^*,\ldots,\mathcal{N}+q^*-1 \tag{2.20}$$

where $q^* \geq 2$. These restrictions require the unidentified higher-order interaction terms to have no net contribution to the moment equations. They are substantially weaker than assuming independence between the market-driven component and the residual, as they restrict only the mixed moments entering the identifying equations while leaving the remaining dependence structure unrestricted. Importantly, the restrictions are imposed exclusively under the risk-neutral measure and should not be interpreted as structural assumptions about the pricing of idiosyncratic risk. Because our framework does not require equivalence between the physical and risk-neutral measures, they neither imply that $\mathbb{E}_t\left[\varepsilon^*_{i,t\to T_1}\right] = 0$ nor restrict higher-order physical moments of $\varepsilon^*_{i,t\to T_1}$ or the pricing covariances

$$\mathbb{COV}_t\left(\frac{m_{t\to T_1}}{\mathbb{E}_t[m_{t\to T_1}]}, \left(\varepsilon^*_{i,t\to T_1}\right)^q\right), \; q = q^*, ..., \mathcal{N} + q^* - 1 \tag{2.21}$$

which may remain nonzero.

Under (2.20),

$$\mathbb{E}^*_t\mathcal{R}^q_{i,t\to T_1} = \mathbb{E}^*_t\left(g_{i,t}\left[\mathcal{R}_{i,t\to T_1}\right]\right)^q \qquad q = q^*, \ldots, \mathcal{N} + q^* - 1. \tag{2.22}$$

In implementation, we replace $g_{i,t}$ in (2.22) by its polynomial approximation $g_{\mathcal{N},i,t}$ in (2.17). This yields $\mathcal{N}$ moment conditions to identify the $\mathcal{N}$ unknown coefficients $\{\underline{\gamma}_{i,1,t}, \ldots, \underline{\gamma}_{i,\mathcal{N},t}\}$, provided that the associated Jacobian matrix has full rank. Since alternative valid sets of identifying moments are available, we verify in the empirical analysis that our results are robust to this choice.[5]

Proposition 2.2. *Under Assumption (2.20), the risk-neutral moments $\mathcal{M}^{*(j)}_{i,M,t}$ can be expressed as*

$$\mathcal{M}^{*(j)}_{i,M,t} = \sum_{k=1}^{\mathcal{N}} \underline{\gamma}_{i,k,t}\mathbb{E}^*_t\left(\mathcal{R}^j_{M,t\to T_1}\left(\mathcal{R}^k_{M,t\to T_1} - \mathbb{E}^*_t\mathcal{R}^k_{M,t\to T_1}\right)\right). \tag{2.23}$$

Proposition 2.2 converts the untruncated stock–market cross-moments required for the lower bound into risk-neutral moments of the market return and moment-matching coefficients obtained from option-implied stock moments. This provides an implementable lower-

[5] Our baseline specification sets $(\mathcal{N}, q^*) = (2, 2)$. As a robustness check, we also estimate the model using $(\mathcal{N}, q^*) = (2, 3)$. The resulting lower and upper bounds are highly correlated with the baseline estimates (pairwise correlations exceeding 0.85), and the corresponding pricing consistency results are reported in Online Appendix Figure OA.1.

bound input without estimating realized covariances or historical betas.

We next apply the same logic to the truncated payoff that enters the upper bound. Define

$$\mathcal{R}^c_{i,t\to T_1} = \mathcal{R}_{i,t\to T_1} 1_{R_{i,t\to T_1} \geq k_0},$$

and write

$$\mathcal{R}^c_{i,t\to T_1} = h_{\mathcal{N},i,t}\left[\mathcal{R}_{M,t\to T_1}\right] - \mathbb{E}^*_t h_{\mathcal{N},i,t}\left[\mathcal{R}_{M,t\to T_1}\right] + \varepsilon^*_{i,t\to T_1},$$

where

$$h_{\mathcal{N},i,t}\left[\mathcal{R}_{M,t\to T_1}\right] = \mathbb{E}^*_t\left[\mathcal{R}^c_{i,t\to T_1} \mid \mathcal{R}_{M,t\to T_1}\right].$$

The function $h_{\mathcal{N},i,t}\left[.\right]$ captures the component of the truncated payoff spanned by the market return. We approximate it by

$$h_{\mathcal{N},i,t}\left[\mathcal{R}_{M,t\to T_1}\right] = \sum_{k=1}^{\mathcal{N}} \overline{\gamma}_{i,k,t} \mathcal{R}^k_{M,t\to T_1}. \tag{2.24}$$

Unlike the untruncated excess return, the truncated payoff need not have zero risk-neutral mean. We therefore match centered moments:

$$\begin{aligned}\mathbb{E}^*_t\left[\left(\mathcal{R}^c_{i,t\to T_1}\right)^q\right] &= \mathbb{E}^*_t\left[\left(h_{\mathcal{N},i,t}\left[\mathcal{R}_{M,t\to T_1}\right] - \mathbb{E}^*_t h_{\mathcal{N},i,t}\left[\mathcal{R}_{M,t\to T_1}\right]\right)^q\right] \\ &\quad + \sum_{j=1}^{q} \frac{q!}{(q-j)!j!} \mathbb{E}^*_t\left[\left(h_{\mathcal{N},i,t}\left[\mathcal{R}_{M,t\to T_1}\right] - \mathbb{E}^*_t h_{\mathcal{N},i,t}\left[\mathcal{R}_{M,t\to T_1}\right]\right)^{q-j} \varepsilon^{*j}_{i,t\to T_1}\right].\end{aligned} \tag{2.25}$$

The first interaction term again vanishes by the conditional expectation property, whereas the remaining higher-order interaction terms are not identified from option prices. Accordingly, we impose the identifying restriction:

$$\sum_{j=1}^{q} \frac{q!}{(q-j)!j!} \mathbb{E}_t^* \left[\left(h_{\mathcal{N},i,t} \left[\mathcal{R}_{M,t\to T_1} \right] - \mathbb{E}_t^* h_{\mathcal{N},i,t} \left[\mathcal{R}_{M,t\to T_1} \right] \right)^{q-j} \varepsilon_{i,t\to T_1}^{*j} \right] = 0, \qquad q = q^*, ..., \mathcal{N}+q^*-1. \tag{2.26}$$

This restriction plays the same identifying role for truncated payoffs as (2.20) does for untruncated payoffs. Under (2.26), the centered moments of truncated returns satisfy

$$\mathbb{E}_t^* \left(\mathcal{R}_{i,t\to T_1}^c - \mathbb{E}_t^* \left[\mathcal{R}_{i,t\to T_1}^c \right] \right)^q = \mathbb{E}_t^* \left(h_{\mathcal{N},i,t} \left[\mathcal{R}_{M,t\to T_1} \right] - \mathbb{E}_t^* h_{\mathcal{N},i,t} \left[\mathcal{R}_{M,t\to T_1} \right] \right)^q, \qquad q = q^*, ..., \mathcal{N}+q^*-1. \tag{2.27}$$

Equation (2.27) provides $\mathcal{N}$ centered moment conditions to identify the $\mathcal{N}$ coefficients $\{\overline{\gamma}_{i,1,t}, \ldots, \overline{\gamma}_{i,\mathcal{N},t}\}$, provided the associated Jacobian has full rank.

Proposition 2.3. *Under Assumption (2.26), the truncated risk-neutral moments* $\mathcal{M}_{i,M,t}^{*(j)}[k_0]$ *can be expressed as*

$$\mathcal{M}_{i,M,t}^{*(j)}[k_0] = \mathbb{E}_t^* \mathcal{R}_{M,t\to T_1}^j \mathbb{E}_t^* \mathcal{R}_{i,t\to T_1}^c + \sum_{k=1}^{\mathcal{N}} \overline{\gamma}_{i,k,t} \mathbb{E}_t^* \left[\mathcal{R}_{M,t\to T_1}^j \left(\mathcal{R}_{M,t\to T_1}^k - \mathbb{E}_t^* \mathcal{R}_{M,t\to T_1}^k \right) \right]. \tag{2.28}$$

Proposition 2.3 provides an implementable approximation to the truncated-return cross-moments required for the upper bound. Together, Propositions 2.2 and 2.3 show how to compute the cross-moments in Proposition 2.1 from option-implied marginal moments of the stock and market, without relying on realized returns.

The static analysis provides a benchmark in which expected returns depend only on contemporaneous stock–market risk-neutral cross-moments. We next extend the framework to a dynamic setting with portfolio rebalancing. In that environment, the SDF depends not only on the contemporaneous market return but also on risk-neutral moments of future market returns, so intertemporal hedging affects individual-stock expected excess returns.

2.2 Expected Excess Return with Intertemporal Hedging

We assume that the representative agent maximizes expected utility recursively over N periods, beginning at time t, according to the following objective:[6]

$$\max_{\omega_t} \mathbb{E}_t \max_{\omega_{T_1}} \mathbb{E}_{T_1} \max_{\omega_{T_2}} \mathbb{E}_{T_2} .... \max_{\omega_{T_{N-1}}} \mathbb{E}_{T_{N-1}} u \left[W_{t \to T_N} \right].$$

We define the wealth evolution recursively by:

$$W_{T_j \to T_{j+1}} = W_{T_{j-1} \to T_j} \left(R_{f,T_j \to T_{j+1}} + \omega_{T_j}^{\top} \left(\mathbf{R}_{T_j \to T_{j+1}} - R_{f,T_j \to T_{j+1}} \mathbf{1} \right) \right),$$

for $j = 0, .., N-1$. In this framework, we assume no interest rate risk and $R_{f,T_j \to T_{j+1}}$ is known at time t for all j. The SDF from time t to T_N is proportional to marginal utility $u' \left[W_{t \to T_N} \right]$. Suppose that we wish to price a two-period payoff formed by investing in asset i over $[t, T_1]$, liquidating the position at T_1, and rolling the proceeds into the risk-free asset over $[T_1, T_N]$. The gross payoff from this rollover strategy equals $R_{i,t \to T_1} R_{f,T_1 \to T_N}$. Subtracting the risk-free gross return over the same horizon, $R_{f,t \to T_1} R_{f,T_1 \to T_N}$, yields the corresponding excess payoff:

$$R_{i,t \to T_1} R_{f,T_1 \to T_N} - R_{f,t \to T_1} R_{f,T_1 \to T_N} = \mathcal{R}_{i,t \to T_1} R_{f,T_1 \to T_N}.$$

[6] Allowing for intermediate consumption is feasible, but it would complicate the analysis and, in practice, preclude real-time implementation because doing so would require specifying and estimating a structural model of consumption dynamics from historical data. We forgo a fully specified consumption-based structure in exchange for parsimony and a purely option-based implementation.

Under no-arbitrage conditions, the expected excess return satisfies

$$\mathbb{E}_t\left(\mathcal{R}_{i,t\to T_1} R_{f,T_1\to T_N}\right) = \mathbb{E}_t^*\left(\frac{\mathbb{E}_t m_{t\to T_N}}{m_{t\to T_N}} \mathcal{R}_{i,t\to T_1} R_{f,T_1\to T_N}\right), \tag{2.29}$$

where the inverse SDF satisfies

$$\frac{\mathbb{E}_t m_{t\to T_N}}{m_{t\to T_N}} = \frac{\vartheta_{t\to T_N}}{\mathbb{E}_t^* \vartheta_{t\to T_N}},$$

with

$$\vartheta_{t\to T_N} = \frac{u'\left[W_t R_{f,t\to T_N}\right]}{u'\left[W_t R_{M,t\to T_N}\right]}.$$

Assuming there is no interest rate risk, $R_{f,T_1\to T_N}$ is known at time t and the expression (2.29) simplifies to

$$\mathbb{E}_t \mathcal{R}_{i,t\to T_1} = \mathbb{E}_t^*\left(\mathcal{R}_{i,t\to T_1} \mathbb{E}_{T_1}^* \frac{\mathbb{E}_t m_{t\to T_N}}{m_{t\to T_N}}\right). \tag{2.30}$$

Since $\mathcal{R}_{i,t\to T_1}$ is an excess return for one period, the standard price relation without arbitrage (2.1) applies. Thus, comparing expression (2.1) and (2.30), and using the uniqueness of the SDF,

$$\frac{\mathbb{E}_t m_{t\to T_1}}{m_{t\to T_1}} = \mathbb{E}_{T_1}^* \frac{\mathbb{E}_t m_{t\to T_N}}{m_{t\to T_N}} = \frac{\upsilon_{t\to T_1}}{\mathbb{E}_t^* \upsilon_{t\to T_1}}. \tag{2.31}$$

Given that $R_{M,t\to T_N} = R_{M,t\to T_1} R_{M,T_1\to T_N}$, $\vartheta_{t\to T_N}$ is a function of $R_{M,t\to T_1}$ and $R_{M,T_1\to T_N}$. Assuming that the necessary regularity conditions in $\vartheta_{t\to T_N}$ are satisfied, a Taylor expansion series of $\vartheta_{t\to T_N}$ around $(\mathcal{R}_{M,t\to T_1}, \mathcal{R}_{M,T_1\to T_N}) = (0,0)$ yields the following.

$$\upsilon_{t\to T_1} = 1 + \sum_{k=1}^{\infty} \sum_{j=0}^{k} \frac{a_{j,k-j,t}}{R_{f,t\to T_1}^{j} R_{f,T_1\to T_N}^{k-j}} f_{T_1}^{(j,k-j)}, \tag{2.32}$$

with

$$f_{T_1}^{(j,k-j)} = \mathcal{R}_{M,t\to T_1}^{j} \mathbb{E}_{T_1}^{*} \mathcal{R}_{M,T_1\to T_N}^{k-j}, \tag{2.33}$$

where the lower-order terms are identified as

$$a_{0,0,t} = 1,\ a_{1,0,t} = a_{1,t},\ a_{2,0,t} = a_{2,t},\ a_{3,0,t} = a_{3,t},\ a_{4,0,t} = a_{4,t}, \tag{2.34}$$

and

$$a_{0,2,t} = a_{2,t},\ a_{0,3,t} = a_{3,t},\ a_{0,4,t} = a_{4,t}, a_{1,2,t} = 2a_{2,t} + 3a_{3,t}, \tag{2.35}$$

and

$$a_{1,3,t} = 3a_{3,t} + 3\left(1 - 2\frac{a_{2,t}}{a_{1,t}^2} + a_{3,t}\right)(a_{1,t} - 1) + 4a_{4.t}, \tag{2.36}$$

$$a_{2,2,t} = a_{2,t} + 6a_{3,t} + 6a_{4,t}. \tag{2.37}$$

The coefficients $a_{j,k,t}$ are analogous to those in (2.6), with T_1 replaced by T_N. The inverse SDF (2.31) is a function of priced factors $f_{T_1}^{(j,k-j)}$ for all pairs $(j, k-j)$ not equal to $(0,0)$ and for pairs where $k-j \neq 1$. When $k-j = 1$, this term vanishes because $\mathbb{E}_{T_1}^{*}\mathcal{R}_{M,T_1\to T_N}$ is zero. In particular, when $j = 0$ and $k - j \geq 2$, each factor simplifies to $f_{T_1}^{(j,k-j)} = \mathbb{E}_{T_1}^{*}\mathcal{R}_{M,T_1\to T_N}^{k-j}$, which corresponds to the time-T_1 conditional risk-neutral variance $(k - j = 2)$, skewness $(k - j = 3)$, and kurtosis $(k - j = 4)$ of future market returns. More generally, the factors $f_{T_1}^{(j,k-j)}$ show that, when intertemporal hedging is relevant, the inverse SDF depends not only on the contemporaneous market return but also on time-T_1 conditional risk-neutral moments of future market returns and their interactions with the contemporaneous market return.

Applying the Carr and Madan (2001) spanning result to both $\mathcal{R}_{M,t\to T_1}^{j}$ and $\mathcal{R}_{M,T_1\to T_N}^{k-j}$, we show in Online Appendix (OA.2.2) that the inverse SDF (2.31) admits a decomposition involving the market return, a continuum of options maturing at T_1, and a continuum of options maturing at T_N that will be sold at T_1.

Using (2.1), (2.2), and (2.32), the expected market excess return (setting $i = M$) can be written as a sum of risk premium terms of the form

$$\underbrace{\frac{a_{j,k-j,t}}{R^j_{f,t\to T_1} R^{k-j}_{f,T_1\to T_N} \mathbb{E}^*_t \upsilon_{t\to T_1}}}_{\text{Price of Risk}} \times \underbrace{\mathbb{COV}^*_t \left(\mathcal{R}_{M,t\to T_1}, \mathcal{R}^j_{M,t\to T_1} \mathbb{E}^*_{T_1} \mathcal{R}^{k-j}_{M,T_1\to T_N} \right)}_{\text{Quantity of Risk}} \geq 0. \tag{2.38}$$

The left-hand side of (2.38) is the compensation for exposure to the priced factor $f^{(j,k-j)}_{T_1}$. This implies that $a_{j,k-j,t} \geq (\leq)\, 0$ if $\mathbb{COV}^*_t \left(\mathcal{R}_{M,t\to T_1}, f^{(j,k-j)}_{T_1} \right) \geq (\leq)\, 0$. When $k - j = 0$, inequality (2.38) coincides with (2.7). When $k-j \geq 2$ and j and $k-j$ are both odd or both even, we posit that $a_{j,k-j,t} \leq 0$. If j is odd (even) and $k - j$ is even (odd), we posit that $a_{j,k-j,t} \geq 0$.

When $i \neq M$, combining (2.1), (2.2), and (2.32) shows that the expected excess return on individual stock is a sum of risk premium terms of the form

$$\underbrace{\frac{a_{j,k-j,t}}{R^j_{f,t\to T_1} R^{k-j}_{f,T_1\to T_N} \mathbb{E}^*_t \upsilon_{t\to T_1}}}_{\text{Price of Risk}} \times \underbrace{\mathbb{COV}^*_t \left(\mathcal{R}_{i,t\to T_1}, \mathcal{R}^j_{M,t\to T_1} \mathbb{E}^*_{T_1} \mathcal{R}^{k-j}_{M,T_1\to T_N} \right)}_{\text{Quantity of Risk}} \geq 0. \tag{2.39}$$

As in the case without intertemporal hedging, restriction (2.39) follows from the economically intuitive assumption that the price of risk times the quantity of risk is positive.[7]

Proposition 2.4. *Assume that for all pairs $(j, k-j)$, inequalities (2.38) and (2.39) hold. Under no-arbitrage conditions, for any $\mathcal{K}$ >0, the expected excess return on individual stock*

[7] The implied sign restrictions are broadly supported by the data; see Online Appendix Table OA.1.

i admits the following lower bound

$$\mathbb{E}_t\left[\mathcal{R}_{i,t\to T_1}\right] \geq \frac{\sum_{k=1}^{\mathcal{K}}\sum_{j=0}^{k}\frac{a_{j,k-j}}{R^j_{f,t\to T_1}R^{k-j}_{f,T_1\to T_N}}\mathcal{M}^{*(j,k-j)}_{i,M,t}}{1+\sum_{k=1}^{\mathcal{K}}\sum_{j=0}^{k}\frac{a_{j,k-j}}{R^j_{f,t\to T_1}R^{k-j}_{f,T_1\to T_N}}\mathbb{E}^*_t f^{(j,k-j)}_{T_1}}, \tag{2.40}$$

with

$$\mathcal{M}^{*(j,k-j)}_{i,M,t} = \mathbb{E}^*_t\left[\mathcal{R}_{i,t\to T_1} f^{(j,k-j)}_{T_1}\right]. \tag{2.41}$$

Furthermore, up to a $\mathcal{K}^{th}$ order expansion of the inverse marginal utility, and for any threshold $k_0 \leq R_{f,t\to T_1}$, the expected excess return on stock i satisfies the following upper bound

$$\mathbb{E}_t\left[\mathcal{R}_{i,t\to T_1}\right] \leq \frac{\mathcal{M}^{*(0)}_{i,M,t}\left[k_0\right]+\sum_{k=1}^{\mathcal{K}}\sum_{j=0}^{k}\frac{a_{j,k-j}}{R^j_{f,t\to T_1}R^{k-j}_{f,T_1\to T_N}}\mathcal{M}^{*(j,k-j)}_{i,M,t}\left[k_0\right]}{1+\sum_{k=1}^{\mathcal{K}}\sum_{j=0}^{k}\frac{a_{j,k-j}}{R^j_{f,t\to T_1}R^{k-j}_{f,T_1\to T_N}}\mathbb{E}^*_t f^{(j,k-j)}_{T_1}}, \tag{2.42}$$

with

$$\mathcal{M}^{*(j,k-j)}_{i,M,t}\left[k_0\right] = \mathbb{E}^*_t\left[\mathcal{R}_{i,t\to T_1} 1_{R_{i,t\to T_1}\geq k_0} f^{(j,k-j)}_{T_1}\right]. \tag{2.43}$$

Proof. See Online Appendix OA.1. □

Proposition 2.4 provides lower and upper bounds for the expected excess return on individual stock i in the presence of intertemporal hedging. Relative to market-level intertemporal hedging formulas, the key additional difficulty is that the individual-stock bounds involve risk-neutral cross-moments between the stock payoff and the terms $f^{(j,k-j)}_{T_1}$, where $f^{(j,k-j)}_{T_1} = \mathcal{R}^j_{M,t\to T_1}\mathbb{E}^*_{T_1}\mathcal{R}^{k-j}_{M,T_1\to T_N}$. These terms combine contemporaneous market excess returns with T_1-conditional risk-neutral moments of future market excess returns.[8] These

[8] Chabi-Yo, Gourier, and Langlois (2025) study market-level premia with intertemporal hedging. Their implementation relies on aggregate market risk-neutral moments, whereas our individual-stock bounds re-

cross-moments are the dynamic counterparts of those in Proposition 2.1 and are not directly observable from traded option prices.

Given the preference parameters, one needs to compute the risk-neutral quantities in (2.40) and (2.42). Since $\mathcal{R}_{M,T_1\to T_N} = R_{M,T_1\to T_N} - R_{f,T_1\to T_N}$, it follows that, for $j_2 \geq 2$,

$$\mathcal{R}^{j_2}_{M,T_1\to T_N} = \sum_{l=0}^{j_2} \frac{j_2!\,(-1)^{j_2-l}\,R^{j_2-l}_{f,T_1\to T_N}}{(j_2-l)!l!} R^l_{M,T_1\to T_N}. \tag{2.44}$$

Taking the conditional expectation yields

$$\mathbb{E}^*_{T_1}\mathcal{R}^{j_2}_{M,T_1\to T_N} = \sum_{l=2}^{j_2} \phi_{j_2,l}\left(\mathbb{E}^*_{T_1} R^l_{M,T_1\to T_N} - R^l_{f,T_1\to T_N}\right), \tag{2.45}$$

with

$$\phi_{j_2,l} = \frac{j_2!\,(-1)^{j_2-l}\,R^{j_2-l}_{f,T_1\to T_N}}{(j_2-l)!l!}. \tag{2.46}$$

When $l \geq 2$, closed-form expressions for $\mathbb{E}^*_{T_1} R^l_{M,T_1\to T_N} - R^l_{f,T_1\to T_N}$ in terms of option prices are not available. Since Jensen's inequality implies $\mathbb{E}^*_{T_1} R^l_{M,T_1\to T_N} \geq R^l_{f,T_1\to T_N}$, a tractable approach is to express the positive term $\mathbb{E}^*_{T_1} R^l_{M,T_1\to T_N} - R^l_{f,T_1\to T_N}$ using time T_1 information, such as $R_{M,t\to T_1}$, by assuming for any $l = 2, 3, 4$ that

$$\mathbb{E}^*_{T_1} R^l_{M,T_1\to T_N} - R^l_{f,T_1\to T_N} = \theta^*_{l,t}\left\{\begin{array}{c} \left(R^l_{M,t\to T_1} - R^l_{f,t\to T_1}\right) 1_{R_{M,t\to T_1} > R_{f,t\to T_1}} \\ +\left(R^l_{f,t\to T_1} - R^l_{M,t\to T_1}\right) 1_{R_{M,t\to T_1} < R_{f,t\to T_1}} \end{array}\right\}. \tag{2.47}$$

The specification assumes that the future positive moment $\mathbb{E}^*_{T_1} R^l_{M,T_1\to T_N} - R^l_{f,T_1\to T_N}$ is solely driven by the intermediate variable $R_{M,t\to T_1}$. The right-hand side of (2.47) can be interpreted as the payoff of a static portfolio of options, and the parameter $\theta^*_{\ell,t}$ is chosen so that the

quire stock–market cross-moments that are not directly observed from traded options.

payoffs on the left- and right-hand sides of (2.47) have identical prices. For completeness, we provide the full motivation and derivations in Online Appendix OA.3. We also consider an alternative specification of (2.47) and obtain qualitatively similar results; details are reported in Online Appendix OA.4.

To determine $\theta^*_{l,t}$, we multiply (2.47) by $R^l_{M,t\to T_1}$, exploit $R^l_{M,t\to T_N} = R^l_{M,t\to T_1} R^l_{M,T_1\to T_N}$, and take expectation, which leads to

$$\theta^*_{l,t} = \frac{\mathbb{E}^*_t R^l_{M,t\to T_N} - R^l_{f,T_1\to T_N}\mathbb{E}^*_t R^l_{M,t\to T_1}}{\left\{\begin{array}{c} \mathbb{E}^*_t\left[R^l_{M,t\to T_1}\left(R^l_{M,t\to T_1} - R^l_{f,t\to T_1}\right)1_{R_{M,t\to T_1} > R_{f,t\to T_1}}\right] \\ -\mathbb{E}^*_t\left[R^l_{M,t\to T_1}\left(R^l_{M,t\to T_1} - R^l_{f,t\to T_1}\right)1_{R_{M,t\to T_1} < R_{f,t\to T_1}}\right] \end{array}\right\}}. \tag{2.48}$$

We now build on (2.48) to provide expressions for (2.41) and (2.43) in terms of observable risk-neutral quantities.

Proposition 2.5. *Denote*

$$\begin{aligned} \mathbb{M}^{*+}_t[j,q,l] &= \mathbb{E}^*_t\left[\mathcal{R}^{j+q}_{M,t\to T_1}\left(R^l_{M,t\to T_1} - R^l_{f,t\to T_1}\right)1_{R_{M,t\to T_1} > R_{f,t\to T_1}}\right], \\ \mathbb{M}^{*-}_t[j,q,l] &= \mathbb{E}^*_t\left[\mathcal{R}^{j+q}_{M,t\to T_1}\left(R^l_{M,t\to T_1} - R^l_{f,t\to T_1}\right)1_{R_{M,t\to T_1} < R_{f,t\to T_1}}\right]. \end{aligned}$$

Assuming (2.47)*, it follows that, for* $k-j \neq \{0,1\}$*,*

$$\mathcal{M}^{(j,k-j)}_{i,M,t} = \sum_{q=1}^{\mathcal{N}} \underline{\gamma}_{i,q} \sum_{l=2}^{k-j} \phi_{k-j,l}\theta^*_{l,t}\mathbb{M}^{*+}_t[j,q,l] - \sum_{q=1}^{\mathcal{N}} \underline{\gamma}_{i,q} \sum_{l=2}^{k-j} \phi_{k-j,l}\theta^*_{l,t}\mathbb{M}^{*-}_t[j,q,l], \tag{2.49}$$

and

$$\mathcal{M}^{(j,k-j)}_{i,M,t}[k_0] = \sum_{q=1}^{\mathcal{N}} \overline{\gamma}_{i,q} \sum_{l=2}^{k-j} \phi_{k-j,l}\theta^*_{l,t}\mathbb{M}^{*+}_t[j,q,l] - \sum_{q=1}^{\mathcal{N}} \overline{\gamma}_{i,q} \sum_{l=2}^{k-j} \phi_{k-j,l}\theta^*_{l,t}\mathbb{M}^{*-}_t[j,q,l], \tag{2.50}$$

and

$$\mathbb{E}_t^* f_{T_1}^{(j,k-j)} = \sum_{l=2}^{k-j} \phi_{k-j,l} \theta_{l,t}^* \mathbb{M}_t^{*+} [j, 0, l] - \sum_{l=2}^{k-j} \phi_{k-j,l} \theta_{l,t}^* \mathbb{M}_t^{*-} [j, 0, l] \,. \tag{2.51}$$

Here, $\phi_{j_2,l}$ is defined in (2.46), while $\overline{\gamma}_{i,k}$ and $\underline{\gamma}_{i,k}$ are defined in (2.17) and (2.24). The risk-neutral quantities $\mathcal{M}_{i,M,t}^{*(j_1)}$ and $\mathcal{M}_{i,M,t}^{*(j_1)}[k_0]$ are defined in (2.23) and (2.28). Finally, $\theta_{l,t}^*$ is defined in (2.48).

Proof. See Online Appendix OA.1. □

Proposition 2.5 provides expressions for the risk-neutral quantities needed to compute the lower and upper bounds in Proposition 2.4. Expressions for the market-return-related risk-neutral quantities appearing in (2.49), (2.50), and (2.51) are provided in Section 3.4 and Online Appendix OA.7.

3 Measuring Bounds from Option Prices

This section describes how we construct empirical counterparts of the theoretical bounds using observable option prices. We first describe the data used in the empirical implementation. We then describe how we choose the local preference parameters, considering both constant and time-varying specifications. Next, we specify the truncation order of the inverse marginal utility expansion. Finally, we explain how the risk-neutral moments entering the bounds are extracted from index and single-name option prices.

3.1 Data

Our sample consists of U.S. firms included in the S&P 500 index between January 1996 and August 2025. Option data on individual equities and on the S&P 500 index are obtained from OptionMetrics. Because options with exact target strikes rarely trade, we use the volatility surface data, which provides daily interpolated implied volatilities and corresponding option premiums over a standardized grid of maturities and deltas.[9] To construct a finer grid of option prices across moneyness levels ranging from 1/3 to 3 (with 1,001 points for each maturity), we interpolate implied volatilities using a piecewise cubic Hermite polynomial and extrapolate flatly outside the boundaries, following Chabi-Yo, Dim, and Vilkov (2023). This procedure, together with our focus on S&P 500 constituents, mitigates concerns about sparse strike coverage and illiquidity in single-name options.[10] Option prices are then recovered from the interpolated volatilities using the Black–Scholes formula. Since the fitted implied volatilities are computed daily using only contemporaneous option quotes and require sufficient data for interpolation, the resulting option prices are free from look-ahead bias and reflect prevailing market valuations.

Underlying index levels and stock prices are obtained from CRSP, and index constituent information from Compustat. For the spot risk-free rate, we use constant-maturity Treasury yields with maturities of 1, 3, 6, and 12 months from the Federal Reserve Economic Database, matching the horizons of the equity premium. Forward risk-free rates between T_1 to T_N are computed from the spot rates at maturities T_1 and T_N.

3.2 Local Preference Parameters

Our formulas for the bounds involve four local risk-preference parameters: τ (risk tolerance), ρ (prudence), κ (temperance), and ξ (hyper-temperance). The restrictions in (2.8) discipline the admissible range of these parameters but do not determine their magnitudes. To con-

[9] Maturities include 30, 60, 91, 122, 152, 182, 273, 365, 547, and 730 days; absolute deltas range from 0.1 to 0.9 in increments of 0.05.

[10] This approach is consistent with recent option-based expected-return studies using volatility surface data, including Martin and Wagner (2019), Kadan and Tang (2020), and Chabi-Yo, Dim, and Vilkov (2023).

struct empirical counterparts of the bounds, we consider two calibration approaches. We first use constant preference parameters, and then allow the parameters to vary over time as functions of observable market conditions. In both specifications, the parameters are chosen to satisfy the theoretical restrictions in (2.8) and to remain within economically plausible ranges.

3.2.1 Calibration with Constant Preference Parameters

Although the preference parameters may vary over time in theory, a constant specification provides a parsimonious benchmark. Our baseline calibration sets $\tau = 1$, $\rho = 2$, $\kappa = 4$, and $\xi = 8$.

The choice of $\tau = 1$ implies local relative risk aversion of $1/\tau = 1$, which lies at the lower end of the range commonly viewed as empirically plausible in finance. A broad empirical literature places relative risk aversion roughly between 1 and 5. Micro-based estimates using household consumption and portfolio data typically suggest low to moderate values, often around 1 to 3 for stockholders, and reject very high levels of risk aversion (Vissing-Jørgensen and Attanasio, 2003; Brunnermeier and Nagel, 2008). Survey and portfolio-choice evidence also supports moderate values, often around 2 to 4 (Guiso and Paiella, 2008; Chiappori and Paiella, 2011). Asset-pricing models frequently use values in this range to match key features of asset returns (Constantinides, 1990; Campbell and Cochrane, 1999; Barberis, Huang, and Santos, 2001; Epstein and Zin, 1989; Bansal and Yaron, 2004). Option-based estimates are also consistent with this view: Bliss and Panigirtzoglou (2004) combine option-implied risk-neutral densities with a parametric utility specification and obtain estimates broadly consistent with moderate relative risk aversion. Meta-analytic evidence reaches a similar conclusion (Elminejad, Havranek, and Irsova, 2025). Taken together, this evidence suggests that $1/\tau = 1$ is a reasonable lower-end benchmark.

The choice of $\rho = 2$ is motivated by theory and evidence on prudence, which captures precautionary saving motives (Kimball, 1990; Gollier, 2001). For our framework, the key implication is that $\rho > 1$. Existing evidence supports this restriction. Noussair, Trautmann, and Van de Kuilen (2014) show in a large representative laboratory experiment that $\rho > 1$ holds for a substantial subset of subjects. Similarly, Ebert and Wiesen (2011, 2014) jointly elicit relative risk aversion and prudence and document many prudent subjects, particularly in the region where $\rho > 1$. Asset-pricing evidence points in the same direction: Chabi-Yo (2012) estimates preference parameters in a stochastic discount factor that depends on market returns and volatility and obtains values consistent with $\rho > 1$. We therefore set $\rho = 2$ as a simple benchmark that lies comfortably within the prudence-consistent region supported by the evidence.

Direct empirical guidance is more limited for κ and ξ. Given $1/\tau = 1$ and $\rho = 2$, we set $\kappa = 4$ and $\xi = 8$, so that the higher-order preference parameters increase approximately in powers of two. This heuristic provides an internally coherent calibration while avoiding implausibly large higher-order values or bounds driven disproportionately by the highest-order terms. We therefore treat κ and ξ as calibration parameters rather than tightly identified structural parameters.

Our decision to first work with constant preference parameters rather than fully estimating a flexible preference process is motivated by both empirical and conceptual considerations. Empirically, Chabi-Yo, Gourier, and Langlois (2025) show, in a market-level setting, that economically reasonable constant-parameter calibrations deliver superior out-of-sample performance to specifications in which preferences are estimated from realized returns. Conceptually, estimating preferences from historical returns would run counter to our goal of deriving ex ante bounds from option prices rather than from realized returns. Accordingly, our default and data-driven parameter sets are disciplined calibrations within a narrow, economically plausible range, not unconstrained statistical estimates. This approach avoids imposing and estimating time-series dynamics for higher-order preference parameters from realized returns, which could introduce look-ahead bias in out-of-sample evaluation. Consistent with this perspective, Chabi-Yo, Dim, and Vilkov (2023) also adopt calibration rather than full estimation. We therefore view calibration as a sound way to bring the theory to the data.

3.2.2 Calibration with Time-Varying Preference Parameters

Allowing the local preference parameters to vary over time serves two purposes. First, it provides a useful check on the plausibility of the constant parameter values used in Section 3.2.1 by comparing them with values disciplined by the data. Second, it allows us to examine whether our conclusions change when the preference parameters are allowed to respond to market conditions over time.

To this end, we consider two complementary calibration approaches. The first chooses the preference parameters to maximize the out-of-sample forecast accuracy of the average bound, defined as the midpoint between the lower and upper bounds, for future returns. Forecast accuracy is evaluated using out-of-sample R^2 statistics that compare predictions based on the average bound under the calibrated parameter set with those based on the default parameter set.[11] Because the calibration is based on the midpoint of the bounds, the resulting parameter set for a given forecast horizon applies to both the lower and upper

[11] This out-of-sample R^2 statistic is widely used in the return predictability literature to compare predictive models; see, for example, Goyal and Welch (2008), Martin and Wagner (2019), and Chabi-Yo, Dim, and Vilkov (2023).

bounds.

The second approach calibrates the preference parameters to match the observed variance risk premium, following Tetlock, McCoy, and Shah (2024). In our framework, the model-implied variance risk premium can be expressed as a function of risk-neutral moments and the preference parameters (see Online Appendix OA.6). This mapping allows us to recover, at each point in time, the parameter values that align the model-implied variance risk premium with its empirical counterpart. Specifically, we proxy for the empirical variance risk premium by the difference between risk-neutral variance and physical variance over the same horizon. Risk-neutral variance is computed from the cross-section of option prices using the model-free option-implied moment formula of Bakshi and Madan (2000) over the available range of out-of-the-money strikes. Physical variance is measured from past daily returns as the cumulative sum of squared daily returns over the previous month. We then calibrate the preference parameters so that the model-implied variance risk premium matches this empirical measure as closely as possible at each point in time. In this way, the observed variance risk premium provides a disciplined moment condition for identifying otherwise unobservable preference-related parameters.

In both approaches, we update the preference parameters each month using an expanding-window scheme. Starting from an initial window of 10 months, we use all available observations up to month t to calibrate the parameter vector for month t. This design allows parameter estimates to respond to evolving market conditions while avoiding the excessive instability that can arise in short-window estimation. We implement the calibration through a grid search over values from 1 to 10 in increments of 0.3 for each parameter, retaining only combinations that satisfy Equation (2.8).

Online Appendix Tables OA.2 and OA.3 summarize the average calibrated time-varying parameter values under the two approaches. Across forecast and investment horizons, the estimated values remain broadly close to our default specification of $(1/\tau, \rho, \kappa, \xi) = (1, 2, 4, 8)$. In particular, $1/\tau$ typically stays close to one, while ρ remains in a moderate range that is generally near or somewhat below two. The higher-order parameters, κ and ξ, also remain of similar magnitudes to the default values, although they exhibit somewhat greater variation across horizon combinations, especially under the variance risk premium calibration. Overall, the calibrated values do not suggest large departures from the benchmark specification, indicating that the constant-parameter choice used in Section 3.2.1 is empirically reasonable.

To illustrate the time-series behavior of these estimates, Online Appendix Figure OA.2 and OA.3 plot the parameter paths for selected forecast and investment horizon combinations under the forecast-accuracy-based and variance-risk-premium-based calibrations, respectively. The figures show that, although the parameters vary over time, their movements are gradual for most of the sample and do not imply persistent deviations large enough to overturn the baseline calibration. This further supports our use of the default parameter values as a parsimonious benchmark.

3.3 Truncating the Inverse Marginal Utility Expansion

We set the Taylor truncation order to $\mathcal{K} = 4$ in the bounds derived in Propositions 2.1 and 2.4. This choice allows the bounds to incorporate variance, skewness, kurtosis, and fifth-moment effects while keeping the empirical implementation tractable.[12]

A natural concern is that truncating the inverse marginal utility expansion at the fourth order omits higher-order terms. The omitted remainder depends on higher-order derivatives

[12] We also considered lower-order truncations with $\mathcal{K} = 2$ and $\mathcal{K} = 3$. While the qualitative results remain similar, the fourth-order specification delivers stronger empirical performance in terms of tighter bounds and improved return predictability. Therefore, we adopt $\mathcal{K} = 4$ as our baseline specification.

of utility and higher-order risk-neutral moments of returns. These objects are not directly observable and, in our setting, involve preference parameters associated with derivatives beyond the sixth order, for which there is limited theoretical or empirical guidance.

Our framework does not require these higher-order terms to be identically zero. Instead, the truncation assumes that their contribution to expected excess returns is quantitatively negligible. Equivalently, we impose that the risk-neutral covariance between individual stock returns and the omitted remainder term is zero. This type of restriction is standard in asset-pricing models based on low-order expansions, including Kraus and Litzenberger (1976), Harvey and Siddique (2000), and Dittmar (2002). Our contribution extends this approach to a fourth-order expansion, allowing richer nonlinearities while preserving empirical discipline.

Extending the expansion beyond the fourth order would require estimating higher-order risk-neutral moments and stock–market cross-moments from option prices. These quantities are noisy and sensitive to the tails of the implied distribution, which would reduce the reliability of the resulting bounds. Moreover, higher-order expansions do not necessarily improve empirical performance; Hlawitschka (1994) shows that adding higher-order terms can fail to improve approximation quality.

The choice $\mathcal{K} = 4$ therefore reflects a trade-off between theoretical generality and empirical implementability. It incorporates the leading higher-order risk channels emphasized in the literature while avoiding the instability associated with estimating very high-order option-implied moments. Under empirically plausible preference parameters and return distributions, higher-order contributions are expected to decay rapidly, so a fourth-order approximation captures the economically relevant variation in the bounds.

3.4 Estimation of Risk-Neutral Moments

We next compute the risk-neutral moments that enter the bound formulas. In total, we require seven types of moments. The first three are fundamental building blocks, while the remaining four can be expressed as combinations of these three.

Marginal risk-neutral moments. The first type consists of marginal risk-neutral moments taken separately for individual stock returns and for the market return,

$$\mathbb{E}_t^*\left[\mathcal{R}_{i,t\to T_1}^q\right].$$

Their computation is straightforward. Following Breeden and Litzenberger (1978) and Bakshi and Madan (2000), each of these moments can be extracted from the cross-section of option prices on individual stocks and on the index, as detailed in Online Appendix OA.7.1.

Truncated risk-neutral moments. The second type is the risk-neutral moments of truncated returns,

$$\mathbb{E}_t^*\left[\mathcal{R}_{i,t\to T_1}\,1_{\{R_{i,t\to T_1}\geq k_0\}}\right].$$

To compute these moments, we must choose the threshold return k_0. Lowering k_0 tightens the bound by reducing the resulting upper bound, but it also requires using deeper out-of-the-money options, whose quotes are noisier and less reliable. We therefore set $k_0 = 0.7$, which delivers a tight bound while maintaining sufficient option-quote quality.[13] Given this threshold, the truncated moments can again be computed from option prices, as explained in Online Appendix OA.7.2.

[13] We verify in robustness checks that an alternative threshold of 0.6 or 0.8 yields qualitatively similar results.

Directional-magnitude risk-neutral co-moments. The third type consists of the interaction between powers of returns and their absolute deviations,

$$\mathbb{E}_t^*\left[\mathcal{R}_{M,t\to T_1}^{j_1} \left|\mathcal{R}_{M,t\to T_1}\right|^l\right].$$

These moments capture the joint effects of two different powers of the market return: the raw power j_1, which preserves the sign and thus reflects the directional component of returns, and the absolute power l, which measures the magnitude of deviations irrespective of sign. In this way, they represent interactions between directional return components and volatility-like magnitudes. The computation relies on the spanning formula and can be implemented from the cross-section of option prices, with details provided in Online Appendix OA.7.4.

Other moments. The remaining four types of risk-neutral moments extend the three basic forms. For clarity, we indicate for each moment how it can be represented as a combination of the basic building blocks (marginal, truncated, and absolute-weighted moments), and we point to the corresponding appendix where the exact computational formula is provided.

1. *Central risk-neutral moments of market returns:*

$$\mathbb{E}_t^*\left(\sum_{k=1}^{\mathcal{N}} \underline{\gamma}_{i,k}\left(\mathcal{R}_{M,t\to T_1}^k - \mathbb{E}_t^*\mathcal{R}_{M,t\to T_1}^k\right)\right)^q, \quad \mathcal{N}=2.$$

   This moment is a demeaned polynomial in market returns that can be represented as a combination of the first building block (marginal risk-neutral moments of market returns). The explicit formula is provided in Online Appendix OA.7.5.

2. *Polynomial truncated risk-neutral moments:*

$$\mathbb{E}_t^*\Big[\big(R_{i,t\to T_1} - R_{f,t\to T_1}\big)^j \, 1_{\{R_{i,t\to T_1}\geq k_0\}}\Big] \, .$$

This reduces to a combination of the first building block (marginal moments of individual-stock returns) and the second building block (truncated moments). The exact reduction and implementation are given in Appendix OA.7.6.

3. *Central risk-neutral moments of truncated returns:*

$$\mathbb{E}_t^*\Big(\mathcal{R}_{i,t\to T_1} \, 1_{\{R_{i,t\to T_1}\geq k_0\}} - \mathbb{E}_t^*\Big[\mathcal{R}_{i,t\to T_1} \, 1_{\{R_{i,t\to T_1}\geq k_0\}}\Big]\Big)^q \, .$$

By binomial expansion, this moment can be constructed from the product of a polynomial truncated risk-neutral moment and a power of the second building block (truncated risk-neutral moments), as detailed in Online Appendix OA.7.7.

4. *Forward-looking cross risk-neutral moments:*

$$\mathbb{E}_t^*\big[f_{T_1}^{(j_1,j_2)}\big], \qquad f_{T_1}^{(j_1,j_2)} = \mathcal{R}_{M,t\to T_1}^{j_1} \, \mathbb{E}_{T_1}^*\big[\mathcal{R}_{M,T_1\to T_N}^{j_2}\big] \, .$$

This can be represented as a combination of the first building block (a marginal moment of the market) and the third building block (absolute-weighted higher-order moments). The precise formula and implementation are provided in Online Appendix OA.7.8.

These derived moments can be interpreted as higher-order conditional risk-neutral moments that capture interactions among return powers, truncation, and deviations from either their means or the risk-free rate. Although the notation may appear cumbersome, each moment can be expressed as a combination of the three fundamental moment types, making their computation tractable.

4 Empirical Performance of the Bounds

This section evaluates the empirical performance of the bounds constructed in Section 3. We first examine the properties and predictive power of the bounds without intertemporal hedging (Section 4.1), then incorporate hedging demands (Section 4.2), and finally compare the two approaches (Section 4.3).

4.1 Bounds Without Intertemporal Hedging

4.1.1 Properties of the Bounds

Table 1 reports summary statistics for the lower bound (LB, Eq. 2.10) and upper bound (UB, Eq. 2.12) of annualized conditional expected excess returns implied by Proposition 2.1. Panel A reports the bounds under the constant-parameter specification, $(1/\tau, \rho, \kappa, \xi) = (1, 2, 4, 8)$, while Panel B reports the bounds under the time-varying-parameter specification, denoted by LB* and UB*, in which the preference parameters are updated over time using the forecast-accuracy-based calibration described in Section 3.2.2.[14]

[Insert Table 1 around here]

Panel A shows that the average annualized lower bound rises from 8.3% at the 30-day horizon to 9.4% at the one-year horizon, while the corresponding upper bound ranges from

[14] For brevity, the main text focuses on the forecast-accuracy-based time-varying specification. The variance-risk-premium-based calibration yields similar qualitative patterns and the empirical results are available upon request.

16.5% to 17.4% at shorter horizons and equals 16.4% at the one-year horizon.[15] Standard deviations are sizable at all horizons, and both bounds exhibit positive skewness, indicating heavy right tails. The percentile spreads further underscore the large cross-sectional dispersion. For example, at the 30-day horizon, the 10th–90th percentile range is 2.9% to 15.6% for the lower bound and 3.3% to 44.2% for the upper bound. Overall, the admissible range of expected returns varies considerably across firms.

Panel B shows that the time-varying-parameter specification yields somewhat higher bounds than the constant-parameter specification. Mean lower bounds range from 10.6% to 13.3% across horizons, while mean upper bounds range from 18.3% to 19.8%. This upward shift in the mean bounds is primarily driven by an increase in the risk-aversion parameter $1/\tau$, which implies greater risk aversion and hence higher required premia. Dispersion remains substantial, although skewness is somewhat lower than in Panel A. Overall, allowing for time variation in preferences changes the level of the bounds only modestly while leaving their main distributional features intact.

We begin by testing the tightness of the bounds to assess whether they can serve as unbiased proxies for expected excess returns. We estimate the pooled panel regression

$$\mathcal{R}_{i,t\to T_1} = \beta_0 + \beta_1 B_{i,t\to T_1} + \varepsilon_{i,t\to T_1}, \tag{4.1}$$

where $\mathcal{R}_{i,t\to T_1}$ denotes the realized annualized excess return on stock i from t to T_1, and $B_{i,t\to T_1}$ is the corresponding bound estimate. If a bound is tight, we should find $\beta_0 = 0$ and $\beta_1 = 1$. We run the regression at the 30-, 91-, 182-, and 365-day horizons using monthly data on S&P 500 stocks. Following Chabi-Yo, Dim, and Vilkov (2023), standard errors and

[15] As a comparison, the average annualized realized returns for the corresponding samples range from 14.47% at the 30-day horizon to 15.45% at the 365-day horizon.

p-values are computed by block bootstrap with 10,000 draws to account for both time-series and cross-sectional dependence. Table 2 reports the results for the lower bound, upper bound, and their midpoint. In each panel, the left side uses the constant-parameter specification and the right side uses the time-varying-parameter specification.

[Insert Table 2 around here]

For the lower bound in Panel A, the intercepts are small and statistically indistinguishable from zero at all horizons under both specifications. The slope estimates exceed one under the constant-parameter specification, consistent with the lower bound understating expected excess returns by construction, and are below one under the time-varying-parameter specification. In both cases, however, we generally fail to reject $\beta_1 = 1$, which is the key implication for tightness.[16] Moreover, the Wald tests do not reject the joint null hypothesis that $\beta_0 = 0$ and $\beta_1 = 1$ at any horizon. Taken together, these results provide preliminary evidence that the lower bound is an unbiased proxy for expected excess returns.

Panel B shows weaker results for the upper bound. Although intercepts are typically close to zero, the slope estimates are well below one in most cases, as expected given that the upper bound overstates expected excess returns by construction.[17] The Wald tests reject the joint null at all horizons except 182 days, indicating that the upper bound is not tight in most cases. Panel C shows that the midpoint remains informative. Intercepts are near zero and slope estimates are close to one.[18] Importantly, the joint null is not rejected at most horizons, implying that the midpoint is a reasonably unbiased proxy for expected excess returns.

[16]Under the constant-parameter specification, the p-values for testing $\beta_1 = 1$ are marginal at the 30-day and 182-day horizons, but neither rejects at the 5% level.

[17]The main exceptions are the 30-day intercepts and the 365-day slope estimates.

[18]The main exception is the 30-day horizon, where the slope estimate departs more noticeably from one.

While the upper bound is empirically less tight than the lower bound, it still plays a useful complementary role. First, the UB, together with the LB, delivers an economically meaningful range for expected excess returns rather than a single point estimate, allowing investors to assess both conservative and optimistic scenarios that are consistent with option prices and our preference assumptions. Second, even when the UB is relatively loose, its combination with the LB through the midpoint produces an unbiased proxy for expected returns, while the distance between the two bounds provides a natural summary of the uncertainty surrounding those expectations. Thus, although the UB on its own is not as informative as the LB in our tightness tests, it remains valuable for bracketing expected returns and for interpreting the economic content and precision of our bound-based measures.

We next assess whether the bounds price assets consistently across aggregation levels by examining their pricing coherence between individual stocks and basket-type securities. Following Chabi-Yo, Dim, and Vilkov (2023), we compare the annualized 30-day expected return bounds of nine S&P 500 sector exchange-traded funds (ETFs) with the value-weighted averages of the bounds of their underlying component stocks. For each day, we compute the difference between the ETF-level and value-weighted constituent-level bounds and then take monthly averages of these daily differences. Figure 2 plots the resulting time series of these differences for our lower bound, upper bound, and their midpoint (LUB), alongside the benchmark bounds proposed by Martin and Wagner (2019, MW), Kadan and Tang (2020, KT), and Chabi-Yo, Dim, and Vilkov (2023, GLB). Grey-shaded areas indicate NBER recession periods.

[Insert Figure 2 around here]

Smaller absolute differences (i.e., values closer to zero) indicate greater pricing consistency between individual stocks and sector portfolios. Among all measures, the difference for our lower bound (solid black line) consistently lies closest to zero and remains remarkably stable over time, suggesting that it achieves stronger pricing coherence between individual stocks and ETFs than the MW and KT bounds. The differences for the GLB bound also exhibit strong pricing consistency but occasionally drift away from zero—particularly during recessions—when our LB difference remains stable and near zero. In contrast, the difference for the upper bound tends to deviate from zero to a greater extent, consistent with the earlier evidence in Table 2 that the upper bound is less tight. Overall, these results demonstrate that our lower bound not only provides a tight proxy for expected returns at the firm level but also achieves high pricing coherence between individual securities and market aggregates.

4.1.2 The Bounds and Future Returns

We next study the relation between the bounds and future returns in two ways. First, we examine whether the bounds convey predictive signals about future returns by analyzing the returns to portfolios formed on the bounds. Second, we assess their out-of-sample forecasting performance relative to benchmark models using the modified out-of-sample R^2 measure proposed in the literature.

Table 3 reports portfolio sorts based on the bounds at monthly frequency. At the end of each month, we sort stocks into quintile portfolios using the lower bound (Panel A), the upper bound (Panel B), or their midpoint (Panel C) as proxies for conditional expected excess returns, and compute equal-weighted annualized realized returns over horizons of 30, 91, 182, and 365 days. To examine whether average returns increase monotonically with the corresponding lower/upper bounds across all portfolios, we employ the monotonicity tests proposed by Patton and Timmermann (2010).[19] The resulting p-values are reported in Table 3. Across all specifications, portfolio returns increase monotonically with the bounds, and the high-minus–low spreads are economically large and statistically significant. Panel A shows that sorting on the lower bound yields sizable return differentials. At the 30-day horizon, average annualized returns increase from 9% in the lowest quintile to 19% in the highest, implying a high–minus-low spread of 10%. The upward trend is also statistically significant under the monotonicity test proposed by Patton and Timmermann (2010), confirming a consistent monotonic increase across all quintile portfolios sorted using our bounds. The spread widens with horizon, reaching 15% at the one-year horizon. The results are similar under the constant-parameter and time-varying-parameter specifications. Panels B and C show similar patterns for the upper bound and the midpoint, with high-minus-low spreads ranging from about 10% to 15% across horizons. Overall, the portfolio sorts indicate that the bounds contain strong information about future stock returns and generate economically meaningful investment signals.[20]

[Insert Table 3 around here]

Next, we turn to a more stringent assessment of the bounds' predictive performance using out-of-sample forecast accuracy tests relative to existing benchmark models. Table 4 compares the forecasts implied by the static lower and upper bounds with a wide set of benchmark models at monthly frequency using the modified out-of-sample R^2 statistic, following Goyal and Welch (2008), Martin and Wagner (2019), Martin and Nagel (2022), and Chabi-Yo, Dim, and Vilkov (2023). Specifically, R^2_{OOS} is defined as

[19]The monotonicity test provides a comprehensive assessment of the relation between our measure and expected returns, whereas the conventional t-test is limited to comparing the extreme portfolios (i.e., the high-minus-low spread).

[20]In an untabulated table, we confirm that the long-short portfolio returns formed on our bounds remain significant and cannot be subsumed by the Fama and French (2015) five-factor model.

$$R^2_{\text{OOS}} = 1 - \frac{\sum_i \sum_t (r_{i,t} - \hat{r}_{i,t})^2}{\sum_i \sum_t (r_{i,t} - \hat{r}^B_{i,t})^2}, \tag{4.2}$$

where $r_{i,t}$ denotes the realized excess return of stock i at time t, $\hat{r}_{i,t}$ is the forecast from our bound, and $\hat{r}^B_{i,t}$ is the forecast from a benchmark model. A positive R^2_{OOS} indicates that our bound produces smaller forecast errors than the benchmark. We test the null hypothesis $R^2_{\text{OOS}} \leq 0$ using a stationary block bootstrap with 10,000 replications.

We consider eight benchmarks: (1) $\overline{RX}_{i,t}$, the historical average excess return of stock i since 1990; (2) 6% p.a., a constant 6% annual excess return; (3) $\overline{MKT}_t$, the historical average market excess return; (4) $\overline{IV}_t$, the historical average market-implied variance; (5) $\overline{IV}_{i,t}$, the historical average stock-level implied variance; (6) $MW_{i,t}$, the bound from Martin and Wagner (2019); (7) $KT_{i,t}$, the bound from Kadan and Tang (2020); and (8) $GLB_{i,t}$, the generalized lower bound from Chabi-Yo, Dim, and Vilkov (2023).

[Insert Table 4 around here]

Panel A reports the lower-bound results for the constant-parameter specification. The lower bound improves forecast accuracy relative to nearly all benchmarks. R^2_{OOS} is positive in all cases except the comparison with GLB at the 30-day horizon. The gains are economically meaningful and tend to increase with horizon. Relative to the stock's own historical mean, for example, R^2_{OOS} rises from 1.9% at 30 days to 17.4% at 365 days. The lower bound consistently outperforms simple benchmarks based on constant returns, market-average returns, and implied variance.

The lower bound also compares favorably with the existing option-based measures. Relative to MW, R^2_{OOS} is positive at all horizons and ranges from 2.7% to 9.0%, indicating that our lower bound delivers materially more accurate forecasts. Relative to KT, the gains are also positive at all horizons, though their statistical significance weakens at longer horizons. Compared with GLB, the results are more nuanced. At the 30-day horizon, R^2_{OOS} is slightly negative, but the difference is not statistically significant, suggesting that the two bounds perform similarly. At the remaining horizons, however, R^2_{OOS} is positive and statistically significant, indicating that our lower bound improves forecast accuracy relative to GLB beyond the shortest horizon. These performance gains likely reflect the greater flexibility of our framework, which dispenses with auxiliary assumptions imposed in earlier studies, including log utility (Martin and Wagner, 2019), first-order approximations of marginal utility (Kadan and Tang, 2020), and the use of realized betas for calibration (Chabi-Yo, Dim, and Vilkov, 2023).

Panel B reports the corresponding results for the upper bound. Its forecasting performance is weaker than that of the lower bound, but the overall pattern remains favorable. R^2_{OOS} is positive in 25 of the 32 benchmark-horizon comparisons, indicating that the upper bound still improves forecast accuracy relative to existing predictors in the large majority of cases. The gains become stronger with horizon: at the 182- and 365-day horizons, the upper bound delivers positive R^2_{OOS} against all eight benchmarks. Relative to MW and KT, the upper bound delivers positive R^2_{OOS} at all horizons. Relative to GLB, the upper bound performs similarly at short horizons, where R^2_{OOS} is negative but statistically insignificant, while R^2_{OOS} becomes positive at the 182- and 365-day horizons.

Taken together, Table 4 shows that the lower bound delivers the strongest and most robust forecasting gains, while the upper bound also improves on existing benchmarks in most cases, particularly at medium and long horizons. Additional results for the time-varying-parameter specification and for the midpoint, reported in Online Appendix Table OA.4, show that allowing for time-varying parameters strengthens the lower-bound performance, while the midpoint results closely track the lower-bound pattern.

4.2 Bounds With Intertemporal Hedging

4.2.1 Properties of the Bounds

We now turn to the multi-period setting and incorporate intertemporal hedging demands. To distinguish the resulting bounds from the static bounds, we refer to them as hedging bounds. Unlike the one-period setting, where only the forecast horizon T_1 matters, the multi-period setting introduces an investment horizon T_N over which investors maximize utility. We consider forecast horizons $T_1 \in \{30, 91, 182, 365 \text{ days}\}$ and investment horizons $T_N \in \{91, 182, 365, 547, 730 \text{ days}\}$, focusing on cases with $T_N > T_1$, since $T_N = T_1$ collapses to the one-period setting. Table 5 reports summary statistics for the hedging bounds. Panel A reports the hedging lower bound (HLB) and Panel B the hedging upper bound (HUB), each under both the constant-parameter and forecast-accuracy-based time-varying-parameter specifications.

Panel A shows that incorporating hedging raises the lower bounds, with the effect becoming more pronounced as the investment horizon lengthens. For example, at the 30-day forecast horizon, the mean HLB rises from 9% when $T_N = 91$ days to 15% when $T_N = 730$ days, compared with 8% in the static one-period setting in Table 1. To quantify the contribution of hedging, we compute the share of the HLB attributable to intertemporal hedging by subtracting the static lower bound from HLB and scaling the difference by HLB, i.e., $(\text{HLB} - \text{LB})/\text{HLB}$. This share rises with T_N, from 6% at $T_N = 91$ days to 47% at $T_N = 730$ days. Similar patterns hold at longer forecast horizons. Under the time-varying-parameter specification, the hedging lower bound also exceeds its static counterpart, but the increase with T_N is more muted. For instance, at the 30-day forecast horizon, the mean HLB* rises only from 11% when $T_N = 91$ days to 12% when $T_N = 730$ days, while the corresponding hedging share increases from 13% to 26%.

Panel B shows a similar pattern for the upper bound. Incorporating hedging raises HUB relative to the static upper bound, and the hedging share, (HUB − UB)/HUB, increases with the investment horizon. At the 30-day forecast horizon, for example, the mean HUB rises from 17% to 25% as T_N increases from 91 to 730 days, while the corresponding hedging share rises from 7% to 47%. The same qualitative pattern holds under the time-varying-parameter specification, although the magnitude is smaller.

[Insert Table 5 around here]

Figure 3 illustrates the effect of intertemporal hedging for representative investment horizons of $T_N = 365$ and 730 days. Two patterns emerge clearly. First, for a given forecast horizon T_1, both the mean bounds and the hedging share ratios increase with T_N. Second, for a given investment horizon T_N, both the mean bounds and the corresponding hedging share decline as T_1 increases. Together, these results indicate that intertemporal hedging plays a more prominent role when the gap between the forecast and investment horizons is larger, underscoring the economic importance of hedging motives in shaping expected returns. Additional time-series evidence on the hedging contribution is reported in the Online Appendix (Figure OA.4), showing pronounced time variation: hedging shares rise sharply during recessions—most notably around the 2008 global financial crisis.

[Insert Figure 3 around here]

The positive contribution of intertemporal hedging to expected returns reflects the underlying preference configuration. In our theoretical framework, the bounds are governed by the four preference parameters $(1/\tau, \rho, \kappa, \xi)$, and Eq.(2.8) specifies a set of inequality restrictions on these parameters that define economically admissible configurations. Our calibration choices satisfy these restrictions and, under such configurations, the intertemporal hedging component is positive, so that hedging raises the expected excess return on individual stocks. By contrast, if the signs of all preference parameters in Eq.(2.8) except $\frac{1}{\tau}$ were reversed, the sign of the hedging component would flip, and intertemporal hedging would lower rather than raise expected excess returns.[21] Chabi-Yo, Gourier, and Langlois (2025) provide an extensive analysis of this mechanism at the market level, showing that the link between intertemporal hedging and the expected market excess return is governed by the investor's utility specification. In the same spirit, we do not impose a particular functional form on preferences; instead, we work with economically reasonable calibrations that determine the sign and magnitude of intertemporal hedging effects on individual expected excess returns. Thus, the increasing effect of hedging on expected excess returns reflects preference configurations that place greater weight on adverse future states in a way that is both theoretically admissible and consistent with empirically plausible parameter values.

We next examine the tightness of the hedging bounds using the regression specification in Eq. (4.1). For each forecast horizon T_1, we report results for the investment horizon T_N that yields the best fit, defined as having the slope coefficient closest to one.[22] Panel A of Table 6 reports the results for the hedging lower bound. Across all forecast horizons, the intercepts are statistically indistinguishable from zero, and the slope estimates are close to one. Notably, the hedging lower bound yields slope estimates that are substantially closer to one than those of the corresponding static lower bound. Consistent with this pattern, the

[21]For illustration, in Section 5.1, we apply our methodology to derive an exact option-based expression for expected excess returns under CRRA utility, both with and without intertemporal hedging. Under CRRA, intertemporal hedging reduces expected excess returns on individual stocks when risk aversion exceeds one and increases them when risk aversion is below one.

[22]Results for other forecast–investment horizon combinations are qualitatively similar and are available upon request.

Wald tests do not reject the joint null hypothesis that $\beta_0 = 0$ and $\beta_1 = 1$ at any horizon. These results indicate that the hedging lower bound remains tight and provides a closer proxy for conditional expected excess returns than its static counterpart.

[Insert Table 6 around here]

Panel B reports the results for the hedging upper bound. The intercepts are again close to zero, while the slope estimates are below one, especially at short and medium horizons. Accordingly, the Wald tests reject the joint null at most horizons under both the constant-parameter and time-varying-parameter specifications. Overall, these results indicate that the hedging upper bound is not as tight a proxy for conditional expected excess returns as the hedging lower bound. Panel C considers the midpoint of the hedging lower and upper bounds. The intercepts are close to zero across horizons, and the slope estimates move closer to one as the forecast horizon lengthens. The joint null is rejected at the 30-day horizon under both specifications, but is not rejected at longer horizons. Thus, as in the static case, the midpoint remains informative, although it exhibits slightly weaker tightness than the lower bound at the shortest horizon.

We also examine whether the hedging bounds remain consistent across levels of aggregation, focusing on the relation between individual stocks and sector ETFs. Using the same ETF–component comparison framework as in Figure 2, we compute the daily differences between the annualized 30-day expected return bounds of the nine S&P 500 sector ETFs and the value-weighted average bounds of their constituent stocks, and then average these differences at the monthly frequency. Figure 4 plots the resulting time series for the hedging lower and upper bounds and their midpoint (HLUB), together with their static counterparts, for the case with investment horizon $T_N = 365$ days.

[Insert Figure 4 around here]

Figure 4 shows that the HLB series closely tracks its static counterpart and is often even closer to zero, indicating slightly improved pricing coherence between ETF-level and component-level bounds.[23] Occasionally, however, the HLB series dips below zero, most notably during recessionary periods, suggesting that intertemporal hedging can temporarily weaken pricing alignment when market uncertainty intensifies. The HUB series nearly overlaps with its static counterpart, implying that the incorporation of hedging has little effect on pricing consistency at the upper end. Overall, the evidence suggests that incorporating intertemporal hedging preserves the ability of the bounds to price individual stocks and aggregated sector portfolios in a coherent way.

4.2.2 The Bounds and Future Returns

This subsection investigates how incorporating intertemporal hedging affects the predictive performance of the bounds. Parallel to Section 4.1.2, we evaluate whether the hedging bounds contain information about future returns and how their predictive content compares with that of benchmark models at monthly frequency. We first examine portfolio returns sorted on the hedging bounds and then evaluate their out-of-sample forecasting accuracy relative to alternative expected-return measures. This parallel design facilitates comparison with the static one-period framework.

Table 7 reports portfolio returns formed on the hedging lower bound (Panel A) and hedging upper bound (Panel B). Each month, stocks are sorted into quintiles based on the respective bound, and we report the annualized realized returns of the lowest and highest

[23] In particular, the average absolute deviation of HLB between ETF-level and component-level bounds is 0.0101, while the corresponding average absolute deviation of LB is 0.0184.

quintiles as well as the high–minus-low spread. The exercise is conducted across forecast horizons $T_1 \in \{30, 91, 182, 365 \text{ days}\}$ and investment horizons $T_N \in \{91, 182, 365, 547, 730 \text{ days}\}$, considering all cases with $T_N > T_1$. Across all specifications, portfolio returns increase monotonically with the hedging bounds, and the high–minus-low spreads are economically meaningful and statistically significant for all quintile portfolios. Thus, incorporating intertemporal hedging preserves the strong predictive content of the bounds.

[Insert Table 7 around here]

Two patterns stand out. First, for a given forecast horizon T_1, the high–minus-low spread tends to decline as the investment horizon T_N lengthens, with the decline most pronounced at short forecast horizons. For example, in Panel A, when $T_1 = 30$ days, the spread decreases from 9.7% at $T_N = 91$ days to 8.5% at $T_N = 730$ days. Second, for a given investment horizon T_N, the spread tends to increase with the forecast horizon T_1. For example, in Panel A with $T_N = 730$ days, the spread rises from 8.5% at $T_1 = 30$ days to 15.2% at $T_1 = 365$ days. Panel B shows a similar pattern for the hedging upper bound, with spreads ranging between 8% and 15% across horizon combinations. Overall, both HLB and HUB contain substantial predictive information for future stock returns and generate economically meaningful investment signals.[24]

We next compare the out-of-sample forecasting performance of the hedging bounds with leading benchmarks using the R^2_{OOS} measure in Eq.(4.2). To conserve space, Table 8 reports results only for the investment horizons $T_N = 365$ and 730 days.[25] Panel A reports the results for the hedging lower bound under the constant-parameter specification. The forecasting

[24]The results are similar when portfolios are formed on the midpoint of HLB and HUB; see Online Appendix Table OA.6. In an untabulated table, we also confirm that the long-short portfolio returns formed on our bounds remain significant and cannot be subsumed by the Fama-French five-factor model.

[25]Results for other investment horizons are similar and available upon request.

gains are strong overall. Out of the 31 comparisons,[26] R^2_{OOS} is positive in 28 cases, and in 24 of those cases the positive value is statistically significant at the 10% level. The gains also tend to increase with the forecast horizon for a given T_N. For example, when $T_N = 365$ days, R^2_{OOS} relative to MW rises from 3% at $T_1 = 30$ days to 10% at $T_1 = 365$ days. Relative to LB, the hedging lower bound also delivers positive incremental gains in most cases.[27] Although these gains are modest in magnitude, ranging from 0.4% to 1.9%, they remain statistically significant at conventional levels. Thus, the hedging lower bound improves forecast accuracy relative to both the nested static bound and the other static benchmarks.

[Insert Table 8 around here]

Panel B reports the corresponding results for the hedging upper bound. Its forecasting performance is noticeably weaker than that of the hedging lower bound. Positive gains remain relative to MW, especially at longer forecast horizons, but the values of R^2_{OOS} relative to GLB and UB are often negative, particularly when $T_N = 730$ days. Thus, unlike the hedging lower bound, the hedging upper bound does not deliver uniformly positive forecasting gains relative to existing benchmarks. Additional results for the time-varying-parameter specification and for the midpoint yield similar conclusions and are relegated to Online Appendix Table OA.7. In brief, the hedging lower bound delivers the strongest and most robust forecasting gains, while those from the hedging upper bound are weaker.

[26] Across the four benchmark models (MW, KT, GLB, and our static lower/upper bounds) and four forecast horizons ($T_1 = 30, 91, 182, 365$ days), this yields 32 cases; since the multi-period hedging bounds collapse to the one-period static bounds when $T_1 = T_N$, we exclude the $T_1 = T_N = 365$ case for the static lower and upper bounds, leaving 31 comparisons. Results for other investment horizons are similar and available upon request.

[27] The main exceptions occur when $T_N = 730$ days, where R^2_{OOS} relative to LB is negative at $T_1 = 30$ and 91 days, but neither difference is statistically significant.

4.3 Comparison of Bounds With and Without Hedging

4.3.1 Prevalence and Cross-Sectional Properties of Hedging Contributions

To assess whether hedging is merely a marginal adjustment or an important component of expected return formation, this subsection examines the prevalence and magnitude of intertemporal hedging effects in the pooled firm-month sample. The previous subsection shows that incorporating hedging raises the level of the bounds on average, but that evidence does not reveal whether the effect is limited to a small subset of observations or pervasive in the pooled sample. To address this, we compute, for each firm-month observation, the share of the hedging bound attributable to intertemporal hedging and examine its distribution in the pooled sample.

For each forecast horizon $T_1 \in \{30, 91, 182, 365\}$ (rows) and investment horizon $T_N \in \{91, 182, 365, 547, 730\}$ (column blocks), Table 9 classifies firm-month observations by the hedging share, measured as (HLB − LB)/HLB for the lower bound and (HUB − UB)/HUB for the upper bound. The distribution is reported across five ranges: $[0\%, 20\%)$, $[20\%, 40\%)$, $[40\%, 60\%)$, $[60\%, 80\%)$, and $[80\%, 100\%]$. A clear pattern emerges: for a given forecast horizon T_1, the distribution shifts toward higher ranges as T_N lengthens. For the hedging lower bound, this shift is economically large. When $T_1 = 30$ days and $T_N = 91$ days, almost all firm-month observations fall in the $[0\%, 20\%)$ range (99.6%). When $T_N = 365$ days, only 19% of firms remain in the lowest range, while most move to $[20\%, 40\%)$ (68%). By $T_N = 730$ days, the mass shifts further upward: only 4% remain in $[0\%, 20\%)$, while 21%, 60%, and 15% fall in $[20\%, 40\%)$, $[40\%, 60\%)$, and $[60\%, 80\%)$, respectively.

[Insert Table 9 around here]

The qualitative pattern for the hedging upper bound is similar but more muted. For a given T_1, increasing T_N shifts observations out of the $[0\%, 20\%)$ range, but less pronounced than for the lower bound. For example, when $T_1 = 30$ and $T_N = 730$, 18% of observations remain in the lowest range for HUB, compared with 4% for HLB; when $T_1 = 91$ and $T_N = 730$, the gap is even more pronounced, with 30% versus 2%. This asymmetry suggests that the lower bound is more responsive to intertemporal hedging components than the upper bound, consistent with the broader evidence that the lower bound tends to be more informative empirically.

The similar broad pattern appears at longer forecast horizons. The greater the gap between T_N and T_1, the larger the fraction of the bound attributable to hedging. This is consistent with the notion that intertemporal hedging motives matter most when investors care about future changes in investment opportunities over horizons that extend beyond the forecasting window. For short forecast horizons paired with long investment horizons, hedging accounts for a nontrivial share of the bounds, with the distribution shifting well beyond the lowest $[0\%, 20\%)$ range. Overall, Table 9 shows that hedging is not a marginal adjustment confined to a small subset of firm-month observations. Rather, it makes a quantitatively important contribution to the bounds for a large fraction of observations, especially when the investment horizon substantially exceeds the forecast horizon.

To further characterize the cross-sectional properties of these hedging contributions, Online Appendix extends the analysis in two directions. First, portfolio sorts and Fama–MacBeth regressions show that the hedging bounds preserve standard cross-sectional patterns in expected returns, while the hedging share exhibits systematic heterogeneity across firm characteristics: it tends to be smaller for firms with greater market and idiosyncratic risk exposures and larger for firms with stronger profitability and recent performance (see Online Appendix OA.8). Second, relating hedging contributions to Campbell et al. (2018)'s news betas reveals that discount-rate news betas explain the largest share of the cross-sectional variation in hedging contributions, followed by volatility-news betas, with cash-flow betas accounting for a relatively small fraction. Although hedging contributions are significantly related to cash-flow, discount-rate, and volatility news betas, they jointly explain only a small portion of the overall variation, suggesting that our forward-looking bounds capture additional dimensions of intertemporal risk beyond the conventional news decomposition (see Online Appendix OA.9).

Motivated by the possibility that hedging demands vary systematically across sectors, we examine industry-level intertemporal hedging components using the Fama–French 12-industry classification (untabulated). Cross-industry dispersion is limited for the lower bound, while the upper bound shows somewhat greater variation. Industries with relatively higher average hedging shares include Consumer Nondurables, Chemicals, and Utilities. Overall, however, average hedging shares are broadly similar across industries, suggesting that the prevalence of intertemporal hedging documented above is not driven by a small set of sectors.

4.3.2 Decomposition of Hedging Contributions

This subsection decomposes the incremental effect of intertemporal hedging into its underlying moment components to identify which aspects of the conditional return distribution drive the difference between the hedging and non-hedging bounds. Unlike the one-period static bounds, the hedging bounds incorporate additional components that reflect investors' concern about future changes in investment opportunities. In particular, the term $\mathcal{M}^{*(j,k-j)}_{i,M,t} = \mathbb{E}^*_t \left[\mathcal{R}_{i,t\to T_1} f^{(j,k-j)}_{T_1}\right]$ contains the factor $f^{(j,k-j)}_{T_1} = \mathcal{R}^{j}_{M,t\to T_1}\, \mathbb{E}^*_{T_1} \mathcal{R}^{k-j}_{M,T_1\to T_N}$, which captures higher-order interactions between contemporaneous and future market returns. The expectation $\mathbb{E}^*_{T_1}\mathcal{R}^{k-j}_{M,T_1\to T_N}$ represents the *forward moments of future market returns*, linking the current pricing kernel to the evolution of market risk beyond the forecast horizon. These forward moments embed the intertemporal hedging channel that distinguishes the multi-period framework from its static counterpart. We classify the terms in the hedging bounds by the order of the forward moments $(k-j)$ and aggregate all terms sharing the same value of $k-j$. The resulting components are interpreted according to the order of the forward moments: when $k-j=2$, the aggregated terms are associated with the future second moment of market returns (*variance-related component*); when $k-j=3$, with the future third moment (*skewness-related component*); and when $k-j=4$, with the future fourth moment (*kurtosis-related component*). We quantify the contribution of variance-, skewness-, and kurtosis-related terms to the total hedging effect.

To illustrate the decomposition, we start from the numerator of the hedging lower bound, denoted as $\mathrm{HLB}_{\mathrm{num}}$. For the fourth-order approximation ($\mathcal{K}=4$) based on the formulation in Eq.(2.40), $\mathrm{HLB}_{\mathrm{num}}$ can be expressed as

$$\mathrm{HLB}_{\mathrm{num}} = \sum_{k=1}^{4}\sum_{j=0}^{k} \frac{a_{j,k-j}}{R^j_{f,t\to T_1}\,R^{k-j}_{f,T_1\to T_N}}\,\mathcal{M}^{*(j,k-j)}_{i,M,t}.$$

We group terms with the same value of $k-j$ (denoted as m), and rewrite it as

$$\mathrm{HLB}_{\mathrm{num}} = \sum_{m=0}^{4}\ \sum_{j=\max\{0,\,1-m\}}^{4-m} \frac{a_{j,m}}{R^j_{f,t\to T_1}\,R^{m}_{f,T_1\to T_N}}\,\mathcal{M}^{*(j,m)}_{i,M,t}.$$

This reformulation allows us to isolate the contribution of each m term and connect it to its economic interpretation:

- When $m=0$, the inner summation coincides exactly with the numerator of the one-period lower bound in Eq.(2.10), denoted as LB_{num}; that is,

$$\sum_{j=1}^{4} \frac{a_{j,0}}{R^{j}_{f,t\to T_1}} \mathcal{M}^{*(j,0)}_{i,M,t} = \text{LB}_{\text{num}}.$$

- When $m = 1$, $\mathcal{M}^{*(j,1)}_{i,M,t} = 0$ by construction, so this term vanishes.
- When $m = 2, 3, 4$, the remaining terms correspond to components associated with the second-, third-, and fourth-order conditional moments of future market returns—namely, variance-, skewness-, and kurtosis-related components—in the intertemporal hedging effect.

Accordingly, the numerator of the hedging lower bound can be expressed as

$$\text{HLB}_{\text{num}} = \text{LB}_{\text{num}} + \underbrace{\sum_{j=0}^{2} \frac{a_{j,2}}{R^{j}_{f,t\to T_1} R^{2}_{f,T_1\to T_N}} \mathcal{M}^{*(j,2)}_{i,M,t}}_{m=2} + \underbrace{\sum_{j=0}^{1} \frac{a_{j,3}}{R^{j}_{f,t\to T_1} R^{3}_{f,T_1\to T_N}} \mathcal{M}^{*(j,3)}_{i,M,t}}_{m=3} + \underbrace{\frac{a_{0,4}}{R^{4}_{f,T_1\to T_N}} \mathcal{M}^{*(0,4)}_{i,M,t}}_{m=4} .$$

Hence, the incremental contribution of intertemporal hedging relative to the static bound can be decomposed as

$$\text{HLB}_{\text{num}} - \text{LB}_{\text{num}} = \underbrace{\text{Variance}}_{m=2} + \underbrace{\text{Skewness}}_{m=3} + \underbrace{\text{Kurtosis}}_{m=4}.$$

and the proportion of each moment-related component in the hedging effect is given by

$$\text{Variance share} = \frac{\text{Variance}}{\text{HLB}_{\text{num}} - \text{LB}_{\text{num}}},$$
$$\text{Skewness share} = \frac{\text{Skewness}}{\text{HLB}_{\text{num}} - \text{LB}_{\text{num}}},$$
$$\text{Kurtosis share} = \frac{\text{Kurtosis}}{\text{HLB}_{\text{num}} - \text{LB}_{\text{num}}}.$$

The same decomposition logic applies to the hedging upper bound, where the corresponding numerator is partitioned into the numerator of the static upper bound and the variance-, skewness-, and kurtosis-related terms in an analogous manner.

Table 10 reports the decomposition results across forecast and investment horizons. Two patterns stand out. First, variance and skewness account for most of the hedging contributions, while kurtosis plays a smaller role.[28] For the lower bound, variance explains about 34–51% and skewness 36–45%, leaving 9–29% for kurtosis. For the upper bound, the corresponding ranges are 42–59%, 27–41%, and 8–27%, respectively. Second, holding T_N fixed, a longer T_1 reduces the variance share and increases the kurtosis share. For example, for the lower bound at $T_N = 730$ days, the variance share falls from 50% to 35%, while the kurtosis share rises from 9% to 28% as T_1 increases from 30 to 365 days. This pattern suggests that as forecast horizons lengthen, the role of variance in the hedging contribution diminishes, whereas the importance of tail risk captured by kurtosis increases.

[Insert Table 10 around here]

Figure 5 illustrates these patterns by fixing the investment horizon at two representative longer values, $T_N = 365$ and 730 days, and varying the forecast horizon T_1. For each fixed

[28]The prominent role of variance-related terms is consistent with evidence that variance-related quantities contain information about risk compensation (Carr and Wu, 2009; Hu, Jacobs, and Seo, 2022).

T_N, the figure plots the average shares of the hedging contribution attributable to variance, skewness, and kurtosis across different values of T_1. The left panels report the lower-bound results, and the right panels the upper-bound results. For both bounds, the trade-off between variance and kurtosis is clear: as T_1 increases, the variance share declines while the kurtosis share rises. The skewness share also tends to decrease with longer forecast horizons, although the pattern is less monotonic across intermediate horizons. Additional time-series evidence is reported in Online Appendix Figure OA.6, which plots the cross-sectional average variance, skewness, and kurtosis shares over time. The same broad pattern emerges: variance and skewness remain the primary drivers of the hedging contribution, while kurtosis becomes relatively more important as T_1 lengthens. As a robustness check, we also compute moment shares using the hedging bound itself (HLB or HUB) as the denominator, rather than the incremental hedging effect (HLB−LB or HUB−UB), and obtain similar results (see Online Appendix Figures OA.7–OA.8 and Table OA.9).

[Insert Figure 5 around here]

5 Preference Restrictions and SDF Implications

This section examines the economic implications of the preference restrictions and the implied stochastic discount factor. We first use the CRRA benchmark to assess how a global utility specification shapes the sign and magnitude of intertemporal hedging. We then examine the implied SDF as a diagnostic of the model's economic implications, focusing on whether it exhibits the non-monotonicity documented in the pricing-kernel literature.

5.1 CRRA Utility as a Restricted Benchmark

Our bounds do not impose a global parametric utility specification. Preferences enter through utility-derivative ratios evaluated locally at the expansion point. CRRA utility provides a useful restricted benchmark for assessing how a global utility specification affects the sign and magnitude of intertemporal hedging.

We derive the CRRA-implied expected-return proxy first without and then with intertemporal hedging. Without intertemporal hedging, the CRRA restriction pins down the inverse SDF as

$$\frac{\mathbb{E}_t m_{t\to T_1}}{m_{t\to T_1}} = \frac{R^{\alpha}_{M,t\to T_1}}{\mathbb{E}^*_t\big(R^{\alpha}_{M,t\to T_1}\big)}. \tag{5.1}$$

This restriction is stronger than our baseline framework. Under CRRA, a single risk-aversion coefficient α determines both the global utility function and the local higher-order preference measures. Specifically, the measures in (2.4) satisfy

$$\frac{1}{\tau_t} = \alpha, \qquad \rho_t = \frac{\alpha+1}{2\alpha}, \qquad \kappa_t = \frac{(\alpha+1)(\alpha+2)}{6\alpha^2}, \qquad \xi_t = \frac{(\alpha+1)(\alpha+2)(\alpha+3)}{24\alpha^3}.$$

By contrast, our baseline framework uses local preference measures evaluated at the risk-free benchmark and remains agnostic about preferences at other wealth levels.

The CRRA restriction also affects the sign of higher-order risk-premium components. In the one-period case, the expected market excess return can be written as

$$\mathbb{E}_t \mathcal{R}_{M,t\to T_1} = \sum_{j=1}^{\infty} \frac{a_{j,t}}{R^j_{f,t\to T_1}\mathbb{E}^*_t \upsilon_{t\to T_1}} \mathbb{E}^*_t \mathcal{R}^{j+1}_{M,t\to T_1}.$$

Under CRRA utility, the expansion coefficients are

$$a_{1,t} = \alpha,\ a_{2,t} = \frac{\alpha\left(\alpha-1\right)}{2},\ a_{3,t} = \frac{\alpha\left(\alpha-1\right)\left(\alpha-2\right)}{6},\ a_{4,t} = \frac{\alpha\left(\alpha-1\right)\left(\alpha-2\right)\left(\alpha-3\right)}{24},\ldots.$$

When the risk-neutral third moment is negative, as is empirically typical, $a_{2,t} > 0$ for $\alpha > 1$ implies that negative market skewness lowers the expected market excess return. Similarly, for $1 < \alpha < 2$, $a_{3,t} < 0$ implies that the fourth risk-neutral moment lowers the expected market excess return. These sign patterns can conflict with the risk-premium restrictions in (2.7) and (2.8); related concerns about the implications of standard utility restrictions for higher-order risk pricing are discussed in Chabi-Yo, Leisen, and Renault (2014) and Chabi-Yo and Loudis (2020).

The same one-period SDF delivers the following CRRA-implied expected-return proxy:

$$\mathbb{E}_t(R_{j,t\to T_1} - R_{f,t\to T_1}) = \frac{\sum_{i=0}^{\alpha} b_{i,0,t}^{\alpha}\,\mathcal{M}_{j,M,t}^{*\,(i,0)}}{\sum_{i=0}^{\alpha} b_{i,0,t}^{\alpha}\,\mathbb{E}_t^*\left[f_{T_1}^{(i,0)}\right]}. \tag{5.2}$$

With intertemporal hedging, marginal utility depends on wealth at the investment horizon T_N. For CRRA utility,

$$u'(W_t R_{M,t\to T_1} R_{M,T_1\to T_N}) \propto W_t^{-\alpha}\left(R_{M,t\to T_1} R_{M,T_1\to T_N}\right)^{-\alpha}.$$

The inverse SDF from t to T_1 becomes

$$\frac{\mathbb{E}_t m_{t\to T_1}}{m_{t\to T_1}} = \frac{\mathbb{E}_{T_1}^*\left[R_{M,t\to T_1}^{\alpha} R_{M,T_1\to T_N}^{\alpha}\right]}{\mathbb{E}_t^*\left[\mathbb{E}_{T_1}^*\left[R_{M,t\to T_1}^{\alpha} R_{M,T_1\to T_N}^{\alpha}\right]\right]}. \tag{5.3}$$

For integer $\alpha > 1$, the binomial expansion gives the option-based expression

$$\mathbb{E}_t(R_{j,t\to T_1} - R_{f,t\to T_1}) = \frac{\sum_{i=0}^{\alpha}\sum_{k=0}^{\alpha} b_{i,k,t}^{\alpha}\, \mathcal{M}_{j,M,t}^{*\,(i,k)}}{\sum_{i=0}^{\alpha}\sum_{k=0}^{\alpha} b_{i,k,t}^{\alpha}\, \mathbb{E}_t^{*}\left[f_{T_1}^{(i,k)}\right]}, \tag{5.4}$$

where

$$b_{i,k,t}^{\alpha} = \frac{\alpha!}{(\alpha-i)!i!}\frac{\alpha!}{(\alpha-k)!k!} R_{f,t\to T_1}^{\alpha-i} R_{f,T_1\to T_N}^{\alpha-k}.$$

Unlike our baseline approach, CRRA delivers a point estimate rather than bounds because the global utility form pins down the SDF. Comparing (5.4) with (5.2) isolates the contribution of intertemporal hedging under the CRRA restriction.

[Insert Figure 6 around here]

Figure 6 illustrates the CRRA-implied expected returns for Apple and JP Morgan when $\alpha = 3$. In contrast to our baseline estimates, incorporating intertemporal hedging under CRRA lowers the implied expected return. The hedged expected return lies below its one-period counterpart, with the gap widening during periods of elevated risk premia.

Additional results in the Online Appendix show that this pattern is robust. Figures OA.10–OA.11 report similar time series for $\alpha = 4$ and $\alpha = 5$. Table OA.13 extends the analysis to the full cross-section of S&P 500 firms and shows that the hedging component is negative in most firm-month observations across a broad set of (T_1, T_N) combinations. We also revisit the pricing-consistency exercise under CRRA. Figures OA.12–OA.14 compare ETF-level CRRA-implied expected returns with the value-weighted averages of constituent-level expected returns for the nine S&P 500 sector ETFs. A pricing-consistent proxy should generate differences close to zero. On the contrary, the CRRA-implied proxy displays larger and more persistent deviations, especially during stress episodes, than our bounds based on calibrated utility-derivative ratios.[29]

Overall, the CRRA evidence highlights that the sign and magnitude of intertemporal hedging effects depend critically on preference restrictions. Under CRRA, the hedging component acts as an offset to expected returns; in our baseline framework, economically motivated sign restrictions and calibrated local preference parameters allow intertemporal hedging to raise stock-level expected excess returns.

5.2 The Economic Behavior of the Implied SDF

Explaining the pricing-kernel puzzle is not the objective of this paper. Nevertheless, because our framework uses option prices to infer stock-level expected excess returns, the behavior of the implied SDF provides a useful diagnostic for the economic implications of the model. We therefore ask whether the implied SDF displays the non-monotonicity documented in the pricing-kernel literature.[30]

A related literature argues that the pricing-kernel puzzle can arise from an information-set mismatch rather than from a fundamental failure of standard asset pricing models. In particular, Linn, Shive, and Shumway (2018) and Barone-Adesi et al. (2020) show that apparent non-monotonicity may arise when the physical distribution is estimated from backward-looking historical returns while the risk-neutral distribution is inferred from forward-looking option prices. Our implementation avoids this mismatch: the objects entering the SDF and the expected-return measures are constructed from option-implied quantities, without

[29]In an untabulated analysis, we also examine tests of tightness and out-of-sample forecast accuracy. The results show that CRRA-implied expected returns consistently underperform relative to the bounds derived from our calibrated local preference parameters.

[30]Seminal evidence on the pricing-kernel puzzle includes Aït-Sahalia and Lo (2000), Jackwerth (2000), and Rosenberg and Engle (2002). Subsequent work documents its empirical relevance and related interpretations in a variety of settings; see, among others, Chabi-Yo, Garcia, and Renault (2008), Bakshi, Madan, and Panayotov (2010), Chabi-Yo (2012), Brown and Jackwerth (2012), Christoffersen, Heston, and Jacobs (2013), and Sichert (2018).

estimating the physical distribution from historical returns.

Another strand of work emphasizes that the SDF may depend on forces beyond contemporaneous market returns. Chabi-Yo (2012) and Christoffersen, Heston, and Jacobs (2013) show that when volatility enters the SDF, the pricing kernel can be monotone in each state variable—decreasing in the market return and increasing in volatility—even though its projection onto the market return alone appears non-monotone. Schreindorfer and Sichert (2025) document that the projected pricing kernel varies with volatility, becoming steeper for negative market returns in low-volatility states and flatter in high-volatility states. In a related but distinct mechanism, Almeida and Freire (2026) show that option-market demand helps shape the pricing kernel: net selling by public investors, which exposes them to variance risk, is associated with a U-shaped pricing kernel. Although our mechanism operates through intertemporal hedging rather than option-demand imbalances, both channels point to the pricing of option-implied risks as an important determinant of the SDF's projected shape. These insights are directly relevant to our setting, because intertemporal hedging introduces exposure to future investment opportunities, summarized by option-implied moments of future market returns.

[Insert Figure 7 around here]

Motivated by these observations, we examine the implied SDF as a function of realized market excess returns. Figure 7 plots the normalized SDF with and without intertemporal hedging. Each subpanel reports a different combination of the forecast horizon T_1 and the investment horizon T_N. The non-hedging SDF, shown in blue, is monotonically decreasing in market excess returns and therefore does not display the pricing-kernel puzzle. By contrast, the hedging SDF, shown in orange, is non-monotonic: it declines over low-to-moderate market returns but rises again at high market returns. This non-monotonicity is visible across the (T_1, T_N) combinations and resembles the puzzling shape documented in the pricing-kernel literature. It is consistent with the additional state dependence introduced by intertemporal hedging: the SDF loads not only on contemporaneous market returns but also on future risk-neutral moments of market returns, including variance, skewness, and kurtosis. The evidence therefore supports the view that, when the SDF depends on additional state variables, its lower-dimensional projection onto market returns can appear non-monotonic even if the underlying SDF is economically well behaved. In our framework, the pricing of future option-implied risks through intertemporal hedging provides precisely such a channel.

Figure 7 is based on the default preference parameters used in our baseline implementation. In the Online Appendix, we report analogous figures based on time-varying preference parameters calibrated either by out-of-sample maximization of the midpoint of the hedging bounds or to match the variance risk premium (Figures OA.15 and OA.16). The resulting SDF displays greater dispersion, reflecting time variation in the calibrated preference parameters, but the qualitative conclusion is unchanged: the non-hedging SDF remains broadly decreasing in market excess returns, whereas the hedging SDF exhibits a pronounced non-monotonic projection. Thus, the SDF implication documented here is not driven by the default preference calibration.

6 Conclusion

This paper develops a framework for bounding the conditional expected excess returns of individual stocks in a dynamic multi-period economy. By nesting the one-period benchmark within a richer setting that allows for portfolio rebalancing, we show how intertemporal hedging considerations alter the stochastic discount factor and thereby shape stock-level risk premia. The resulting lower and upper bounds are expressed in terms of higher-order risk-neutral cross-moments between the market and individual stocks, quantities that can be recovered from option prices and implemented without reliance on realized returns.

Empirically, our results show that the proposed bounds are tight, strongly related to future returns, and generate economically large and statistically significant investment signals. They also improve out-of-sample forecast accuracy relative to leading benchmarks. Incorporating intertemporal hedging further strengthens these results, underscoring the importance of dynamic hedging motives for stock-level risk premia. Finally, by contrasting our functional-form-free bounds with the CRRA case—under which the intertemporal hedging component turns negative and the implied expected return proxy performs worse in the data—we show that the effect of intertemporal hedging depends critically on preference restrictions. Overall, our analysis complements the option-implied equity premium and intertemporal asset pricing literature by providing tractable, forward-looking, and stock-specific measures of expected returns.

References

Aït-Sahalia, Y., and A. W. Lo. 2000. Nonparametric risk management and implied risk aversion. *Journal of Econometrics* 94:9–51.

Almeida, C., and G. Freire. 2026. Demand in the option market and the pricing kernel. *Journal of Finance (Forthcoming)* .

Bakshi, G., and D. Madan. 2000. Spanning and derivative-security valuation. *Journal of Financial Economics* 55:205–38.

Bakshi, G., D. Madan, and G. Panayotov. 2010. Returns of claims on the upside and the viability of U-shaped pricing kernels. *Journal of Financial Economics* 97:130–54.

Bansal, R., and A. Yaron. 2004. Risks for the long run: A potential resolution of asset pricing puzzles. *Journal of Finance* 59:1481–509.

Barberis, N., M. Huang, and T. Santos. 2001. Prospect theory and asset prices. *Quarterly Journal of Economics* 116:1–53.

Barone-Adesi, G., N. Fusari, A. Mira, and C. Sala. 2020. Option market trading activity and the estimation of the pricing kernel: A Bayesian approach. *Journal of Econometrics* 216:430–49.

Bliss, R. R., and N. Panigirtzoglou. 2004. Option-implied risk aversion estimates. *Journal of Finance* 59:407–46.

Breeden, D. T., and R. H. Litzenberger. 1978. Prices of state-contingent claims implicit in option prices. *Journal of Business* 51:621–51.

Brennan, M. J., E. S. Schwartz, and R. Lagnado. 1997. Strategic asset allocation. *Journal of Economic Dynamics and Control* 21:1377–403.

Brennan, M. J., and Y. Xia. 2002. Dynamic asset allocation under inflation. *Journal of Finance* 57:1201–38.

Brown, D. P., and J. C. Jackwerth. 2012. The pricing kernel puzzle: reconciling index option data and economic theory .

Brunnermeier, M. K., and S. Nagel. 2008. Do wealth fluctuations generate time-varying risk aversion? Micro-evidence on individuals' asset allocation. *American Economic Review* 98:713–36.

Campbell, J. Y., Y. L. Chan, and L. M. Viceira. 2003. A multivariate model of strategic asset allocation. *Journal of Financial Economics* 67:41–80.

Campbell, J. Y., and J. H. Cochrane. 1999. By force of habit: A consumption-based explanation of aggregate stock market behavior. *Journal of Political Economy* 107:205–51.

Campbell, J. Y., S. Giglio, and C. Polk. 2013. Hard times. *Review of Asset Pricing Studies* 3:95–132.

Campbell, J. Y., S. Giglio, C. Polk, and R. Turley. 2018. An intertemporal CAPM with stochastic volatility. *Journal of Financial Economics* 128:207–33.

Campbell, J. Y., C. Polk, and T. Vuolteenaho. 2010. Growth or glamour? Fundamentals and systematic risk in stock returns. *Review of Financial Studies* 23:305–44.

Campbell, J. Y., and R. J. Shiller. 1988. The dividend-price ratio and expectations of future dividends and discount factors. *Review of Financial Studies* 1:195–228.

Campbell, J. Y., and L. M. Viceira. 1999. Consumption and portfolio decisions when expected returns are time varying. *Quarterly Journal of Economics* 114:433–95.

Campbell, J. Y., and T. Vuolteenaho. 2004. Bad beta, good beta. *American Economic Review* 94:1249–75.

Carhart, M. 1997. On persistence in mutual fund performance. *Journal of Finance* 52:57–82.

Carr, P., and D. Madan. 2001. Optimal positioning in derivative securities. *Quantitative Finance* 1:19–37.

Carr, P., and L. Wu. 2009. Variance Risk Premia. *Review of Financial Studies* 22:1311–41.

Chabi-Yo, F. 2012. Pricing kernels with stochastic skewness and volatility risk. *Management Science* 58:624–40.

Chabi-Yo, F., C. Dim, and G. Vilkov. 2023. Generalized bounds on the conditional expected excess return on individual stocks. *Management Science* 69:922–39.

Chabi-Yo, F., R. Garcia, and E. Renault. 2008. State dependence can explain the risk aversion puzzle. *Review of Financial Studies* 21:973–1011.

Chabi-Yo, F., A. S. Gonçalves, and J. A. Loudis. 2025. An intertemporal risk factor model. *Management Science* 71:6518–44.

Chabi-Yo, F., E. Gourier, and H. Langlois. 2025. Option-implied risk premia with intertemporal hedging. *Available at SSRN 5404768* .

Chabi-Yo, F., D. P. Leisen, and E. Renault. 2014. Aggregation of preferences for skewed asset returns. *Journal of Economic Theory* 154:453–89.

Chabi-Yo, F., and J. Loudis. 2020. The conditional expected market return. *Journal of Financial Economics* 137:752–86.

Chacko, G., and L. M. Viceira. 2005. Dynamic consumption and portfolio choice with stochastic volatility in incomplete markets. *Review of Financial Studies* 18:1369–402.

Chang, B. Y., P. Christoffersen, and K. Jacobs. 2013. Market skewness risk and the cross section of stock returns. *Journal of Financial Economics* 107:46–68.

Chang, B.-Y., P. Christoffersen, K. Jacobs, and G. Vainberg. 2012. Option-implied measures of equity risk. *Review of Finance* 16:385–428.

Chiappori, P.-A., and M. Paiella. 2011. Relative risk aversion is constant: Evidence from panel data. *Journal of the European Economic Association* 9:1021–52.

Christoffersen, P., M. Fournier, K. Jacobs, and M. Karoui. 2021. Option-based estimation of the price of coskewness and cokurtosis risk. *Journal of Financial and Quantitative Analysis* 56:65–91.

Christoffersen, P., S. Heston, and K. Jacobs. 2013. Capturing option anomalies with a variance-dependent pricing kernel. *Review of Financial Studies* 26:1963–2006.

Constantinides, G. M. 1990. Habit formation: A resolution of the equity premium puzzle. *Journal of Political Economy* 98:519–43.

Dittmar, R. F. 2002. Nonlinear pricing kernels, kurtosis preference, and evidence from the cross section of equity returns. *Journal of Finance* 57:369–403.

Ebert, S., and D. Wiesen. 2011. Testing for prudence and skewness seeking. *Management Science* 57:1334–49.

———. 2014. Joint measurement of risk aversion, prudence, and temperance. *Journal of Risk and Uncertainty* 48:231–52.

Elminejad, A., T. Havranek, and Z. Irsova. 2025. Relative risk aversion: A meta-analysis. *Journal of Economic Surveys* 39:2315–33.

Epstein, L. G., and S. E. Zin. 1989. Substitution, Risk Aversion, and the Temporal Behavior of Consumption and Asset Returns: A Theoretical Framework. *Econometrica* 57:937–69.

Fama, E. F., and K. R. French. 1992. The cross-section of expected stock returns. *Journal of Finance* 47:427–65.

———. 2015. A five-factor asset pricing model. *Journal of Financial Economics* 116:1–22.

Fama, E. F., and J. MacBeth. 1973. Risk, return, and equilibrium: Empirical tests. *Journal of Political Economy* 81:607–36.

Fournier, M., K. Jacobs, and P. Orłowski. 2024. Modeling conditional factor risk premia implied by index option returns. *Journal of Finance* 79:2289–338.

Gollier, C. 2001. Should we beware of the precautionary principle? *Economic Policy* 16:302–27.

Goyal, A., and I. Welch. 2008. A comprehensive look at the empirical performance of equity premium prediction. *Review of Financial Studies* 21:1455–508.

Guiso, L., and M. Paiella. 2008. Risk aversion, wealth, and background risk. *Journal of the European Economic Association* 6:1109–50.

Harvey, C. R., and A. Siddique. 2000. Conditional skewness in asset pricing tests. *Journal of Finance* 55:1263–95.

Hlawitschka, W. 1994. The empirical nature of Taylor-series approximations to expected utility. *American Economic Review* 84:713–9.

Hou, K., C. Xue, and L. Zhang. 2015. Digesting anomalies: An investment approach. *Review of Financial Studies* 28:650–705.

Hu, G., K. Jacobs, and S. B. Seo. 2022. Characterizing the variance risk premium: The role of the leverage effect. *Review of Asset Pricing Studies* 12:500–42.

Jackwerth, J. C. 2000. Recovering risk aversion from option prices and realized returns. *Review of Financial Studies* 13:433–51.

Kadan, O., and X. Tang. 2020. A bound on expected stock returns. *Review of Financial Studies* 33:1565–617.

Kim, T. S., and E. Omberg. 1996. Dynamic nonmyopic portfolio behavior. *Review of Financial Studies* 9:141–61.

Kimball, M. S. 1990. Precautionary saving and the marginal propensity to consume.

Kraus, A., and R. H. Litzenberger. 1976. Skewness preference and the valuation of risk assets. *Journal of Finance* 31:1085–100.

Linn, M., S. Shive, and T. Shumway. 2018. Pricing kernel monotonicity and conditional information. *Review of Financial Studies* 31:493–531.

Liu, J. 2007. Portfolio selection in stochastic environments. *Review of Financial Studies* 20:1–39.

Martin, I. 2017. What is the expected return on the market? *Quarterly Journal of Economics* 132:367–433.

Martin, I. W., and S. Nagel. 2022. Market efficiency in the age of big data. *Journal of Financial Economics* 145:154–77.

Martin, I. W., and C. Wagner. 2019. What is the expected return on a stock? *Journal of Finance* 74:1887–929.

Merton, R. C. 1969. Lifetime portfolio selection under uncertainty: The continuous-time case. *Review of Economics and Statistics* 51:247–57.

———. 1971. Optimum consumption and portfolio rules in a continuous-time model. *Journal of Economic Theory* 3:373–413.

———. 1973. An intertemporal capital asset pricing model. *Econometrica: Journal of the Econometric Society* 41:867–87.

Newey, W. K., and K. D. West. 1987. A simple, positive semi-definite, heteroskedasticity and autocorrelation consistent covariance matrix. *Econometrica* 55:703–8.

Noussair, C. N., S. T. Trautmann, and G. Van de Kuilen. 2014. Higher order risk attitudes, demographics, and financial decisions. *Review of Economic Studies* 81:325–55.

Patton, A. J., and A. Timmermann. 2010. Monotonicity in asset returns: New tests with applications to the term structure, the CAPM, and portfolio sorts. *Journal of Financial Economics* 98:605–25.

Rosenberg, J. V., and R. F. Engle. 2002. Empirical pricing kernels. *Journal of Financial Economics* 64:341–72.

Samuelson, P. A. 1969. Lifetime portfolio selection by dynamic stochastic programming. *Review of Economics and Statistics* 51:239–46.

Schneider, P., and F. Trojani. 2019. (Almost) model-free recovery. *Journal of Finance* 74:323–70.

Schneider, S. O., and M. Sutter. 2026. Risk preferences and field behavior: The relevance of higher-order risk preferences. *American Economic Review* 116:88–118.

Schreindorfer, D., and T. Sichert. 2025. Conditional risk and the pricing kernel. *Journal of Financial Economics* 171:104106–.

Seo, S. B., and J. A. Wachter. 2019. Option prices in a model with stochastic disaster risk. *Management Science* 65:3449–69.

Sichert, T. 2018. The pricing kernel is U-shaped. *Available at SSRN 3095551* .

Tetlock, P. C., J. McCoy, and N. Shah. 2024. The implied equity premium. *Available at SSRN 4373579* .

Tsai, J., and J. A. Wachter. 2015. Disaster risk and its implications for asset pricing. *Annual Review of Financial Economics* 7:219–52.

Vissing-Jørgensen, A., and O. P. Attanasio. 2003. Stock-market participation, intertemporal substitution, and risk-aversion. *American Economic Review* 93:383–91.

Wachter, J. A. 2002. Portfolio and consumption decisions under mean-reverting returns: An exact solution for complete markets. *Journal of Financial and Quantitative Analysis* 37:63–91.

———. 2013. Can time-varying risk of rare disasters explain aggregate stock market volatility? *Journal of Finance* 68:987–1035.

Table 1 Summary Statistics of Static Bounds

This table reports descriptive statistics for the static bounds on conditional expected excess returns at the individual-stock level. Panel A uses the default preference parameters $[1/\tau, \rho, \kappa, \xi]$=[1, 2, 4, 8] and reports the mean, standard deviation, skewness, and selected percentiles of the annualized lower and upper bounds (LB and UB). Panel B reports the corresponding statistics for optimized bounds (LB^* and UB^*), where preference parameters are chosen to maximize out-of-sample forecast accuracy of the midpoint (LB+UB)/2 relative to the default parameter values [1, 2, 4, 8] up to each point of time using an expanding widow. The optimal parameter values are changing over time and illustrated in Figure OA.2. The sample spans January 1996 to August 2025 at monthly frequency.

Panel A. With Constant Preference Parameters								
	30 Days		91 Days		182 Days		365 Days	
Statistics	LB	UB	LB	UB	LB	UB	LB	UB
Mean	0.083	0.165	0.083	0.174	0.086	0.168	0.094	0.164
Standard Deviation	0.070	0.175	0.065	0.140	0.063	0.119	0.069	0.111
Skewness	3.081	1.771	3.101	1.549	3.084	1.764	3.039	2.016
1%	0.017	0.015	0.020	0.024	0.024	0.027	0.027	0.034
10%	0.029	0.033	0.032	0.042	0.036	0.054	0.040	0.066
50%	0.063	0.090	0.064	0.133	0.068	0.139	0.074	0.131
90%	0.156	0.442	0.151	0.360	0.152	0.321	0.167	0.302
99%	0.376	0.750	0.356	0.669	0.350	0.611	0.392	0.595
Panel B. With Time-Varying Preference Parameters								
	30 Days		91 Days		182 Days		365 Days	
Statistics	LB^*	UB^*	LB^*	UB^*	LB^*	UB^*	LB^*	UB^*
Mean	0.106	0.183	0.111	0.193	0.129	0.198	0.133	0.192
Standard Deviation	0.098	0.182	0.100	0.151	0.092	0.136	0.101	0.133
Skewness	2.033	1.500	2.076	1.401	1.601	1.469	2.026	1.732
1%	0.016	0.014	0.021	0.025	0.027	0.031	0.033	0.039
10%	0.029	0.032	0.034	0.044	0.044	0.063	0.049	0.074
50%	0.069	0.110	0.073	0.152	0.099	0.163	0.099	0.151
90%	0.239	0.471	0.250	0.403	0.256	0.382	0.262	0.369
99%	0.471	0.753	0.481	0.703	0.441	0.669	0.525	0.678

Table 2 Tightness Test of Static Bounds

This table presents Wald tests of $H_0 : \beta_0 = 0, \beta_1 = 1$ and $H_0 : \beta_1 = 1$ based on a pooled panel regression specified in Equation (4.1) using all stocks in the sample, with observations winsorized at the 1% level. Reported p-values (in parentheses) for the estimated coefficients and the two Wald tests are based on 10,000 bootstrap replications used to estimate the covariance matrix and account for overlapping observations. Tests are conducted for the lower bound (LB; Panel A), the upper bound (UB; Panel B), and their midpoint ($(LB + UB)/2$; Panel C) across maturities from 30 to 365 days. Preference parameters for the optimized bounds (LB^* and UB^*) are chosen to maximize out-of-sample forecast accuracy of the midpoint relative to the default calibration [1, 2, 4, 8] up to each time using an expanding window. The sample spans January 1996 to August 2025 at monthly frequency.

Panel A. Lower Bound

	LB				LB^*			
Statistics	30 Days	91 Days	182 Days	365 Days	30 Days	91 Days	182 Days	365 Days
β_0	−0.010	−0.004	−0.058	−0.049	0.034	0.043	0.003	0.044
	(0.726)	(0.928)	(0.174)	(0.339)	(0.243)	(0.256)	(0.950)	(0.461)
β_1	1.681	1.591	2.161	1.785	0.887	0.746	0.879	0.542
	(0.000)	(0.016)	(0.000)	(0.018)	(0.032)	(0.177)	(0.003)	(0.369)
$R^2(\%)$	0.81	1.72	5.30	7.57	0.42	1.06	4.98	3.79
$H_0 : \beta_0 = 0, \beta_1 = 1$	0.134	0.256	0.138	0.579	0.384	0.393	0.817	0.745
$H_0 : \beta_1 = 1$	0.094	0.371	0.052	0.296	0.784	0.645	0.686	0.448

Panel B. Upper Bound

	UB				UB^*			
Statistics	30 Days	91 Days	182 Days	365 Days	30 Days	91 Days	182 Days	365 Days
β_0	0.061	0.038	−0.018	−0.052	0.058	0.044	0.010	0.042
	(0.004)	(0.189)	(0.691)	(0.296)	(0.007)	(0.115)	(0.719)	(0.461)
β_1	0.334	0.485	0.841	1.043	0.313	0.397	0.539	0.377
	(0.000)	(0.020)	(0.010)	(0.013)	(0.000)	(0.031)	(0.000)	(0.354)
$R^2(\%)$	0.43	0.99	3.27	6.57	0.40	1.06	4.16	3.45
$H_0 : \beta_0 = 0, \beta_1 = 1$	0.000	0.028	0.187	0.097	0.000	0.002	0.000	0.080
$H_0 : \beta_1 = 1$	0.000	0.013	0.626	0.919	0.000	0.001	0.001	0.126

Panel C. Midpoint

	$(LB + UB)/2$				$(LB^* + UB^*)/2$			
Statistics	30 Days	91 Days	182 Days	365 Days	30 Days	91 Days	182 Days	365 Days
β_0	0.038	0.021	−0.038	−0.056	0.042	0.033	0.001	0.042
	(0.101)	(0.547)	(0.417)	(0.281)	(0.090)	(0.320)	(0.978)	(0.479)
β_1	0.635	0.801	1.275	1.350	0.528	0.586	0.703	0.448
	(0.000)	(0.017)	(0.004)	(0.014)	(0.001)	(0.048)	(0.001)	(0.369)
$R^2(\%)$	0.56	1.25	4.05	7.11	0.46	1.18	4.70	3.61
$H_0 : \beta_0 = 0, \beta_1 = 1$	0.059	0.823	0.709	0.416	0.009	0.372	0.089	0.399
$H_0 : \beta_1 = 1$	0.019	0.553	0.532	0.523	0.002	0.162	0.157	0.268

Table 3 Portfolios Sorted by Static Bounds

This table reports average annualized excess returns for portfolios sorted on the static lower bound (LB; Panel A), static upper bound (UB; Panel B), or their midpoint (LB + UB)/2 (Panel C), with maturities shown at the top of each column. Reported p-values (in parentheses) are based on the monotonicity test of Patton and Timmermann (2010) using 10,000 stationary block bootstrap replications across all portfolios formed by LB/UB. Preference parameters for the optimized bounds (LB^* and UB^*) are chosen to maximize out-of-sample forecast accuracy of the midpoint relative to the default calibration [1, 2, 4, 8] up to each time using an expanding window. The sample spans January 1996 to August 2025 at monthly frequency.

Panel A. Sorting by Lower Bound (LB)

	30 Days		91 Days		182 Days		365 Days	
Portfolio	LB	LB^*	LB	LB^*	LB	LB^*	LB	LB^*
Low	0.092	0.091	0.087	0.088	0.087	0.088	0.089	0.088
2	0.107	0.108	0.105	0.105	0.104	0.104	0.107	0.107
3	0.128	0.125	0.118	0.117	0.117	0.117	0.116	0.114
4	0.144	0.145	0.142	0.141	0.140	0.139	0.137	0.136
High	0.192	0.191	0.197	0.195	0.211	0.210	0.241	0.236
High − Low	0.100	0.100	0.110	0.107	0.124	0.122	0.152	0.148
p-Value	(0.001)	(0.001)	(0.002)	(0.003)	(0.005)	(0.006)	(0.007)	(0.008)

Panel B. Sorting by Upper Bound (UB)

	30 Days		91 Days		182 Days		365 Days	
Portfolio	UB	UB^*	UB	UB^*	UB	UB^*	UB	UB^*
Low	0.096	0.096	0.088	0.087	0.087	0.087	0.088	0.088
2	0.107	0.104	0.105	0.104	0.104	0.104	0.107	0.106
3	0.126	0.126	0.119	0.119	0.117	0.117	0.118	0.116
4	0.145	0.145	0.141	0.142	0.139	0.143	0.137	0.135
High	0.196	0.196	0.192	0.190	0.209	0.208	0.241	0.237
High − Low	0.100	0.099	0.104	0.103	0.122	0.121	0.153	0.149
p-Value	(0.006)	(0.016)	(0.001)	(0.001)	(0.024)	(0.009)	(0.005)	(0.009)

Panel C. Sorting by (LB+UB)/2

	30 Days		91 Days		182 Days		365 Days	
Portfolio	$\frac{(LB+UB)}{2}$	$\frac{(LB^*+UB^*)}{2}$	$\frac{(LB+UB)}{2}$	$\frac{(LB^*+UB^*)}{2}$	$\frac{(LB+UB)}{2}$	$\frac{(LB^*+UB^*)}{2}$	$\frac{(LB+UB)}{2}$	$\frac{(LB^*+UB^*)}{2}$
Low	0.094	0.094	0.086	0.086	0.087	0.087	0.089	0.088
2	0.107	0.104	0.105	0.104	0.104	0.104	0.107	0.106
3	0.121	0.122	0.119	0.119	0.116	0.117	0.117	0.115
4	0.149	0.149	0.140	0.142	0.141	0.143	0.136	0.134
High	0.195	0.192	0.196	0.193	0.210	0.210	0.242	0.238
High − Low	0.101	0.098	0.109	0.106	0.123	0.123	0.153	0.150
p-Value	(0.001)	(0.003)	(0.001)	(0.001)	(0.013)	(0.010)	(0.005)	(0.007)

Table 4 Out-of-Sample Forecast Accuracy Relative to Existing Methodologies (Static Bounds)

This table reports out-of-sample R^2 (in percent) from predicting future realized excess returns using the lower bound (Panel A) and upper bound (Panel B) computed with the default preference parameters $[1/\tau, \rho, \kappa, \xi]$=[1, 2, 4, 8]. The benchmarks include the recursive historical mean excess return for stock i from 1990 ($\overline{RX}_{i,t}$), a constant 6% annual excess return (6% p.a.), the recursive historical mean market excess returns from 1996 ($\overline{MKT}_{i,t}$), the historical mean market-implied variance ($\overline{IV}_t$), the historical mean stock-level implied variance ($\overline{IV}_{i,t}$), and the option-based one-period measures $MW_{i,t}$ (Martin and Wagner (2019)), $KT_{i,t}$ (Kadan and Tang (2020)), and $GLB_{i,t}$ (Chabi-Yo, Dim, and Vilkov (2023)). Reported p-values (in parentheses) test $H_0 : R^2 \leq 0$ and are computed using a stationary block bootstrap with 10,000 replications. The sample spans January 1996 to August 2025 at monthly frequency.

Panel A. Lower Bound								
	$\overline{RX}_{i,t}$	$6\%\,p.a.$	$\overline{MKT}_t$	$\overline{IV}_t$	$\overline{IV}_{i,t}$	$MW_{i,t}$	$KT_{i,t}$	$GLB_{i,t}$
30 Days	1.909	0.891	0.862	0.993	1.904	2.671	3.719	−0.096
	(0.000)	(0.003)	(0.003)	(0.003)	(0.000)	(0.009)	(0.002)	(0.782)
91 Days	5.122	1.994	1.888	2.327	4.231	4.725	4.114	0.764
	(0.000)	(0.011)	(0.008)	(0.010)	(0.000)	(0.000)	(0.021)	(0.082)
182 Days	10.022	4.621	4.440	5.219	7.791	5.010	4.016	1.435
	(0.000)	(0.004)	(0.002)	(0.003)	(0.000)	(0.006)	(0.206)	(0.054)
365 Days	17.362	7.441	7.126	8.313	11.797	8.981	3.415	3.475
	(0.000)	(0.008)	(0.002)	(0.007)	(0.000)	(0.067)	(0.345)	(0.049)
Panel B. Upper Bound								
	$\overline{RX}_{i,t}$	$6\%\,p.a.$	$\overline{MKT}_t$	$\overline{IV}_t$	$\overline{IV}_{i,t}$	$MW_{i,t}$	$KT_{i,t}$	$GLB_{i,t}$
30 Days	−0.035	−1.045	−1.081	−0.942	0.018	1.709	2.109	−2.032
	(0.622)	(0.926)	(0.934)	(0.908)	(0.563)	(0.254)	(0.054)	(0.999)
91 Days	3.249	0.074	−0.035	0.412	2.446	3.334	2.395	−1.188
	(0.010)	(0.497)	(0.506)	(0.459)	(0.018)	(0.069)	(0.000)	(0.759)
182 Days	9.152	3.697	3.514	4.299	6.926	4.442	3.172	0.479
	(0.000)	(0.154)	(0.149)	(0.134)	(0.000)	(0.025)	(0.011)	(0.444)
365 Days	16.982	7.010	6.694	7.885	11.386	8.571	2.966	3.019
	(0.000)	(0.133)	(0.108)	(0.120)	(0.000)	(0.008)	(0.102)	(0.053)

Table 5 Summary Statistics of Hedging Bounds

This table reports descriptive statistics for the annualized hedging lower bound (HLB, Panel A) and the annualized hedging upper bound (HUB, Panel B) across horizons defined by T_1 and $T_N > T_1$. The table reports mean, standard deviation, and the hedging share, defined as (HLB-LB)/HLB or (HUB-UB)/HUB. The default preference parameters are $[1/\tau, \rho, \kappa, \xi]$=[1, 2, 4, 8]. For the optimized bounds (HLB^* and HUB^*), preference parameters are chosen to maximize out-of-sample forecast accuracy of the midpoint relative to the default calibration [1, 2, 4, 8] up to each time using an expanding window. The sample spans January 1996 to August 2025 at monthly frequency.

Panel A. Hedging Lower Bound

		$T_N = 91$		$T_N = 182$		$T_N = 365$		$T_N = 547$		$T_N = 730$	
	$[T_1, T_N]$	HLB	HLB^*	HLB	HLB^*	HLB	HLB^*	HLB	HLB^*	HLB	HLB^*
30	Mean	0.089	0.111	0.098	0.115	0.116	0.114	0.134	0.115	0.154	0.119
	Standard Deviation	0.076	0.098	0.082	0.102	0.092	0.102	0.101	0.102	0.110	0.103
	(Hedge-Unhedge)/Hedge	0.064	0.129	0.150	0.179	0.285	0.197	0.389	0.224	0.471	0.264
91	Mean			0.091	0.116	0.106	0.116	0.121	0.114	0.136	0.117
	Standard Deviation			0.073	0.102	0.084	0.103	0.090	0.102	0.098	0.103
	(Hedge-Unhedge)/Hedge			0.081	0.177	0.212	0.201	0.313	0.199	0.397	0.231
182	Mean					0.101	0.123	0.116	0.122	0.131	0.124
	Standard Deviation					0.077	0.092	0.086	0.091	0.092	0.092
	(Hedge-Unhedge)/Hedge					0.141	0.223	0.252	0.249	0.344	0.268
365	Mean							0.109	0.136	0.124	0.136
	Standard Deviation							0.080	0.108	0.089	0.107
	(Hedge-Unhedge)/Hedge							0.132	0.255	0.242	0.253

Panel B. Hedging Upper Bound

		$T_N = 91$		$T_N = 182$		$T_N = 365$		$T_N = 547$		$T_N = 730$	
	$[T_1, T_N]$	HUB	HUB^*	HUB	HUB^*	HUB	HUB^*	HUB	HUB^*	HUB	HUB^*
30	Mean	0.170	0.190	0.180	0.195	0.199	0.195	0.221	0.198	0.245	0.202
	Standard Deviation	0.175	0.182	0.175	0.182	0.172	0.182	0.171	0.181	0.170	0.180
	(Hedge-Unhedge)/Hedge	0.067	0.104	0.156	0.165	0.291	0.197	0.391	0.230	0.470	0.271
91	Mean			0.180	0.201	0.193	0.203	0.206	0.203	0.221	0.206
	Standard Deviation			0.143	0.156	0.147	0.157	0.150	0.157	0.154	0.158
	(Hedge-Unhedge)/Hedge			0.049	0.109	0.136	0.133	0.212	0.147	0.279	0.172
182	Mean					0.180	0.198	0.193	0.202	0.206	0.205
	Standard Deviation					0.125	0.135	0.131	0.138	0.136	0.141
	(Hedge-Unhedge)/Hedge					0.077	0.131	0.147	0.160	0.211	0.181
365	Mean							0.176	0.197	0.189	0.201
	Standard Deviation							0.120	0.138	0.127	0.139
	(Hedge-Unhedge)/Hedge							0.075	0.115	0.145	0.162

Table 6 Tightness Test of Hedging Bounds

This table presents Wald tests of $H_0 : \beta_0 = 0, \beta_1 = 1$ and $H_0 : \beta_1 = 1$ based on a pooled panel regression specified in Equation (4.1) using all stocks in the sample, with observations winsorized at the 1% level. Reported p-values (in parentheses) for the estimated coefficients and the two Wald tests are based on 10,000 bootstrap replications used to estimate the covariance matrix and account for overlapping observations. Tests are conducted for the hedging lower bound (Panel A), the hedging upper bound (Panel B), and their midpoint (HLB + HUB)/2 (Panel C) across maturities T_1 from 30 to 365 days. For each T_1, we report the value of T_N that minimizes $|\beta_1 - 1|$ over candidate values of T_N. Preference parameters for the optimized bounds (HLB^* and HUB^*) are chosen to maximize out-of-sample forecast accuracy of the midpoint relative to the default calibration [1, 2, 4, 8] up to each time using an expanding window. The sample spans January 1996 to August 2025 at monthly frequency.

Panel A. Hedging Lower Bound

	HLB				HLB^*			
	$[T_1, T_N]$	$[T_1, T_N]$	$[T_1, T_N]$	$[T_1, T_N]$	$[T_1, T_N]$	$[T_1, T_N]$	$[T_1, T_N]$	$[T_1, T_N]$
Statistics	[30, 365]	[91, 365]	[182, 730]	[365, 730]	[30, 730]	[91, 547]	[182, 730]	[365, 547]
β_0	−0.003	0.016	−0.013	−0.013	0.009	0.024	−0.060	−0.026
	(0.928)	(0.740)	(0.728)	(0.812)	(0.758)	(0.510)	(0.241)	(0.566)
β_1	1.058	1.004	0.982	1.006	1.003	0.901	1.517	1.126
	(0.001)	(0.065)	(0.007)	(0.081)	(0.002)	(0.070)	(0.001)	(0.028)
$R^2(\%)$	0.96	1.67	5.23	6.64	0.66	1.40	5.53	6.46
$H_0 : \beta_0 = 0, \beta_1 = 1$	0.980	0.756	0.815	0.877	0.921	0.712	0.489	0.763
$H_0 : \beta_1 = 1$	0.854	0.995	0.961	0.992	0.993	0.842	0.262	0.806

Panel B. Hedging Upper Bound

	HUB				HUB^*			
	$[T_1, T_N]$	$[T_1, T_N]$	$[T_1, T_N]$	$[T_1, T_N]$	$[T_1, T_N]$	$[T_1, T_N]$	$[T_1, T_N]$	$[T_1, T_N]$
Statistics	[30, 365]	[91, 182]	[182, 365]	[365, 547]	[30, 730]	[91, 182]	[182, 365]	[365, 547]
β_0	0.040	0.035	−0.022	−0.043	0.047	0.032	−0.039	−0.035
	(0.096)	(0.232)	(0.609)	(0.361)	(0.054)	(0.291)	(0.433)	(0.455)
β_1	0.349	0.479	0.794	0.905	0.327	0.445	0.816	0.797
	(0.000)	(0.018)	(0.005)	(0.016)	(0.000)	(0.023)	(0.004)	(0.022)
$R^2(\%)$	0.58	1.06	3.73	6.64	0.48	1.04	4.11	6.01
$H_0 : \beta_0 = 0, \beta_1 = 1$	0.000	0.015	0.068	0.051	0.000	0.004	0.013	0.030
$H_0 : \beta_1 = 1$	0.000	0.010	0.468	0.798	0.000	0.005	0.519	0.560

Panel C. Hedging Midpoint

	$(HLB + HUB)/2$				$(HLB^* + HUB^*)/2$			
	$[T_1, T_N]$	$[T_1, T_N]$	$[T_1, T_N]$	$[T_1, T_N]$	$[T_1, T_N]$	$[T_1, T_N]$	$[T_1, T_N]$	$[T_1, T_N]$
Statistics	[30, 91]	[91, 182]	[182, 547]	[365, 547]	[30, 730]	[91, 182]	[182, 730]	[365, 730]
β_0	0.033	0.019	−0.031	−0.042	0.025	0.024	−0.051	−0.035
	(0.182)	(0.577)	(0.444)	(0.393)	(0.359)	(0.481)	(0.304)	(0.464)
β_1	0.637	0.762	0.968	1.111	0.565	0.629	1.058	0.954
	(0.000)	(0.016)	(0.002)	(0.021)	(0.000)	(0.030)	(0.002)	(0.025)
$R^2(\%)$	0.63	1.34	4.69	6.99	0.60	1.24	4.78	6.28
$H_0 : \beta_0 = 0, \beta_1 = 1$	0.062	0.746	0.340	0.350	0.003	0.394	0.211	0.232
$H_0 : \beta_1 = 1$	0.018	0.451	0.918	0.819	0.002	0.200	0.863	0.914

Table 7 Portfolios Sorted by Hedging Bounds

This table reports average annualized excess returns for portfolios sorted on the hedging lower bound (HLB, Panel A) or hedging upper bound (HUB, Panel B), for each forecast horizon $T_1 \in \{30, 91, 182, 365\}$ (rows) and investment horizon $T_N \in \{91, 182, 365, 547, 730\}$ (column blocks). Reported p-values (in parentheses) are based on the monotonicity test of Patton and Timmermann (2010) using 10,000 stationary block bootstrap replications across all portfolios formed by HLB/HUB. Preference parameters for the optimized bounds (HLB^* and HUB^*) are chosen to maximize out-of-sample forecast accuracy of the midpoint relative to the default calibration [1, 2, 4, 8] up to each time using an expanding window. The sample spans January 1996 to August 2025 at monthly frequency.

Panel A. Hedging Lower Bound

		$T_N = 91$		$T_N = 182$		$T_N = 365$		$T_N = 547$		$T_N = 730$	
	$[T_1, T_N]$	HLB	HLB^*	HLB	HLB^*	HLB	HLB^*	HLB	HLB^*	HLB	HLB^*
	Low	0.093	0.099	0.096	0.102	0.101	0.103	0.106	0.109	0.105	0.109
30	High	0.191	0.196	0.189	0.194	0.191	0.192	0.188	0.193	0.189	0.193
	High − Low	0.097	0.097	0.093	0.092	0.090	0.089	0.083	0.084	0.085	0.084
	p-Value	(0.001)	(0.003)	(0.001)	(0.015)	(0.002)	(0.033)	(0.008)	(0.041)	(0.005)	(0.018)
	Low			0.088	0.092	0.089	0.091	0.091	0.091	0.092	0.091
91	High			0.197	0.194	0.197	0.193	0.196	0.191	0.196	0.191
	High − Low			0.109	0.102	0.107	0.102	0.105	0.100	0.104	0.101
	p-Value			(0.001)	(0.002)	(0.001)	(0.004)	(0.002)	(0.003)	(0.002)	(0.007)
	Low					0.087	0.087	0.087	0.087	0.088	0.087
182	High					0.210	0.212	0.211	0.212	0.210	0.213
	High − Low					0.123	0.125	0.123	0.126	0.122	0.126
	p-Value					(0.004)	(0.002)	(0.009)	(0.006)	(0.013)	(0.012)
	Low							0.089	0.089	0.089	0.089
365	High							0.242	0.241	0.241	0.240
	High − Low							0.153	0.152	0.152	0.151
	p-Value							(0.010)	(0.008)	(0.005)	(0.004)

Panel B. Hedging Upper Bound

		$T_N = 91$		$T_N = 182$		$T_N = 365$		$T_N = 547$		$T_N = 730$	
	$[T_1, T_N]$	HUB	HUB^*	HUB	HUB^*	HUB	HUB^*	HUB	HUB^*	HUB	HUB^*
	Low	0.095	0.097	0.097	0.099	0.102	0.098	0.107	0.098	0.111	0.099
30	High	0.194	0.198	0.194	0.198	0.193	0.192	0.194	0.194	0.192	0.197
	High − Low	0.099	0.101	0.098	0.099	0.092	0.094	0.087	0.096	0.081	0.098
	p-Value	(0.002)	(0.016)	(0.001)	(0.014)	(0.011)	(0.008)	(0.015)	(0.010)	(0.004)	(0.002)
	Low			0.088	0.089	0.089	0.088	0.089	0.088	0.090	0.088
91	High			0.193	0.191	0.193	0.191	0.194	0.191	0.194	0.191
	High − Low			0.105	0.103	0.104	0.103	0.105	0.103	0.104	0.103
	p-Value			(0.002)	(0.001)	(0.001)	(0.001)	(0.008)	(0.009)	(0.001)	(0.003)
	Low					0.087	0.087	0.087	0.087	0.086	0.087
182	High					0.209	0.210	0.209	0.209	0.208	0.208
	High − Low					0.122	0.122	0.122	0.121	0.122	0.121
	p-Value					(0.003)	(0.006)	(0.019)	(0.014)	(0.006)	(0.003)
	Low							0.088	0.088	0.088	0.088
365	High							0.241	0.241	0.242	0.240
	High − Low							0.153	0.152	0.153	0.152
	p-Value							(0.004)	(0.003)	(0.021)	(0.008)

Table 8 Out-of-Sample Forecast Accuracy Relative to Existing Methodologies (Hedging Bounds)

The table reports out-of-sample R^2 (percent) from predicting future realized excess returns using the hedging lower bound (Panel A) and hedging upper bound (Panel B) computed with the default preference parameters $1/\tau = 1, \rho = 2, \kappa = 4$, and $\xi = 8$. Results are reported for each forecast horizon $T_1 \in \{30, 91, 182, 365\}$ (rows) and investment horizon $T_N \in \{365, 730\}$ (column blocks). Benchmarks, shown in the column headers, include $MW_{i,t}$, $KT_{i,t}$, $GLB_{i,t}$, and the corresponding static bounds (LB/UB). Reported p-values (in parentheses) test $H_0 : R^2 \leq 0$ and are computed using a stationary block bootstrap with 10,000 replications. When $T_1 = T_N$, since HLB (HUB) converges to LB (UB), we set R^2 (p-value) to 0.000 ((0.000)). The sample spans January 1996 to August 2025 at monthly frequency.

Panel A. Hedging Lower Bound

	$T_N = 365$				$T_N = 730$			
	$MW_{i,t}$	$KT_{i,t}$	$GLB_{i,t}$	$LB_{i,t}$	$MW_{i,t}$	$KT_{i,t}$	$GLB_{i,t}$	$LB_{i,t}$
$T_1 = 30$	3.019	4.062	0.261	0.358	2.656	3.704	−0.112	−0.012
	(0.001)	(0.000)	(0.295)	(0.052)	(0.108)	(0.005)	(0.640)	(0.549)
$T_1 = 91$	5.115	4.507	1.170	1.424	4.026	3.411	0.036	−0.698
	(0.000)	(0.002)	(0.052)	(0.035)	(0.084)	(0.072)	(0.542)	(0.657)
$T_1 = 182$	6.148	5.165	2.615	1.234	6.691	5.714	3.179	1.896
	(0.000)	(0.089)	(0.005)	(0.013)	(0.000)	(0.016)	(0.049)	(0.058)
$T_1 = 365$	9.729	4.208	4.269	0.000	9.547	4.016	4.076	0.775
	(0.028)	(0.084)	(0.056)	(0.000)	(0.014)	(0.075)	(0.048)	(0.108)

Panel B. Hedging Upper Bound

	$T_N = 365$				$T_N = 730$			
	$MW_{i,t}$	$KT_{i,t}$	$GLB_{i,t}$	$UB_{i,t}$	$MW_{i,t}$	$KT_{i,t}$	$GLB_{i,t}$	$UB_{i,t}$
$T_1 = 30$	1.019	1.421	−2.749	−2.630	−0.850	−0.440	−4.689	−0.717
	(0.320)	(0.208)	(0.999)	(1.000)	(0.636)	(0.589)	(1.000)	(0.998)
$T_1 = 91$	2.335	1.387	−2.233	−4.049	−0.602	−1.578	−5.307	−1.026
	(0.122)	(0.132)	(0.831)	(0.991)	(0.546)	(0.724)	(0.922)	(0.950)
$T_1 = 182$	4.248	2.975	0.277	−2.425	2.000	0.698	−2.063	−0.163
	(0.041)	(0.004)	(0.465)	(0.933)	(0.077)	(0.370)	(0.663)	(0.599)
$T_1 = 365$	7.718	2.060	2.114	0.000	5.644	−0.141	−0.086	−3.029
	(0.034)	(0.079)	(0.090)	(0.000)	(0.047)	(0.613)	(0.510)	(0.922)

Table 9 Distribution of Firms by Hedging Contributions

This table summarizes the proportion of firms whose intertemporal hedging contributions fall within each specified range. For each forecast horizon $T_1 \in \{30, 91, 182, 365\}$ (rows) and investment horizon $T_N \in \{91, 182, 365, 547, 730\}$ (column blocks), we compute the incremental contribution of intertemporal hedging relative to the static bound—(HLB − LB)/HLB and (HUB − UB)/HUB—and classify firm-month observations by these ratios. The distribution is reported across five percentage ranges: $[0\%, 20\%)$, $[20\%, 40\%)$, $[40\%, 60\%)$, $[60\%, 80\%)$, and $[80\%, 100\%]$. The sample spans January 1996 to August 2025 at monthly frequency.

		$T_N = 91$		$T_N = 182$		$T_N = 365$		$T_N = 547$		$T_N = 730$	
	$[T_1, T_N]$	HLB	HUB	HLB	HUB	HLB	HUB	HLB	HUB	HLB	HUB
	$[0\%, 20\%)$	99.60	98.60	81.03	69.97	19.13	35.88	7.01	24.22	3.84	17.50
30	$[20\%, 40\%)$	0.40	1.38	18.89	27.91	68.04	38.68	43.63	28.11	21.10	22.19
	$[40\%, 60\%)$	0.00	0.00	0.09	2.09	12.73	22.55	46.64	34.45	59.87	31.46
	$[60\%, 80\%)$	0.00	0.02	0.00	0.01	0.10	2.87	2.71	12.89	15.14	26.32
	$[80\%, 100\%]$	0.00	0.00	0.00	0.02	0.00	0.02	0.01	0.33	0.07	2.54
	$[0\%, 20\%)$			99.37	99.92	45.70	81.58	6.69	49.74	2.24	30.48
91	$[20\%, 40\%)$			0.62	0.08	52.65	18.21	78.71	46.19	48.05	51.89
	$[40\%, 60\%)$			0.00	0.00	1.64	0.20	14.45	3.99	47.39	17.16
	$[60\%, 80\%)$			0.00	0.00	0.01	0.01	0.14	0.08	2.31	0.45
	$[80\%, 100\%]$			0.00	0.00	0.00	0.00	0.00	0.00	0.01	0.01
	$[0\%, 20\%)$					90.58	98.74	21.12	82.09	1.93	49.59
182	$[20\%, 40\%)$					9.40	1.24	75.97	17.71	76.48	46.67
	$[40\%, 60\%)$					0.01	0.02	2.90	0.18	20.60	3.69
	$[60\%, 80\%)$					0.01	0.01	0.01	0.02	0.98	0.04
	$[80\%, 100\%]$					0.00	0.00	0.01	0.00	0.01	0.01
	$[0\%, 20\%)$							94.78	99.67	24.26	84.56
365	$[20\%, 40\%)$							5.19	0.32	73.52	15.36
	$[40\%, 60\%)$							0.03	0.02	2.19	0.06
	$[60\%, 80\%)$							0.00	0.00	0.03	0.02
	$[80\%, 100\%]$							0.00	0.00	0.00	0.00

Table 10 Decomposition of Hedging Contributions

This table summarizes the decomposition of the hedging component into contributions from variance, skewness, and kurtosis. We compute the variance-, skewness-, and kurtosis-related components by aggregating the forward moment terms corresponding to the coefficients $a_{j,k-j}$ in Proposition 2.4 for each $k-j$ with varying j to derive the total contribution of each moment in the intertemporal hedging case. Specifically, the component associated with $k-j=2$ captures the variance-related contribution, $k-j=3$ captures the skewness-related contribution, and $k-j=4$ captures the kurtosis-related contribution. We then calculate the incremental contribution of intertemporal hedging relative to the static bound (e.g., HLB−LB). The contribution of each forward moment is then calculated as the ratio of the respective forward moment to the incremental contribution (e.g., HLB−LB or HUB−UB). The sample spans January 1996 to August 2025 at monthly frequency.

		$T_N=91$		$T_N=182$		$T_N=365$		$T_N=547$		$T_N=730$	
	$[T_1, T_N]$	HLB-LB	HUB-UB	HLB-LB	HUB-UB	HLB-LB	HUB-UB	HLB-LB	HUB-UB	HLB-LB	HUB-UB
30	Variance (%)	49.98	57.79	50.52	58.28	50.28	57.20	50.08	56.35	49.88	55.58
	Skewness (%)	40.36	33.39	40.45	33.94	40.65	34.35	40.96	34.52	41.19	34.54
	Kurtosis (%)	9.66	8.82	9.03	7.78	9.07	8.45	8.97	9.13	8.93	9.88
91	Variance (%)			37.85	41.41	38.92	44.47	39.80	45.87	40.61	46.63
	Skewness (%)			43.17	38.29	43.58	38.74	44.27	39.54	45.15	40.56
	Kurtosis (%)			18.98	20.29	17.49	16.79	15.93	14.59	14.24	12.81
182	Variance (%)					34.12	41.52	35.01	43.67	35.95	45.47
	Skewness (%)					40.67	32.88	41.37	33.64	42.24	34.71
	Kurtosis (%)					25.21	25.60	23.62	22.68	21.82	19.82
365	Variance (%)							34.48	46.74	35.16	48.23
	Skewness (%)							36.06	26.64	36.63	27.07
	Kurtosis (%)							29.46	26.62	28.21	24.69

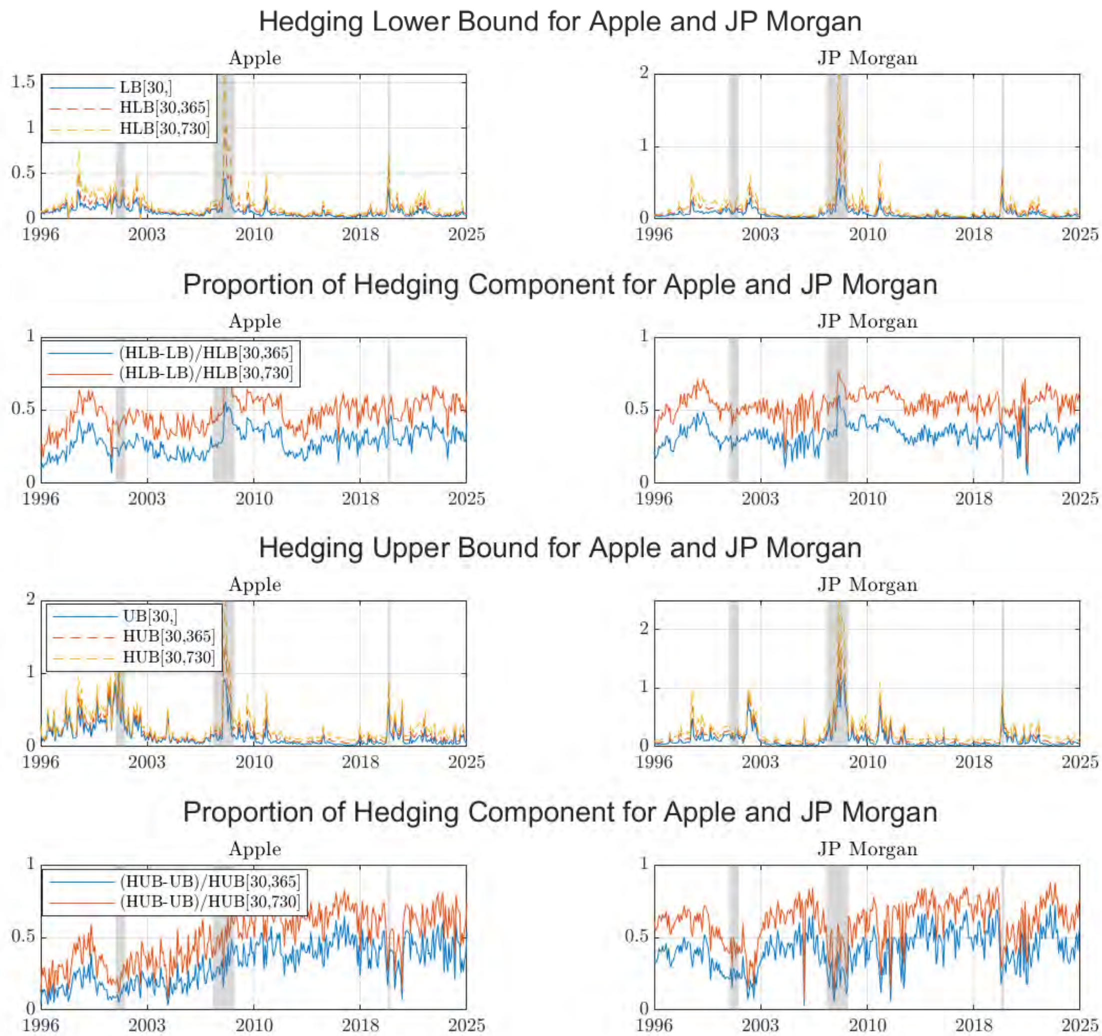

Fig. 1: Time Series of Expected Excess Return Bounds for AAPL and JPM This figure plots the time series of lower and upper bounds on expected excess returns for Apple and JP Morgan with and without hedging (LB/UB and HLB/HUB). Bounds are computed using the default preference parameters: $1/\tau = 1, \rho = 2, \kappa = 4$, and $\xi = 8$. The figure also reports the hedging share, defined as (HLB-LB)/HLB and (HUB-UB)/HUB, with $T_1 = 30$ and $T_N = 365/730$. The sample spans January 1996 to August 2025. The grey areas indicate NBER recessions.

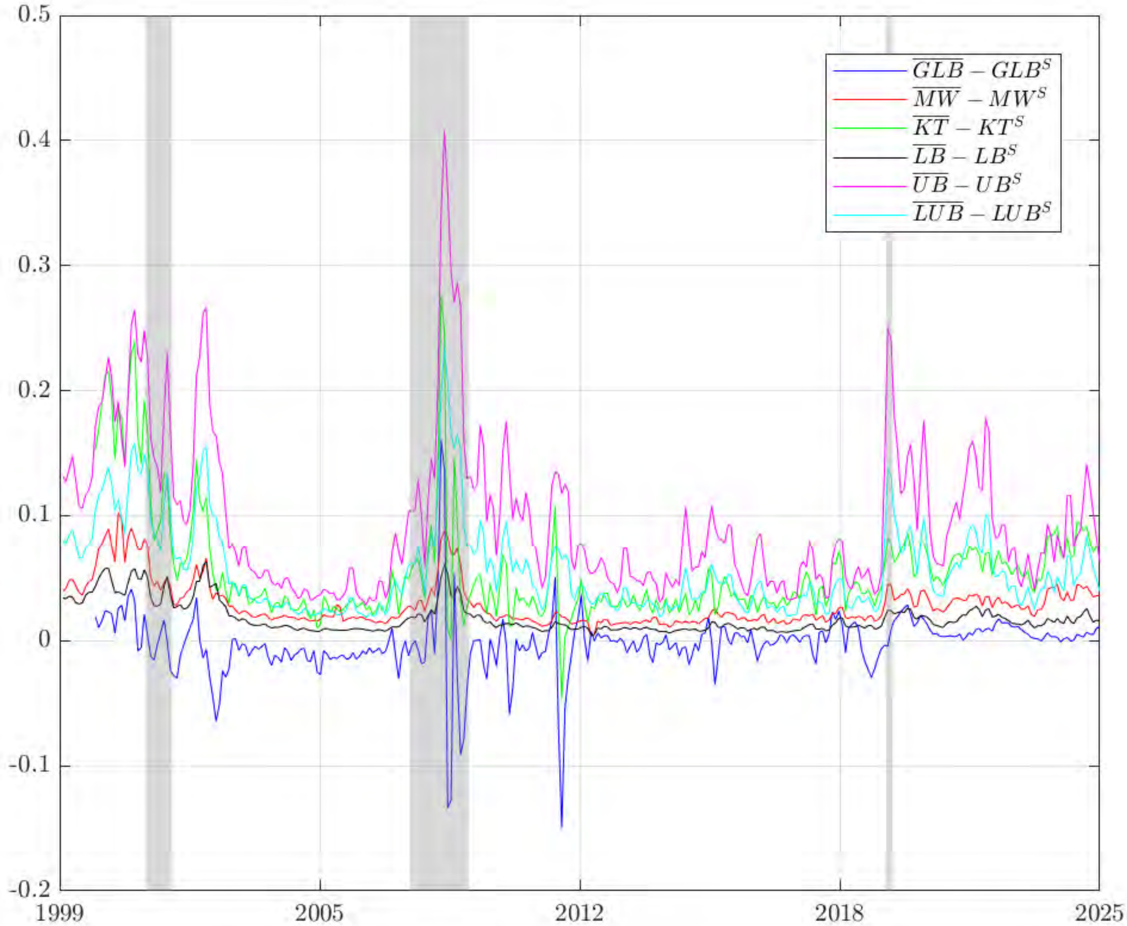

Fig. 2: Pricing Consistency of Static Bounds This figure reports average differences in 30-day annualized expected excess return bounds between nine S&P500-based SPDR ETFs (X^S) and the value-weighted bounds of their underlying constituents ($\bar{X}$). The figure includes MW (Martin and Wagner (2019)), KT (Kadan and Tang (2020)), GLB (Chabi-Yo, Dim, and Vilkov (2023)), the static bounds (LB and UB), and the midpoint (LUB=(LB+UB)/2). The static bounds are computed using the default preference parameters $1/\tau = 1, \rho = 2, \kappa = 4$, and $\xi = 8$. The series are monthly averages of annualized daily values from January 1999 (the start of sector-ETF option trading) to August 2025. The grey areas indicate NBER recessions.

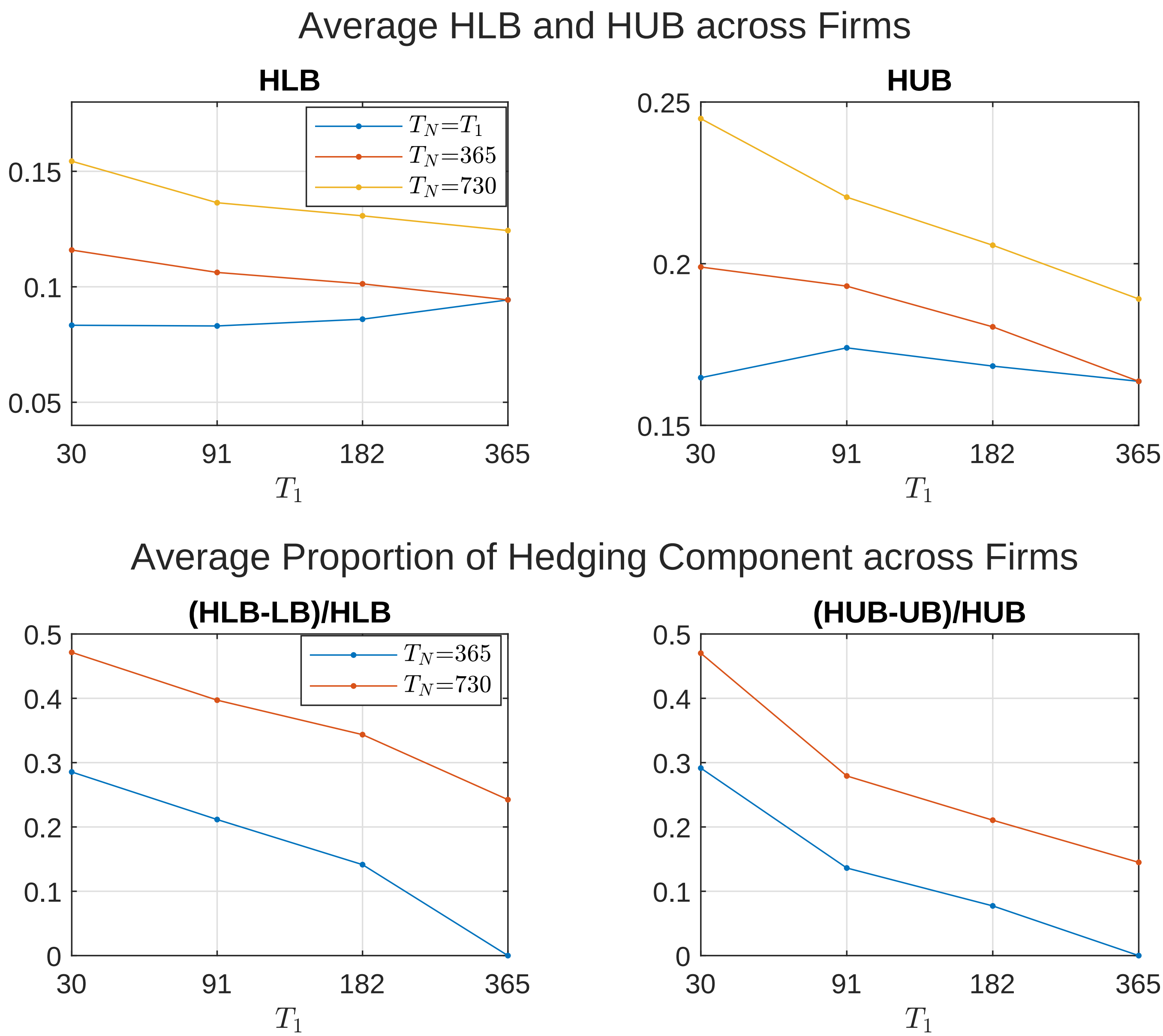

Fig. 3: Average Hedging Bounds across Forecast Horizons This figure plots averages of the hedging bounds (HLB and HUB) across all firms for maturities from 30 to 365 days. The figure also reports the hedging share, defined as (HLB−LB)/HLB and (HUB−UB)/HUB, averaged across firms at each maturity. The sample spans January 1996 to August 2025.

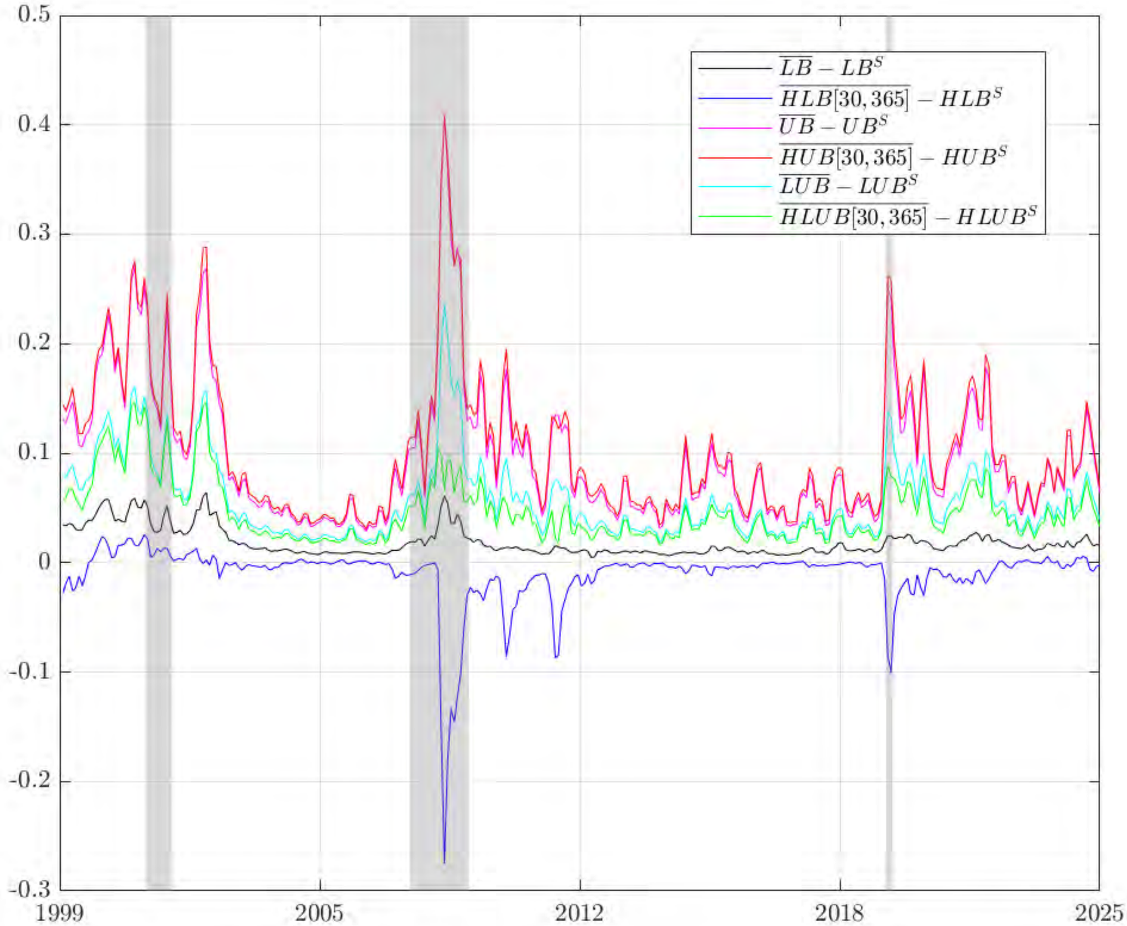

Fig. 4: Pricing Consistency: Hedging vs. Static Bounds This figure reports average differences in 30-day annualized expected excess return bounds between nine S&P500-based SPDR ETFs (X^S) and the value-weighted bounds of their underlying constituents ($\bar{X}$). The figure includes the static bounds (LB and UB) and midpoint (LUB=(LB+UB)/2), as well as the hedging bounds (HLB and HUB) and midpoint (HLUB=(HLB+HUB)/2). The series are monthly averages of annualized daily values from January 1999 to August 2025. The grey areas indicate NBER recessions.

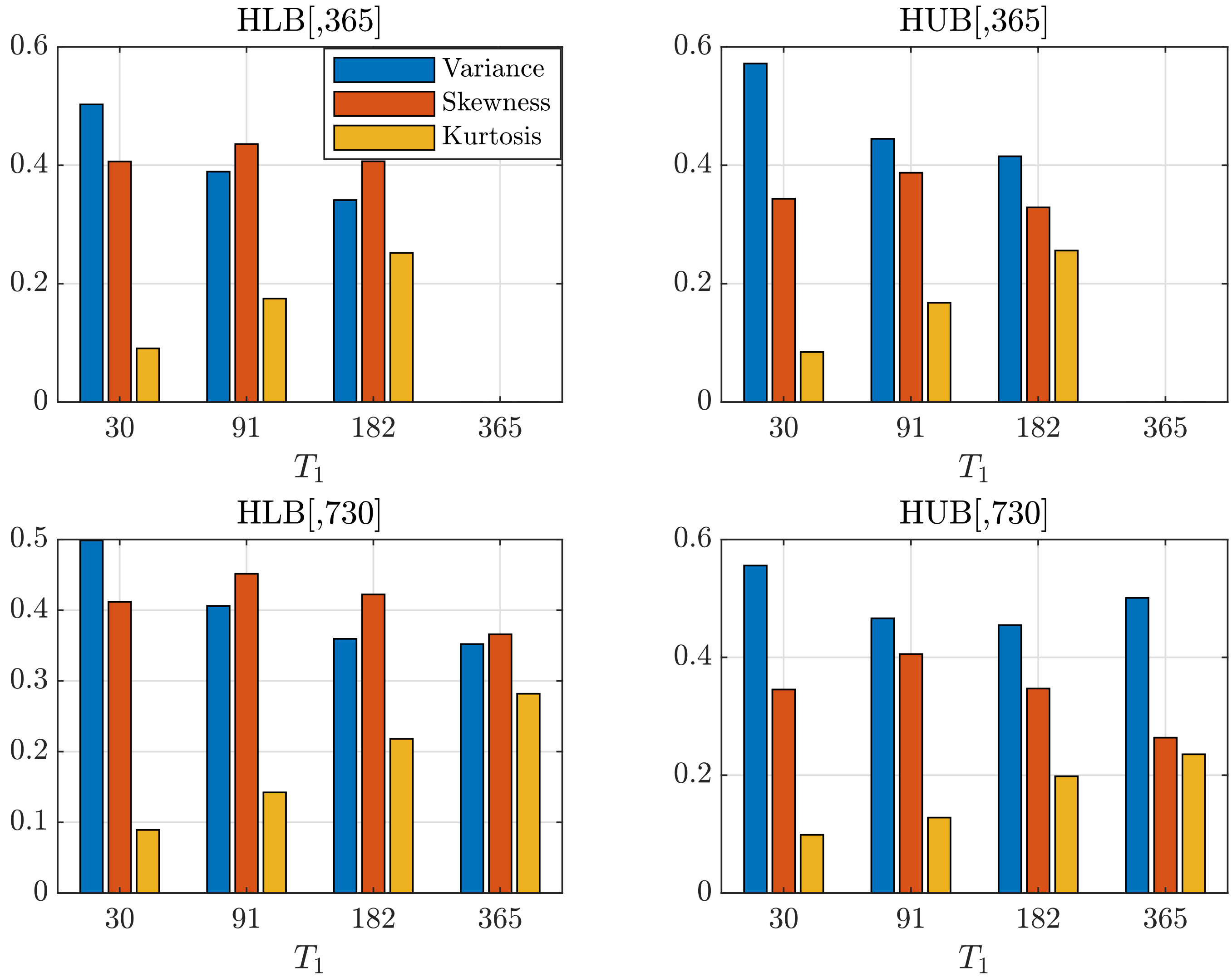

Fig. 5: Decomposition of Hedging Contributions This figure depicts the average decomposition of the hedging components of the lower bound (HLB) and upper bound (HUB) across all firms in the sample, with maturities ranging from 30 to 365 days. We compute the variance-, skewness-, and kurtosis-related components by aggregating the forward moment terms corresponding to the coefficients $a_{j,k-j}$ in Proposition 2.4 for each $k-j$ with varying j to derive the total contribution of each moment in the intertemporal hedging case. Specifically, the component associated with $k-j=2$ captures the variance-related contribution, $k-j=3$ captures the skewness-related contribution, and $k-j=4$ captures the kurtosis-related contribution. We then calculate the incremental contribution of intertemporal hedging relative to the static bound (e.g., HLB−LB). The contribution of each forward moment is then calculated as the ratio of the respective forward moment to the incremental contribution (e.g., HLB−LB or HUB−UB). The sample spans January 1996 to August 2025.

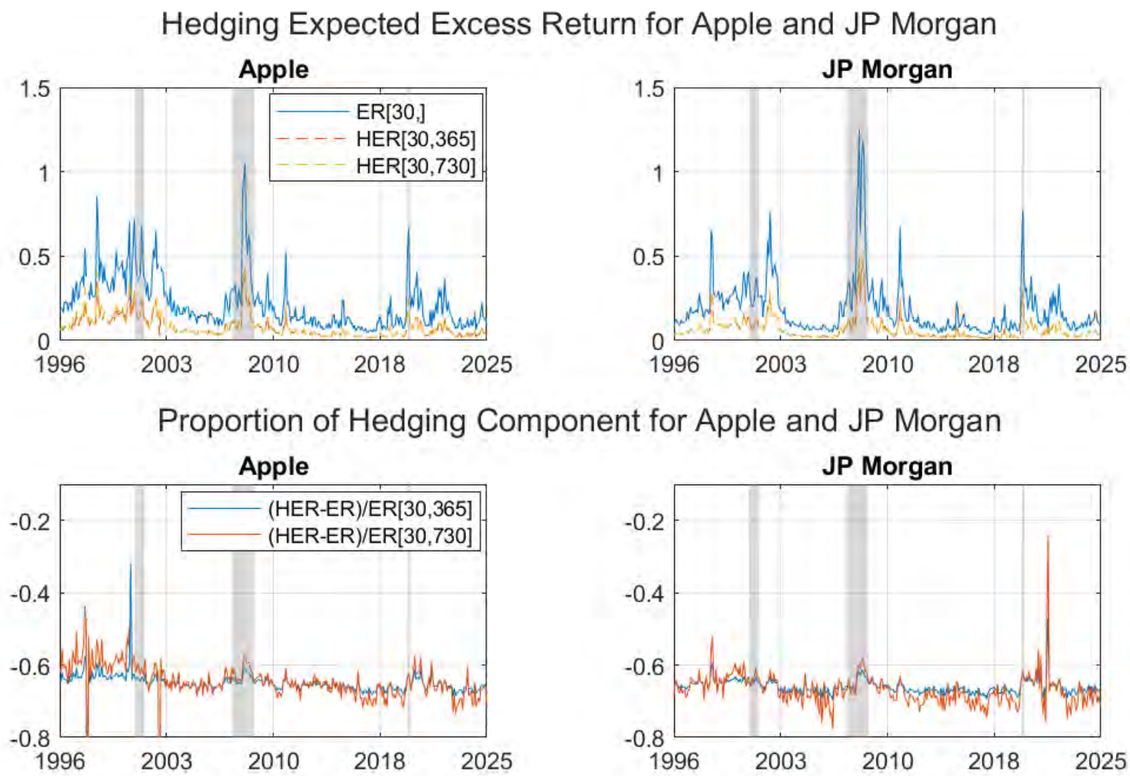

Fig. 6: Time Series of Expected Excess Return for AAPL and JPM Under the CRRA Utility (Risk Aversion=3) This figure depicts the time series of expected excess returns (ER) for two stocks, Apple and JP Morgan, with and without hedging, under the case of CRRA utility. In particular, we set the preference parameters with risk aversion equal to 3. The figure also plots time-series proportion of the hedging component, measured as the difference between hedging expected excess return (HER) and ER scaled by ER with $T_1 = 30$ and $T_N = 365/730$. The sample period spans from January 1996 to August 2025. The grey areas indicate the National Bureau of Economic Research (NBER) recession periods.

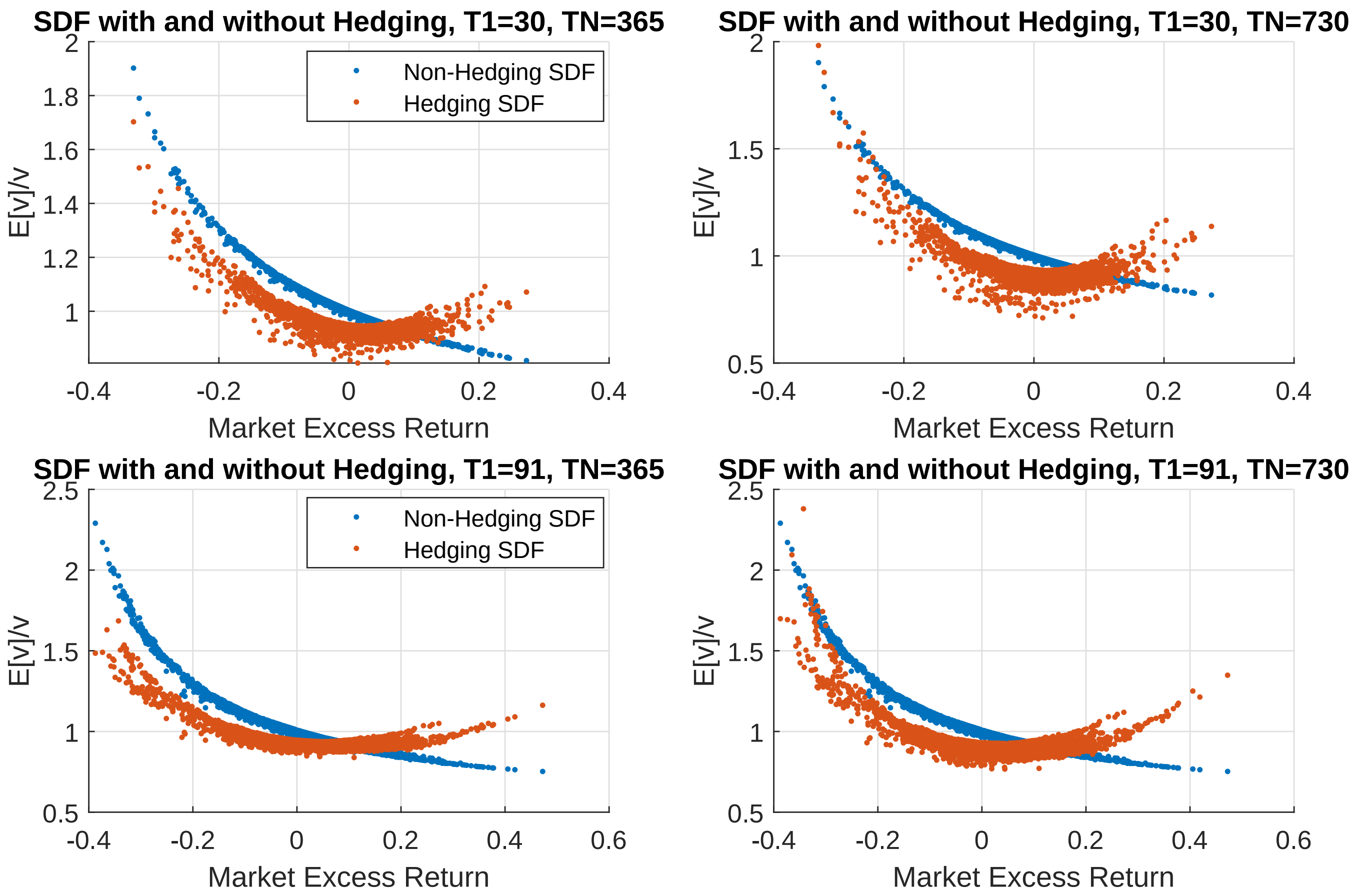

Fig. 7: SDF Estimation with and without Intertemporal Hedging This figure depicts the estimation of the SDF using our approximation based on realized market returns with and with intertemporal hedging. The SDFs are computed using the default preference parameters $1/\tau = 1, \rho = 2, \kappa = 4$, and $\xi = 8$. The sample periods to estimate SDF spans from January 1996 to August 2025.

Online Appendix for

"Conditional Expected Returns on Individual Stocks with and without Intertemporal Hedging"

OA.1 Proofs for Propositions

Proof of the SDF in Absence of Intertemporal Hedging. This section provides the proofs for all propositions. Set $x_0 = R_{f,t\to T_1}$ and $x = R_{M,t\to T_1}$. Set $\Delta x = x - x_0$. A Taylor expansion-series of $\upsilon_{t\to T_1}$ around $\Delta x = 0$ yields

$$\upsilon_{t\to T_1} = 1 + \sum_{j=1}^{\infty} \frac{1}{j!} \left(\frac{\partial^j \upsilon_{t\to T_1}}{\partial^j x} \right)_{x=x_0} (\Delta x)^j .$$

Observe that

$$\left(\frac{\partial \upsilon_{t\to T_1}}{\partial x} \right)_{x=x_0} = \left\{ -\frac{W_t u' \left[W_t x_0\right] u'' \left[W_t x\right]}{\left(u' \left[W_t x\right]\right)^2} \right\}_{x=x_0} = \frac{1}{x_0} \frac{1}{\tau_t}.$$

Next,

$$\left(\frac{\partial^2 \upsilon_{t\to T_1}}{\partial^2 x} \right)_{x=x_0} = \left\{ -\frac{\left(W_t\right)^2 u' \left[W_t x_0\right] u''' \left[W_t x\right]}{\left(u' \left[W_t x\right]\right)^2} + 2 \frac{\left(W_t\right)^2 u' \left[W_t x\right] u' \left[W_t x_0\right] \left(u'' \left[W_t x\right]\right)^2}{\left(u' \left[W_t x\right]\right)^4} \right\}_{x=x_0} = \frac{2\left(1-\rho_t\right)}{\tau_t^2 x_0^2}.$$

Observe that

$$\left(\frac{\partial^3 \upsilon_{t\to T_1}}{\partial^3 x} \right)_{x=x_0} = \left\{ \begin{array}{c} -\frac{(W_t)^3 u'[W_t x_0] u''''[W_t x]}{\left(u'[W_t x]\right)^2} + \frac{6 u''[W_t x] (W_t)^3 u'[W_t x_0] u'''[W_t x]}{\left(u'[W_t x]\right)^3} \\ -6 \frac{(W_t)^3 u'[W_t x_0] \left(u'[W_t x]\right)^2 \left(u''[W_t x]\right)^3}{\left(u'[W_t x]\right)^6} \end{array} \right\}_{x=x_0} = \frac{6\kappa_t + 6 - 12\rho_t}{\tau_t^3 x_0^3}.$$

Next,

$$\left(\frac{\partial^4 \upsilon_{t\to T_1}}{\partial^4 x}\right)_{x=x_0}$$
$$= \left\{\begin{array}{c} -\frac{(W_t)^4 u^{\prime}[W_t x_0] u^{\prime\prime\prime\prime\prime}[W_t x]}{\left(u^{\prime}[W_t x]\right)^2} + 2\frac{(W_t)^4 u^{\prime\prime}[W_t x] u^{\prime}[W_t x_0] u^{\prime\prime\prime\prime}[W_t x]}{\left(u^{\prime}[W_t x]\right)^3} + \frac{6u^{\prime\prime\prime}[W_t x](W_t)^4 u^{\prime}[W_t x_0] u^{\prime\prime\prime}[W_t x]}{\left(u^{\prime}[W_t x]\right)^3} \\ + \frac{6u^{\prime\prime}[W_t x](W_t)^4 u^{\prime}[W_t x_0] u^{\prime\prime\prime\prime}[W_t x]}{\left(u^{\prime}[W_t x]\right)^3} - \frac{18\left(u^{\prime\prime}[W_t x]\right)^2 (W_t)^4 u^{\prime}[W_t x_0] u^{\prime\prime\prime}[W_t x]}{\left(u^{\prime}[W_t x]\right)^4} \\ -18\frac{(W_t)^4 u^{\prime}[W_t x_0]\left(u^{\prime\prime}[W_t x]\right)^2 u^{\prime\prime\prime}[W_t x]}{\left(u^{\prime}[W_t x]\right)^4} + 24\frac{(W_t)^4 u^{\prime}[W_t x_0]\left(u^{\prime\prime}[W_t x]\right)^4}{\left(u^{\prime}[W_t x]\right)^5} \end{array}\right\}_{x=x_0}.$$

This simplifies to

$$\left(\frac{\partial^4 \upsilon_{t\to T_1}}{\partial^4 x}\right)_{x=x_0} = \frac{24\rho_t^2 - 72\rho_t + 24 + 48\kappa_t - 24\xi_t}{\tau_t^4 x_0^4}.$$

The replacement of $\upsilon_{t\to T_1}$ in (2.2) yields the final result. □

Proof of Proposition 2.1. Let us first derive the lower bound. Replace the inverse SDF obtained in Proposition 1 with expression (2.1). It follows that

$$\begin{aligned} \mathbb{E}_t\left[\mathcal{R}_{i,t\to T_1}\right] &= \mathbb{E}_t^*\left(\frac{\mathbb{E}_t m_{t\to T_1}}{m_{t\to T_1}}\mathcal{R}_{i,t\to T_1}\right) \\ &= \sum_{j=1}^{\infty}\underbrace{\frac{a_{j,t}}{\mathcal{R}^j_{f,t\to T_1}\mathbb{E}_t^*\upsilon_{t\to T_1}}}_{\text{Price of Risk}}\underbrace{\mathbb{COV}_t^*\left(\mathcal{R}_{i,t\to T_1},\mathcal{R}^j_{M,t\to T_1}\right)}_{\text{Quantity of Risk}}, \end{aligned} \tag{OA.1.1}$$

where $a_{j,t}$ are defined as

$$a_{j,t} = \left\{\frac{\partial^j \upsilon_{t\to T_1}}{\partial^j R_{M,t\to T_1}}\right\}_{\mathcal{R}_{M,t\to T_1}=0}. \tag{OA.1.2}$$

The expected ecess return expands to

$$\mathbb{E}_t\mathcal{R}_{i,t\to T_1}$$
$$= \frac{1+\sum_{j=1}^{\mathcal{K}}\frac{a_{j,t}}{R^j_{f,t\to T_1}}\mathbb{E}_t^*\left[\mathcal{R}^j_{M,t\to T_1}\right]}{1+\sum_{j=1}^{\infty}\frac{a_{j,t}}{R^j_{f,t\to T_1}}\mathbb{E}_t^*\left[\mathcal{R}^j_{M,t\to T_1}\right]} \times \frac{\sum_{j=1}^{\mathcal{K}}\frac{a_{j,t}}{R^j_{f,t\to T_1}}\mathbb{E}_t^*\left[\mathcal{R}^j_{M,t\to T_1}\mathcal{R}_{i,t\to T_1}\right]}{1+\sum_{j=1}^{\mathcal{K}}\frac{a_{j,t}}{R^j_{f,t\to T_1}}\mathbb{E}_t^*\left[\mathcal{R}^j_{M,t\to T_1}\right]} + \frac{\sum_{j=\mathcal{K}+1}^{\infty}\frac{a_{j,t}}{R^j_{f,t\to T_1}}\mathbb{E}_t^*\left[\mathcal{R}^j_{M,t\to T_1}\mathcal{R}_{i,t\to T_1}\right]}{1+\sum_{j=1}^{\infty}\frac{a_{j,t}}{R^j_{f,t\to T_1}}\mathbb{E}_t^*\left[\mathcal{R}^j_{M,t\to T_1}\right]}.$$

Since $\frac{a_{j,t}}{R^j_{f,t\to T_1}} \mathbb{COV}^*_t \left[\mathcal{R}^j_{M,t\to T_1}, R_{i,t\to T_1}\right] \geq 0$, it follows that

$$\frac{\sum\limits_{j=\mathcal{K}+1}^{\infty} \frac{a_{j,t}}{R^j_{f,t\to T_1}} \mathbb{E}^*_t \left[\mathcal{R}^j_{M,t\to T_1} \mathcal{R}_{i,t\to T_1}\right]}{1+\sum\limits_{j=1}^{\infty} \frac{a_{j,t}}{R^j_{f,t\to T_1}} \mathbb{E}^*_t \left[\mathcal{R}^j_{M,t\to T_1}\right]} \geq 0.$$

Since $a_{2j+1,t} \geq 0$, $a_{2j,t} \leq 0$, $\mathbb{E}^*_t \mathcal{R}^{2j+1}_{M,t\to T_1}$, and $\mathbb{E}^*_t \mathcal{R}^{2j}_{M,t\to T_1} \geq 0$, it follows that

$$0 \leq 1+\sum_{j=1}^{\infty} \frac{a_{j,t}}{R^j_{f,t\to T_1}} \mathbb{E}^*_t \mathcal{R}^j_{M,t\to T_1} \leq 1+\sum_{j=1}^{\mathcal{K}} \frac{a_{j,t}}{R^j_{f,t\to T_1}} \mathbb{E}^*_t \mathcal{R}^j_{M,t\to T_1}.$$

Hence,

$$\frac{1+\sum\limits_{j=1}^{\mathcal{K}} \frac{a_{j,t}}{R^j_{f,t\to T_1}} \mathbb{E}^*_t \left[\mathcal{R}^j_{M,t\to T_1}\right]}{1+\sum\limits_{j=1}^{\infty} \frac{a_{j,t}}{R^j_{f,t\to T_1}} \mathbb{E}^*_t \left[\mathcal{R}^j_{M,t\to T_1}\right]} \geq 1.$$

Thus it implies

$$\left(\frac{1+\sum\limits_{j=1}^{\mathcal{K}} \frac{a_{j,t}}{R^j_{f,t\to T_1}} \mathbb{E}^*_t \left[\mathcal{R}^j_{M,t\to T_1}\right]}{1+\sum\limits_{j=1}^{\infty} \frac{a_{j,t}}{R^j_{f,t\to T_1}} \mathbb{E}^*_t \left[\mathcal{R}^j_{M,t\to T_1}\right]}\right) \left\{\frac{\sum\limits_{j=1}^{\mathcal{K}} \frac{a_{j,t}}{R^j_{f,t\to T_1}} \mathbb{E}^*_t \left[\mathcal{R}^j_{M,t\to T_1} \mathcal{R}_{i,t\to T_1}\right]}{1+\sum\limits_{j=1}^{\mathcal{K}} \frac{a_{j,t}}{R^j_{f,t\to T_1}} \mathbb{E}^*_t \left[\mathcal{R}^j_{M,t\to T_1}\right]}\right\} \geq \frac{\sum\limits_{j=1}^{\mathcal{K}} \frac{a_{j,t}}{R^j_{f,t\to T_1}} \mathbb{E}^*_t \left[\mathcal{R}^j_{M,t\to T_1} \mathcal{R}_{i,t\to T_1}\right]}{1+\sum\limits_{j=1}^{\mathcal{K}} \frac{a_{j,t}}{R^j_{f,t\to T_1}} \mathbb{E}^*_t \left[\mathcal{R}^j_{M,t\to T_1}\right]}.$$

and hence

$$\mathbb{E}_t\, \mathcal{R}_{i,t\to T_1} \geq \frac{\sum\limits_{j=1}^{\mathcal{K}} \frac{a_{j,t}}{R^j_{f,t\to T_1}} \mathbb{E}^*_t \left[\mathcal{R}^j_{M,t\to T_1}\, \mathcal{R}_{i,t\to T_1}\right]}{1+\sum\limits_{j=1}^{\mathcal{K}} \frac{a_{j,t}}{R^j_{f,t\to T_1}} \mathbb{E}^*_t \left[\mathcal{R}^j_{M,t\to T_1}\right]}.$$

Next, we derive the upper bound. For any threshold $0 \leq k_0 \leq R_{f,t\to T_1}$,

$$\mathbb{E}_t \mathcal{R}_{i,t\to T_1} \leq \mathbb{E}_t \left(\mathcal{R}_{i,t\to T_1} 1_{R_{i,t\to T_1} \geq k_0}\right).$$

Up to the $\mathcal{K}^{\text{th}}$-order expansion of the inverse marginal utility, under no-arbitrage

$$\mathbb{E}_t^* \left[\frac{\mathbb{E}_t m_{t\to T_1}}{m_{t\to T_1}} \mathcal{R}_{i,t\to T_1} 1_{R_{i,t\to T_1}\geq k_0} \right] = \mathbb{E}_t^* \left\{ \frac{1 + \sum_{j=1}^{\mathcal{K}} \frac{a_{j,t}}{R_{f,t\to T_1}^j} \mathcal{R}_{M,t\to T_1}^j}{1 + \sum_{j=1}^{\mathcal{K}} \frac{a_{j,t}}{R_{f,t\to T_1}^j} \mathbb{E}_t^* \left[\mathcal{R}_{M,t\to T_1}^j \right]} \mathcal{R}_{i,t\to T_1} 1_{R_{i,t\to T_1}\geq k_0} \right\}.$$

Since, under arbitrage $\mathbb{E}_t \left[\mathcal{R}_{i,t\to T_1} 1_{R_{i,t\to T_1}\geq k_0} \right] = \mathbb{E}_t^* \left[\frac{\mathbb{E}_t m_{t\to T_1}}{m_{t\to T_1}} \mathcal{R}_{i,t\to T_1} 1_{R_{i,t\to T_1}\geq k_0} \right]$, we obtain

$$\mathbb{E}_t \left\{ \mathcal{R}_{i,t\to T_1} 1_{R_{i,t\to T_1}\geq k_0} \right\} = \frac{\mathbb{E}_t^* \left[\mathcal{R}_{i,t\to T_1} 1_{R_{i,t\to T_1}\geq k_0} \right] + \sum_{j=1}^{\mathcal{K}} \frac{a_{j,t}}{R_{f,t\to T_1}^j} \mathbb{E}_t^* \left[\mathcal{R}_{M,t\to T_1}^j \mathcal{R}_{i,t\to T_1} 1_{R_{i,t\to T_1}\geq k_0} \right]}{1 + \sum_{j=1}^{\mathcal{K}} \frac{a_{j,t}}{R_{f,t\to T_1}^j} \mathbb{E}_t^* \left[\mathcal{R}_{M,t\to T_1}^j \right]}.$$

This ends the proof. □

Proof of the SDF in Presence of Intertemporal Hedging. Comparing expression (2.1) and (2.30), and using the uniqueness of the SDF it follows that

$$\frac{\mathbb{E}_t m_{t\to T_1}}{m_{t\to T_1}} = \frac{\upsilon_{t\to T_1}}{\mathbb{E}_t^* \upsilon_{t\to T_1}},$$

where

$$\upsilon_{t\to T_1} = \mathbb{E}_{T_1}^* \vartheta_{t\to T_N} \text{ with } \vartheta_{t\to T_N} = \frac{u^{'} \left[W_t x_0 y_0 \right]}{u^{'} \left[W_t x y \right]}. \tag{OA.1.3}$$

Setting $x_0 = R_{f,t\to T_1}, y_0 = R_{f,T_1\to T_N}$ and $x = R_{M,t\to T_1}, y = R_{M,T_1\to T_N}$ Let's set $\Delta x = x - x_0$ and $\Delta y = y - y_0$.

$$\vartheta_{t\to T_N} = \sum_{j_1=0}^{\mathcal{K}} \sum_{j_1=0}^{\mathcal{K}} \frac{a_{j_1,j_2}}{R_{f,t\to T_1}^{j_1} R_{f,T_1\to T_N}^{j_2}} \Delta x^{j_1} \Delta y^{j_2}. \tag{OA.1.4}$$

Hence,

$$\begin{aligned}
\vartheta_{t\to T_N} = 1 &+ \left(\frac{\partial \vartheta_{t\to T_N}}{\partial x}\right)_{x=x_0} \Delta x + \left(\frac{\partial \vartheta_{t\to T_N}}{\partial y}\right)_{y=y_0} \Delta y \\
&+ \frac{1}{2}\left(\frac{\partial^2 \vartheta_{t\to T_N}}{\partial x^2}\right)_{x=x_0} (\Delta x)^2 + \frac{1}{2}\left(\frac{\partial^2 \vartheta_{t\to T_N}}{\partial y^2}\right)_{y=y_0} (\Delta y)^2 \\
&+ \left(\frac{\partial^2 \vartheta_{t\to T_N}}{\partial x\, \partial y}\right)_{(x,y)=(x_0,y_0)} \Delta x\, \Delta y \\
&+ \frac{1}{3!}\left(\frac{\partial^3 \vartheta_{t\to T_N}}{\partial x^3}\right)_{x=x_0} (\Delta x)^3 + \frac{1}{3!}\left(\frac{\partial^3 \vartheta_{t\to T_N}}{\partial y^3}\right)_{y=y_0} (\Delta y)^3 \\
&+ \frac{3}{3!}\left(\frac{\partial^3 \vartheta_{t\to T_N}}{\partial y^2 \partial x}\right)_{(x,y)=(x_0,y_0)} (\Delta y)^2 \Delta x + \frac{3}{3!}\left(\frac{\partial^3 \vartheta_{t\to T_N}}{\partial x^2 \partial y}\right)_{(x,y)=(x_0,y_0)} (\Delta x)^2 \Delta y \\
&+ \frac{1}{4!}\left(\frac{\partial^4 \vartheta_{t\to T_N}}{\partial x^4}\right)_{x=x_0} (\Delta x)^4 + \frac{1}{4!}\left(\frac{\partial^4 \vartheta_{t\to T_N}}{\partial y^4}\right)_{y=y_0} (\Delta y)^4 \\
&+ \frac{4}{4!}\left(\frac{\partial^4 \vartheta_{t\to T_N}}{\partial x^3 \partial y}\right)_{(x,y)=(x_0,y_0)} (\Delta x)^3 (\Delta y) + \frac{4}{4!}\left(\frac{\partial^4 \vartheta_{t\to T_N}}{\partial y^3 \partial x}\right)_{(x,y)=(x_0,y_0)} (\Delta y)^3 (\Delta x) \\
&+ \frac{6}{4!}\left(\frac{\partial^4 \vartheta_{t\to T_N}}{\partial x^2 \partial y^2}\right)_{(x,y)=(x_0,y_0)} (\Delta x)^2 (\Delta y)^2.
\end{aligned}$$

and

$$
\begin{aligned}
\mathbb{E}^*_{T_1}\frac{u'(W_t x_0 y_0)}{u'(W_t x y)} = 1 &+ \left(\frac{\partial \vartheta_{t\to T_N}}{\partial x}\right)_{x=x_0}\Delta x + \frac{1}{2}\left(\frac{\partial^2 \vartheta_{t\to T_N}}{\partial x^2}\right)_{x=x_0}(\Delta x)^2 \\
&+ \frac{1}{2}\left(\frac{\partial^2 \vartheta_{t\to T_N}}{\partial y^2}\right)_{y=y_0}\mathbb{E}^*_{T_1}(\Delta y)^2 \\
&+ \frac{1}{3!}\left(\frac{\partial^3 \vartheta_{t\to T_N}}{\partial x^3}\right)_{x=x_0}(\Delta x)^3 + \frac{1}{3!}\left(\frac{\partial^3 \vartheta_{t\to T_N}}{\partial y^3}\right)_{y=y_0}\mathbb{E}^*_{T_1}(\Delta y)^3 \\
&+ \frac{3}{3!}\left(\frac{\partial^3 \vartheta_{t\to T_N}}{\partial y^2 \partial x}\right)_{(x,y)=(x_0,y_0)}\Delta x\,\mathbb{E}^*_{T_1}(\Delta y)^2 \\
&+ \frac{1}{4!}\left(\frac{\partial^4 \vartheta_{t\to T_N}}{\partial x^4}\right)_{x=x_0}(\Delta x)^4 + \frac{1}{4!}\left(\frac{\partial^4 \vartheta_{t\to T_N}}{\partial y^4}\right)_{y=y_0}\mathbb{E}^*_{T_1}(\Delta y)^4 \\
&+ \frac{4}{4!}\left(\frac{\partial^4 \vartheta_{t\to T_N}}{\partial y^3 \partial x}\right)_{(x,y)=(x_0,y_0)}(\Delta x)\,\mathbb{E}^*_{T_1}(\Delta y)^3 \\
&+ \frac{6}{4!}\left(\frac{\partial^4 \vartheta_{t\to T_N}}{\partial x^2 \partial y^2}\right)_{(x,y)=(x_0,y_0)}(\Delta x)^2\mathbb{E}^*_{T_1}(\Delta y)^2.
\end{aligned}
$$

Observe that (details are provided in the Online Appendix OA.5)

$$
\left(\frac{\partial \vartheta_{t\to T_N}}{\partial x}\right)_{x=x_0} = \frac{1}{x_0}\frac{1}{\tau_t},
$$

$$
\left(\frac{\partial \vartheta_{t\to T_N}}{\partial y}\right)_{y=y_0} = \frac{1}{y_0}\frac{1}{\tau_t},
$$

$$
\begin{aligned}
\left(\frac{\partial^2 \vartheta_{t\to T_N}}{\partial^2 x}\right)_{x=x_0} &= \frac{2\,(1-\rho_t)}{\tau_t^2 x_0^2}, \\
\left(\frac{\partial^2 \vartheta_{t\to T_N}}{\partial^2 y}\right)_{x=x_0} &= \frac{2\,(1-\rho_t)}{\tau_t^2 y_0^2}, \\
\left(\frac{\partial^3 \vartheta_{t\to T_N}}{\partial^3 x}\right)_{x=x_0} &= \frac{6\kappa_t + 6 - 12\rho_t}{\tau_t^3 x_0^3}, \\
\left(\frac{\partial^3 \vartheta_{t\to T_N}}{\partial^3 y}\right)_{y=x_0} &= \frac{6\kappa_t + 6 - 12\rho_t}{\tau_t^3 y_0^3},
\end{aligned}
$$

$$\left(\frac{\partial^3\vartheta_{t\to T_N}}{\partial^2 y\partial x}\right)_{y=x_0} = \frac{4\left(1-\rho_t\right)}{\tau_t^2 x_0 y_0^2}+\frac{6\left(\kappa_t+1-2\rho_t\right)}{\tau_t^3 x_0 y_0^2},$$

$$\frac{1}{24}\left(\frac{\partial^4\vartheta_{t\to T_N}}{\partial^4 x}\right)_{x=x_0} = \frac{\rho_t^2-3\rho_t+1+2\kappa_t-\xi_t}{\tau_t^4 x_0^4},$$

$$\left(\frac{\partial^4\vartheta_{t\to T_N}}{\partial^2 y\partial^2 x}\right)_{(x,y)=(x_0,y_0)} = \frac{4\left(1-\rho_t\right)}{\tau_t^2 x_0^2 y_0^2}+\frac{24\left(\kappa_t-2\rho_t+1\right)}{\tau_t^3 x_0^2 y_0^2}+\frac{24\left(2\kappa_t-\xi_t+\rho_t^2-3\rho_t+1\right)}{\tau_t^4 x_0^2 y_0^2},$$

$$\begin{aligned}\left(\frac{\partial^4\vartheta_{t\to T_N}}{\partial^3 y\partial x}\right)_{(x,y)=(x_0,y_0)} &= \frac{18-36\rho_t}{\tau_t^3 x_0 y_0^3}+\frac{18\kappa_t+48\kappa_t-24\xi_t+24\rho_t^2-72\rho_t+24}{\tau_t^4 x_0 y_0^3}\\ &= \frac{6}{x_0 y_0^3}\left\{3a_{3,t}+3\left(1-2\frac{a_{2,t}}{a_{1,t}^2}+a_{3,t}\right)\left(a_{1,t}-1\right)+4a_{4.t}\right\}.\end{aligned}$$

Hence

$$\begin{aligned}\upsilon_{t\to T_1} &= \mathbb{E}^*_{T_1}\frac{u'\left[W_t x_0 y_0\right]}{u'\left[W_t x y\right]}\\ &= 1+\frac{1}{R_{f,t\to T_1}}a_{1,t}\Delta x+\frac{a_{2,t}}{R^2_{f,t\to T_1}}\left(\Delta x\right)^2+\frac{a_{2,t}}{R^2_{f,T_1\to T_N}}\mathbb{E}^*_{T_1}\left(\Delta y\right)^2\\ &\quad+\frac{a_{3,t}}{R^3_{f,t\to T_1}}\left(\Delta x\right)^3+\frac{a_{3,t}}{R^3_{f,T_1\to T_N}}\mathbb{E}^*_{T_1}\left(\Delta y\right)^3+\frac{a_{5,t}}{R_{f,t\to T_1}R^2_{f,T_1\to T_N}}\Delta x\mathbb{E}^*_{T_1}\left(\Delta y\right)^2\\ &\quad+\frac{a_{4,t}}{R^4_{f,t\to T_1}}\left(\Delta x\right)^4+\frac{a_{4,t}}{R^4_{f,T_1\to T_N}}\mathbb{E}^*_{T_1}\left(\Delta y\right)^4+\frac{a_{6,t}}{R_{f,t\to T_1}R^3_{f,T_1\to T_N}}\left(\Delta x\right)\mathbb{E}^*_{T_1}\left(\Delta y\right)^3\\ &\quad+\frac{a_{7,t}}{R^2_{f,t\to T_1}R^2_{f,T_1\to T_N}}\left(\Delta x\right)^2\mathbb{E}^*_{T_1}\left(\Delta y\right)^2.\end{aligned}$$

This ends the proof. □

Proof of Proposition 2.4. Consider $\vartheta_{t\to T_N}$ defined in (OA.1.3). A $\mathcal{K}$ order ($\mathcal{K}$ can be finite or infinite) Taylor expansion-series of $\vartheta_{t\to T_N}$ around $\left(\mathcal{R}_{M,t\to T_1},\mathcal{R}_{M,T_1\to T_N}\right)=(0,0)$ yields

$$\upsilon_{t\to T_1}=1+\sum_{k=1}^{\infty}\sum_{j=0}^{k}\frac{a_{j,k-j,t}}{R^j_{f,t\to T_1}R^{k-j}_{f,T_1\to T_N}}f^{(j,k-j)}_{T_1}, \tag{OA.1.5}$$

with

$$f^{(j,k-j)}_{T_1}=\mathcal{R}^j_{M,t\to T_1}\mathbb{E}^*_t\mathcal{R}^{k-j}_{M,t\to T_1}.$$

Replace the inverse SDF

$$\frac{\mathbb{E}_t m_{t\to T_1}}{m_{t\to T_1}} = \frac{\upsilon_{t\to T_1}}{\mathbb{E}_t^* \upsilon_{t\to T_1}} \tag{OA.1.6}$$

in (2.1), it follows that the expected excess return is

$$\mathbb{E}_t\left(R_{M,t\to T_1} - R_{f,t\to T_1}\right) = \frac{\sum_{k=1}^{\infty}\sum_{j=0}^{k} \frac{a_{j,k-j,t}}{R^j_{f,t\to T_1} R^{k-j}_{f,T_1\to T_N}} \mathbb{COV}_t^*\left(f_{T_1}^{(j,k-j)}, R_{M,t\to T_1}\right)}{1 + \sum_{k=1}^{\infty}\sum_{j=0}^{k} \frac{a_{j,k-j,t}}{R^j_{f,t\to T_1} R^{k-j}_{f,T_1\to T_N}} \mathbb{E}_t^* f_{T_1}^{(j,k-j)}}.$$

By definition, $\upsilon_{t\to T_1}$ is positive, thus, its expectation is also positive:

$$1 + \sum_{k=1}^{\infty}\sum_{j=0}^{k} \frac{a_{j,k-j,t}}{R^j_{f,t\to T_1} R^{k-j}_{f,T_1\to T_N}} \mathbb{E}_t^* f_{T_1}^{(j,k-j)} \geq 0.$$

Thus,

$$\lim_{\mathcal{K}\to\infty} \sum_{\substack{j_1,j_2=0 \\ j_1+j_2\leq\mathcal{K}}}^{\mathcal{K}} \frac{a_{j_1,j_2,t}}{R^{j_1}_{f,t\to T_1} R^{j_2}_{f,T_1\to T_N}} \mathbb{E}_t^*\left[\mathcal{R}^{j_1}_{M,t\to T_1} \mathbb{E}^*_{T_1} \mathcal{R}^{j_2}_{M,T_1\to T_N}\right] \geq 0.$$

Notice that each term of the numerator above is a risk premium which by definition is compensation for an exposure to $\mathcal{R}^{j_1}_{M,t\to T_1} \mathbb{E}^*_{T_1} \mathcal{R}^{j_2}_{M,T_1\to T_N}$. It is viewed as a price of risk $\frac{a_{j_1,j_2,t}}{R^{j_1}_{f,t\to T_1} R^{j_2}_{f,T_1\to T_N}}$ times the quantity of risk $\mathbb{COV}_t^*\left[\mathcal{R}_{i,t\to T_1}, \mathcal{R}^{j_1}_{M,t\to T_1} \mathbb{E}^*_{T_1} \mathcal{R}^{j_2}_{M,T_1\to T_N}\right]$. According to economic theory, the risk premium is positive. As a result

$$\begin{aligned}
\mathbb{E}_t\left(R_{M,t\to T_1} - R_{f,t\to T_1}\right) &\geq \frac{\sum_{k=1}^{\infty}\sum_{j=0}^{\mathcal{K}} \frac{a_{j,k-j,t}}{R^j_{f,t\to T_1} R^{k-j}_{f,T_1\to T_N}} \mathbb{COV}_t^*\left(f_{T_1}^{(j,k-j)}, R_{M,t\to T_1}\right)}{1 + \sum_{k=1}^{\infty}\sum_{j=0}^{k} \frac{a_{j,k-j,t}}{R^j_{f,t\to T_1} R^{k-j}_{f,T_1\to T_N}} \mathbb{E}_t^* f_{T_1}^{(j,k-j)}} \\
&\geq \frac{\sum_{k=1}^{\infty}\sum_{j=0}^{\mathcal{K}} \frac{a_{j,k-j,t}}{R^j_{f,t\to T_1} R^{k-j}_{f,T_1\to T_N}} \mathbb{COV}_t^*\left(f_{T_1}^{(j,k-j)}, R_{M,t\to T_1}\right)}{1 + \sum_{k=1}^{\infty}\sum_{j=0}^{\mathcal{K}} \frac{a_{j,k-j,t}}{R^j_{f,t\to T_1} R^{k-j}_{f,T_1\to T_N}} \mathbb{E}_t^* f_{T_1}^{(j,k-j)}} \\
&\quad \times \frac{1 + \sum_{k=1}^{\infty}\sum_{j=0}^{\mathcal{K}} \frac{a_{j,k-j,t}}{R^j_{f,t\to T_1} R^{k-j}_{f,T_1\to T_N}} \mathbb{E}_t^* f_{T_1}^{(j,k-j)}}{1 + \sum_{k=1}^{\infty}\sum_{j=0}^{k} \frac{a_{j,k-j,t}}{R^j_{f,t\to T_1} R^{k-j}_{f,T_1\to T_N}} \mathbb{E}_t^* f_{T_1}^{(j,k-j)}}.
\end{aligned}$$

Provided that

$$a_{j_1,j_2,t}\mathbb{E}_t^*\left[\mathcal{R}_{M,t\to T_1}^{j_1}\mathbb{E}_{T_1}^*\mathcal{R}_{M,T_1\to T_N}^{j_2}\right]\leq 0,$$

it follows that

$$\frac{1+\sum_{k=1}^{\infty}\sum_{j=0}^{\mathcal{K}}\frac{a_{j,k-j,t}}{R_{f,t\to T_1}^{j}R_{f,T_1\to T_N}^{k-j}}\mathbb{E}_t^*f_{T_1}^{(j,k-j)}}{1+\sum_{k=1}^{\infty}\sum_{j=0}^{k}\frac{a_{j,k-j,t}}{R_{f,t\to T_1}^{j}R_{f,T_1\to T_N}^{k-j}}\mathbb{E}_t^*f_{T_1}^{(j,k-j)}}\geq 1$$

and hence

$$\mathbb{E}_t\left(R_{M,t\to T_1}-R_{f,t\to T_1}\right)\geq\frac{\sum_{k=1}^{\infty}\sum_{j=0}^{\mathcal{K}}\frac{a_{j,k-j,t}}{R_{f,t\to T_1}^{j}R_{f,T_1\to T_N}^{k-j}}\mathbb{COV}_t^*\left(f_{T_1}^{(j,k-j)},R_{M,t\to T_1}\right)}{1+\sum_{k=1}^{\infty}\sum_{j=0}^{\mathcal{K}}\frac{a_{j,k-j,t}}{R_{f,t\to T_1}^{j}R_{f,T_1\to T_N}^{k-j}}\mathbb{E}_t^*f_{T_1}^{(j,k-j)}}.$$

We follow a similar approach as in Proposition 2.1 to derive the proof of (2.42). □

Proof of Proposition 2.5. Before we provide expressions for $\mathcal{M}_{i,M,t}^{(j,k-j)}$ and $\mathcal{M}_{i,M,t}^{(j,k-j)}[k_0]$, we provide closed-form expressions of the risk neutral quantities in $\theta_{l,t}^*$

$$\begin{aligned}H^{(j,l)}\left[S_{T_1}\right] &= R_{M,t\to T_1}^{j}\left(R_{M,t\to T_1}^{l}-R_{f,t\to T_1}^{l}\right)\\ &= \left(\frac{S_{T_1}}{S_t}\right)^{j}\left(\left(\frac{S_{T_1}}{S_t}\right)^{l}-R_{f,t\to T_1}^{l}\right),\ l\neq\{0,1\},\end{aligned}$$

where

$$\begin{aligned}\mathbb{E}_t^*\left[H^{(i,j)}\left[S_{T_1}\right]1_{S_{T_1}<S_tR_{f,t\to T_1}}\right] &= -R_{f,t\to T_1}H_S^{(i,j)}\left[S_tR_{f,t\to T_1}\right]P_t\left[S_tR_{f,t\to T_1}\right]\\ &\quad+R_{f,t\to T_1}\int_0^{S_tR_{f,t\to T_1}}H_{SS}^{(i,j)}\left[K\right]P_t\left[K\right]dK\end{aligned} \quad \text{(OA.1.7)}$$

and

$$\begin{aligned}\mathbb{E}_t^*\left[H^{(i,j)}\left[S_{T_1}\right]1_{S_{T_1}>S_tR_{f,t\to T_1}}\right] &= R_{f,t\to T_1}H_S^{(i,j)}\left[S_tR_{f,t\to T_1}\right]C_t\left[S_tR_{f,t\to T_1}\right]\\ &\quad+R_{f,t\to T_1}\int_{S_tR_{f,t\to T_1}}^{\infty}H_{SS}^{(i,j)}\left[K\right]C_t\left[K\right]dK.\end{aligned} \quad \text{(OA.1.8)}$$

Next, we focus on providing expressions for $\mathcal{M}_{i,M,t}^{(j,k-j)}$ and $\mathcal{M}_{i,M,t}^{(j,k-j)}[k_0]$. When $k-j=1$,

$$\mathcal{M}_{i,M,t}^{(j,1)} = \mathbb{E}_t^*\left[\mathcal{R}_{i,t\to T_1} f_{T_1}^{(j,1)}\right] = 0,$$

with

$$f_{T_1}^{(j,1)} = \mathcal{R}_{M,t\to T_1}^{j}\mathbb{E}_{T_1}^*\mathcal{R}_{M,T_1\to T_N} = 0.$$

Similarly

$$\mathcal{M}_{i,M,t}^{(j,1)}[k_0] = 0.$$

When $k-j=0$, $\mathcal{M}_{i,M,t}^{(j,0)} = \mathcal{M}_{i,M,t}^{(j)}$:

$$\mathcal{M}_{i,M,t}^{(j,0)} = \mathbb{E}_t^*\left[\mathcal{R}_{i,t\to T_1} f_{T_1}^{(j,0)}\right],$$

with

$$f_{T_1}^{(j,0)} = \mathcal{R}_{M,t\to T_1}^{j}\mathbb{E}_{T_1}^*\mathcal{R}_{M,T_1\to T_N}^{0} = \mathcal{R}_{M,t\to T_1}^{j}.$$

Thus

$$\mathcal{M}_{i,M,t}^{(j,0)} = \mathbb{E}_t^*\left[\mathcal{R}_{i,t\to T_1}\mathcal{R}_{M,t\to T_1}^{j}\right] = \mathcal{M}_{i,M,t}^{(j)}.$$

Similarly

$$\mathcal{M}_{i,M,t}^{(j,0)}[k_0] = \mathcal{M}_{i,M,t}^{(j)}[k_0].$$

Our goal is to compute $\mathcal{M}_{i,M,t}^{(j,k-j)}$ and $\mathcal{M}_{i,M,t}^{(j,k-j)}[k_0]$ when $k-j\neq\{0,1\}$ Notice that

$$\mathcal{M}_{i,M,t}^{(j,k-j)} = \mathbb{E}_t^*\left[\mathcal{R}_{i,t\to T_1} f_{T_1}^{(j,k-j)}\right],$$

with

$$f_{T_1}^{(j,k-j)} = \mathcal{R}_{M,t\to T_1}^{j}\mathbb{E}_{T_1}^*\mathcal{R}_{M,T_1\to T_N}^{k-j}.$$

That is

$$\begin{aligned}
\mathcal{M}_{i,M,t}^{(j,k-j)} &= \mathbb{E}_t^*\left[\mathcal{R}_{i,t\to T_1}\mathcal{R}_{M,t\to T_1}^{j}\mathbb{E}_{T_1}^*\mathcal{R}_{M,T_1\to T_N}^{k-j}\right] \\
&= \mathbb{E}_t^*\left[\mathcal{R}_{M,t\to T_1}^{j}\mathbb{E}_{T_1}^*\mathcal{R}_{M,T_1\to T_N}^{k-j} g_i\left[\mathcal{R}_{M,t\to T_1}\right]\right], \qquad \text{(OA.1.9)}
\end{aligned}$$

where

$$g_i\left[\mathcal{R}_{M,t\to T_1}\right] = \mathbb{E}_t^*\left[\mathcal{R}_{i,t\to T_1}|\mathcal{R}_{M,t\to T_1}\right]$$

is given in our Eq.(2.17):

$$g_i\left[\mathcal{R}_{M,t\to T_1}\right] = \sum_{q=1}^{\mathcal{N}}\underline{\gamma}_{i,q}\mathcal{R}_{M,t\to T_1}^{q}.$$

Hence,

$$\mathcal{M}_{i,M,t}^{(j,k-j)} = \sum_{q=1}^{\mathcal{N}} \underline{\gamma}_{i,q} \mathbb{E}_t^* \left[\mathcal{R}_{M,t\to T_1}^{j+q} \left(\mathbb{E}_{T_1}^* \mathcal{R}_{M,T_1\to T_N}^{k-j} \right) \right]. \tag{OA.1.10}$$

We then replace $\mathbb{E}_{T_1}^* \mathcal{R}_{M,T_1\to T_N}^{k-j}$ by using expression

$$\mathbb{E}_{T_1}^* \mathcal{R}_{M,T_1\to T_N}^{j_2} = \sum_{l=2}^{j_2} \phi_{j_2,l} \left(\mathbb{E}_{T_1}^* R_{M,T_1\to T_N}^l - R_{f,T_1\to T_N}^l \right),$$

where

$$\mathbb{E}_{T_1}^* R_{M,T_1\to T_N}^l - R_{f,T_1\to T_N}^l = \theta_{l,t}^* \left\{ \begin{array}{c} \left(R_{M,t\to T_1}^l - R_{f,t\to T_1}^l \right) 1_{R_{M,t\to T_1} > R_{f,t\to T_1}} \\ + \left(R_{f,t\to T_1}^l - R_{M,t\to T_1}^l \right) 1_{R_{M,t\to T_1} < R_{f,t\to T_1}} \end{array} \right\}. \tag{OA.1.11}$$

Therefore,

$$\begin{aligned} \mathbb{E}_{T_1}^* \mathcal{R}_{M,T_1\to T_N}^{j_2} &= \sum_{l=2}^{j_2} \phi_{j_2,l} \theta_{l,t}^* \left\{ \begin{array}{c} \left(R_{M,t\to T_1}^l - R_{f,t\to T_1}^l \right) 1_{R_{M,t\to T_1} > R_{f,t\to T_1}} \\ + \left(R_{f,t\to T_1}^l - R_{M,t\to T_1}^l \right) 1_{R_{M,t\to T_1} < R_{f,t\to T_1}} \end{array} \right\} \\ &= \sum_{l=2}^{j_2} \phi_{j_2,l} \theta_{l,t}^* \left(R_{M,t\to T_1}^l - R_{f,t\to T_1}^l \right) 1_{R_{M,t\to T_1} > R_{f,t\to T_1}} \\ &\quad + \sum_{l=2}^{j_2} \phi_{j_2,l} \theta_{l,t}^* \left(R_{f,t\to T_1}^l - R_{M,t\to T_1}^l \right) 1_{R_{M,t\to T_1} < R_{f,t\to T_1}}. \end{aligned} \tag{OA.1.12}$$

Setting $j_2 = k - j$, it follows that

$$\begin{aligned} \mathcal{M}_{i,M,t}^{(j,k-j)} &= \sum_{q=1}^{\mathcal{N}} \underline{\gamma}_{i,q} \sum_{l=2}^{k-j} \phi_{k-j,l} \theta_{l,t}^* \mathbb{E}_t^* \left[\mathcal{R}_{M,t\to T_1}^{j+q} \left(R_{M,t\to T_1}^l - R_{f,t\to T_1}^l \right) 1_{R_{M,t\to T_1} > R_{f,t\to T_1}} \right] \\ &\quad - \sum_{q=1}^{\mathcal{N}} \underline{\gamma}_{i,q} \sum_{l=2}^{k-j} \phi_{k-j,l} \theta_{l,t}^* \mathbb{E}_t^* \left[\mathcal{R}_{M,t\to T_1}^{j+q} \left(R_{M,t\to T_1}^l - R_{f,t\to T_1}^l \right) 1_{R_{M,t\to T_1} < R_{f,t\to T_1}} \right] \end{aligned} \tag{OA.1.13}$$

Set

$$\begin{aligned} G^{(j,l)} \left[S_{T_1} \right] &= \mathcal{R}_{M,t\to T_1}^j \left(R_{M,t\to T_1}^l - R_{f,t\to T_1}^l \right) \\ &= \left(\frac{S_{T_1}}{S_t} - R_{f,t\to T_1} \right)^j \left(\left(\frac{S_{T_1}}{S_t} \right)^l - R_{f,t\to T_1}^l \right) \; l \neq \{0,1\}. \end{aligned} \tag{OA.1.14}$$

Thus

$$\begin{aligned}\mathcal{M}_{i,M,t}^{(j,k-j)} = & \sum_{q=1}^{\mathcal{N}} \underline{\gamma}_{i,q} \sum_{l=2}^{k-j} \phi_{k-j,l} \theta_{l,t}^{*} \mathbb{E}_t^{*} \left[G^{(j+q,l)} \left[S_{T_1} \right] 1_{R_{M,t\to T_1} > R_{f,t\to T_1}} \right] \\ & - \sum_{q=1}^{\mathcal{N}} \underline{\gamma}_{i,q} \sum_{l=2}^{k-j} \phi_{k-j,l} \theta_{l,t}^{*} \mathbb{E}_t^{*} \left[G^{(j+q,l)} \left[S_{T_1} \right] 1_{R_{M,t\to T_1} < R_{f,t\to T_1}} \right].\end{aligned} \tag{OA.1.15}$$

where

$$\begin{aligned}\mathbb{E}_t^{*} \left[G^{(i,j)} \left[S_{T_1} \right] 1_{S_{T_1} < S_t R_{f,t\to T_1}} \right] & = -R_{f,t\to T_1} G_S^{(i,j)} \left[S_t R_{f,t\to T_1} \right] P_t \left[S_t R_{f,t\to T_1} \right] \\ & \quad + R_{f,t\to T_1} \int_0^{S_t R_{f,t\to T_1}} G_{SS}^{(i,)} \left[K \right] P_t \left[K \right] dK\end{aligned} \tag{OA.1.16}$$

and

$$\begin{aligned}\mathbb{E}_t^{*} \left[G^{(i,j)} \left[S_{T_1} \right] 1_{S_{T_1} > S_t R_{f,t\to T_1}} \right] & = R_{f,t\to T_1} G_S^{(i,j)} \left[S_t R_{f,t\to T_1} \right] C_t \left[S_t R_{f,t\to T_1} \right] \\ & \quad + R_{f,t\to T_1} \int_{S_t R_{f,t\to T_1}}^{\infty} G_{SS}^{(i,j)} \left[K \right] C_t \left[K \right] dK.\end{aligned} \tag{OA.1.17}$$

Next, notice that

$$\begin{aligned}\mathcal{M}_{i,M,t}^{(j,k-j)} \left[k_0 \right] & = \mathbb{E}_t^{*} \left[\mathcal{R}_{i,t\to T_1}^{c} \mathcal{R}_{M,t\to T_1}^{j} \mathbb{E}_{T_1}^{*} \mathcal{R}_{M,T_1\to T_N}^{k-j} \right] \\ & = \mathbb{E}_t^{*} \left[\mathcal{R}_{M,t\to T_1}^{j} \mathbb{E}_{T_1}^{*} \mathcal{R}_{M,T_1\to T_N}^{k-j} h_i \left[\mathcal{R}_{M,t\to T_1} \right] \right],\end{aligned} \tag{OA.1.18}$$

with

$$h_i \left[\mathcal{R}_{M,t\to T_1} \right] = \mathbb{E}_t^{*} \left[\mathcal{R}_{i,t\to T_1}^{c} | \mathcal{R}_{M,t\to T_1} \right]$$

given in Eq. (2.24):

$$h_i \left[\mathcal{R}_{M,t\to T_1} \right] = \sum_{q=1}^{\mathcal{N}} \overline{\gamma}_{i,q} \mathcal{R}_{M,t\to T_1}^{q}.$$

Hence

$$\begin{aligned}\mathcal{M}_{i,M,t}^{(j,k-j)}[k_0] &= \mathbb{E}_t^*\left[\mathcal{R}_{i,t\to T_1}^c \mathcal{R}_{M,t\to T_1}^j \mathbb{E}_{T_1}^* \mathcal{R}_{M,T_1\to T_N}^{k-j}\right] \\ &= \mathbb{E}_t^*\left[\mathcal{R}_{M,t\to T_1}^j \mathbb{E}_{T_1}^* \mathcal{R}_{M,T_1\to T_N}^{k-j} h_i\left[\mathcal{R}_{M,t\to T_1}\right]\right] \\ &= \sum_{q=1}^{\mathcal{N}} \overline{\gamma}_{i,q} \mathbb{E}_t^*\left[\mathcal{R}_{M,t\to T_1}^{j+q}\left(\mathbb{E}_{T_1}^* \mathcal{R}_{M,T_1\to T_N}^{k-j}\right)\right]. \qquad \text{(OA.1.19)}\end{aligned}$$

Let's replace $\mathbb{E}_{T_1}^* \mathcal{R}_{M,T_1\to T_N}^{k-j}$ by its expression, it follows that

$$\begin{aligned}\mathcal{M}_{i,M,t}^{(j,k-j)}[k_0] &= \sum_{q=1}^{\mathcal{N}} \overline{\gamma}_{i,q} \sum_{l=2}^{k-j} \phi_{k-j,l} \theta_{l,t}^* \mathbb{E}_t^*\left[\mathcal{R}_{M,t\to T_1}^{j+q}\left(R_{M,t\to T_1}^l - R_{f,t\to T_1}^l\right) 1_{R_{M,t\to T_1} > R_{f,t\to T_1}}\right] \\ &\quad - \sum_{q=1}^{\mathcal{N}} \overline{\gamma}_{i,q} \sum_{l=2}^{k-j} \phi_{k-j,l} \theta_{l,t}^* \mathbb{E}_t^*\left[\mathcal{R}_{M,t\to T_1}^{j+q}\left(R_{M,t\to T_1}^l - R_{f,t\to T_1}^l\right) 1_{R_{M,t\to T_1} < R_{f,t\to T_1}}\right] \qquad \text{(OA.1.20)}\end{aligned}$$

Using (OA.1.11), it follows that

$$\begin{aligned}\mathcal{M}_{i,M,t}^{(j,k-j)}[k_0] &= \sum_{q=1}^{\mathcal{N}} \overline{\gamma}_{i,q} \sum_{l=2}^{k-j} \phi_{k-j,l} \theta_{l,t}^* \mathbb{E}_t^*\left[G^{(j+q,l)}\left[S_{T_1}\right] 1_{R_{M,t\to T_1} > R_{f,t\to T_1}}\right] \\ &\quad - \sum_{q=1}^{\mathcal{N}} \overline{\gamma}_{i,q} \sum_{l=2}^{k-j} \phi_{k-j,l} \theta_{l,t}^* \mathbb{E}_t^*\left[G^{(j+q,l)}\left[S_{T_1}\right] 1_{R_{M,t\to T_1} < R_{f,t\to T_1}}\right] \qquad \text{(OA.1.21)}\end{aligned}$$

Our next goal is to compute $\mathbb{E}_t^* f_{T_1}^{(j,k-j)}$, observe that

$$f_{T_1}^{(j,k-j)} = \mathcal{R}_{M,t\to T_1}^j \mathbb{E}_{T_1}^* \mathcal{R}_{M,T_1\to T_N}^{k-j}.$$

Computing

$$\mathbb{E}_t^* f_{T_1}^{(j,k-j)} = \mathbb{E}_t^*\left(\mathcal{R}_{M,t\to T_1}^j \mathbb{E}_{T_1}^* \mathcal{R}_{M,T_1\to T_N}^{k-j}\right)$$

- When $k - j = 0$

$$\mathbb{E}_t^* f_{T_1}^{(j,0)} = \mathbb{E}_t^*\left(\mathcal{R}_{M,t\to T_1}^j \mathbb{E}_{T_1}^* \mathcal{R}_{M,T_1\to T_N}^0\right) = \mathbb{E}_t^* \mathcal{R}_{M,t\to T_1}^j.$$

- When $k-j=1$

$$\begin{aligned}\mathbb{E}_t^* f_{T_1}^{(j,1)} &= \mathbb{E}_t^* \left(\mathcal{R}_{M,t\to T_1}^{j} \mathbb{E}_{T_1}^* \mathcal{R}_{M,T_1\to T_N}\right)\\ &= \mathbb{E}_t^* \left(\mathcal{R}_{M,t\to T_1}^{j} 0\right)\\ &= 0.\end{aligned}$$

Now, let's find $\mathbb{E}_t^* f_{T_1}^{(j,k-j)}$ when $k-j\neq\{0,1\}$:

$$\begin{aligned}\mathbb{E}_t^* f_{T_1}^{(j,k-j)} &= \mathbb{E}_t^* \left(\mathcal{R}_{M,t\to T_1}^{j} \mathbb{E}_{T_1}^* \mathcal{R}_{M,T_1\to T_N}^{k-j}\right)\\ &= \mathbb{E}_t^* \left(\mathcal{R}_{M,t\to T_1}^{j} \left(\begin{array}{c} \sum_{l=2}^{k-j} \phi_{k-j,l}\theta_{l,t}^* \left(R_{M,t\to T_1}^{l} - R_{f,t\to T_1}^{l}\right) 1_{R_{M,t\to T_1} > R_{f,t\to T_1}} \\ + \sum_{l=2}^{k-j} \phi_{k-j,l}\theta_{l,t}^* \left(R_{f,t\to T_1}^{l} - R_{M,t\to T_1}^{l}\right) 1_{R_{M,t\to T_1} < R_{f,t\to T_1}} \end{array}\right)\right)\\ &= \sum_{l=2}^{k-j} \phi_{k-j,l}\theta_{l,t}^* \mathbb{E}_t^* \left(\mathcal{R}_{M,t\to T_1}^{j} \left(R_{M,t\to T_1}^{l} - R_{f,t\to T_1}^{l}\right) 1_{R_{M,t\to T_1} > R_{f,t\to T_1}}\right)\\ &\quad - \sum_{l=2}^{k-j} \phi_{k-j,l}\theta_{l,t}^* \mathbb{E}_t^* \left(\mathcal{R}_{M,t\to T_1}^{j} \left(R_{M,t\to T_1}^{l} - R_{f,t\to T_1}^{l}\right) 1_{R_{M,t\to T_1} < R_{f,t\to T_1}}\right)\\ &= \sum_{l=2}^{k-j} \phi_{k-j,l}\theta_{l,t}^* \mathbb{E}_t^* \left[G^{(j,l)}\left[S_{T_1}\right] 1_{S_{T_1} > S_t R_{f,t\to T_1}}\right]\\ &\quad - \sum_{l=2}^{k-j} \phi_{k-j,l}\theta_{l,t}^* \mathbb{E}_t^* \left[G^{(j,l)}\left[S_{T_1}\right] 1_{S_{T_1} < S_t R_{f,t\to T_1}}\right]. \end{aligned} \tag{OA.1.22}$$

□

OA.2 Interpretation of the Inverse SDF

OA.2.1 Interpretation of the Inverse SDF (2.2)

We apply the Carr and Madan (2001) spanning formula to $\mathcal{R}^j_{M,t\to T_1}$, $j > 1$:

$$\mathcal{R}^j_{M,t\to T_1} = \frac{j(j-1)}{S_t^2}\left\{\begin{aligned}&\int_{S_t R_{f,t\to T_1}}^{\infty}\left(\frac{K}{S_t} - R_{f,t\to T_1}\right)^{j-2}(S_{T_1}-K)^+\,dK\\&+\int_0^{S_t R_{f,t\to T_1}}\left(\frac{K}{S_t} - R_{f,t\to T_1}\right)^{j-2}(K-S_{T_1})^+\,dK\end{aligned}\right\}.$$

Substituting into (2.5) becomes

$$\upsilon_{t\to T_1} = 1 + \sum_{j=1}^{\mathcal{K}}\frac{a_{j,t}}{R^j_{f,t\to T_1}}\frac{j(j-1)}{S_t^2}\left\{\begin{aligned}&\int_{S_t R_{f,t\to T_1}}^{\infty}\left(\frac{K}{S_t} - R_{f,t\to T_1}\right)^{j-2}(S_{T_1}-K)^+\,dK\\&+\int_0^{S_t R_{f,t\to T_1}}\left(\frac{K}{S_t} - R_{f,t\to T_1}\right)^{j-2}(K-S_{T_1})^+\,dK\end{aligned}\right\}.$$

Since $\mathbb{E}^*_t\upsilon_{t\to T_1}$ is constant at time t, the inverse SDF

$$\frac{\mathbb{E}_t m_{t\to T_1}}{m_{t\to T_1}} = \frac{\upsilon_{t\to T_1}}{\mathbb{E}^*_t\upsilon_{t\to T_1}}$$

is the payoff of a portfolio holding the market return and a continuum of options maturing at T_1.

OA.2.2 Interpretation of the Inverse SDF (2.31)

This appendix shows that the inverse SDF in (2.31) admits an equivalent option-spanning representation. By the Carr–Madan spanning result, each basis function entering the inverse SDF can be represented using the market asset together with a continuum of European call and put options. When $k - j = 0$, we have

$$f^{(j,k-j)}_{T_1} = \mathcal{R}^j_{M,t\to T_1} = \left(\frac{S_{T_1}}{S_t} - R_{f,t\to T_1}\right)^j.$$

For $j > 1$, the Carr–Madan spanning formula gives

$$f_{T_1}^{(j,k-j)} = \frac{j(j-1)}{S_t^2} \left\{ \begin{aligned} &\int_{S_t R_{f,t\to T_1}}^{\infty} \left(\frac{K}{S_t} - R_{f,t\to T_1}\right)^{j-2} (S_{T_1} - K)^+ \, dK \\ &+ \int_0^{S_t R_{f,t\to T_1}} \left(\frac{K}{S_t} - R_{f,t\to T_1}\right)^{j-2} (K - S_{T_1})^+ \, dK \end{aligned} \right\}.$$

Thus, the current-period component of the inverse SDF can be represented by the market return and options maturing at T_1. Next consider $k - j > 1$. Applying the Carr and Madan (2001) spanning formula to

$$\mathcal{R}_{M,T_1\to T_N}^{k-j} = \left(\frac{S_{T_N}}{S_{T_1}} - R_{f,T_1\to T_N}\right)^{k-j}$$

yields

$$\mathcal{R}_{M,T_1\to T_N}^{k-j} = \frac{(k-j)(k-j-1)}{S_{T_1}^2} \left\{ \begin{aligned} &\int_{S_{T_1} R_{f,T_1\to T_N}}^{\infty} \left(\frac{K}{S_{T_1}} - R_{f,T_1\to T_N}\right)^{k-j-2} (S_{T_N} - K)^+ \, dK \\ &+ \int_0^{S_{T_1} R_{f,T_1\to T_N}} \left(\frac{K}{S_{T_1}} - R_{f,T_1\to T_N}\right)^{k-j-2} (K - S_{T_N})^+ \, dK \end{aligned} \right\}.$$

Taking the time-T_1 risk-neutral expectation gives

$$\mathbb{E}_{T_1}^* \mathcal{R}_{M,T_1\to T_N}^{k-j} = (k-j)(k-j-1) R_{f,T_1\to T_N} \left\{ \begin{aligned} &\int_{R_{f,T_1\to T_N}}^{\infty} (K - R_{f,T_1\to T_N})^{k-j-2} \frac{C_{T_1}[K]}{S_{T_1}} \, dK \\ &+ \int_0^{R_{f,T_1\to T_N}} (K - R_{f,T_1\to T_N})^{k-j-2} \frac{P_{T_1}[K]}{S_{T_1}} \, dK \end{aligned} \right\}.$$

Thus, when $j = 0$ and $k - j \geq 2$, the factor

$$f_{T_1}^{(j,k-j)} = \mathbb{E}_{T_1}^* \mathcal{R}_{M,T_1\to T_N}^{k-j}$$

is represented by the time-T_1 value of a continuum of options maturing at T_N, that is, by T_N-maturity options unwound at T_1. Finally, when both $j > 0$ and $k - j > 0$, the basis function is

$$f_{T_1}^{(j,k-j)} = \mathcal{R}_{M,t\to T_1}^{j} \mathbb{E}_{T_1}^* \mathcal{R}_{M,T_1\to T_N}^{k-j}.$$

This product is a nonlinear function of S_{T_1} and therefore admits the same Carr–Madan option-spanning representation in terms of the market asset and options maturing at T_1, with the second component reflecting the time-T_1 value of T_N-maturity options. Taken together, every basis function entering the inverse SDF admits an equivalent option-spanning representation. Consequently, the inverse SDF itself can be represented by a dynamically equivalent portfolio consisting of the market asset and a continuum of European call and put options. The same conclusion follows from the parameterized specification in Eqs. (2.44)–(2.47), which provides an alternative option-based representation of the inverse SDF.

OA.3 Motivation for Assuming that $\mathbb{E}^*_{T_1} R^k_{M,T_1\to T_N} - R^k_{f,T_1\to T_N}$ is a Function of $R_{M,t\to T_1}$

We begin by showing that the right-hand side of (2.47) can be represented as the payoff of a portfolio of options. Using the spanning relations of Carr and Madan (2001), we may write

$$\begin{aligned}\left(R^k_{M,t\to T_1} - R^k_{f,t\to T_1}\right) 1_{R_{M,t\to T_1} > R_{f,t\to T_1}} &= \frac{k}{S_t} R^{k-1}_{f,t\to T_1} \left(S_{T_1} - S_t R_{f,t\to T_1}\right)^+ \\ &\quad + \frac{k\,(k-1)}{S_t^2} \int_{S_t R_{f,t\to T_1}}^{\infty} \left(\frac{K}{S_t}\right)^{k-2} \left(S_{T_1} - K\right)^+ dK\end{aligned}$$

and

$$\begin{aligned}\left(R^k_{f,t\to T_1} - R^k_{M,t\to T_1}\right) 1_{R_{M,t\to T_1} < R_{f,t\to T_1}} &= \frac{k}{S_t} R^{k-1}_{f,t\to T_1} \left(S_t R_{f,t\to T_1} - S_{T_1}\right)^+ \\ &\quad + \frac{k\,(k-1)}{S_t^2} \int_0^{S_t R_{f,t\to T_1}} \left(\frac{K}{S_t}\right)^{k-2} \left(K - S_{T_1}\right)^+ dK.\end{aligned}$$

Combining these expressions yields

$$\begin{aligned}\mathbb{E}^*_{T_1} R^k_{M,T_1\to T_N} - R^k_{f,T_1\to T_N} &= \frac{\theta^*_{k,t} k}{S_t} R^{k-1}_{f,t\to T_1} \left(\left(S_{T_1} - S_t R_{f,t\to T_1}\right)^+ + \left(S_t R_{f,t\to T_1} - S_{T_1}\right)^+\right) \\ &\quad + \frac{\theta^*_{k,t} k\,(k-1)}{S_t^2} \left(\begin{array}{c} \int_{S_t R_{f,t\to T_1}}^{\infty} \left(\frac{K}{S_t}\right)^{k-2} \left(S_{T_1} - K\right)^+ dK \\ + \int_0^{S_t R_{f,t\to T_1}} \left(\frac{K}{S_t}\right)^{k-2} \left(K - S_{T_1}\right)^+ dK \end{array}\right)\end{aligned} \quad \text{(OA.3.1)}$$

Thus, the right-hand side of (OA.3.1) is the payoff of a portfolio of calls and puts with weights proportional to

$$\frac{\theta^*_{k,t} k}{S_t} R^{k-1}_{f,t\to T_1} \quad \text{and} \quad \frac{\theta^*_{k,t} k\,(k-1)}{S_t^2} \left(\frac{K}{S_t}\right)^{k-2},$$

where $\theta^*_{k,t}$ is determined uniquely by the option prices with maturities T_1 and T_N.

Define the payoff

$$H\left[S_{T_N}\right] = R^k_{M,T_1\to T_N} - R^k_{f,T_1\to T_N} = \left(\frac{S_{T_N}}{S_{T_1}}\right)^k - R^k_{f,T_1\to T_N}, \quad k \geq 2.$$

Applying the Carr and Madan (2001) spanning representation around the reference point $S_{T_N} = S_{T_1} R_{f,T_1\to T_N}$ yields

$$\begin{aligned} H\left[S_{T_N}\right] &= H\left[S_{T_1} R_{f,T_1\to T_N}\right] + H_S\left[S_{T_1} R_{f,T_1\to T_N}\right]\left(S_{T_N} - S_{T_1} R_{f,T_1\to T_N}\right) \\ &\quad + \int_{S_{T_1} R_{f,T_1\to T_N}}^{\infty} H_{SS}\left[K\right]\left(S_{T_N} - K\right)^+ \, dK + \int_0^{S_{T_1} R_{f,T_1\to T_N}} H_{SS}\left[K\right]\left(K - S_{T_N}\right)^+ \, dK. \end{aligned}$$

Taking risk-neutral expectations yields

$$\mathbb{E}^*_{T_1} R^k_{M,T_1\to T_N} - R^k_{f,T_1\to T_N} = \frac{k\left(k-1\right) R_{f,T_1\to T_N}}{S^2_{T_1}} \left(\begin{array}{c} \int_{S_{T_1} R_{f,T_1\to T_N}}^{\infty} \left(\frac{K}{S_{T_1}}\right)^{k-2} C_{T_1}\left[K\right] \, dK \\ + \int_0^{S_{T_1} R_{f,T_1\to T_N}} \left(\frac{K}{S_{T_1}}\right)^{k-2} P_{T_1}\left[K\right] \, dK \end{array}\right). \tag{OA.3.2}$$

At time T_1, the volatility surface pins down

$$\mathbb{VAR}^*_{T_1} \log R_{M,T_1\to T_N}, \ K, \ S_{T_1}, \ R_{f,T_1\to T_N}, \ T_N - T_1,$$

which uniquely determine the option prices $C_{T_1}\left[K\right]$ and $P_{T_1}\left[K\right]$. Thus,

$$C_{T_1}\left[K\right] = \pi^{\text{call}}\left[\mathbb{VAR}^*_{T_1} \log R_{M,T_1\to T_N}, K, S_{T_1}, R_{f,T_1\to T_N}, T_N - T_1\right]$$

and

$$P_{T_1}\left[K\right] = \pi^{\text{put}}\left[\mathbb{VAR}^*_{T_1} \log R_{M,T_1\to T_N}, K, S_{T_1}, R_{f,T_1\to T_N}, T_N - T_1\right]$$

for known functions π^{call} and π^{put}.

For the case $k = 2$, (OA.3.2) becomes

$$\begin{aligned} \mathbb{VAR}^*_{T_1} R_{M,T_1\to T_N} = \frac{R_{f,T_1\to T_N}}{S^2_{T_1}} \Bigg(&\int_{S_{T_1} R_{f,T_1\to T_N}}^{\infty} \pi^{\text{call}}\Big[\mathbb{VAR}^*_{T_1} \log R_{M,T_1\to T_N}, K, S_{T_1}, R_{f,T_1\to T_N}, T_N - T_1\Big] \, dK \\ &+ \int_0^{S_{T_1} R_{f,T_1\to T_N}} \pi^{\text{put}}\Big[\mathbb{VAR}^*_{T_1} \log R_{M,T_1\to T_N}, K, S_{T_1}, R_{f,T_1\to T_N}, T_N - T_1\Big] \, dK \Bigg). \end{aligned} \tag{OA.3.3}$$

If $\log R_{M,T_1\to T_N}$ is conditionally lognormal, then

$$\mathbb{VAR}^*_{T_1}\log R_{M,T_1\to T_N} = \log\left(\frac{\mathbb{VAR}^*_{T_1} R_{M,T_1\to T_N}}{R^2_{f,T_1\to T_N}} + 1\right). \tag{OA.3.4}$$

Substituting (OA.3.4) into (OA.3.3) shows that

$$x = \mathbb{VAR}^*_{T_1}\log R_{M,T_1\to T_N}$$

solves the fixed-point equation

$$x = \frac{R_{f,T_1\to T_N}}{S^2_{T_1}}\left(\begin{array}{c} \int_{S_{T_1}R_{f,T_1\to T_N}}^{\infty} \pi^{\text{ call}}\left[\log\left(1+\frac{x}{R^2_{f,T_1\to T_N}}\right), K, S_{T_1}, R_{f,T_1\to T_N}, T_N - T_1\right] dK \\ +\int_0^{S_{T_1}R_{f,T_1\to T_N}} \pi^{\text{put}}\left[\log\left(1+\frac{x}{R^2_{f,T_1\to T_N}}\right), K, S_{T_1}, R_{f,T_1\to T_N}, T_N - T_1\right] dK \end{array}\right).$$

Since the solution must be strictly positive, we may write

$$\mathbb{VAR}^*_{T_1} R_{M,T_1\to T_N} = g\left[S_{T_1}, R_{f,T_1\to T_N}, T_N - T_1\right] > 0.$$

This observation motivates specification (2.47) in the paper, where the parameter $\theta^*_{\ell,t}$ is recovered in a model-free manner. Because $\mathbb{VAR}^*_{T_1} R_{M,T_1\to T_N}$ is a function of S_{T_1}, it follows that $\mathbb{VAR}^*_{T_1}\log R_{M,T_1\to T_N}$ is also a function of S_{T_1}. Consequently, the right-hand side of (OA.3.2) is a function of S_{T_1}. Therefore,

$$\mathbb{E}^*_{T_1} R^k_{M,T_1\to T_N} - R^k_{f,T_1\to T_N} \text{ is a function of } S_{T_1}, \quad k \geq 2.$$

This observation provides the economic and technical motivation for specification (2.47).

OA.4 Alternative Representation of $\mathbb{E}^*_{T_1} R^l_{M,T_1\to T_N} - R^l_{f,T_1\to T_N}$

This section provides an alternative representation of the term

$$\mathbb{E}^*_{T_1} R^l_{M,T_1\to T_N} - R^l_{f,T_1\to T_N}$$

which appears in Equation (2.47) and serves as a robustness check for our bounds. Using the Carr and Madan (2001) spanning formula and applying it to

$$R^l_{M,T_1\to T_N} - R^l_{f,T_1\to T_N}$$

with $R_{M,T_1\to T_N} = S_{T_N}/S_{T_1}$ leads to

$$\begin{aligned}
&\mathbb{E}^*_{T_1} R^l_{M,T_1\to T_N} - R^l_{f,T_1\to T_N} \\
&\quad = \frac{R_{f,T_1\to T_N}\, l(l-1)}{S^2_{T_1}} \left\{ \begin{aligned} &\int_{R_{f,T_1\to T_N} S_{T_1}}^{\infty} \left(\frac{K}{S_{T_1}}\right)^{l-2} C_{T_1}[K]\, dK \\ &\quad + \int_0^{R_{f,T_1\to T_N} S_{T_1}} \left(\frac{K}{S_{T_1}}\right)^{l-2} P_{T_1}[K]\, dK \end{aligned} \right\}, \qquad l \geq 2.
\end{aligned}$$

Here, $C_{T_1}[K]$ and $P_{T_1}[K]$ denote call and put prices observed at time T_1 with maturity T_N written on the market index.

Because we work with the implied-volatility surface, option prices can be expressed as

$$C_{T_1}[K_0] = \mathbb{BS}^c \left[S_{T_1}, \log\left(\frac{K_0}{S_{T_1}}\right), \sigma^*_{T_1}[K_0], R_{f,T_1\to T_N}, T_N - T_1\right] \tag{OA.4.1}$$

and

$$P_{T_1}[K_0] = \mathbb{BS}^p \left[S_{T_1}, \log\left(\frac{K_0}{S_{T_1}}\right), \sigma^*_{T_1}[K_0], R_{f,T_1\to T_N}, T_N - T_1\right] \tag{OA.4.2}$$

where $\mathbb{BS}^c$ and $\mathbb{BS}^p$ denote Black–Scholes call and put prices, respectively, and $\sigma^*_{T_1}[K_0]$ is the implied volatility associated with strike K_0. The volatility surface is parameterized as a function of log-moneyness. We specify

$$\sigma^*_{T_1}[K_0] = \exp\left(\alpha_t \log\left(\frac{S_{T_1}}{S_t}\right) + \sum_{j=0}^{J} d_{j,t}\left(\log\left(\frac{K_0}{S_{T_1}}\right)\right)^j\right),$$

where the coefficients α_t and $d_{j,t}$ are known at time t and must be estimated. To recover these coefficients, note that under the risk-neutral measure,

$$\mathbb{E}^*_t \frac{C_{T_1}[K_0]}{C_t[K_0]} = R_{f,t\to T_1} \quad \text{and} \quad \mathbb{E}^*_t \frac{P_{T_1}[K_0]}{P_t[K_0]} = R_{f,t\to T_1}.$$

Note that $C_t[K_0]$ and $P_t[K_0]$ denote the prices of call and put options that mature at T_N. We then express (OA.4.1) and (OA.4.2) as

$$R_{f,t\to T_1} C_t[K_0] = \mathbb{E}^*_t \mathbb{BS}^c \left[S_{T_1}, \log\left(\frac{K_0}{S_{T_1}}\right), \sigma^*_{T_1}[K_0], R_{f,T_1\to T_N}, T_N - T_1\right], \tag{OA.4.3}$$

$$R_{f,t\to T_1} P_t[K_0] = \mathbb{E}^*_t \mathbb{BS}^p \left[S_{T_1}, \log\left(\frac{K_0}{S_{T_1}}\right), \sigma^*_{T_1}[K_0], R_{f,T_1\to T_N}, T_N - T_1\right]. \tag{OA.4.4}$$

The right-hand sides of (OA.4.3) and (OA.4.4) can themselves be evaluated using the Carr–

Madan spanning formula because the Black–Scholes pricing functions are ultimately functions of S_{T_1}. Specifically, for any twice-differentiable function $H[S_{T_1}]$,

$$\begin{aligned}\mathbb{E}_t^* H[S_{T_1}] = H[S_t R_{f,t\to T_1}] \\ + R_{f,t\to T_1} \left\{ \begin{aligned} \int_{S_t R_{f,t\to T_1}}^{\infty} H_{SS}[K] C_t[K] \, dK \\ + \int_0^{S_t R_{f,t\to T_1}} H_{SS}[K] C_t[K] \, dK \end{aligned} \right\},\end{aligned}$$

where $H_{SS}[\cdot]$ is the second derivative of H with respect to S_{T_1}. We estimate the coefficients $\{\alpha_t, d_{j,t}\}$ at each date by solving

$$\min_{\{\alpha_t, d_{j,t}\}} \sum_{q=1}^{Q} \left\{ \left(R_{f,t\to T_1} C_t[K_q] - \mathbb{E}_t^* \mathbb{BS}_q^c \right)^2 + \left(R_{f,t\to T_1} P_t[K_q] - \mathbb{E}_t^* \mathbb{BS}_q^p \right)^2 \right\}$$

with

$$\begin{aligned}\mathbb{BS}_q^c &= \mathbb{BS}^c \left[S_{T_1}, \log\left(\frac{K_q}{S_{T_1}} \right), \sigma_{T_1}^*[K_q], R_{f,T_1\to T_N}, T_N - T_1 \right], \\ \mathbb{BS}_q^p &= \mathbb{BS}^p \left[S_{T_1}, \log\left(\frac{K_q}{S_{T_1}} \right), \sigma_{T_1}^*[K_q], R_{f,T_1\to T_N}, T_N - T_1 \right].\end{aligned}$$

Once the coefficients $\{\alpha_t, d_{j,t}\}$ have been recovered, the quantities

$$\mathbb{E}_{T_1}^* R_{M,T_1\to T_N}^l - R_{f,T_1\to T_N}^l, \qquad l = 2, 3, 4,$$

can be expressed as functions of S_{T_1}. These expressions can then be substituted into Equation (2.47) and used as inputs in the computation of our expected excess-return bounds.

We implement this alternative approach by estimating α_t and $d_{j,t}$ at each date using 60 options (30 calls and 30 puts) drawn from an equally spaced moneyness grid ranging from 0.5 to 1.5. Figure OA.17 reports pricing-consistency results obtained from the resulting HLB and HUB. Overall, the alternative specification replicates closely the HLB and HUB used in the main analysis. The correlation between the two HLB measures is 0.94, while the corresponding correlation for HUB is 0.80. Moreover, the pricing-consistency performance of the alternative HLB remains comparable to that of the main-specification HLB, although the alternative series is somewhat more volatile and exhibits greater estimation noise. Overall, the close correspondence between the two sets of bounds indicates that our main findings are not driven by the particular representation adopted for Equation (2.47).

OA.5 Detailed Proof of the SDF in Presence of Intertemporal Hedging.

Proof.

$$\vartheta_{t\to T_N} = \sum_{j_1=0}^{\mathcal{K}}\sum_{j_1=0}^{\mathcal{K}} \frac{a_{j_1,j_2}}{R_{f,t\to T_1}^{j_1} R_{f,T_1\to T_N}^{j_2}} \Delta x^{j_1} \Delta y^{j_2}. \tag{OA.5.1}$$

Observe that

$$\left(\frac{\partial \vartheta_{t\to T_N}}{\partial x}\right)_{x=x_0} = \left\{-\frac{W_t y u'\left[W_t x_0 y_0\right] u''\left[W_t x y\right]}{\left(u'\left[W_t x y\right]\right)^2}\right\}_{x=x_0} = \frac{1}{x_0}\frac{1}{\tau_t}.$$

Similarly

$$\left(\frac{\partial \vartheta_{t\to T_N}}{\partial y}\right)_{y=y_0} = \left\{-\frac{W_t x u'\left[W_t x_0 y_0\right] u''\left[W_t x y\right]}{\left(u'\left[W_t x y\right]\right)^2}\right\}_{x=x_0} = \frac{1}{y_0}\frac{1}{\tau_t}$$

and

$$\begin{aligned}\left(\frac{\partial^2 \vartheta_{t\to T_N}}{\partial^2 x}\right)_{x=x_0} &= \left\{-\frac{\left(W_t y\right)^2 u'\left[W_t x_0 y_0\right] u'''\left[W_t x y\right]}{\left(u'\left[W_t x y\right]\right)^2} + 2\frac{\left(W_t y\right)^2 u'\left[W_t x y\right] u'\left[W_t x_0 y_0\right]\left(u''\left[W_t x y\right]\right)^2}{\left(u'\left[W_t x y\right]\right)^4}\right\}_{x=x_0} \\ &= \frac{2\left(1-\rho_t\right)}{\tau_t^2 x_0^2}.\end{aligned}$$

Similarly, we show

$$\left(\frac{\partial^2 \vartheta_{t\to T_N}}{\partial^2 y}\right)_{x=x_0} = \frac{2\left(1-\rho_t\right)}{\tau_t^2 y_0^2}.$$

Observe that

$$\left(\frac{\partial^3 \vartheta_{t\to T_N}}{\partial^3 x}\right)_{x=x_0} = \left\{\begin{array}{c} -\frac{(W_t y)^3 u'[W_t x_0 y_0] u''''[W_t x y]}{\left(u'[W_t x y]\right)^2} + \frac{6u''[W_t x y](W_t y)^3 u'[W_t x_0 y_0] u'''[W_t x y]}{\left(u'[W_t x y]\right)^3} \\ -6\frac{(W_t y)^3 u'[W_t x_0 y_0]\left(u'[W_t x y]\right)^2\left(u''[W_t x y]\right)^3}{\left(u'[W_t x y]\right)^6} \end{array}\right\}_{x=x_0}$$

which simplifies to

$$\left(\frac{\partial^3 \vartheta_{t\to T_N}}{\partial^3 x}\right)_{x=x_0} = \frac{6\kappa_t + 6 - 12\rho_t}{\tau_t^3 x_0^3}.$$

Similarly

$$\left(\frac{\partial^3 \vartheta_{t\to T_N}}{\partial^3 y}\right)_{y=x_0} = \frac{6\kappa_t + 6 - 12\rho_t}{\tau_t^3 y_0^3}.$$

Now, observe that

$$\left(\frac{\partial^2 \vartheta_{t\to T_N}}{\partial^2 y}\right)_{y=x_0} = \left\{-\frac{(W_t x)^2\, u'\,[W_t x_0 y_0]\, u'''\,[W_t xy]}{(u'\,[W_t xy])^2} + 2\frac{(W_t x)^2\, u'\,[W_t x_0 y_0]\,\left(u''\,[W_t xy]\right)^2}{(u'\,[W_t xy])^3}\right\}_{y=y_0}$$

and

$$\left(\frac{\partial^3 \vartheta_{t\to T_N}}{\partial^2 y \partial x}\right)_{(x,y)=(x_0,y_0)} = \left\{\begin{array}{c} -\frac{2(W_t x)W_t u'[W_t x_0 y_0]u'''[W_t xy]}{\left(u'[W_t xy]\right)^2} \\ -\frac{(W_t x)^2 W_t y u'[W_t x_0 y_0]u''''[W_t xy]}{\left(u'[W_t xy]\right)^2} \\ +\frac{2\left(u'[W_t xy]\right)\left(u''[W_t xy]\right)(W_t x)^2 W_t y u'[W_t x_0 y_0]u'''[W_t xy]}{\left(u'[W_t xy]\right)^4} \\ +4\frac{(W_t x)W_t u'[W_t x_0 y_0]\left(u''[W_t xy]\right)^2}{\left(u'[W_t xy]\right)^3} \\ +4\frac{(W_t x)^2 W_t y u'[W_t x_0 y_0]u''[W_t xy]u'''[W_t xy]}{\left(u'[W_t xy]\right)^3} \\ -6\frac{\left(u'[W_t xy]\right)^2 u''[W_t xy]W_t y(W_t x)^2 u'[W_t x_0 y_0]\left(u''[W_t xy]\right)^2}{\left(u'[W_t xy]\right)^6} \end{array}\right\}_{(x,y)=(x_0,y_0)}.$$

This simplifies to

$$\left(\frac{\partial^3 \vartheta_{t\to T_N}}{\partial^2 y \partial x}\right)_{y=x_0} = \frac{4\left(1-\rho_t\right)}{\tau_t^2 x_0 y_0^2} + \frac{6\left(\kappa_t + 1 - 2\rho_t\right)}{\tau_t^3 x_0 y_0^2}.$$

Now, observe that

$$\left(\frac{\partial^3 \vartheta_{t\to T_N}}{\partial^3 x}\right)_{x=x_0} = \left\{\begin{array}{c} -\frac{(W_t y)^3 u'[W_t x_0 y_0]u''''[W_t xy]}{\left(u'[W_t xy]\right)^2} + \frac{6u''[W_t xy](W_t y)^3 u'[W_t x_0 y_0]u'''[W_t xy]}{\left(u'[W_t xy]\right)^3} \\ -6\frac{(W_t y)^3 u'[W_t x_0 y_0]\left(u'[W_t xy]\right)^2\left(u''[W_t xy]\right)^3}{\left(u'[W_t xy]\right)^6} \end{array}\right\}_{x=x_0}.$$

Hence,

$$\left(\frac{\partial^4\vartheta_{t\to T_N}}{\partial^4 x}\right)_{x=x_0}=\left\{\begin{array}{c}-\frac{(W_ty)^4u^{'}[W_tx_0y_0]u^{'''''}[W_txy]}{\left(u^{'}[W_txy]\right)^2}+2\frac{(W_ty)^4u^{''}[W_txy]u^{'}[W_tx_0y_0]u^{''''}[W_txy]}{\left(u^{'}[W_txy]\right)^3}\\ +\frac{6u^{'''}[W_txy](W_ty)^4u^{'}[W_tx_0y_0]u^{'''}[W_txy]}{\left(u^{'}[W_txy]\right)^3}\\ +\frac{6u^{''}[W_txy](W_ty)^4u^{'}[W_tx_0y_0]u^{''''}[W_txy]}{\left(u^{'}[W_txy]\right)^3}\\ -\frac{18\left(u^{''}[W_txy]\right)^2(W_ty)^4u^{'}[W_tx_0y_0]u^{'''}[W_txy]}{\left(u^{'}[W_txy]\right)^4}\\ -18\frac{(W_ty)^4u^{'}[W_tx_0y_0]\left(u^{''}[W_txy]\right)^2u^{'''}[W_txy]}{\left(u^{'}[W_txy]\right)^4}\\ +24\frac{(W_ty)^4u^{'}[W_tx_0y_0]\left(u^{''}[W_txy]\right)^4}{\left(u^{'}[W_txy]\right)^5}\end{array}\right\}_{x=x_0}.$$

This simplifies to

$$\frac{1}{24}\left(\frac{\partial^4\vartheta_{t\to T_N}}{\partial^4 x}\right)_{x=x_0}=\frac{\rho_t^2-3\rho_t+1+2\kappa_t-\xi_t}{\tau_t^4x_0^4}.$$

Finally, recall that:

$$\left(\frac{\partial^3\vartheta_{t\to T_N}}{\partial^2 y\partial x}\right)_{(x,y)=(x_0,y_0)}=\left\{\begin{array}{c}-\frac{2(W_tx)W_tu^{'}[W_tx_0y_0]u^{'''}[W_txy]}{\left(u^{'}[W_txy]\right)^2}\\ -\frac{(W_tx)^2W_tyu^{'}[W_tx_0y_0]u^{''''}[W_txy]}{\left(u^{'}[W_txy]\right)^2}\\ +\frac{6\left(u^{''}[W_txy]\right)(W_tx)^2W_tyu^{'}[W_tx_0y_0]u^{'''}[W_txy]}{\left(u^{'}[W_txy]\right)^3}\\ +4\frac{(W_tx)W_tu^{'}[W_tx_0y_0]\left(u^{''}[W_txy]\right)^2}{\left(u^{'}[W_txy]\right)^3}\\ -6\frac{W_ty(W_tx)^2u^{'}[W_tx_0y_0]\left(u^{''}[W_txy]\right)^3}{\left(u^{'}[W_txy]\right)^4}\end{array}\right\}_{(x,y)=(x_0,y_0)}.$$

Set

$$A_1=-\frac{2(W_tx)W_tu^{'}[W_tx_0y_0]u^{'''}[W_txy]}{\left(u^{'}[W_txy]\right)^2},\ A_2=-\frac{(W_tx)^2W_tyu^{'}[W_tx_0y_0]u^{''''}[W_txy]}{\left(u^{'}[W_txy]\right)^2},$$
$$A_3=\frac{6\left(u^{''}[W_txy]\right)(W_tx)^2W_tyu^{'}[W_tx_0y_0]u^{'''}[W_txy]}{\left(u^{'}[W_txy]\right)^3},\ A_4=4\frac{(W_tx)W_tu^{'}[W_tx_0y_0]\left(u^{''}[W_txy]\right)^2}{\left(u^{'}[W_txy]\right)^3},$$
$$A_5=-6\frac{W_ty(W_tx)^2u^{'}[W_tx_0y_0]\left(u^{''}[W_txy]\right)^3}{\left(u^{'}[W_txy]\right)^4}.$$

It follows that

$$\begin{aligned}\left(\frac{\partial A_1}{\partial x}\right)_{(x,y)=(x_0,y_0)} &= -\frac{4\rho_t}{\tau_t^2 x_0^2 y_0^2}+\frac{12\kappa_t}{\tau_t^3 x_0^2 y_0^2}-\frac{8\rho_t}{\tau_t^3 x_0^2 y_0^2}\\ &= -\frac{4\rho_t}{\tau_t^2 x_0^2 y_0^2}+\frac{4\left(3\kappa_t-2\rho_t\right)}{\tau_t^3 x_0^2 y_0^2}\end{aligned}$$

and

$$\left(\frac{\partial A_2}{\partial x}\right)_{(x,y)=(x_0,y_0)} = \frac{12\kappa_t}{\tau_t^3 x_0^2 y_0^2}+\frac{12\left(\kappa_t-2\xi_t\right)}{\tau_t^4 x_0^2 y_0^2}$$

and

$$\left(\frac{\partial A_3}{\partial x}\right)_{(x,y)=(x_0,y_0)} = \frac{12\left(2\rho_t^2+3\kappa_t-3\rho_t\right)}{\tau_t^4 x_0^2 y_0^2}-\frac{24\rho_t}{\tau_t^3 x_0^2 y_0^2}$$

and

$$\left(\frac{\partial A_4}{\partial x}\right)_{(x,y)=(x_0,y_0)} = \frac{4}{\tau_t^2 x_0^2 y_0^2}+\frac{4\left(3-4\rho_t\right)}{\tau_t^3 x_0^2 y_0^2}$$

and

$$\begin{aligned}\left(\frac{\partial A_5}{\partial x}\right)_{(x,y)=(x_0,y_0)} &= -12\frac{W_t y\left(W_t x\right)W_t u'\left[W_t x_0 y_0\right]\left(u''\left[W_t xy\right]\right)^3}{\left(u'\left[W_t xy\right]\right)^4}\\ &\quad -18\frac{\left(W_t y\right)^2\left(W_t x\right)^2 u'\left[W_t x_0 y_0\right]\left(u''\left[W_t xy\right]\right)^2 u'''\left[W_t xy\right]}{\left(u'\left[W_t xy\right]\right)^4}\\ &\quad +24\frac{\left(W_t y\right)^2\left(W_t x\right)^2 u'\left[W_t x_0 y_0\right]\left(u'\left[W_t xy\right]\right)^3\left(u''\left[W_t xy\right]\right)^4}{\left(u'\left[W_t xy\right]\right)^8}\end{aligned}$$

and

$$\left(\frac{\partial A_5}{\partial x}\right)_{(x,y)=(x_0,y_0)} = \frac{12}{\tau_t^3 x_0^2 y_0^2}+\frac{12\left(2-3\rho_t\right)}{\tau_t^4 x_0^2 y_0^2}.$$

Finally

$$
\begin{aligned}
\left(\frac{\partial^4 \vartheta_{t\to T_N}}{\partial^2 y \partial^2 x}\right)_{(x,y)=(x_0,y_0)} = & -\frac{4\rho_t}{\tau_t^2 x_0^2 y_0^2} + \frac{4\left(3\kappa_t - 2\rho_t\right)}{\tau_t^3 x_0^2 y_0^2} \\
& + \frac{12\kappa_t}{\tau_t^3 x_0^2 y_0^2} + \frac{12\left(\kappa_t - 2\xi_t\right)}{\tau_t^4 x_0^2 y_0^2} \\
& + \frac{12\left(2\rho_t^2 + 3\kappa_t - 2\rho_t\right)}{\tau_t^4 x_0^2 y_0^2} - \frac{24\rho_t}{\tau_t^3 x_0^2 y_0^2} \\
& + \frac{4}{\tau_t^2 x_0^2 y_0^2} + \frac{4\left(3 - 4\rho_t\right)}{\tau_t^3 x_0^2 y_0^2} \\
& + \frac{12}{\tau_t^3 x_0^2 y_0^2} + \frac{12\left(2 - 3\rho_t\right)}{\tau_t^4 x_0^2 y_0^2},
\end{aligned}
$$

which simplifies to

$$
\begin{aligned}
\left(\frac{\partial^4 \vartheta_{t\to T_N}}{\partial^2 y \partial^2 x}\right)_{(x,y)=(x_0,y_0)} = & \frac{4\left(1 - \rho_t\right)}{\tau_t^2 x_0^2 y_0^2} + \frac{24\left(\kappa_t - 2\rho_t + 1\right)}{\tau_t^3 x_0^2 y_0^2} \\
& + \frac{24\left(2\kappa_t - \xi_t + \rho_t^2 - 3\rho_t + 1\right)}{\tau_t^4 x_0^2 y_0^2}.
\end{aligned}
$$

Set

$$
\begin{aligned}
B_1 &= -\frac{\left(W_t x\right)^3 u'\left[W_t x_0 y_0\right] u''''\left[W_t x y\right]}{\left(u'\left[W_t x y\right]\right)^2}, \\
B_2 &= \frac{6u''\left[W_t x y\right]\left(W_t x\right)^3 u'\left[W_t x_0 y_0\right] u'''\left[W_t x y\right]}{\left(u'\left[W_t x y\right]\right)^3}, \\
B_3 &= -6\frac{\left(W_t x\right)^3 u'\left[W_t x_0 y_0\right]\left(u''\left[W_t x y\right]\right)^3}{\left(u'\left[W_t x y\right]\right)^4}.
\end{aligned}
$$

Then

$$
\left(\frac{\partial^4 \vartheta_{t\to T_N}}{\partial^3 y \partial x}\right) = \frac{\partial B_1}{\partial x} + \frac{\partial B_2}{\partial x} + \frac{\partial B_3}{\partial x},
$$

where

$$
\frac{\partial B_1}{\partial x} = \left\{\begin{array}{c}
-\frac{3(W_t x)^2 W_t u'[W_t x_0 y_0] u''''[W_t x y]}{\left(u'[W_t x y]\right)^2} \\
-\frac{W_t y (W_t x)^3 u'[W_t x_0 y_0] u'''''[W_t x y]}{\left(u'[W_t x y]\right)^2} \\
+\frac{2(W_t x)^3 W_t y u''[W_t x y] u''''[W_t x y]}{\left(u'[W_t x y]\right)^2}
\end{array}\right\}_{(x,y)=(x_0,y_0)}.
$$

Hence

$$\left(\frac{\partial B_1}{\partial x}\right)_{(x,y)=(x_0,y_0)} = \frac{18\kappa_t}{\tau_t^4 x_0 y_0^3} + \frac{(12\kappa_t - 24\xi_t)}{\tau_t^4 x_0 y_0^3}$$

and

$$\left(\frac{\partial B_2}{\partial x}\right)_{(x,y)=(x_0,y_0)} = \left\{\begin{array}{c} \frac{6W_t y (W_t x)^3 \left(u'''[W_t xy]\right)^2}{\left(u'[W_t xy]\right)^2} \\ +\frac{18u''[W_t xy](W_t x)^2 W_t u'''[W_t xy]}{\left(u'[W_t xy]\right)^2} \\ +\frac{6u''[W_t xy] W_t y (W_t x)^3 u''''[W_t xy]}{\left(u'[W_t xy]\right)^2} \\ -\frac{18\left(u''[W_t xy]\right)^2 (W_t x)^3 W_t y u'''[W_t xy]}{\left(u'[W_t xy]\right)^3} \end{array}\right\}_{(x,y)=(x_0,y_0)}$$

and

$$\left(\frac{\partial B_2}{\partial x}\right)_{(x,y)=(x_0,y_0)} = \frac{24\rho_t^2}{\tau_t^4 x_0 y_0^3} - \frac{36\rho_t}{\tau_t^3 x_0 y_0^3} + \frac{36\kappa_t}{\tau_t^4 x_0 y_0^3} - \frac{36\rho_t}{\tau_t^4 x_0 y_0^3}$$

and

$$\frac{\partial B_3}{\partial x} = \left\{\begin{array}{c} -18\frac{(W_t x)^2 W_t \left(u''[W_t xy]\right)^3}{\left(u'[W_t xy]\right)^3} \\ -18\frac{(W_t x)^3 W_t y \left(u''[W_t xy]\right)^2 u'''[W_t xy]}{\left(u'[W_t xy]\right)^3} \\ +24\frac{(W_t x)^3 W_t y \left(u''[W_t xy]\right)^4}{\left(u'[W_t xy]\right)^4} \end{array}\right\}_{(x,y)=(x_0,y_0)},$$

which simplifies to

$$\frac{\partial B_3}{\partial x} = \frac{18}{\tau_t^3 x_0 y_0^3} - \frac{36\rho_t}{\tau_t^4 x_0 y_0^3} + \frac{24}{\tau_t^4 x_0 y_0^3}.$$

Hence

$$\begin{aligned}
\left(\frac{\partial^4 \vartheta_{t\to T_N}}{\partial^3 y \partial x}\right)_{(x,y)=(x_0,y_0)} &= \frac{18 - 36\rho_t}{\tau_t^3 x_0 y_0^3} + \frac{18\kappa_t + 48\kappa_t - 24\xi_t + 24\rho_t^2 - 72\rho_t + 24}{\tau_t^4 x_0 y_0^3} \\
&= \frac{6}{x_0 y_0^3}\left\{\begin{array}{c} \frac{3-6\rho_t}{\tau_t^3} + \frac{3\kappa_t}{\tau_t^4} \\ +\frac{4\left(2\kappa_t - \xi_t + \rho_t^2 - 3\rho_t + 1\right)}{\tau_t^4} \end{array}\right\} \\
&= \frac{6}{x_0 y_0^3}\left\{3a_{3,t} + 3\left(1 - 2\frac{a_{2,t}}{a_{1,t}^2} + a_{3,t}\right)(a_{1,t} - 1) + 4a_{4.t}\right\}.
\end{aligned}$$

As a result:

$$
\begin{aligned}
\upsilon_{t\to T_1} &= \mathbb{E}^*_{T_N} \frac{u'\left[W_t x_0 y_0\right]}{u'\left[W_t x y\right]} \\
&= 1 + \frac{1}{R_{f,t\to T_1}} a_{1,t} \Delta x + \frac{a_{2,t}}{R^2_{f,t\to T_1}} \left(\Delta x\right)^2 + \frac{a_{2,t}}{R^2_{f,T_1\to T_N}} \mathbb{E}^*_{T_1} \left(\Delta y\right)^2 \\
&\quad + \frac{a_{3,t}}{R^3_{f,t\to T_1}} \left(\Delta x\right)^3 + \frac{a_{3,t}}{R^3_{f,T_1\to T_N}} \mathbb{E}^*_{T_1} \left(\Delta y\right)^3 + \frac{a_{5,t}}{R_{f,t\to T_1} R^2_{f,T_1\to T_N}} \Delta x \mathbb{E}^*_{T_1} \left(\Delta y\right)^2 \\
&\quad + \frac{a_{4,t}}{R^4_{f,t\to T_1}} \left(\Delta x\right)^4 + \frac{a_{4,t}}{R^4_{f,T_1\to T_N}} \mathbb{E}^*_{T_1} \left(\Delta y\right)^4 + \frac{a_{6,t}}{R_{f,t\to T_1} R^3_{f,T_1\to T_N}} \left(\Delta x\right) \mathbb{E}^*_{T_1} \left(\Delta y\right)^3 \\
&\quad + \frac{a_{7,t}}{R^2_{f,t\to T_1} R^2_{f,T_1\to T_N}} \left(\Delta x\right)^2 \mathbb{E}^*_{T_1} \left(\Delta y\right)^2,
\end{aligned}
$$

with

$$
\begin{aligned}
a_{5,t} &= 2a_{2,t} + 3a_{3,t} \\
a_{6,t} &= 3a_{3,t} + 3\left(1 - 2\frac{a_{2,t}}{a^2_{1,t}} + a_{3,t}\right)\left(a_{1,t} - 1\right) + 4a_{4.t} \\
a_{7,t} &= a_{2,t} + 6a_{3,t} + 6a_{4,t}.
\end{aligned}
$$

This ends the proof. $\square$

OA.6 Model-Implied Variance Risk Premium

$$
\begin{aligned}
\mathbb{VRP}_t &= \mathbb{E}_t^*(R_{M,t\to T_1} - R_{f,t\to T_1})^2 - \mathbb{E}_t(R_{M,t\to T_1} - R_{f,t\to T_1})^2 \\
&= -\mathbb{COV}_t^*\left(\frac{\mathbb{E}_t m_{t\to T_1}}{m_{t\to T_1}},\ (R_{M,t\to T_1} - R_{f,t\to T_1})^2\right) \\
&= -\mathbb{COV}_t^*\left(\frac{\vartheta_{t\to T_1}}{\mathbb{E}_t^*\vartheta_{t\to T_1}},\ (R_{M,t\to T_1} - R_{f,t\to T_1})^2\right) \\
&= -\mathbb{COV}_t^*\left(\frac{1+\sum_{k=1}^{K}\sum_{j=0}^{k}\frac{a_{j,k-j}}{R_{f,t\to T_1}^{j}R_{f,T_1\to T_N}^{k-j}}f^{(j,k-j)}}{\mathbb{E}_t^*\left(1+\sum_{k=1}^{K}\sum_{j=0}^{k}\frac{a_{j,k-j}}{R_{f,t\to T_1}^{j}R_{f,T_1\to T_N}^{k-j}}f^{(j,k-j)}\right)},\ (R_{M,t\to T_1} - R_{f,t\to T_1})^2\right) \\
&= -\frac{\sum_{k=1}^{K}\sum_{j=0}^{k}\frac{a_{j,k-j}}{R_{f,t\to T_1}^{j}R_{f,T_1\to T_N}^{k-j}}\left\{\mathbb{E}_t^*\left(f^{(j,k-j)}\,(R_{M,t\to T_1} - R_{f,t\to T_1})^2\right) - \mathbb{E}_t^* f^{(j,k-j)}\ \mathbb{E}_t^*(R_{M,t\to T_1} - R_{f,t\to T_1})^2\right\}}{1+\sum_{k=1}^{K}\sum_{j=0}^{k}\frac{a_{j,k-j}}{R_{f,t\to T_1}^{j}R_{f,T_1\to T_N}^{k-j}}\mathbb{E}_t^* f^{(j,k-j)}} \\
&= -\frac{\sum_{k=1}^{K}\sum_{j=0}^{k}\frac{a_{j,k-j}}{R_{f,t\to T_1}^{j}R_{f,T_1\to T_N}^{k-j}}\left\{\begin{array}{c}\mathbb{E}_t^*\left[\mathbb{M}_{T_1\to T_N}^{*(k-j)}\,(R_{M,t\to T_1} - R_{f,t\to T_1})^{j+2}\right] \\ -\,\mathbb{E}_t^* f^{(j,k-j)}\ \mathbb{E}_t^*(R_{M,t\to T_1} - R_{f,t\to T_1})^2\end{array}\right\}}{1+\sum_{k=1}^{K}\sum_{j=0}^{k}\frac{a_{j,k-j}}{R_{f,t\to T_1}^{j}R_{f,T_1\to T_N}^{k-j}}\mathbb{E}_t^* f^{(j,k-j)}}.
\end{aligned}
$$

OA.7 Computation of the Risk Neutral Moments

OA.7.1 Computation of $\mathbb{E}_t^*\mathcal{R}_{i,t\to T_1}^q$

Notice that for $q \geq 2$

$$
\mathbb{E}_t^*\mathcal{R}_{i,t\to T_1}^q = \mathbb{E}_t^*\left(\frac{S_{i,T_1}}{S_{i,t}} - R_{f,t\to T_1}\right)^q = \frac{q\,(q-1)\,R_{f,t\to T_1}}{S_{i,t}^2}\left\{\begin{array}{c}\int_{S_{i,t}R_{f,t\to T_1}}^{\infty}\left(\frac{K}{S_{i,t}} - R_{f,t\to T_1}\right)^{q-2}C_{i,t}\,[K]\,dK \\ +\int_0^{S_tR_{f,t\to T_1}}\left(\frac{K}{S_{i,t}} - R_{f,t\to T_1}\right)^{q-2}P_{i,t}\,[K]\,dK.\end{array}\right\} \tag{OA.7.1}
$$

OA.7.2 Computation of $\mathbb{E}_t^*\left[\mathcal{R}_{i,t\to T_1} 1_{R_{i,t\to T_1}\geq k_0}\right]$

Next,

$$\begin{aligned}
\mathbb{E}_t^*\left[\mathcal{R}_{i,t\to T_1} 1_{R_{i,t\to T_1}\geq k_0}\right] &= \frac{1}{S_{i,t}}\left\{\mathbb{E}_t^*\left[\left(S_{i,T_1} - S_{i,t}k_0 + S_{i,t}k_0 - S_{i,t}R_{f,t\to T_1}\right) 1_{S_{i,T_1}\geq S_{i,t}k_0}\right]\right\} \\
&= \frac{R_{f,t\to T_1} C_{i,t}\left[S_{i,t}k_0\right]}{S_{i,t}} + \frac{\left(S_{i,t}k_0 - S_{i,t}R_{f,t\to T_1}\right)}{S_{i,t}}\mathbb{P}_t^*\left[S_{i,T_1} \geq S_{i,t}k_0\right].
\end{aligned}$$

OA.7.3 Computation of $\mathbb{E}_t^*\left[R_{M,t\to T_1}^{j_1}\left|R_{M,t\to T_1} - R_{f,t\to T_1}\right|^l\right] = \mathbb{E}_t^*\left[R_{M,t\to T_1}^{j_1}\left|\mathcal{R}_{M,t\to T_1}\right|^l\right]$

Observe that

$$\left|\mathcal{R}_{M,t\to T_1}\right|^l = \mathcal{R}_{M,t\to T_1}^l 1_{R_{M,t\to T_1} > R_{f,t\to T_1}} + (-1)^l \mathcal{R}_{M,t\to T_1}^l 1_{R_{M,t\to T_1} < R_{f,t\to T_1}}.$$

Hence,

$$\begin{aligned}
\mathbb{E}_t^*\left(R_{M,t\to T_1}^{j_1}\left|\mathcal{R}_{M,t\to T_1}\right|^l\right) &= \mathbb{E}_t^*\left[R_{M,t\to T_1}^{j_1}\mathcal{R}_{M,t\to T_1}^l 1_{R_{M,t\to T_1} > R_{f,t\to T_1}}\right] \\
&\quad + (-1)^l \mathbb{E}_t^*\left[R_{M,t\to T_1}^{j_1}\mathcal{R}_{M,t\to T_1}^l 1_{R_{M,t\to T_1} < R_{f,t\to T_1}}\right].
\end{aligned}$$

Notice that

$$\mathbb{E}_t^*\left[R_{M,t\to T_1}^{j_1}\mathcal{R}_{M,t\to T_1}^l 1_{R_{M,t\to T_1} > R_{f,t\to T_1}}\right] = \mathbb{E}_t^*\left[\mathcal{G}\left[S_{T_1}\right] 1_{S_{T_1} > S_t R_{f,t\to T_1}}\right],$$

with

$$\mathcal{G}\left[S_{T_1}\right] = \left(\frac{S_{T_1}}{S_t}\right)^{j_1}\left(\frac{S_{T_1}}{S_t} - R_{f,t\to T_1}\right)^l.$$

Thus, if $l > 0$,

$$\begin{aligned}
\mathbb{E}_t^*\left[\mathcal{G}\left[S_{T_1}\right] 1_{S_{T_1} > S_t R_{f,t\to T_1}}\right] &= R_{f,t\to T_1}\mathcal{G}_S\left[S_t R_{f,t\to T_1}\right] C_t\left[S_t R_{f,t\to T_1}\right] \\
&\quad + R_{f,t\to T_1}\int_{S_t R_{f,t\to T_1}}^{\infty}\mathcal{G}_{SS}\left[K\right] C_t\left[K\right] dK.
\end{aligned}$$

Similarly,

$$\mathbb{E}_t^*\left[\mathcal{G}\left[S_{T_1}\right] 1_{R_{M,t\to T_1} < R_{f,t\to T_1}}\right] = \mathbb{E}_t^*\left[\mathcal{G}\left[S_{T_1}\right] 1_{S_{T_1} < S_t R_{f,t\to T_1}}\right].$$

Thus, if $l > 0$,

$$\begin{aligned}\mathbb{E}_t^*\left[\mathcal{G}\left[S_{T_1}\right]1_{S_{T_1}<S_tR_{f,t\to T_1}}\right] &= -R_{f,t\to T_1}\mathcal{G}_S\left[S_tR_{f,t\to T_1}\right]P_t\left[S_tR_{f,t\to T_1}\right]\\ &\quad +R_{f,t\to T_1}\int_0^{S_tR_{f,t\to T_1}}\mathcal{G}_{SS}\left[K\right]P_t\left[K\right]dK.\end{aligned}$$

OA.7.4 Computation of $\mathbb{E}_t^*\left[\mathcal{R}_{M,t\to T_1}^{j_1}\left|R_{M,t\to T_1}-R_{f,t\to T_1}\right|^l\right] = \mathbb{E}_t^*\left[\mathcal{R}_{M,t\to T_1}^{j_1}\left|\mathcal{R}_{M,t\to T_1}\right|^l\right]$

Observe that

$$\left|\mathcal{R}_{M,t\to T_1}\right|^l = \left(\mathcal{R}_{M,t\to T_1}\right)^l 1_{R_{M,t\to T_1}>R_{f,t\to T_1}} + (-1)^l\left(\mathcal{R}_{M,t\to T_1}\right)^l 1_{R_{M,t\to T_1}<R_{f,t\to T_1}}.$$

Hence,

$$\begin{aligned}\mathbb{E}_t^*\left(\mathcal{R}_{M,t\to T_1}^{j_1}\left|\mathcal{R}_{M,t\to T_1}\right|^l\right) &= \mathbb{E}_t^*\left[\mathcal{R}_{M,t\to T_1}^{j_1+l}1_{R_{M,t\to T_1}>R_{f,t\to T_1}}\right]\\ &\quad +(-1)^l\mathbb{E}_t^*\left[\mathcal{R}_{M,t\to T_1}^{j_1+l}1_{R_{M,t\to T_1}<R_{f,t\to T_1}}\right].\end{aligned}$$

Notice that

$$\mathbb{E}_t^*\left[\mathcal{R}_{M,t\to T_1}^{j_1+l}1_{R_{M,t\to T_1}>R_{f,t\to T_1}}\right] = \mathbb{E}_t^*\left[G\left[S_{T_1}\right]1_{S_{T_1}>S_tR_{f,t\to T_1}}\right],$$

with

$$G\left[S_{T_1}\right] = \left(\frac{S_{T_1}}{S_t} - R_{f,t\to T_1}\right)^{j_1+l}.$$

Thus, if $j_1 + l > 0$,

$$\begin{aligned}\mathbb{E}_t^*\left[G\left[S_{T_1}\right]1_{S_{T_1}>S_tR_{f,t\to T_1}}\right] &= R_{f,t\to T_1}G_S\left[S_tR_{f,t\to T_1}\right]C_t\left[S_tR_{f,t\to T_1}\right]\\ &\quad +R_{f,t\to T_1}\int_{S_tR_{f,t\to T_1}}^{\infty}G_{SS}\left[K\right]C_t\left[K\right]dK.\end{aligned}$$

Similarly,

$$\mathbb{E}_t^*\left[\mathcal{R}_{M,t\to T_1}^{j_1+l}1_{R_{M,t\to T_1}<R_{f,t\to T_1}}\right] = \mathbb{E}_t^*\left[H\left[S_{T_1}\right]1_{S_{T_1}<S_tR_{f,t\to T_1}}\right],$$

with

$$H\left[S_{T_1}\right] = \left(\frac{S_{T_1}}{S_t} - R_{f,t\to T_1}\right)^{j_1+l}.$$

Thus, if $j_1 + l > 0$,

$$\begin{aligned}\mathbb{E}_t^*\left[H\left[S_{T_1}\right]1_{S_{T_1}<S_tR_{f,t\to T_1}}\right] &= -R_{f,t\to T_1}H_S\left[S_tR_{f,t\to T_1}\right]P_t\left[S_tR_{f,t\to T_1}\right]\\ &\quad +R_{f,t\to T_1}\int_0^{S_tR_{f,t\to T_1}}H_{SS}\left[K\right]P_t\left[K\right]dK.\end{aligned}$$

OA.7.5 Computation of $\mathbb{E}_t^*\left(\sum_{k=1}^{\mathcal{N}}\underline{\gamma}_{i,k}\left(\mathcal{R}_{M,t\to T_1}^k-\mathbb{E}_t^*\mathcal{R}_{M,t\to T_1}^k\right)\right)^q$

The key here is to expand the term within the risk-neutral expectation and then use (OA.7.1) to compute the risk-neutral quantities.

- Assume $\mathcal{N}$ =2 then $q = 2, 3$. For $q = 2$,

$$\begin{aligned}&\mathbb{E}_t^*\left(\underline{\gamma}_{i,1}\mathcal{R}_{M,t\to T_1}+\underline{\gamma}_{i,2}\left(\mathcal{R}_{M,t\to T_1}^2-\mathbb{E}_t^*\mathcal{R}_{M,t\to T_1}^2\right)\right)^2\\ =\;&\underline{\gamma}_{i,1}^2\mathbb{E}_t^*\mathcal{R}_{M,t\to T_1}^2+\underline{\gamma}_{i,2}^2\mathbb{E}_t^*\left(\mathcal{R}_{M,t\to T_1}^2-\mathbb{E}_t^*\mathcal{R}_{M,t\to T_1}^2\right)^2\\ &+2\underline{\gamma}_{i,2}\underline{\gamma}_{i,1}\mathbb{E}_t^*\left(\mathcal{R}_{M,t\to T_1}\left(\mathcal{R}_{M,t\to T_1}^2-\mathbb{E}_t^*\mathcal{R}_{M,t\to T_1}^2\right)\right).\end{aligned}$$

  For $q = 3$,

$$\begin{aligned}&\mathbb{E}_t^*\left(\underline{\gamma}_{i,1}\mathcal{R}_{M,t\to T_1}+\underline{\gamma}_{i,2}\left(\mathcal{R}_{M,t\to T_1}^2-\mathbb{E}_t^*\mathcal{R}_{M,t\to T_1}^2\right)\right)^3\\ =\;&\underline{\gamma}_{i,1}^3\mathbb{E}_t^*\mathcal{R}_{M,t\to T_1}^3+\underline{\gamma}_{i,2}^3\mathbb{E}_t^*\left(\mathcal{R}_{M,t\to T_1}^2-\mathbb{E}_t^*\mathcal{R}_{M,t\to T_1}^2\right)^3\\ &+3\underline{\gamma}_{i,1}^2\underline{\gamma}_{i,2}\mathbb{E}_t^*\left(\mathcal{R}_{M,t\to T_1}^2\left(\mathcal{R}_{M,t\to T_1}^2-\mathbb{E}_t^*\mathcal{R}_{M,t\to T_1}^2\right)\right)\\ &+3\underline{\gamma}_{i,1}\underline{\gamma}_{i,2}^2\mathbb{E}_t^*\left(\mathcal{R}_{M,t\to T_1}\left(\mathcal{R}_{M,t\to T_1}^2-\mathbb{E}_t^*\mathcal{R}_{M,t\to T_1}^2\right)^2\right).\end{aligned}$$

- Assume $\mathcal{N}$ =3 then $q = 2, 3, 4$. For $q = 2$,

$$\begin{aligned}&\mathbb{E}_t^*\left(\underline{\gamma}_{i,1}\mathcal{R}_{M,t\to T_1}+\underline{\gamma}_{i,2}\left(\mathcal{R}_{M,t\to T_1}^2-\mathbb{E}_t^*\mathcal{R}_{M,t\to T_1}^2\right)+\underline{\gamma}_{i,3}\left(\mathcal{R}_{M,t\to T_1}^3-\mathbb{E}_t^*\mathcal{R}_{M,t\to T_1}^3\right)\right)^2\\ =\;&\underline{\gamma}_{i,1}^2\mathbb{E}_t^*\mathcal{R}_{M,t\to T_1}^2+\underline{\gamma}_{i,2}^2\mathbb{E}_t^*\left(\mathcal{R}_{M,t\to T_1}^2-\mathbb{E}_t^*\mathcal{R}_{M,t\to T_1}^2\right)^2\\ &+\underline{\gamma}_{i,3}^2\mathbb{E}_t^*\left(\mathcal{R}_{M,t\to T_1}^3-\mathbb{E}_t^*\mathcal{R}_{M,t\to T_1}^3\right)^2\\ &+2\underline{\gamma}_{i,2}\underline{\gamma}_{i,1}\mathbb{E}_t^*\left(\mathcal{R}_{M,t\to T_1}\left(\mathcal{R}_{M,t\to T_1}^2-\mathbb{E}_t^*\mathcal{R}_{M,t\to T_1}^2\right)\right)\\ &+2\underline{\gamma}_{i,1}\underline{\gamma}_{i,3}\mathbb{E}_t^*\left(\mathcal{R}_{M,t\to T_1}\left(\mathcal{R}_{M,t\to T_1}^3-\mathbb{E}_t^*\mathcal{R}_{M,t\to T_1}^3\right)\right)\\ &+2\underline{\gamma}_{i,3}\underline{\gamma}_{i,2}\mathbb{E}_t^*\left(\left(\mathcal{R}_{M,t\to T_1}^2-\mathbb{E}_t^*\mathcal{R}_{M,t\to T_1}^2\right)\left(\mathcal{R}_{M,t\to T_1}^3-\mathbb{E}_t^*\mathcal{R}_{M,t\to T_1}^3\right)\right),\end{aligned}$$

for $q = 3$,

$$\begin{aligned}
& \mathbb{E}_t^* \left(\underline{\gamma}_{i,1} \mathcal{R}_{M,t\to T_1} + \underline{\gamma}_{i,2} \left(\mathcal{R}_{M,t\to T_1}^2 - \mathbb{E}_t^* \mathcal{R}_{M,t\to T_1}^2 \right) + \underline{\gamma}_{i,3} \left(\mathcal{R}_{M,t\to T_1}^3 - \mathbb{E}_t^* \mathcal{R}_{M,t\to T_1}^3 \right) \right)^3 \\
= \; & \underline{\gamma}_{i,1}^3 \mathbb{E}_t^* \mathcal{R}_{M,t\to T_1}^3 + \underline{\gamma}_{i,2}^3 \mathbb{E}_t^* \left(\mathcal{R}_{M,t\to T_1}^2 - \mathbb{E}_t^* \mathcal{R}_{M,t\to T_1}^2 \right)^3 + \underline{\gamma}_{i,3}^3 \mathbb{E}_t^* \left(\mathcal{R}_{M,t\to T_1}^3 - \mathbb{E}_t^* \mathcal{R}_{M,t\to T_1}^3 \right)^3 \\
& +3 \underline{\gamma}_{i,2} \underline{\gamma}_{i,1}^2 \mathbb{E}_t^* \left(\mathcal{R}_{M,t\to T_1}^2 \left(\mathcal{R}_{M,t\to T_1}^2 - \mathbb{E}_t^* \mathcal{R}_{M,t\to T_1}^2 \right) \right) \\
& +3 \underline{\gamma}_{i,1}^2 \underline{\gamma}_{i,3} \mathbb{E}_t^* \left(\mathcal{R}_{M,t\to T_1}^2 \left(\mathcal{R}_{M,t\to T_1}^3 - \mathbb{E}_t^* \mathcal{R}_{M,t\to T_1}^3 \right) \right) \\
& +3 \underline{\gamma}_{i,1} \underline{\gamma}_{i,2}^2 \mathbb{E}_t^* \left(\mathcal{R}_{M,t\to T_1} \left(\mathcal{R}_{M,t\to T_1}^2 - \mathbb{E}_t^* \mathcal{R}_{M,t\to T_1}^2 \right)^2 \right) \\
& +3 \underline{\gamma}_{i,3} \underline{\gamma}_{i,2}^2 \mathbb{E}_t^* \left(\left(\mathcal{R}_{M,t\to T_1}^2 - \mathbb{E}_t^* \mathcal{R}_{M,t\to T_1}^2 \right)^2 \left(\mathcal{R}_{M,t\to T_1}^2 - \mathbb{E}_t^* \mathcal{R}_{M,t\to T_1}^2 \right) \right) \\
& +3 \underline{\gamma}_{i,1} \underline{\gamma}_{i,3}^2 \mathbb{E}_t^* \left(\mathcal{R}_{M,t\to T_1} \left(\mathcal{R}_{M,t\to T_1}^3 - \mathbb{E}_t^* \mathcal{R}_{M,t\to T_1}^3 \right)^2 \right) \\
& +3 \underline{\gamma}_{i,2} \underline{\gamma}_{i,3}^2 \mathbb{E}_t^* \left(\left(\mathcal{R}_{M,t\to T_1}^2 - \mathbb{E}_t^* \mathcal{R}_{M,t\to T_1}^2 \right) \left(\mathcal{R}_{M,t\to T_1}^3 - \mathbb{E}_t^* \mathcal{R}_{M,t\to T_1}^3 \right)^2 \right) \\
& +6 \underline{\gamma}_{i,1} \underline{\gamma}_{i,2} \underline{\gamma}_{i,3} \mathbb{E}_t^* \left(\mathcal{R}_{M,t\to T_1} \left(\mathcal{R}_{M,t\to T_1}^2 - \mathbb{E}_t^* \mathcal{R}_{M,t\to T_1}^2 \right) \left(\mathcal{R}_{M,t\to T_1}^3 - \mathbb{E}_t^* \mathcal{R}_{M,t\to T_1}^3 \right) \right),
\end{aligned}$$

and for $q = 4$,

$$
\begin{aligned}
& \mathbb{E}_t^* \left(\underline{\gamma}_{i,1}\mathcal{R}_{M,t\to T_1} + \underline{\gamma}_{i,2}\left(\mathcal{R}^2_{M,t\to T_1} - \mathbb{E}_t^*\mathcal{R}^2_{M,t\to T_1}\right) + \underline{\gamma}_{i,3}\left(\mathcal{R}^3_{M,t\to T_1} - \mathbb{E}_t^*\mathcal{R}^3_{M,t\to T_1}\right)\right)^4 \\
= \; & \underline{\gamma}^4_{i,1}\mathbb{E}_t^*\mathcal{R}^4_{M,t\to T_1} + \underline{\gamma}^4_{i,2}\mathbb{E}_t^*\left(\mathcal{R}^2_{M,t\to T_1} - \mathbb{E}_t^*\mathcal{R}^2_{M,t\to T_1}\right)^4 + \underline{\gamma}^4_{i,3}\mathbb{E}_t^*\left(\mathcal{R}^3_{M,t\to T_1} - \mathbb{E}_t^*\mathcal{R}^3_{M,t\to T_1}\right)^4 \\
& +4\underline{\gamma}^3_{i,1}\underline{\gamma}_{i,2}\mathbb{E}_t^*\left(\mathcal{R}^3_{M,t\to T_1}\left(\mathcal{R}^2_{M,t\to T_1} - \mathbb{E}_t^*\mathcal{R}^2_{M,t\to T_1}\right)\right) \\
& +4\underline{\gamma}^3_{i,1}\underline{\gamma}_{i,3}\mathbb{E}_t^*\left(\mathcal{R}^3_{M,t\to T_1}\left(\mathcal{R}^3_{M,t\to T_1} - \mathbb{E}_t^*\mathcal{R}^3_{M,t\to T_1}\right)\right) \\
& +4\underline{\gamma}_{i,1}\underline{\gamma}^3_{i,2}\mathbb{E}_t^*\left(\mathcal{R}_{M,t\to T_1}\left(\mathcal{R}^2_{M,t\to T_1} - \mathbb{E}_t^*\mathcal{R}^2_{M,t\to T_1}\right)^3\right) \\
& +4\underline{\gamma}_{i,3}\underline{\gamma}^3_{i,2}\mathbb{E}_t^*\left(\left(\mathcal{R}^2_{M,t\to T_1} - \mathbb{E}_t^*\mathcal{R}^2_{M,t\to T_1}\right)^3\left(\mathcal{R}^2_{M,t\to T_1} - \mathbb{E}_t^*\mathcal{R}^2_{M,t\to T_1}\right)\right) \\
& +4\underline{\gamma}_{i,1}\underline{\gamma}^3_{i,3}\mathbb{E}_t^*\left(\mathcal{R}_{M,t\to T_1}\left(\mathcal{R}^3_{M,t\to T_1} - \mathbb{E}_t^*\mathcal{R}^3_{M,t\to T_1}\right)^3\right) \\
& +4\underline{\gamma}_{i,2}\underline{\gamma}^3_{i,3}\mathbb{E}_t^*\left(\left(\mathcal{R}^2_{M,t\to T_1} - \mathbb{E}_t^*\mathcal{R}^2_{M,t\to T_1}\right)\left(\mathcal{R}^3_{M,t\to T_1} - \mathbb{E}_t^*\mathcal{R}^3_{M,t\to T_1}\right)^3\right) \\
& +6\underline{\gamma}^2_{i,1}\underline{\gamma}^2_{i,2}\mathbb{E}_t^*\left(\mathcal{R}^2_{M,t\to T_1}\left(\mathcal{R}^2_{M,t\to T_1} - \mathbb{E}_t^*\mathcal{R}^2_{M,t\to T_1}\right)^2\right) \\
& +6\underline{\gamma}^2_{i,1}\underline{\gamma}^2_{i,3}\mathbb{E}_t^*\left(\mathcal{R}^2_{M,t\to T_1}\left(\mathcal{R}^3_{M,t\to T_1} - \mathbb{E}_t^*\mathcal{R}^3_{M,t\to T_1}\right)^2\right) \\
& +6\underline{\gamma}^2_{i,2}\underline{\gamma}^2_{i,3}\mathbb{E}_t^*\left(\left(\mathcal{R}^2_{M,t\to T_1} - \mathbb{E}_t^*\mathcal{R}^2_{M,t\to T_1}\right)^2\left(\mathcal{R}^3_{M,t\to T_1} - \mathbb{E}_t^*\mathcal{R}^3_{M,t\to T_1}\right)^2\right) \\
& +12\underline{\gamma}^2_{i,1}\underline{\gamma}_{i,3}\underline{\gamma}_{i,2}\mathbb{E}_t^*\left(\mathcal{R}^2_{M,t\to T_1}\left(\mathcal{R}^2_{M,t\to T_1} - \mathbb{E}_t^*\mathcal{R}^2_{M,t\to T_1}\right)\left(\mathcal{R}^3_{M,t\to T_1} - \mathbb{E}_t^*\mathcal{R}^3_{M,t\to T_1}\right)\right) \\
& +12\underline{\gamma}_{i,1}\underline{\gamma}^2_{i,2}\underline{\gamma}_{i,3}\mathbb{E}_t^*\left(\mathcal{R}_{M,t\to T_1}\left(\mathcal{R}^2_{M,t\to T_1} - \mathbb{E}_t^*\mathcal{R}^2_{M,t\to T_1}\right)^2\left(\mathcal{R}^3_{M,t\to T_1} - \mathbb{E}_t^*\mathcal{R}^3_{M,t\to T_1}\right)\right) \\
& +12\underline{\gamma}_{i,1}\underline{\gamma}_{i,2}\underline{\gamma}^2_{i,3}\mathbb{E}_t^*\left(\mathcal{R}_{M,t\to T_1}\left(\mathcal{R}^2_{M,t\to T_1} - \mathbb{E}_t^*\mathcal{R}^2_{M,t\to T_1}\right)\left(\mathcal{R}^3_{M,t\to T_1} - \mathbb{E}_t^*\mathcal{R}^3_{M,t\to T_1}\right)^2\right).
\end{aligned}
$$

OA.7.6 Computation of $\mathbb{E}_t^*\left[\left(R_{i,t\to T_1} - R_{f,t\to T_1}\right)^j 1_{R_{i,t\to T_1}\geq k_0}\right]$

Observe that

$$\mathbb{E}_t^*\left[\mathcal{R}^j_{i,t\to T_1}1_{R_{i,t\to T_1}\geq k_0}\right] = \mathbb{E}_t^*\left[\left(R_{i,t\to T_1} - R_{f,t\to T_1}\right)^j 1_{R_{i,t\to T_1}\geq k_0}\right].$$

For $j = 0$

$$\mathbb{E}_t^*\left[\mathcal{R}^j_{i,t\to T_1}1_{R_{i,t\to T_1}\geq k_0}\right] = \mathbb{E}_t^*\left[1_{R_{i,t\to T_1}\geq k_0}\right] = \mathbb{P}_t^*\left[R_{i,t\to T_1} \geq k_0\right].$$

For $j = 1$

$$\mathbb{E}_t^*\left[\mathcal{R}^j_{i,t\to T_1}1_{R_{i,t\to T_1}\geq k_0}\right] = \mathbb{E}_t^*\left[\mathcal{R}_{i,t\to T_1}1_{R_{i,t\to T_1}\geq k_0}\right].$$

This is already provided. For $j > 1$

$$
\begin{aligned}
\mathbb{E}_t^*\left[\left(R_{i,t\to T_1} - R_{f,t\to T_1}\right)^j 1_{R_{i,t\to T_1}\geq k_0}\right] &= \left(k_0 - R_{f,t\to T_1}\right)^j \mathbb{P}_t^*\left[R_{i,t\to T_1} \geq k_0\right] \\
&\quad + j\frac{R_{f,t\to T_1}}{S_{i,t}}\left(k_0 - R_{f,t\to T_1}\right)^{j-1} C_{i,t}\left[k_0 S_{i,t}\right] \\
&\quad + \frac{j\,(j-1)}{S_t^2} R_{f,t\to T_1}\int_{k_0 S_{i,t}}^{\infty}\left(\frac{K}{S_{i,t}} - R_{f,t\to T_1}\right)^{j-2} C_{i,t}\left[K\right] dK.
\end{aligned}
\tag{OA.7.2}
$$

OA.7.7 Computation of $\mathbb{E}_t^*\left(\mathcal{R}_{i,t\to T_1} 1_{R_{i,t\to T_1}\geq k_0} - \mathbb{E}_t^*\left[\mathcal{R}_{i,t\to T_1} 1_{R_{i,t\to T_1}\geq k_0}\right]\right)^q$

Next, how do we compute

$$
\mathbb{E}_t^*\left(\mathcal{R}_{i,t\to T_1} 1_{R_{i,t\to T_1}\geq k_0} - \mathbb{E}_t^*\left[\mathcal{R}_{i,t\to T_1} 1_{R_{i,t\to T_1}\geq k_0}\right]\right)^q .
$$

Observe that

$$
\begin{aligned}
&\left(\mathcal{R}_{i,t\to T_1} 1_{R_{i,t\to T_1}\geq k_0} - \mathbb{E}_t^*\left[\mathcal{R}_{i,t\to T_1} 1_{R_{i,t\to T_1}\geq k_0}\right]\right)^q \\
= &\sum_{j=0}^{q} \frac{q!}{(q-j)!j!}\left(\mathcal{R}_{i,t\to T_1} 1_{R_{i,t\to T_1}\geq k_0}\right)^j (-1)^{q-j}\left(\mathbb{E}_t^*\left[\mathcal{R}_{i,t\to T_1} 1_{R_{i,t\to T_1}\geq k_0}\right]\right)^{q-j} .
\end{aligned}
$$

Thus

$$
\begin{aligned}
&\mathbb{E}_t^*\left(\mathcal{R}_{i,t\to T_1} 1_{R_{i,t\to T_1}\geq k_0} - \mathbb{E}_t^*\left[\mathcal{R}_{i,t\to T_1} 1_{R_{i,t\to T_1}\geq k_0}\right]\right)^q \\
= &\sum_{j=0}^{q} \frac{q!\,(-1)^{q-j}}{(q-j)!j!}\left(\mathbb{E}_t^*\left[\mathcal{R}_{i,t\to T_1}^j 1_{R_{i,t\to T_1}\geq k_0}\right]\right)\left(\mathbb{E}_t^*\left[\mathcal{R}_{i,t\to T_1} 1_{R_{i,t\to T_1}\geq k_0}\right]\right)^{q-j} .
\end{aligned}
$$

OA.7.8 Computation of $\mathbb{E}_t^* f_{T_1}^{(j_1,j_2)}$

Notice that

$$
f_{T_1}^{(j_1,j_2)} = \mathcal{R}_{M,t\to T_1}^{j_1}\mathbb{E}_{T_1}^*\left[\mathcal{R}_{M,T_1\to T_N}^{j_2}\right]
$$

and

$$
\mathbb{E}_{T_1}^*\mathcal{R}_{M,T_1\to T_N}^{j_2} = \sum_{l=0}^{j_2}\phi_{j_2,l}R_{f,T_1\to T_N}^{l} + \sum_{l=2}^{j_2}\phi_{j_2,l}\left(\mathbb{E}_{T_1}^* R_{M,T_1\to T_N}^{l} - R_{f,T_1\to T_N}^{l}\right).
$$

Thus

$$
\begin{aligned}
f_{T_1}^{(j_1,j_2)} &= \mathcal{R}_{M,t\to T_1}^{j_1}\left(\sum_{l=0}^{j_2}\phi_{j_2,l}R_{f,T_1\to T_N}^{l}+\sum_{l=2}^{j_2}\phi_{j_2,l}\left(\mathbb{E}_{T_1}^{*}R_{M,T_1\to T_N}^{l}-R_{f,T_1\to T_N}^{l}\right)\right)\\
&= \sum_{l=0}^{j_2}\phi_{j_2,l}R_{f,T_1\to T_N}^{l}\mathcal{R}_{M,t\to T_1}^{j_1}+\sum_{l=2}^{j_2}\phi_{j_2,l}\mathcal{R}_{M,t\to T_1}^{j_1}\left(\mathbb{E}_{T_1}^{*}R_{M,T_1\to T_N}^{l}-R_{f,T_1\to T_N}^{l}\right).
\end{aligned}
$$

Since

$$
\mathbb{E}_{T_1}^{*}R_{M,T_1\to T_N}^{l}-R_{f,T_1\to T_N}^{l}=\theta_{l,t}^{*}\left|R_{M,t\to T_1}-R_{f,t\to T_1}\right|^{l},
$$

it follows that

$$
f_{T_1}^{(j_1,j_2)}=\sum_{l=0}^{j_2}\phi_{j_2,l}R_{f,T_1\to T_N}^{l}\mathcal{R}_{M,t\to T_1}^{j_1}+\sum_{l=2}^{j_2}\phi_{j_2,l}\theta_{l,t}^{*}\mathcal{R}_{M,t\to T_1}^{j_1}\left|R_{M,t\to T_1}-R_{f,t\to T_1}\right|^{l}
$$

and

$$
\mathbb{E}_{t}^{*}f_{T_1}^{(j_1,j_2)}=\sum_{l=0}^{j_2}\phi_{j_2,l}R_{f,T_1\to T_N}^{l}\mathbb{E}_{t}^{*}\left[\mathcal{R}_{M,t\to T_1}^{j_1}\right]+\sum_{l=2}^{j_2}\phi_{j_2,l}\theta_{l,t}^{*}\mathbb{E}_{t}^{*}\left[\mathcal{R}_{M,t\to T_1}^{j_1}\left|R_{M,t\to T_1}-R_{f,t\to T_1}\right|^{l}\right].
$$

OA.8 Variation with Firm Characteristics

OA.8.1 Bounds Without Intertemporal Hedging

This subsection examines how the predictive performance of our bounds varies with stock characteristics. The characteristics considered include market beta, size, book-to-market ratio, momentum, profitability, investment, idiosyncratic volatility, and illiquidity, which are standard predictors for the cross-section of stock returns in the asset pricing literature (e.g., Fama and French, 1992; Carhart, 1997; Hou, Xue, and Zhang, 2015).

[Insert Table OA.5 around here]

Table OA.5 reports the Fama and MacBeth (1973) regressions of prediction errors—defined as the difference between realized returns and our bound estimates—on these firm characteristics. We consider both signed prediction errors and their absolute values. Results for the lower bound are shown in Panel A and for the upper bound in Panel B under the default preference parameters.[31]

For the lower bound (Panel A), the signed error regressions show that most traditional characteristics—such as beta, momentum, profitability, investment, and idiosyncratic volatility—are insignificant, suggesting that the lower bound already captures much of the cross-sectional variation in expected returns typically associated with these factors. By contrast, firm size loads with significantly negative coefficients, indicating that the bound tends to overstate expected returns for larger firms. Illiquidity enters with significantly positive coefficients (up to the 182-day horizon), implying that the bound understates returns for illiquid stocks. For the absolute errors, beta and idiosyncratic volatility are positively related, whereas size, momentum, and profitability are negatively related. These results suggest that prediction errors are larger for firms with high systematic or idiosyncratic risk, but smaller for large, well-performing, and profitable firms.

For the upper bound (Panel B), the overall patterns resemble those for the lower bound, but two differences stand out in the signed error regressions. First, firm size is not significant at the 30-day horizon, though it becomes significantly negative from 91 days onward. This indicates that the upward bias of the upper bound for large firms emerges more clearly at longer horizons. Second, idiosyncratic volatility loads with significantly negative coefficients at all horizons, suggesting that the upper bound systematically overstates expected returns for firms with high firm-specific risk.

OA.8.2 Bounds With Intertemporal Hedging

This subsection examines how the performance of the hedging bounds varies with firm characteristics using Fama–MacBeth regressions of realized returns minus the hedging bounds (i.e., signed prediction errors) and of the absolute prediction errors on standard firm characteristics. For brevity, we report results only for an investment horizon of $T_N = 365$ days in Table OA.8. Panel A presents results for the hedging lower bound (HLB) and Panel B for the hedging upper bound (HUB).

[Insert Table OA.8 around here]

The results broadly mirror those obtained for the static bounds in Table OA.5. For the hedging lower bound (Panel A), most conventional predictors show little relation to the signed errors, while firm size loads with significantly negative coefficients and illiquidity with significantly positive coefficients, indicating that the bound tends to overstate returns for large firms and understate returns for illiquid firms. For the absolute errors, beta and idiosyncratic volatility are positively related, whereas size, momentum, and profitability are negatively related, implying larger errors for firms with high systematic or idiosyncratic risk,

[31] Results based on calibrated parameters are omitted for brevity but are very similar and available upon request.

but smaller errors for large, profitable, and past winners. For the hedging upper bound (Panel B), the patterns are broadly similar to those for Panel A but with two notable differences. In the signed error regressions, firm size is insignificant at the 30-day horizon but becomes significantly negative from 91 days onward, and idiosyncratic volatility loads negatively at all horizons, indicating that the HUB systematically overstates returns for firms with high firm-specific risk.

Overall, the hedging bounds display patterns very similar to those of their static counterparts, reinforcing the conclusion that while the hedging bounds absorb much of the variation typically attributed to traditional firm characteristics, certain sources of risk remain systematically linked to their prediction errors.

OA.8.3 Hedging Contributions

To further explore the cross-sectional sources of variation in our bounds and the role of firm characteristics in shaping hedging effects, we begin by examining how the bounds behave across portfolios sorted by key firm attributes. Figure OA.5 displays the average lower and upper bounds, with and without hedging (LB, HLB, UB, HUB), across deciles of four representative characteristics—market beta, size, book-to-market ratio, and illiquidity—using S&P 500 firms at a 30-day forecast horizon and a 365-day investment horizon.[32] The figure reveals patterns that align closely with well-established cross-sectional regularities in expected returns. Both the lower and upper bounds rise monotonically with beta and book-to-market, and decline with firm size, consistent with higher expected returns for high-beta, value, and small-capitalization firms. Bounds also increase with illiquidity, suggesting that stocks facing higher trading frictions are priced with higher expected returns. Across all characteristics, the hedging versions of the bounds (HLB, HUB) lie systematically above their static counterparts (LB, UB), confirming that intertemporal hedging raises the level of expected returns in a way that is broadly consistent with the cross-sectional structure documented in the literature.

[Insert Figure OA.5 and Table OA.10 around here]

Table OA.10 provides a more formal test of which firm attributes are most closely associated with intertemporal hedging effects. We regress the hedging share ratios—(HLB − LB)/HLB and (HUB−UB)/HUB—on standard firm characteristics following a Fama–MacBeth procedure. For brevity, we report results for investment horizons of $T_N = 365$ days (for $T_1 = 30, 91, 182$) and $T_N = 730$ days (for $T_1 = 365$), as other combinations yield similar patterns. The results indicate that firms with higher market betas and greater idiosyncratic volatility tend to exhibit smaller hedging shares, while those that are larger or have stronger recent performance (momentum) show larger shares. Profitability also enters with a positive

[32] Results for other horizon combinations are very similar and omitted for brevity.

sign, although its significance weakens in some specifications. In contrast, book-to-market, investment, and illiquidity coefficients vary in sign and significance across specifications. Economically, these results suggest that intertemporal hedging plays a more important role for firms that are less exposed to market or idiosyncratic risk but have stronger fundamentals or recent price momentum—firms whose expected returns are more sensitive to gradual shifts in investment opportunities rather than immediate risk shocks.

The apparent difference between the univariate sorts in Figure OA.5 and the multivariate regressions in Table OA.10 can be reconciled by recognizing that the hedging share is a residual component of expected return formation, not a simple function of any single characteristic. While univariate sorts capture broad return patterns shared by all bounds, the regression isolates how hedging intensity covaries with firm traits after controlling for their joint effects. Together, the two analyses indicate that our hedging bounds both reflect established cross-sectional patterns in expected returns and reveal additional dimensions of heterogeneity linked to firms' exposure to intertemporal risk.

OA.9 Relation to Cash-Flow, Discount-Rate, and Volatility News Betas

Building on Campbell et al. (2018), who decompose unexpected market returns into news about cash flows, discount rates, and volatility, this subsection investigates how the intertemporal hedging contributions in our framework relate to these distinct news components. Campbell et al. (2018) show that these three sources of news jointly explain much of the time variation in expected returns through their respective betas, capturing distinct channels of risk compensation. Integrating this perspective into our setting allows us to explore whether and how the component of expected returns arising from investors' intertemporal hedging motives is systematically associated with any of these news-based betas.

Following Campbell et al. (2018), we estimate three factor loadings—β_{CF}, β_{DR}, and β_V—that capture a stock's exposure to news about cash flows, discount rates, and volatility, respectively. Specifically, we estimate a vector autoregression (VAR) for the aggregate market return, realized variance, and a set of state variables such as the price–dividend ratio, short rate, default spread, and value spread. The VAR yields one-step-ahead forecasts of market returns and variance, which allow us to extract the unexpected component of the market return. Using the Campbell–Shiller log-linear approximation, this unexpected return innovation is then decomposed into three orthogonal components: innovations to expected cash flows (N_{CF}), to expected discount rates (N_{DR}), and to expected volatility (N_V). Each firm's return innovation is then regressed on these three aggregate news series using a

60-month rolling window to obtain monthly factor loadings:

$$\beta_{CF,i} = \frac{\text{Cov}(\tilde{r}_i, N_{CF})}{\text{Var}(N_{CF})}, \qquad \beta_{DR,i} = \frac{\text{Cov}(\tilde{r}_i, N_{DR})}{\text{Var}(N_{DR})}, \qquad \beta_{V,i} = \frac{\text{Cov}(\tilde{r}_i, N_{V})}{\text{Var}(N_{V})}.$$

These betas quantify how each stock co-moves with shocks to future cash flows, discount rates, and volatility in the aggregate economy, thereby capturing the three distinct channels of risk compensation in the stochastic-volatility ICAPM.

[Insert Table OA.11 around here]

Using monthly Fama–MacBeth regressions, we then relate the intertemporal hedging contributions to firm characteristics and the three news betas. Table OA.11 reports the results. Across all combinations of forecast and investment horizons and for both the lower and upper bounds, three clear patterns emerge. First, the coefficients on β_{CF} are positive and highly significant throughout, indicating that stocks more exposed to favorable cash-flow news tend to exhibit larger hedging shares. This suggests that intertemporal hedging amplifies the expected-return component linked to revisions in firms' future cash-flow prospects, consistent with the idea that cash-flow news represents a key source of priced risk. Second, the coefficients on β_{DR} are negative and significant across all horizons, consistent with a discount-rate-hedge effect: firms that covary more strongly with declines in expected discount rates (i.e., with rising valuations) require smaller intertemporal hedging adjustments. Third, β_V also enters negatively and significantly, implying a volatility-hedge channel. Stocks that move closely with increases in aggregate volatility—thus providing a hedge against worsening investment opportunities—tend to have smaller hedging contributions in expected-return terms. Taken together, these results indicate that the intertemporal hedging component in expected returns is systematically linked to the three sources of market news identified by Campbell et al. (2018). Cash-flow news amplifies the compensations embedded in the hedging bounds, whereas discount-rate and volatility news act as hedging forces that dampen them.

[Insert Table OA.12 around here]

Table OA.12 reports the average proportion of the intertemporal hedging contributions explained by the three news betas. For each firm and month, we regress the hedging contribution (HC)—defined as (HLB − LB)/HLB or (HUB − UB)/HUB—on the three betas as

$$\text{HC}_{i,t} = \alpha_t + \lambda_{CF,t}\beta_{i,CF} + \lambda_{DR,t}\beta_{i,DR} + \lambda_{V,t}\beta_{i,V} + \varepsilon_{i,t}.$$

The total variance of the hedging contribution can then be decomposed as

$$\text{Var}(\text{HC}_{i,t}) = \lambda_{CF,t}\text{Cov}(\text{HC}_{i,t}, \beta_{i,CF}) + \lambda_{DR,t}\text{Cov}(\text{HC}_{i,t}, \beta_{i,DR}) + \lambda_{V,t}\text{Cov}(\text{HC}_{i,t}, \beta_{i,V}) + \text{Cov}(\text{HC}_{i,t}, \varepsilon_{i,t}).$$

The proportion of $\mathrm{HC}_{i,t}$ attributable to each beta is thus computed as

$$\frac{\lambda_{k,t}\mathrm{Cov}(\mathrm{HC}_{i,t}, \beta_{i,k})}{\mathrm{Var}(\mathrm{HC}_{i,t})}, \quad \text{for } k \in \{CF, DR, V\},$$

which sum to one together with the residual term. Table OA.12 reports the time-series averages of these proportions across firms.

Across all forecast–investment horizon combinations, discount-rate news betas (β_{DR}) explain the largest share of the hedging contributions, followed by volatility-news betas (β_V), while cash-flow betas (β_{CF}) account for a relatively small fraction. Moreover, for a given investment horizon T_N, the shares attributed to discount-rate and volatility news rise as the forecast horizon T_1 lengthens. For example, with $T_N = 365$ days and for the hedging lower bound, the fraction explained by β_{DR} increases from about 3% at $T_1 = 30$ days to about 7% at $T_1 = 182$ days, while the share explained by β_V rises from roughly 2% to 4% over the same range. Figure OA.9 visualizes these patterns for representative investment horizons ($T_N = 365$ and 730 days). The panels show that discount-rate news dominates across horizons, and the shares of discount-rate and volatility news generally increase with T_1 (more pronounced for the HLB), while the cash-flow share remains small and comparatively flat.

[Insert Figure OA.9 around here]

Overall, although our bounds are significantly related to cash-flow, discount-rate, and volatility news betas, only a small fraction of the hedging contributions is explained by these three sources. This finding suggests that the intertemporal hedging components captured by our bounds reflect additional dimensions of risk beyond the cash-flow, discount-rate, and volatility channels identified by Campbell et al. (2018). This limited explanatory power is unsurprising for two reasons. First, our measure is forward looking, whereas the Campbell et al. (2018) news series are constructed from past returns and are therefore essentially in-sample, backward-looking measures rather than out-of-sample forecasts of future risks. Second, these news measures are derived under the assumption of conditionally normal market returns, so that hedging demand reflects exposure to future variance only within a world governed by normal return dynamics. In contrast, our framework relaxes this normality assumption and extends the intertemporal hedging component beyond the variance implied by normality, capturing the influence of higher-order dynamics under a general, non-normal return distribution. The resulting hedging bounds incorporate multiple forward-looking elements linked to higher-order moments of the future market return distribution—specifically variance, skewness, and kurtosis—thereby capturing richer, non-Gaussian sources of intertemporal risk that the conventional ICAPM under normality cannot account for.

OA.10 Supplementary Tables and Figures

Table OA.1 Percentage of Theory-Consistent Quantity of Risk

This table reports the percentage of firms with theory-consistent quantities of risk implied by the SDF in Eq (2.9) and Eq (2.39). Specifically, we estimate $\mathcal{R}^j_{M,t\to T_1} = \alpha + \beta_{i,j}\left(\frac{m_{t\to T_1}}{\mathbb{E}_t m_{t\to T_1}}\mathcal{R}_{i,t\to T_1}\right) + \varepsilon_{T_1}$ in the single-period setting without intertemporal hedging, and $\mathcal{R}^j_{M,t\to T_1} = \alpha + \beta_{i,j}\left(\mathbb{E}^*_{T_1}\frac{m_{t\to T_N}}{\mathbb{E}_t m_{t\to T_N}}\mathcal{R}_{i,t\to T_1}\right) + \varepsilon_{T_1}$ in the multi-period setting with intertemporal hedging. The regressions are estimated at the firm level for $j = 1, 2, 3, 4$. A theory-consistent quantity of risk is defined as a positive β for odd j and a negative β for even j. The reported percentage is computed as 100% minus the percentage of statistically significant violations of these sign restrictions. A violation is classified as significant when β has the opposite sign implied by the theory and its t-statistics exceeds 2 in absolute value. When $T_1 = T_N$ ($T_1 \neq T_N$), the βs are computed using the SDF from the single-period setting without intertemporal hedging (the multi-period setting with intertemporal hedging). The sample period spans from January 1996 to August 2025 at monthly frequency.

	$[T_1, T_N]$ (%)	$T_N = 30$	$T_N = 91$	$T_N = 182$	$T_N = 365$	$T_N = 547$	$T_N = 730$
30	$j = 1$	100.00	100.00	100.00	100.00	100.00	100.00
	$j = 2$	99.80	99.80	99.80	99.80	99.80	99.80
	$j = 3$	100.00	100.00	100.00	100.00	100.00	100.00
	$j = 4$	99.80	99.90	99.80	99.80	99.80	99.80
91	$j = 1$		100.00	100.00	100.00	100.00	100.00
	$j = 2$		98.29	97.59	97.59	97.79	97.79
	$j = 3$		99.80	99.80	99.80	99.80	99.80
	$j = 4$		98.70	98.40	98.29	98.29	98.09
182	$j = 1$			99.59	99.70	99.70	99.70
	$j = 2$			92.60	89.96	90.37	91.78
	$j = 3$			99.49	99.70	99.70	99.70
	$j = 4$			94.83	94.32	94.32	94.22
365	$j = 1$				93.08	97.33	97.33
	$j = 2$				83.22	81.19	82.84
	$j = 3$				94.09	98.87	98.77
	$j = 4$				84.95	85.82	87.78

Table OA.2 Average of Time-varying Preference Parameters Calibrated based on Out-of-sample Performance

This table summarizes the average of time-varying preference parameters calibrated to maximize out-of-sample (OOS) forecast accuracy. The preference is calibrated at end of each month based on the OOS performance of the midpoint of LB/HLB and UB/HUB relative to the default parameter values [1, 2, 4, 8] using an expanding window. We then take the average of those parameter values over months. When $T_1 = T_N$ ($T_1 \neq T_N$) the preference parameters are calibrated based on non-hedging (hedging) SDF. The sample period spans from January 1996 to August 2025 at monthly frequency.

	$[T_1, T_N]$	$T_N = 30$	$T_N = 91$	$T_N = 182$	$T_N = 365$	$T_N = 547$	$T_N = 730$
	$1/\tau$	1.19	1.12	1.08	1.04	1.02	1.01
30	ρ	1.33	1.32	1.31	1.30	1.30	1.30
	κ	4.44	2.62	2.15	2.03	1.96	1.98
	ξ	8.03	6.83	5.16	3.66	3.25	3.14
	$1/\tau$		1.24	1.10	1.07	1.05	1.03
91	ρ		1.31	1.36	1.58	1.69	1.63
	κ		3.09	2.62	2.86	2.88	2.69
	ξ		8.03	6.53	5.20	5.11	4.71
	$1/\tau$			1.35	1.03	1.02	1.02
182	ρ			1.32	1.87	2.05	2.01
	κ			2.45	4.64	4.31	3.94
	ξ			9.33	8.56	8.10	7.33
	$1/\tau$				1.25	1.08	1.06
365	ρ				1.48	1.78	2.08
	κ				3.69	3.17	3.87
	ξ				8.89	7.19	7.63

Table OA.3 Average of Time-varying Preference Parameters Calibrated based on Variance Risk Premium

This table summarizes the average of time-varying preference parameters calibrated based on variance risk premium (VRP). The preference is calibrated at end of each month based on the past daily observations of option prices and VRP using an expanding window. We then take the average of those parameter values over months. When $T_1 = T_N$ ($T_1 \neq T_N$) the preference parameters are calibrated based on non-hedging (hedging) SDF. The sample period spans from January 1996 to August 2025 at monthly frequency.

	$[T_1, T_N]$	$T_N = 30$	$T_N = 91$	$T_N = 182$	$T_N = 365$	$T_N = 547$	$T_N = 730$
	$1/\tau$	1.11	2.32	1.63	1.35	1.17	1.17
30	ρ	1.40	1.69	1.66	1.30	1.30	1.30
	κ	2.13	3.97	3.63	3.03	3.48	3.12
	ξ	3.33	7.03	6.35	5.12	6.05	5.31
	$1/\tau$		1.20	1.61	1.19	1.18	1.00
91	ρ		1.45	1.31	1.30	1.30	1.30
	κ		2.42	3.43	3.54	3.09	3.57
	ξ		4.16	6.13	6.31	5.40	6.30
	$1/\tau$			1.15	1.22	1.04	1.03
182	ρ			1.42	1.34	1.33	1.34
	κ			3.84	2.71	2.84	2.62
	ξ			7.58	4.73	4.94	4.43
	$1/\tau$				1.08	1.49	1.64
365	ρ				1.50	2.32	2.18
	κ				2.54	3.98	3.69
	ξ				5.03	7.96	6.90

Table OA.4 Out-of-sample Forecast Accuracy of Static Bounds

This table reports out-of-sample (OOS) R^2 (expressed as a percentage) from predicting future realized excess returns using the lower bound (LB) and upper bound (UB), based on the default preference parameters: $1/\tau = 1, \rho = 2, \kappa = 4$, and $\xi = 8$. The benchmarks include the recursive historical average excess return for stock i from 1990 ($\overline{RX}_{i,t}$), a constant annual return of 6% for all stocks (6% p.a.), the recursive average market excess returns from 1996 ($\overline{MKT}_{i,t}$), the recursive average market implied variance from 1996 ($\overline{IV}_t$), the recursive average implied variance of stock i from 1996 ($\overline{IV}_{i,t}$), the expected excess return measure of Martin and Wagner (2019) ($MW_{i,t}$), the lower bound by Kadan and Tang (2020) ($KT_{i,t}$), and the lower bound by Chabi-Yo, Dim, and Vilkov (2023) ($GLB_{i,t}$). p-values (in parentheses) are for the hypothesis $H_0 : R^2 <= 0$, computed using the stationary block bootstrap procedure with 10,000 replications. For the optimized lower bound (LB^*) and upper bound (UB^*), preference parameters are chosen to maximize out-of-sample forecast accuracy of the midpoint relative to the default calibration [1, 2, 4, 8] up to each time using an expanding window. The sample period spans from January 1996 to August 2025 at monthly frequency.

Panel A. Out-of-sample Forecast Accuracy for LB^*								
	$\overline{RX}_{i,t}$	$6\%\,p.a.$	$\overline{MKT}_t$	$\overline{IV}_t$	$\overline{IV}_{i,t}$	$MW_{i,t}$	$KT_{i,t}$	$GLB_{i,t}$
30 Days	1.696	0.660	0.632	0.758	1.687	2.448	3.508	−0.335
	(0.000)	(0.015)	(0.013)	(0.013)	(0.000)	(0.032)	(0.003)	(0.925)
91 Days	4.866	1.686	1.586	2.008	3.973	4.441	3.855	1.437
	(0.000)	(0.052)	(0.036)	(0.041)	(0.000)	(0.000)	(0.016)	(0.029)
182 Days	11.296	6.001	5.819	6.592	9.106	6.384	5.385	2.859
	(0.000)	(0.019)	(0.014)	(0.015)	(0.000)	(0.002)	(0.034)	(0.045)
365 Days	12.895	2.159	1.796	3.050	7.093	4.062	−1.591	−1.530
	(0.004)	(0.384)	(0.386)	(0.351)	(0.087)	(0.339)	(0.669)	(0.587)

Panel B. Out-of-sample Forecast Accuracy for UB^*								
	$\overline{RX}_{i,t}$	$6\%\,p.a.$	$\overline{MKT}_t$	$\overline{IV}_t$	$\overline{IV}_{i,t}$	$MW_{i,t}$	$KT_{i,t}$	$GLB_{i,t}$
30 Days	−0.456	−1.486	−1.520	−1.387	−0.404	1.285	1.698	−2.482
	(0.798)	(0.959)	(0.963)	(0.949)	(0.759)	(0.279)	(0.124)	(1.000)
91 Days	1.429	−1.850	−1.955	−1.518	0.611	1.512	0.559	−3.152
	(0.109)	(0.664)	(0.676)	(0.630)	(0.241)	(0.250)	(0.077)	(0.864)
182 Days	5.524	−0.119	−0.312	0.511	3.220	0.668	−0.683	−3.465
	(0.018)	(0.501)	(0.509)	(0.458)	(0.084)	(0.430)	(0.649)	(0.789)
365 Days	3.639	−8.236	−8.638	−7.251	−2.792	−6.145	−12.411	−12.323
	(0.347)	(0.692)	(0.709)	(0.667)	(0.597)	(0.666)	(0.847)	(0.767)

Panel C. Out-of-sample Forecast Accuracy for $(LB+UB)/2$								
	$\overline{RX}_{i,t}$	$6\%\,p.a.$	$\overline{MKT}_t$	$\overline{IV}_t$	$\overline{IV}_{i,t}$	$MW_{i,t}$	$KT_{i,t}$	$GLB_{i,t}$
30 Days	1.704	0.712	0.677	0.813	1.758	3.418	3.812	−0.256
	(0.000)	(0.118)	(0.111)	(0.103)	(0.000)	(0.000)	(0.000)	(0.875)
91 Days	5.028	1.911	1.804	2.243	4.241	5.134	4.191	0.672
	(0.000)	(0.123)	(0.105)	(0.108)	(0.000)	(0.000)	(0.001)	(0.148)
182 Days	10.461	5.085	4.905	5.679	8.267	5.820	4.567	1.914
	(0.000)	(0.028)	(0.025)	(0.024)	(0.000)	(0.000)	(0.053)	(0.110)
365 Days	17.972	8.118	7.806	8.983	12.442	9.661	4.122	4.175
	(0.000)	(0.031)	(0.020)	(0.029)	(0.000)	(0.002)	(0.086)	(0.073)

Panel D. Out-of-sample Forecast Accuracy for $(LB^*+UB^*)/2$								
	$\overline{RX}_{i,t}$	$6\%\,p.a.$	$\overline{MKT}_t$	$\overline{IV}_t$	$\overline{IV}_{i,t}$	$MW_{i,t}$	$KT_{i,t}$	$GLB_{i,t}$
30 Days	1.384	0.345	0.317	0.443	1.375	2.133	3.185	−0.651
	(0.001)	(0.250)	(0.248)	(0.221)	(0.000)	(0.135)	(0.000)	(0.964)
91 Days	4.334	1.137	1.037	1.461	3.434	3.900	3.313	−0.119
	(0.000)	(0.251)	(0.238)	(0.221)	(0.000)	(0.001)	(0.000)	(0.530)
182 Days	9.603	4.207	4.022	4.810	7.372	4.463	3.576	1.007
	(0.000)	(0.106)	(0.093)	(0.091)	(0.001)	(0.067)	(0.125)	(0.122)
365 Days	9.216	−1.974	−2.352	−1.045	3.169	0.009	−5.889	−5.82
	(0.111)	(0.566)	(0.582)	(0.535)	(0.327)	(0.515)	(0.786)	(0.686)

Table OA.5 Cross-Sectional Regressions of Static Bound Prediction Errors

This table presents the results of Fama-MacBeth regressions analyzing the prediction errors of the lower bound (LB) and upper bound (UB). We regress the pricing errors (indicated at the top of each column) on a set of commonly used stock characteristics, including CAPM beta, size, book-to-market ratio, momentum, profitability, investment growth, idiosyncratic volatility, and Amihud illiquidity. The analysis is conducted using all available stocks in our sample, with all variables winsorized at the 1% level on a monthly basis. Reported p-values (in parentheses) are based on the standard errors corrected using the Newey and West (1987) method. The sample period spans from January 1996 to August 2025 at monthly frequency.

Panel A. Lower Bound (LB)								
	30 Days		91 Days		182 Days		365 Days	
	Ret-LB	|Ret-LB|	Ret-LB	|Ret-LB|	Ret-LB	|Ret-LB|	Ret-LB	|Ret-LB|
Constant	0.157	0.399	0.109	0.268	0.088	0.228	0.183	0.284
	(0.049)	(0.000)	(0.167)	(0.000)	(0.255)	(0.000)	(0.036)	(0.000)
β	0.011	0.242	0.004	0.131	0.006	0.087	0.004	0.051
	(0.732)	(0.000)	(0.890)	(0.000)	(0.844)	(0.000)	(0.886)	(0.007)
Size	−0.017	−0.026	−0.013	−0.020	−0.012	−0.018	−0.019	−0.023
	(0.018)	(0.000)	(0.062)	(0.000)	(0.083)	(0.000)	(0.019)	(0.002)
B/M	−0.020	−0.003	−0.011	0.003	−0.011	0.004	−0.022	−0.008
	(0.034)	(0.695)	(0.182)	(0.464)	(0.206)	(0.235)	(0.121)	(0.462)
Momentum	0.040	−0.181	0.054	−0.088	0.054	−0.051	−0.018	−0.079
	(0.292)	(0.000)	(0.108)	(0.000)	(0.108)	(0.011)	(0.794)	(0.236)
Profitability	0.027	−0.039	0.033	−0.019	0.026	−0.017	−0.061	−0.069
	(0.325)	(0.005)	(0.184)	(0.025)	(0.319)	(0.111)	(0.168)	(0.087)
Investment	−0.005	0.016	−0.021	−0.001	−0.023	0.005	−0.042	−0.001
	(0.695)	(0.092)	(0.098)	(0.892)	(0.079)	(0.435)	(0.005)	(0.918)
Idio. Vol.	−2.007	27.156	−0.869	17.651	−0.767	12.935	0.234	10.805
	(0.120)	(0.000)	(0.495)	(0.000)	(0.571)	(0.000)	(0.913)	(0.000)
Illiquidity	0.186	−0.026	0.212	−0.081	0.272	−0.088	0.395	−0.012
	(0.044)	(0.556)	(0.030)	(0.031)	(0.021)	(0.017)	(0.152)	(0.917)
R^2 (%)	14.78	19.74	14.85	20.93	15.59	21.27	17.78	21.96

Panel B. Upper Bound (UB)								
	30 Days		91 Days		182 Days		365 Days	
	Ret-UB	|Ret-UB|	Ret-UB	|Ret-UB|	Ret-UB	|Ret-UB|	Ret-UB	|Ret-UB|
Constant	−0.064	0.448	0.108	0.254	0.099	0.202	0.172	0.254
	(0.547)	(0.000)	(0.183)	(0.000)	(0.193)	(0.000)	(0.043)	(0.001)
β	−0.027	0.241	−0.037	0.131	−0.028	0.089	−0.019	0.054
	(0.447)	(0.000)	(0.249)	(0.000)	(0.351)	(0.000)	(0.546)	(0.004)
Size	0.009	−0.031	−0.007	−0.020	−0.009	−0.016	−0.017	−0.022
	(0.321)	(0.000)	(0.315)	(0.000)	(0.169)	(0.000)	(0.037)	(0.004)
B/M	−0.029	0.001	−0.013	0.004	−0.010	0.006	−0.022	−0.008
	(0.004)	(0.997)	(0.131)	(0.286)	(0.225)	(0.090)	(0.139)	(0.452)
Momentum	0.083	−0.198	0.066	−0.096	0.063	−0.056	−0.010	−0.083
	(0.030)	(0.000)	(0.046)	(0.000)	(0.055)	(0.001)	(0.880)	(0.207)
Profitability	0.044	−0.049	0.044	−0.029	0.033	−0.026	−0.056	−0.072
	(0.123)	(0.000)	(0.087)	(0.002)	(0.212)	(0.013)	(0.210)	(0.070)
Investment	0.013	0.008	−0.016	0.001	−0.023	0.007	−0.044	0.006
	(0.404)	(0.431)	(0.206)	(1.000)	(0.075)	(0.347)	(0.003)	(0.419)
Idio. Vol.	−8.074	28.548	−6.801	18.796	−5.226	14.134	−2.785	11.981
	(0.000)	(0.000)	(0.000)	(0.000)	(0.000)	(0.000)	(0.191)	(0.000)
Illiquidity	0.265	−0.042	0.251	−0.090	0.296	−0.125	0.425	−0.092
	(0.019)	(0.327)	(0.019)	(0.021)	(0.018)	(0.011)	(0.131)	(0.412)
R^2 (%)	15.60	20.91	15.80	22.43	16.78	23.45	19.11	25.05

Table OA.6 Portfolios Sorted by Average Hedging Bounds

This table reports average annualized excess returns for portfolios sorted on the average of hedging lower bound (HLB) and hedging upper bound (HUB), for each forecast horizon $T_1 \in \{30, 91, 182, 365\}$ (rows) and investment horizon $T_N \in \{91, 182, 365, 547, 730\}$ (column blocks). Reported p-values (in parentheses) are based on the monotonicity test of Patton and Timmermann (2010) using 10,000 stationary block bootstrap replications across all portfolios formed by HLB+HUB. For the optimized bounds (HLB^* and HUB^*), preference parameters are chosen to maximize out-of-sample forecast accuracy of the midpoint relative to the default calibration [1, 2, 4, 8] up to each time using an expanding window. The sample spans January 1996 to August 2025 at monthly frequency.

		$T_N = 91$		$T_N = 182$		$T_N = 365$		$T_N = 547$		$T_N = 730$	
	$[T_1, T_N]$	(HLB+ HUB)/2	(HLB*+ HUB*)/2	(HLB+ HUB)/2	(HLB*+ HUB*)/2	(HLB+ HUB)/2	(HLB*+ HUB*)/2	(HLB+ HUB)/2	(HLB*+ HUB*)/2	(HLB+ HUB)/2	(HLB*+ HUB*)/2
	Low	0.097	0.098	0.096	0.102	0.100	0.100	0.106	0.100	0.109	0.100
30	High	0.194	0.197	0.192	0.196	0.189	0.194	0.192	0.196	0.192	0.196
	High − Low	0.097	0.099	0.096	0.095	0.089	0.094	0.086	0.096	0.083	0.096
	p-Value	(0.004)	(0.013)	(0.003)	(0.017)	(0.007)	(0.002)	(0.004)	(0.006)	(0.001)	(0.004)
	Low			0.087	0.087	0.088	0.087	0.088	0.087	0.089	0.087
91	High			0.195	0.193	0.195	0.191	0.194	0.191	0.194	0.191
	High − Low			0.107	0.105	0.107	0.104	0.106	0.104	0.104	0.104
	p-Value			(0.002)	(0.001)	(0.002)	(0.002)	(0.006)	(0.009)	(0.003)	(0.002)
	Low					0.087	0.087	0.087	0.087	0.088	0.087
182	High					0.209	0.210	0.210	0.209	0.211	0.209
	High − Low					0.122	0.122	0.123	0.122	0.123	0.121
	p-Value					(0.003)	(0.001)	(0.009)	(0.016)	(0.019)	(0.009)
	Low							0.089	0.088	0.088	0.089
365	High							0.242	0.241	0.242	0.241
	High − Low							0.154	0.153	0.154	0.152
	p-Value							(0.006)	(0.003)	(0.008)	(0.004)

Table OA.7 Out-of-sample Forecast Accuracy of Hedging Bounds

The table reports out-of-sample R^2 (expressed as a percentage) from predicting future realized excess returns using the hedging lower bound (HLB) and hedging upper bound (HUB), based on the default preference set: $1/\tau = 1, \rho = 2, \kappa = 4$, and $\xi = 8$. The benchmarks, indicated in the column headers, include the expected excess return measure of Martin and Wagner (2019) ($MW_{i,t}$), the expected excess return lower bound by Kadan and Tang (2020) ($KT_{i,t}$), the expected excess return lower bound proposed by Chabi-Yo, Dim, and Vilkov (2023) ($GLB_{i,t}$), and LB/UB without hedging. Reported p-values (in parentheses) are for the hypothesis $H_0 : R^2 <= 0$, computed using the stationary block bootstrap procedure with 10,000 replications. For the optimized HLB^* and HUB^*, preference parameters are chosen to maximize out-of-sample forecast accuracy of the midpoint relative to the default calibration [1, 2, 4, 8] up to each time using an expanding window. HLB^* and HUB^* are identical for each maturity. When $T_1 = T_N$, since HLB (HUB) converges to LB (UB), we set R^2 (p-value) to 0.000 ((0.000)). The sample period spans from January 1996 to August 2025 at monthly frequency.

Panel A. Out-of-sample Forecast Accuracy for HLB^*

	$T_N = 365$				$T_N = 730$			
	$MW_{i,t}$	$KT_{i,t}$	$GLB_{i,t}$	$LB^*_{i,t}$	$MW_{i,t}$	$KT_{i,t}$	$GLB_{i,t}$	$LB^*_{i,t}$
$T_1 = 30$	3.396	3.936	−0.187	−0.023	3.623	4.045	−0.053	0.104
	(0.000)	(0.001)	(0.858)	(0.320)	(0.000)	(0.000)	(0.688)	(0.143)
$T_1 = 91$	5.365	4.445	0.868	0.279	5.380	4.459	0.885	0.299
	(0.000)	(0.006)	(0.145)	(0.191)	(0.000)	(0.007)	(0.117)	(0.146)
$T_1 = 182$	7.332	5.942	3.337	1.776	7.027	5.634	3.018	1.928
	(0.000)	(0.018)	(0.012)	(0.021)	(0.000)	(0.035)	(0.015)	(0.021)
$T_1 = 365$	9.347	3.818	3.888	0.000	9.366	3.827	3.887	1.264
	(0.015)	(0.280)	(0.162)	(0.000)	(0.017)	(0.280)	(0.148)	(0.176)

Panel B. Out-of-sample Forecast Accuracy for HUB^*

	$T_N = 365$				$T_N = 730$			
	$MW_{i,t}$	$KT_{i,t}$	$GLB_{i,t}$	$UB^*_{i,t}$	$MW_{i,t}$	$KT_{i,t}$	$GLB_{i,t}$	$UB^*_{i,t}$
$T_1 = 30$	1.105	1.519	−2.668	−0.605	0.967	1.381	−2.813	−0.790
	(0.291)	(0.161)	(1.000)	(0.999)	(0.302)	(0.193)	(1.000)	(0.999)
$T_1 = 91$	1.920	0.971	−2.726	−1.312	1.222	0.267	−3.456	−2.195
	(0.213)	(0.028)	(0.846)	(0.968)	(0.292)	(0.178)	(0.889)	(0.994)
$T_1 = 182$	4.089	2.784	0.098	−0.272	3.382	2.068	−0.638	−0.984
	(0.053)	(0.004)	(0.476)	(0.547)	(0.112)	(0.029)	(0.544)	(0.743)
$T_1 = 365$	5.779	0.008	0.052	0.000	5.370	−0.424	−0.381	−2.781
	(0.112)	(0.566)	(0.487)	(0.000)	(0.126)	(0.641)	(0.505)	(0.899)

Panel C. Out-of-sample Forecast Accuracy for $(HLB + HUB)/2$								
	$T_N = 365$				$T_N = 730$			
	$MW_{i,t}$	$KT_{i,t}$	$GLB_{i,t}$	$\frac{(LB_{i,t}+UB_{i,t})}{2}$	$MW_{i,t}$	$KT_{i,t}$	$GLB_{i,t}$	$\frac{(LB_{i,t}+UB_{i,t})}{2}$
$T_1 = 30$	2.355	3.392	−0.418	−0.350	1.324	2.373	−1.477	−1.405
	(0.120)	(0.000)	(0.871)	(0.828)	(0.299)	(0.116)	(0.969)	(0.965)
$T_1 = 91$	4.306	3.698	0.339	−0.419	2.284	1.664	−1.766	−2.524
	(0.016)	(0.000)	(0.484)	(0.640)	(0.269)	(0.258)	(0.746)	(0.831)
$T_1 = 182$	5.773	4.917	2.367	1.014	4.878	4.014	1.440	0.164
	(0.000)	(0.011)	(0.047)	(0.041)	(0.020)	(0.011)	(0.134)	(0.446)
$T_1 = 365$	9.598	4.059	4.100	0.000	8.454	2.845	2.887	−0.380
	(0.001)	(0.060)	(0.162)	(0.000)	(0.017)	(0.181)	(0.129)	(0.535)

Panel D. Out-of-sample Forecast Accuracy for $(HLB^* + HUB^*)/2$								
	$T_N = 365$				$T_N = 730$			
	$MW_{i,t}$	$KT_{i,t}$	$GLB_{i,t}$	$\frac{(LB^*_{i,t}+UB^*_{i,t})}{2}$	$MW_{i,t}$	$KT_{i,t}$	$GLB_{i,t}$	$\frac{(LB^*_{i,t}+UB^*_{i,t})}{2}$
$T_1 = 30$	2.969	3.500	−0.623	−0.510	3.110	3.524	−0.579	−0.496
	(0.039)	(0.000)	(0.950)	(0.848)	(0.010)	(0.000)	(0.932)	(0.830)
$T_1 = 91$	4.503	3.579	−0.023	−0.627	4.334	3.407	−0.198	−0.794
	(0.000)	(0.000)	(0.504)	(0.611)	(0.001)	(0.000)	(0.554)	(0.649)
$T_1 = 182$	6.474	5.203	2.583	1.024	6.200	4.927	2.297	1.226
	(0.000)	(0.000)	(0.064)	(0.055)	(0.000)	(0.000)	(0.103)	(0.051)
$T_1 = 365$	8.368	2.766	2.818	0.000	8.332	2.719	2.760	0.188
	(0.010)	(0.254)	(0.326)	(0.000)	(0.009)	(0.242)	(0.326)	(0.445)

Table OA.8 Cross-Sectional Regressions of Hedging Bound Prediction Errors

This table presents the results of Fama–MacBeth regressions analyzing the prediction errors of the hedging lower bound (HLB) and hedging upper bound (HUB). Specifically, we regress the pricing errors (indicated at the top of each column) on a set of commonly used stock characteristics, including CAPM beta, size, book-to-market ratio, momentum, profitability, investment growth, idiosyncratic volatility, and Amihud illiquidity. The analysis is conducted using all available stocks in our sample, with all variables winsorized at the 1% level on a monthly basis. The reported p-values (in parentheses) are based on standard errors corrected using the Newey and West (1987) method. The sample period spans from January 1996 to August 2025 at monthly frequency.

Panel A. Lower Bound with Hedging (HLB)

	$[T_1, T_N]$=[30, 365]		$[T_1, T_N]$=[91, 365]		$[T_1, T_N]$=[182, 365]		$[T_1, T_N]$=[365, 730]	
	Ret-HLB	|Ret-HLB|	Ret-HLB	|Ret-HLB|	Ret-HLB	|Ret-HLB|	Ret-HLB	|Ret-HLB|
Constant	0.124	0.394	0.093	0.262	0.078	0.223	0.172	0.274
	(0.117)	(0.000)	(0.238)	(0.000)	(0.309)	(0.000)	(0.047)	(0.000)
β	0.004	0.241	−0.002	0.130	0.002	0.086	0.002	0.051
	(0.915)	(0.000)	(0.960)	(0.000)	(0.935)	(0.000)	(0.961)	(0.007)
Size	−0.016	−0.026	−0.013	−0.020	−0.012	−0.017	−0.019	−0.023
	(0.025)	(0.000)	(0.065)	(0.000)	(0.085)	(0.000)	(0.021)	(0.003)
B/M	−0.021	−0.002	−0.012	0.004	−0.011	0.005	−0.023	−0.008
	(0.031)	(0.763)	(0.177)	(0.371)	(0.205)	(0.185)	(0.120)	(0.469)
Momentum	0.031	−0.181	0.051	−0.087	0.054	−0.050	−0.017	−0.078
	(0.414)	(0.000)	(0.122)	(0.000)	(0.106)	(0.008)	(0.799)	(0.243)
Profitability	0.027	−0.040	0.033	−0.020	0.026	−0.017	−0.061	−0.069
	(0.326)	(0.005)	(0.186)	(0.018)	(0.317)	(0.101)	(0.170)	(0.087)
Investment	−0.005	0.015	−0.022	−0.001	−0.023	0.006	−0.042	0.001
	(0.697)	(0.145)	(0.091)	(0.881)	(0.077)	(0.424)	(0.004)	(0.876)
Idio. Vol.	−2.316	27.335	−1.130	17.807	−0.972	13.063	−0.003	10.999
	(0.073)	(0.000)	(0.375)	(0.000)	(0.472)	(0.000)	(0.999)	(0.000)
Illiquidity	0.184	−0.027	0.215	−0.084	0.274	−0.094	0.398	−0.020
	(0.043)	(0.531)	(0.029)	(0.029)	(0.020)	(0.014)	(0.150)	(0.865)
R^2 (%)	14.77	19.81	14.83	21.04	15.57	21.39	17.79	22.29

Panel B. Upper Bound with Hedging (HUB)								
	$[T_1, T_N]$=[30, 365]		$[T_1, T_N]$=[91, 365]		$[T_1, T_N]$=[182, 365]		$[T_1, T_N]$=[365, 730]	
	Ret-HUB	|Ret-HUB|	Ret-HUB	|Ret-HUB|	Ret-HUB	|Ret-HUB|	Ret-HUB	|Ret-HUB|
Constant	−0.077	0.451	0.099	0.250	0.092	0.197	0.163	0.244
	(0.467)	(0.000)	(0.221)	(0.000)	(0.224)	(0.000)	(0.053)	(0.002)
β	−0.028	0.240	−0.041	0.132	−0.031	0.090	−0.022	0.055
	(0.431)	(0.000)	(0.213)	(0.000)	(0.312)	(0.000)	(0.489)	(0.004)
Size	0.006	−0.031	−0.008	−0.019	−0.009	−0.015	−0.016	−0.021
	(0.530)	(0.000)	(0.273)	(0.000)	(0.166)	(0.000)	(0.040)	(0.005)
B/M	−0.029	0.001	−0.013	0.005	−0.010	0.007	−0.021	−0.008
	(0.005)	(0.881)	(0.139)	(0.231)	(0.230)	(0.074)	(0.140)	(0.451)
Momentum	0.076	−0.198	0.065	−0.094	0.064	−0.054	−0.009	−0.082
	(0.048)	(0.000)	(0.049)	(0.000)	(0.052)	(0.001)	(0.891)	(0.211)
Profitability	0.045	−0.050	0.045	−0.030	0.033	−0.026	−0.055	−0.071
	(0.121)	(0.000)	(0.084)	(0.002)	(0.208)	(0.013)	(0.215)	(0.069)
Investment	0.014	0.007	−0.016	0.001	−0.023	0.007	−0.044	0.008
	(0.375)	(0.523)	(0.204)	(0.996)	(0.074)	(0.338)	(0.003)	(0.277)
Idio. Vol.	−8.117	28.788	−7.054	19.011	−5.423	14.296	−3.049	12.211
	(0.000)	(0.000)	(0.000)	(0.000)	(0.000)	(0.000)	(0.152)	(0.000)
Illiquidity	0.250	−0.043	0.249	−0.094	0.296	−0.131	0.427	−0.095
	(0.021)	(0.324)	(0.019)	(0.019)	(0.019)	(0.010)	(0.129)	(0.400)
R^2 (%)	15.52	21.05	15.83	22.61	16.81	23.65	19.21	25.44

Table OA.9 Contribution of Forward Market Moments to Hedging Bounds

This table summarizes the decomposition of the hedging component into contributions from variance, skewness, and kurtosis. We compute the variance-, skewness-, and kurtosis-related components by aggregating the forward moment terms corresponding to the coefficients $a_{j,k-j}$ in Proposition 2.4 for each $k-j$ with varying j to derive the total contribution of each moment in the intertemporal hedging case. Specifically, the component associated with $k-j=2$ captures the variance-related contribution, $k-j=3$ captures the skewness-related contribution, and $k-j=4$ captures the kurtosis-related contribution. The contribution of each forward moment is then calculated as the ratio of the respective forward moment to the total corresponding hedging bound (e.g., HLB or HUB). The sample period spans from January 1996 to August 2025 at monthly frequency.

		$T_N=91$		$T_N=182$		$T_N=365$		$T_N=547$		$T_N=730$	
	$[T_1,T_N]$	HLB	HUB	HLB	HUB	HLB	HUB	HLB	HUB	HLB	HUB
30	Variance (%)	2.84	4.00	6.57	8.91	12.01	15.25	15.65	18.99	18.12	21.28
	Skewness (%)	2.25	1.88	5.20	4.42	9.61	8.06	12.60	10.33	14.64	11.71
	Kurtosis (%)	0.56	0.34	1.19	0.96	2.29	2.24	3.05	3.35	3.64	4.32
91	Variance (%)			2.43	1.51	6.25	4.02	9.05	5.99	11.16	7.53
	Skewness (%)			2.83	1.51	7.23	4.05	10.44	6.04	12.83	7.60
	Kurtosis (%)			1.24	0.60	2.88	1.54	3.74	2.16	4.08	2.56
182	Variance (%)					3.40	1.53	5.93	2.80	7.86	3.86
	Skewness (%)					4.19	1.65	7.31	3.02	9.69	4.20
	Kurtosis (%)					2.57	1.06	4.11	1.78	4.93	2.23
365	Variance (%)							2.77	1.21	4.90	2.24
	Skewness (%)							3.00	0.90	5.33	1.67
	Kurtosis (%)							2.40	0.82	4.02	1.42

Table OA.10 Cross-Sectional Determinants of Hedging Contributions

This table presents the results of Fama–MacBeth regressions analyzing the determinants of the hedging contributions. Specifically, we regress the hedging contributions (indicated at the top of each column) on a set of commonly used stock characteristics, including CAPM beta, size, book-to-market ratio, momentum, profitability, investment growth, idiosyncratic volatility, and Amihud illiquidity. The analysis is conducted using all available stocks in our sample, with all variables winsorized at the 1% level on a monthly basis. The reported p-values are based on standard errors corrected using the Newey and West (1987) method. The sample period spans from January 1996 to August 2025 at monthly frequency.

	$[T_1, T_N]$=[30, 365]		$[T_1, T_N]$=[91, 365]		$[T_1, T_N]$=[182, 365]		$[T_1, T_N]$=[365, 730]	
	$\frac{(HLB-LB)}{HLB}$	$\frac{(HUB-UB)}{HUB}$	$\frac{(HLB-LB)}{HLB}$	$\frac{(HUB-UB)}{HUB}$	$\frac{(HLB-LB)}{HLB}$	$\frac{(HUB-UB)}{HUB}$	$\frac{(HLB-LB)}{HLB}$	$\frac{(HUB-UB)}{HUB}$
Constant	0.234	0.001	0.208	0.130	0.143	0.093	0.136	0.155
	(0.000)	(0.993)	(0.000)	(0.000)	(0.000)	(0.000)	(0.000)	(0.000)
β	−0.008	−0.065	−0.008	−0.041	−0.005	−0.018	−0.005	−0.015
	(0.000)	(0.000)	(0.000)	(0.000)	(0.000)	(0.000)	(0.000)	(0.000)
Size	0.010	0.048	0.004	0.011	0.002	0.003	0.001	0.003
	(0.000)	(0.000)	(0.000)	(0.000)	(0.000)	(0.000)	(0.000)	(0.000)
B/M	−0.001	−0.008	0.000	−0.002	0.000	−0.001	0.002	0.000
	(0.075)	(0.000)	(0.457)	(0.000)	(0.164)	(0.003)	(0.621)	(0.076)
Momentum	0.073	0.051	0.027	0.010	0.007	0.003	0.003	0.003
	(0.000)	(0.000)	(0.000)	(0.000)	(0.000)	(0.000)	(0.000)	(0.001)
Profitability	0.006	0.007	0.004	−0.001	0.002	0.003	0.001	0.002
	(0.000)	(0.010)	(0.000)	(0.413)	(0.000)	(0.922)	(0.000)	(0.000)
Investment	−0.001	−0.007	−0.001	−0.006	−0.001	−0.002	−0.001	−0.002
	(0.556)	(0.073)	(0.241)	(0.000)	(0.085)	(0.000)	(0.023)	(0.000)
Idio. Vol.	−2.324	−6.284	−1.755	−3.503	−0.888	−1.473	−0.631	−1.346
	(0.000)	(0.000)	(0.000)	(0.000)	(0.000)	(0.000)	(0.000)	(0.000)
Illiquidity	0.034	0.175	−0.003	0.053	−0.002	0.017	0.009	0.032
	(0.003)	(0.001)	(0.378)	(0.002)	(0.205)	(0.004)	(0.009)	(0.002)
R^2 (%)	25.46	54.37	42.04	55.66	55.77	53.77	60.73	53.40

Table OA.11 Cross-Sectional Regressions of Hedging Contributions with Cash-Flow, Discount-Rate, and Volatilit News Betas

This table presents the results of Fama–MacBeth regressions analyzing the determinants of the hedging contributions. Specifically, we regress the hedging contributions (indicated at the top of each column) on a set of commonly used stock characteristics, including three betas (i.e., $\beta_{CF}, \beta_{DR}, \beta_V$) computed following the approach of Campbell et al. (2018), as well as size, book-to-market ratio, momentum, profitability, investment growth, idiosyncratic volatility, and Amihud illiquidity. The analysis is conducted using all available stocks in our sample, with all variables winsorized at the 1% level on a monthly basis. The reported p-values are based on standard errors corrected using the Newey and West (1987) method. The sample period spans from January 1996 to August 2025 at monthly frequency.

	$[T_1, T_N]$=[30, 365]		$[T_1, T_N]$=[91, 365]		$[T_1, T_N]$=[182, 365]		$[T_1, T_N]$=[365, 730]	
	$\frac{(HLB-LB)}{HLB}$	$\frac{(HUB-UB)}{HUB}$	$\frac{(HLB-LB)}{HLB}$	$\frac{(HUB-UB)}{HUB}$	$\frac{(HLB-LB)}{HLB}$	$\frac{(HUB-UB)}{HUB}$	$\frac{(HLB-LB)}{HLB}$	$\frac{(HUB-UB)}{HUB}$
Constant	0.258	0.045	0.206	0.138	0.139	0.097	0.135	0.161
	(0.000)	(0.439)	(0.000)	(0.000)	(0.000)	(0.000)	(0.000)	(0.000)
β_{CF}	0.004	0.018	0.003	0.012	0.001	0.006	0.001	0.004
	(0.025)	(0.000)	(0.003)	(0.000)	(0.059)	(0.000)	(0.061)	(0.000)
β_{DR}	−0.010	−0.053	−0.006	−0.034	−0.003	−0.014	−0.002	−0.011
	(0.106)	(0.000)	(0.020)	(0.000)	(0.015)	(0.000)	(0.022)	(0.000)
β_V	0.023	0.013	0.006	−0.014	0.003	−0.010	0.002	−0.008
	(0.251)	(0.728)	(0.558)	(0.530)	(0.553)	(0.387)	(0.610)	(0.412)
Size	0.008	0.043	0.004	0.010	0.002	0.002	0.001	0.002
	(0.000)	(0.000)	(0.000)	(0.000)	(0.000)	(0.000)	(0.000)	(0.000)
B/M	−0.001	−0.008	0.000	−0.001	0.000	0.000	0.000	−0.001
	(0.155)	(0.000)	(0.435)	(0.028)	(0.718)	(0.248)	(0.830)	(0.039)
Momentum	0.064	0.037	0.024	0.006	0.007	0.002	0.004	0.001
	(0.000)	(0.000)	(0.000)	(0.085)	(0.000)	(0.201)	(0.000)	(0.230)
Profitability	0.001	0.001	0.001	−0.001	0.000	0.000	0.000	0.001
	(0.456)	(0.540)	(0.135)	(0.078)	(0.008)	(0.499)	(0.000)	(0.008)
Investment	0.003	−0.003	0.001	−0.003	0.001	−0.002	0.000	−0.001
	(0.148)	(0.395)	(0.656)	(0.015)	(0.496)	(0.001)	(0.630)	(0.137)
Idio. Vol.	−2.655	−8.035	−1.769	−4.306	−0.878	−1.834	−0.624	−1.657
	(0.000)	(0.000)	(0.000)	(0.000)	(0.000)	(0.000)	(0.000)	(0.000)
Illiquidity	0.017	0.099	−0.005	0.025	−0.003	0.006	0.002	0.012
	(0.016)	(0.000)	(0.085)	(0.000)	(0.139)	(0.001)	(0.489)	(0.001)
R^2 (%)	25.90	51.59	37.88	49.72	45.90	44.80	46.91	43.86

Table OA.12 Proportion of Hedging Contributions Explained by Cash-Flow, Discount-Rate, and Volatility News Betas

This table summarizes the decomposition of the hedging component based on the three betas proposed by Campbell et al. (2018). Following their approach, we first decompose market excess returns into three components: cash-flows news (CF), discount-rate news (DR), and volatility news (V). For each stock in our sample, we then compute the stock's beta with respect to each of these market excess return components using a 60-month rolling window. Next, we estimate a cross-sectional regression of the hedging component (e.g., (HLB−LB)/HLB) on the three betas (i.e., $\beta_{CF}, \beta_{DR}, \beta_V$) for each month. The proportion of the hedging component attributable to each beta is calculated as the corresponding regression coefficient multiplied by the covariance between the beta and the hedging component, and then scaled by the variance of the hedging component. The sample period spans from January 1996 to August 2025 at monthly frequency.

		$T_N = 91$		$T_N = 182$		$T_N = 365$		$T_N = 547$		$T_N = 730$	
	$[T_1, T_N]$	HLB-LB	HUB-UB	HLB-LB	HUB-UB	HLB-LB	HUB-UB	HLB-LB	HUB-UB	HLB-LB	HUB-UB
30	β_{CF} (%)	1.00	1.91	1.03	1.93	1.04	1.93	1.04	1.91	1.01	1.92
	β_{DR} (%)	3.27	6.48	3.39	6.60	3.41	6.67	3.42	6.65	3.40	6.62
	β_V (%)	2.20	2.89	2.31	3.11	2.46	3.34	2.46	3.43	2.32	3.53
91	β_{CF} (%)			1.49	2.28	1.57	2.38	1.58	2.40	1.58	2.40
	β_{DR} (%)			5.22	7.15	5.43	7.38	5.43	7.50	5.51	7.58
	β_V (%)			2.80	3.27	3.10	3.57	3.30	3.69	3.44	3.78
182	β_{CF} (%)					1.79	2.31	1.84	2.38	1.88	2.46
	β_{DR} (%)					6.18	6.87	6.28	7.10	6.27	7.25
	β_V (%)					3.45	3.21	3.66	3.50	3.76	3.72
365	β_{CF} (%)							1.65	1.79	1.70	1.85
	β_{DR} (%)							5.40	5.25	5.63	5.49
	β_V (%)							2.92	2.37	3.09	2.54

Table OA.13 Percentage of Negative Hedging Contributions Under CRRA Utility

This table summarizes the percentage of negative proportion of the hedging component by CRRA utility, measured as the difference between hedging expected excess return (HER) and non-hedging expected excess return (ER) scaled by ER with various T_1 and T_N. The risk aversions for CRRA utility are 3, 4, and 5. The negative percentage is first computed by calculating the percentage of negative (HER-ER) out of all available firm in our sample by the end of each month, and then taking the average over months. The sample period spans from January 1996 to August 2025 at monthly frequency.

	$[T_1, T_N]$ (%)	$T_N = 91$	$T_N = 182$	$T_N = 365$	$T_N = 547$	$T_N = 730$
	Risk Aversion=3	98.95	97.25	97.19	98.92	98.94
30	Risk Aversion=4	98.97	98.83	97.56	98.92	96.91
	Risk Aversion=5	98.98	98.26	98.09	97.32	95.91
	Risk Aversion=3		98.80	98.74	97.96	98.80
91	Risk Aversion=4		98.14	98.37	96.11	98.04
	Risk Aversion=5		98.42	98.87	98.55	98.27
	Risk Aversion=3			96.57	97.82	95.18
182	Risk Aversion=4			97.62	96.12	97.38
	Risk Aversion=5			95.68	96.10	98.29
	Risk Aversion=3				98.32	98.48
365	Risk Aversion=4				98.95	98.36
	Risk Aversion=5				98.03	98.79

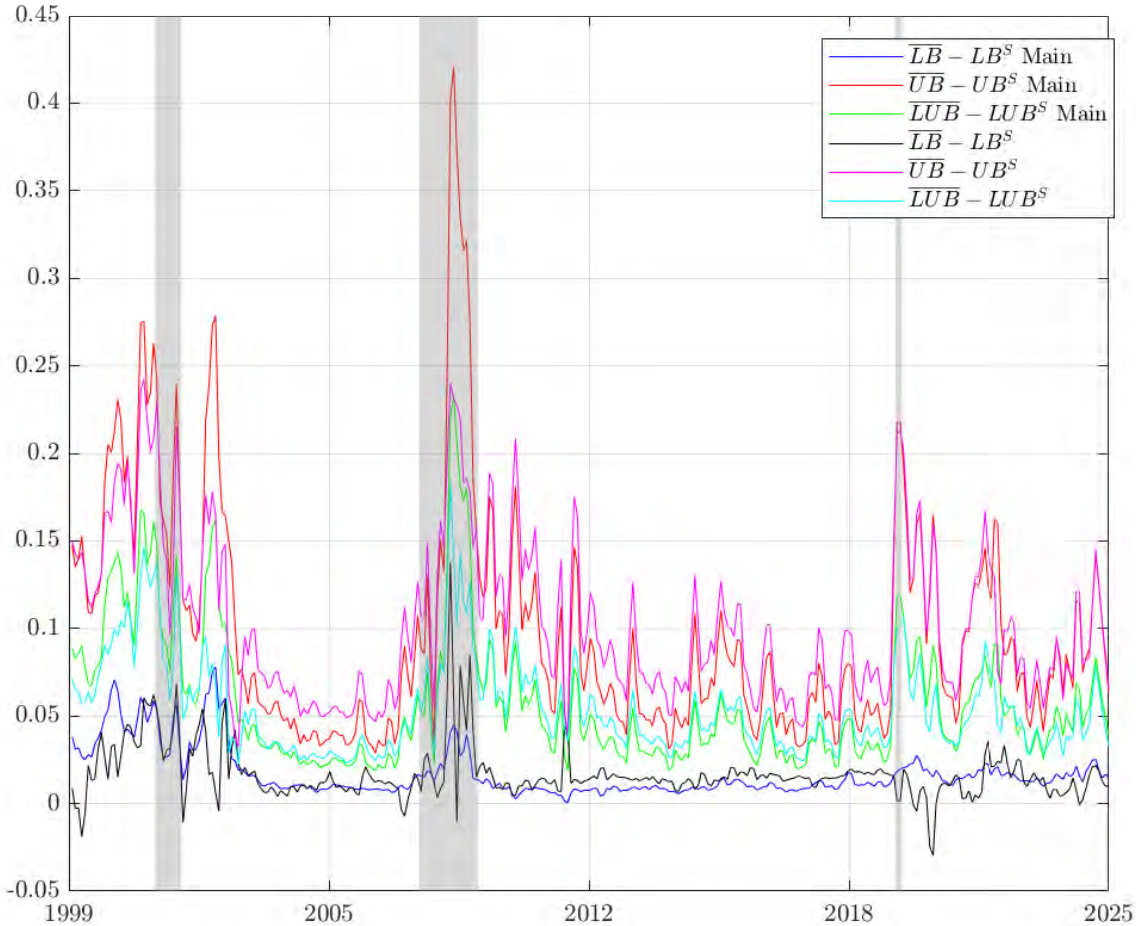

Fig. OA.1: Pricing Consistency: Robustness to an Alternative Set of Identifying Moments (2.22) This figure reports pricing-consistency results obtained using an alternative set of identifying moments. Our main specification uses $(\mathcal{N}, q^*) = (2, 2)$, corresponding to moment conditions based on $q = 2, 3$, whereas the robustness specification uses $(\mathcal{N}, q^*) = (2, 3)$, corresponding to moment conditions based on $q = 3, 4$, to estimate $\underline{\gamma}_{i,k,t}$ and $\overline{\gamma}_{i,k,t}$. This figure reports average differences in 30-day annualized expected excess return bounds between nine S&P500-based SPDR ETFs (X^S) and the value-weighted bounds of their underlying constituents ($\bar{X}$) based on the new approach. The figure includes the static bounds (LB and UB) and midpoint (LUB=(LB+UB)/2), as well as the hedging bounds (HLB and HUB) and midpoint (HLUB=(HLB+HUB)/2). We compare them with the main results as in Figure 2 denoted as "LB/UB/LUB Main". The series are monthly averages of annualized daily values from January 1999 to August 2025. The grey areas indicate NBER recessions.

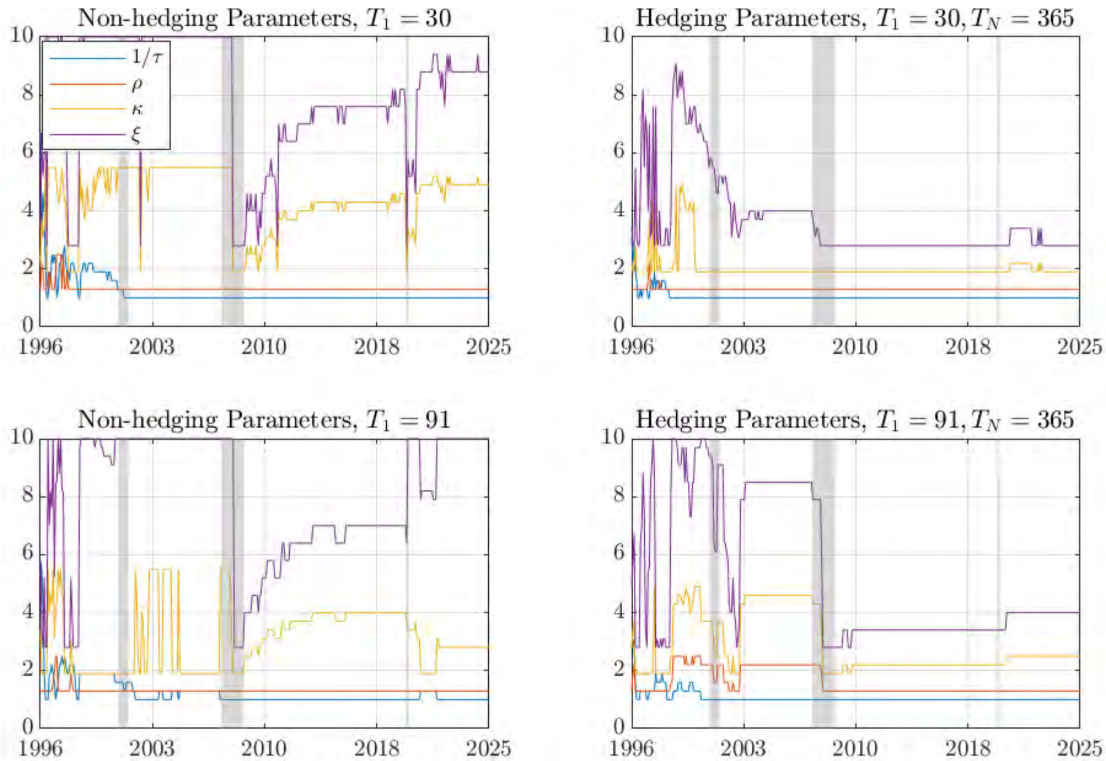

Fig. OA.2: Time Series of Time-Varying Preference Parameters Calibrated based on Out-of-sample Performance This figure displays the time-varying preference parameters calibrated based on out-of-sample (OOS) performance. The preference is calibrated at end of each month to maximize OOS forecast accuracy of the midpoint (i.e., (LB+UB)/2 for the non-hedging case and (HLB+HUB)/2 for the hedging case) relative to the default calibration [1, 2, 4, 8] up to each time using an expanding window. As an example, we choose $T_1 = 30/91$ and $T_N = 365$. The grey areas indicate the National Bureau of Economic Research (NBER) recession periods. The sample periods spans from January 1996 to August 2025 at monthly frequency.

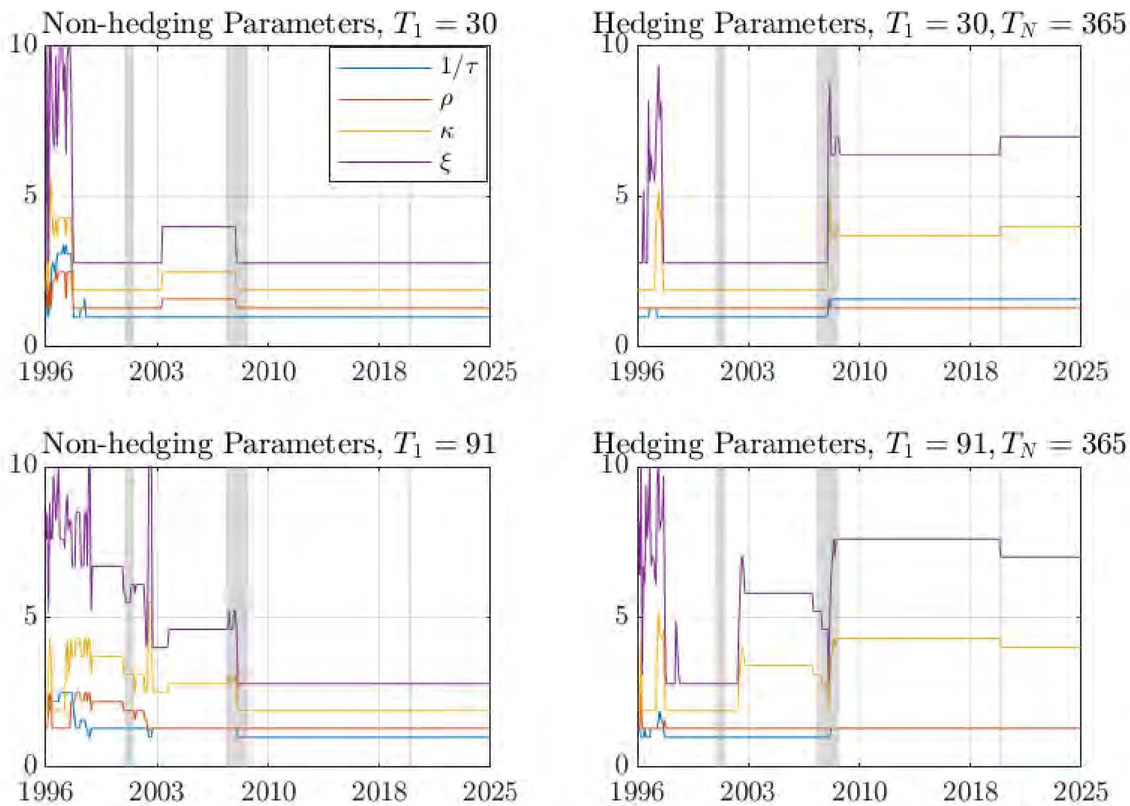

Fig. OA.3: Time Series of Time-Varying Preference Parameters Calibrated based on Variance Risk Premium This figure displays the time-varying preference parameters calibrated based on variance risk premium (VRP). The preference is calibrated at end of each month based on the past daily observations of option prices and VRP using an expanding window. As an example, we choose $T_1 = 30/91$ and $T_N = 365$. The grey areas indicate the National Bureau of Economic Research (NBER) recession periods. The sample periods spans from January 1996 to August 2025 at monthly frequency.

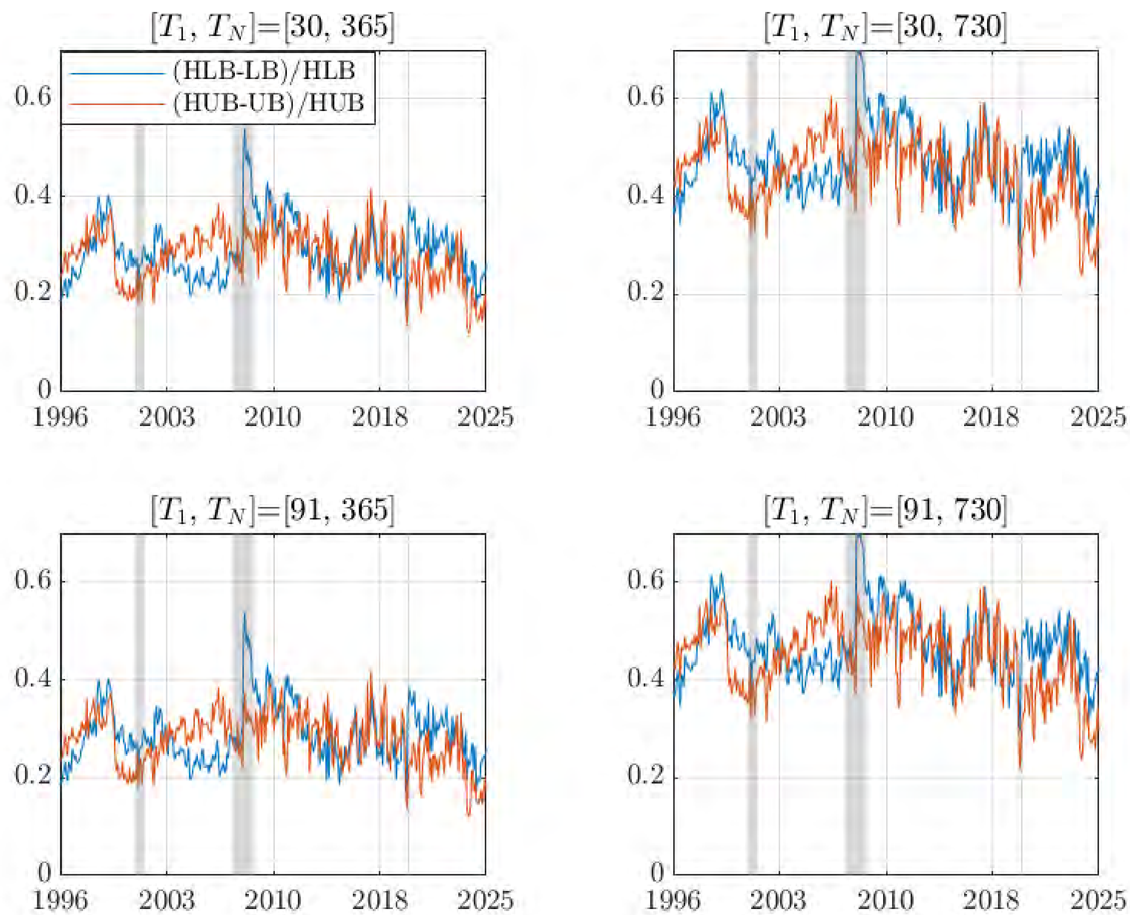

Fig. OA.4: Time Series of Hedging Contributions This figure displays the time series of average proportion of the hedging component, measured as (HLB−LB)/HLB or (HUB−UB)/UB over time. Each subfigure corresponds to a specific maturity pair, with T_1 set to either 30 or 91 days and T_N set to either 365 or 730 days, as indicated in the respective title. The sample period spans from January 1996 to August 2025 at monthly frequency. The grey areas indicate the National Bureau of Economic Research (NBER) recession periods.

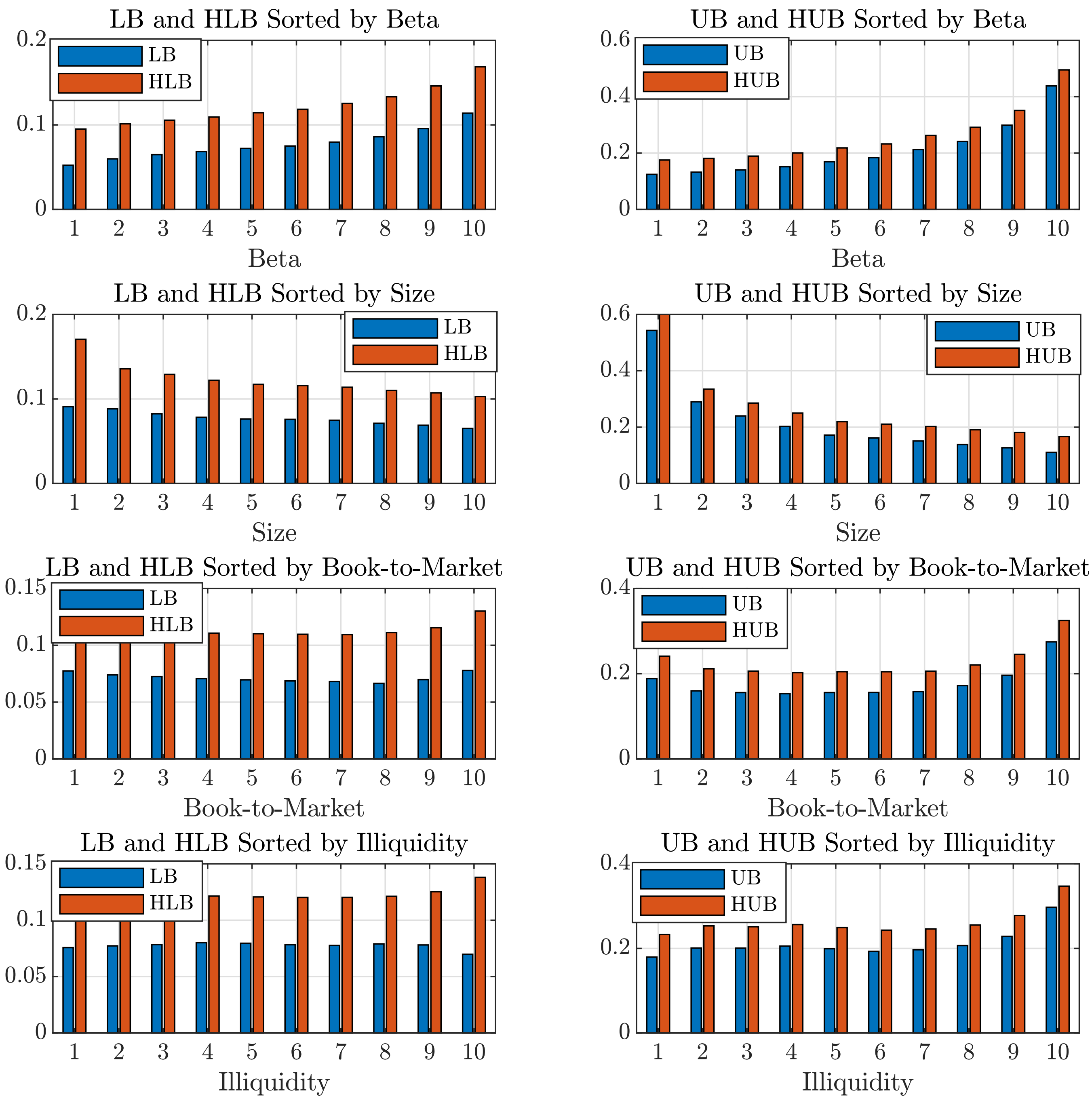

Fig. OA.5: Static vs. Hedging Bounds for Portfolios Sorted by Firm Characteristics This figure displays the average portfolio-level hedging lower bound (HLB) and hedging upper bound (HUB), as well as the unhedged lower bound (LB) and upper bound (UB), sorted by various stock characteristics, including CAPM beta, size, book-to-market ratio, and Amihud illiquidity. We set $T_1 = 30$ and $T_N = 365$. At the end of each month, we first sort all available stocks' LB, UB, HLB, and HUB into deciles ranging from 1 (smallest) to 10 (largest), and then compute the average across all firms' bounds within each decile. The sample period spans from January 1996 to August 2025 at monthly frequency.

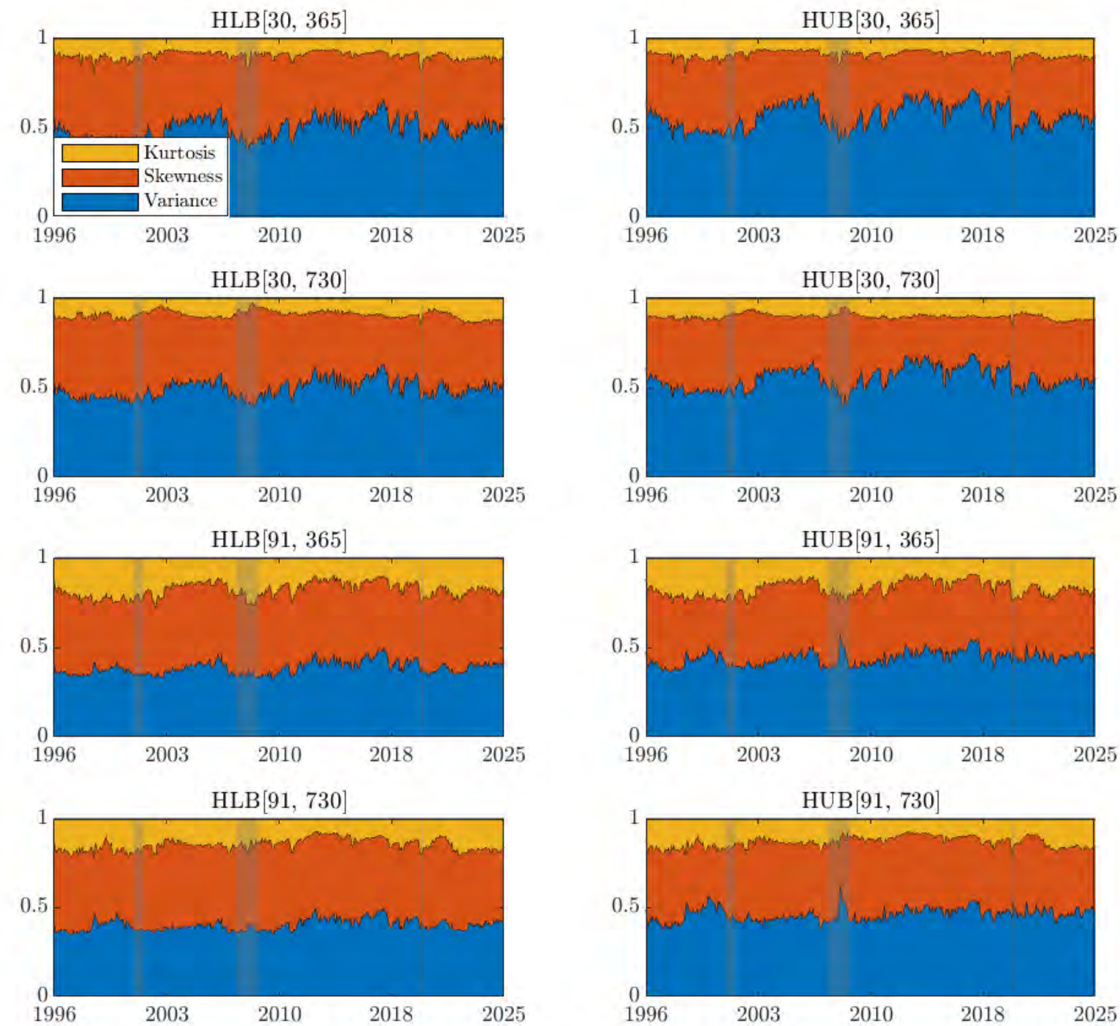

Fig. OA.6: Time Series of Decomposed Hedging Contributions This figure depicts the time-series decomposition of the hedging lower bound (HLB) and hedging upper bound (HUB) across all firms in the sample. The detailed decomposition process is described in under Figure 5. Each subfigure corresponds to a specific maturity pair, with T_1 set to either 30 or 91 days and T_N set to either 365 or 730 days, as indicated in the respective title. The sample period spans from January 1996 to August 2025 at monthly frequency. The grey areas indicate the National Bureau of Economic Research (NBER) recession periods.

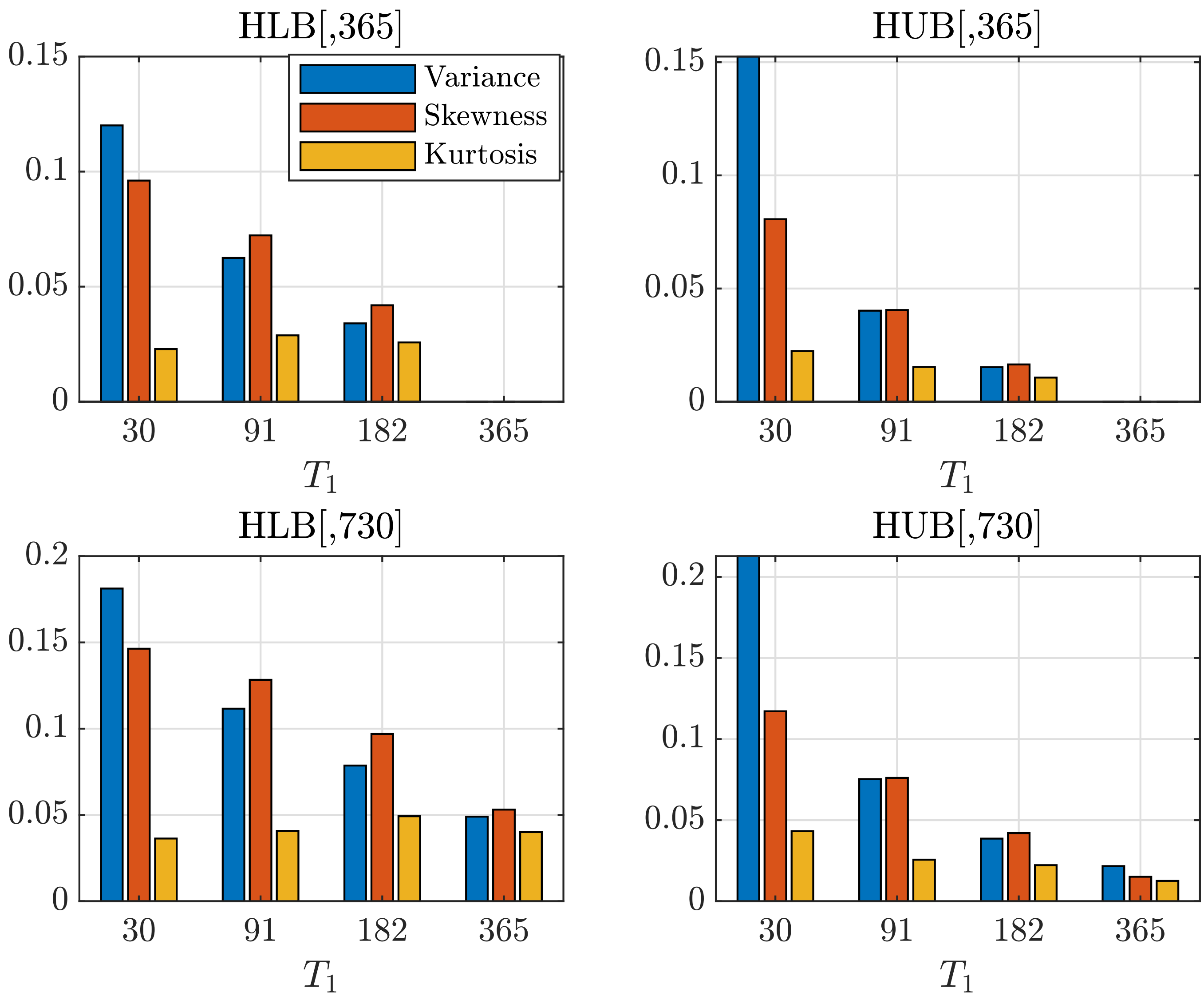

Fig. OA.7: Contribution of Forward Market Moments to Hedging Bounds This figure depicts the average decomposition of the hedging lower bound (HLB) and upper bound (HUB) across all firms in the sample, with maturities ranging from 30 to 365 days. We compute the variance-, skewness-, and kurtosis-related components by aggregating the forward moment terms corresponding to the coefficients $a_{j,k-j}$ in Proposition 2.4 for each $k-j$ with varying j to derive the total contribution of each moment in the intertemporal hedging case. Specifically, the component associated with $k-j=2$ captures the variance-related contribution, $k-j=3$ captures the skewness-related contribution, and $k-j=4$ captures the kurtosis-related contribution. The contribution of each forward moment is then calculated as the ratio of the respective forward moment to the total corresponding hedging bound (e.g., HLB or HUB). The sample period is from January 1996 to August 2025 at monthly frequency.

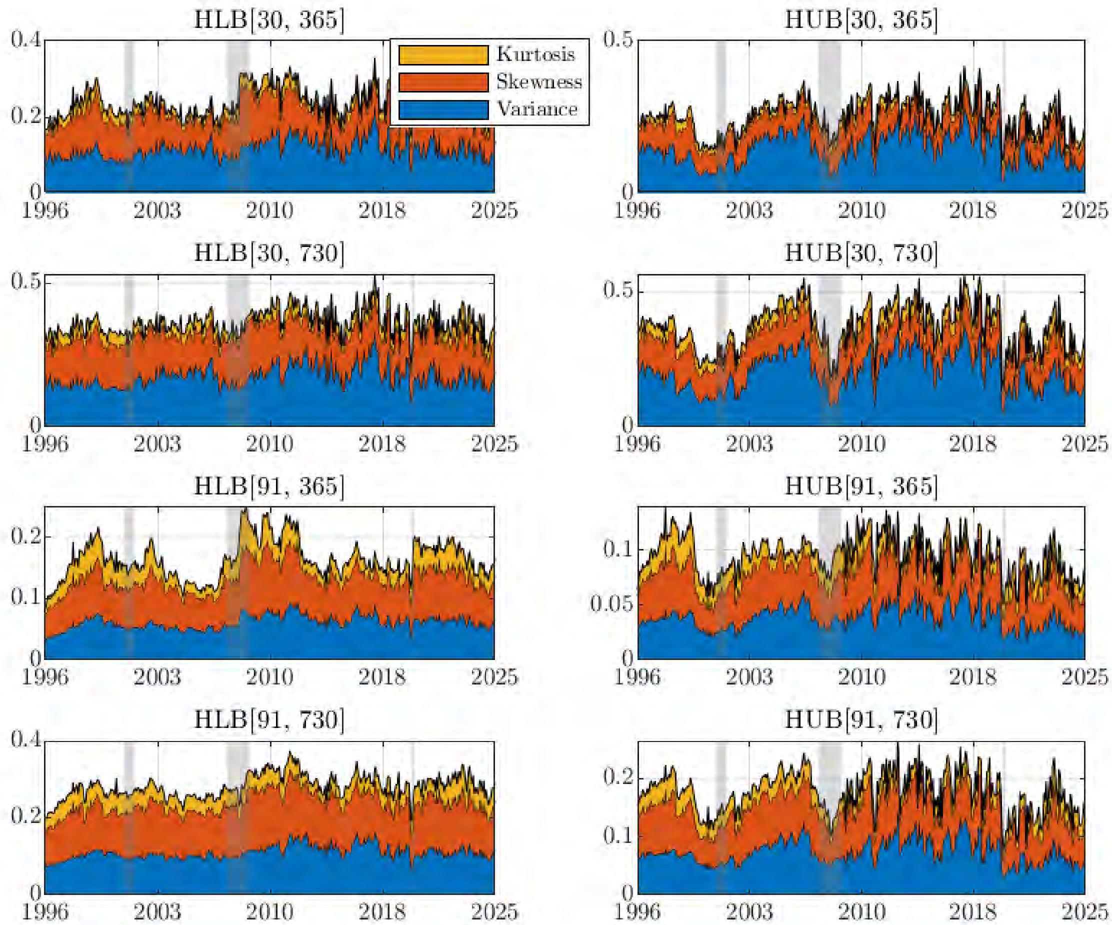

Fig. OA.8: Time Series of Forward Market Moments' Contribution to Hedging Bounds This figure depicts the time-series decomposition of the hedging lower bound (HLB) and hedging upper bound (HUB) across all firms in the sample. The detailed decomposition process is described under Figure OA.7. Each subfigure corresponds to a specific maturity pair, with T_1 set to either 30 or 91 days and T_N set to either 365 or 730 days, as indicated in the respective title. The sample period spans from January 1996 to August 2025 at monthly frequency. The grey areas indicate the National Bureau of Economic Research (NBER) recession periods.

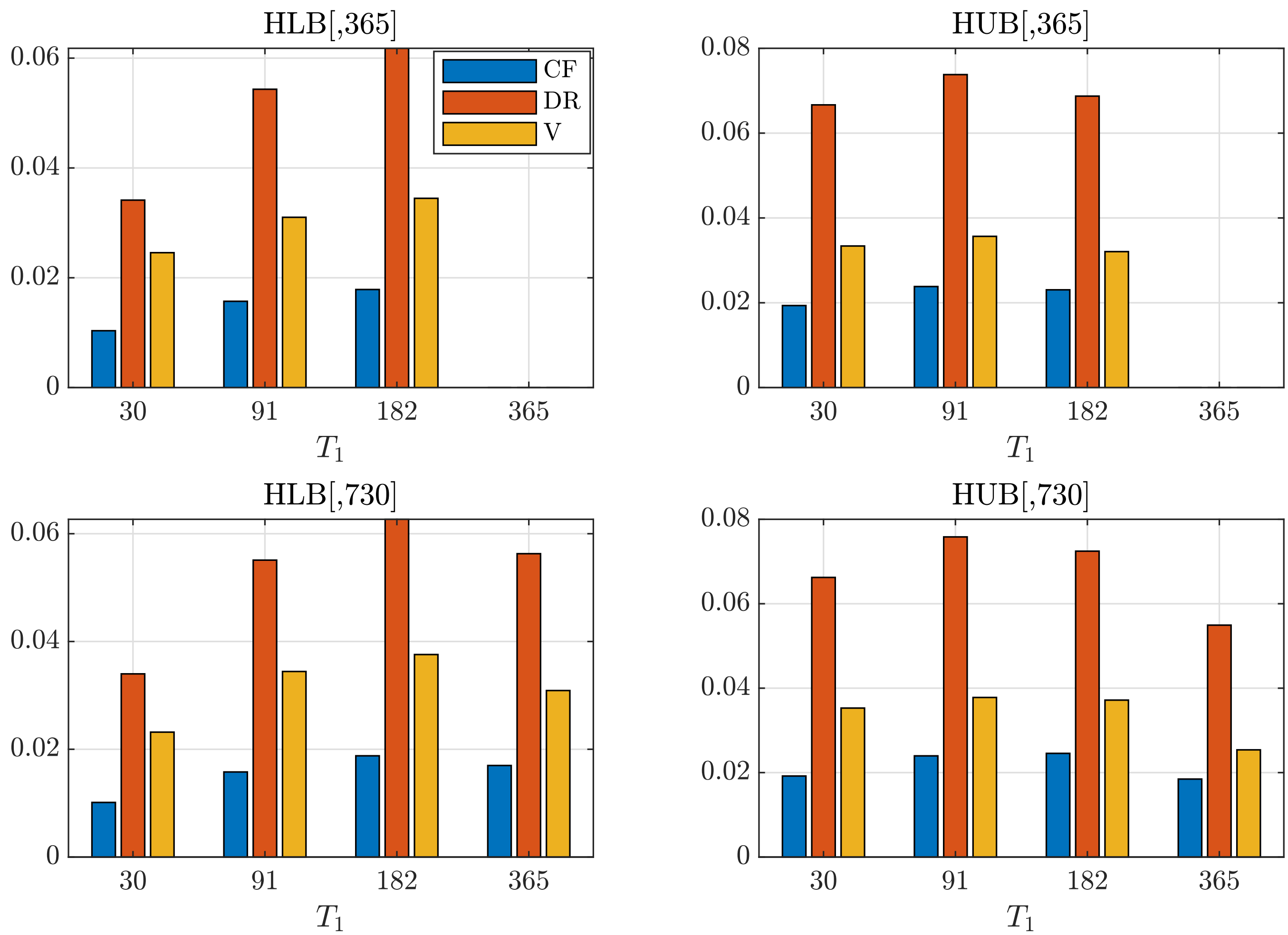

Fig. OA.9: Proportion of Hedging Contributions Explained by Cash-Flow, Discount-Rate, and Volatility News Betas This figure depicts the average decomposition of the hedging components of the hedging lower bound (HLB) and hedging upper bound (HUB) with respect to the framework of Campbell et al. (2018), across all firms in the sample, using maturities ranging from 30 to 365 days. Following their approach, we first decompose market excess returns into three components: cash-flows news (CF), discount-rate news (DR), and volatility news (V). For each stock in our sample, we then compute the stock's beta with respect to each of these market excess return components using a 60-month rolling window. Next, we estimate a cross-sectional regression of the hedging component (e.g., (HLB−LB)/HLB) on the three betas (i.e., $\beta_{CF}, \beta_{DR}, \beta_V$) for each month. The proportion of the hedging component attributable to each beta is calculated as the corresponding regression coefficient multiplied by the covariance between the beta and the hedging component, and then scaled by the variance of the hedging component. We then average these proportions across all firms. The sample period spans from January 1996 to August 2025 at monthly frequency.

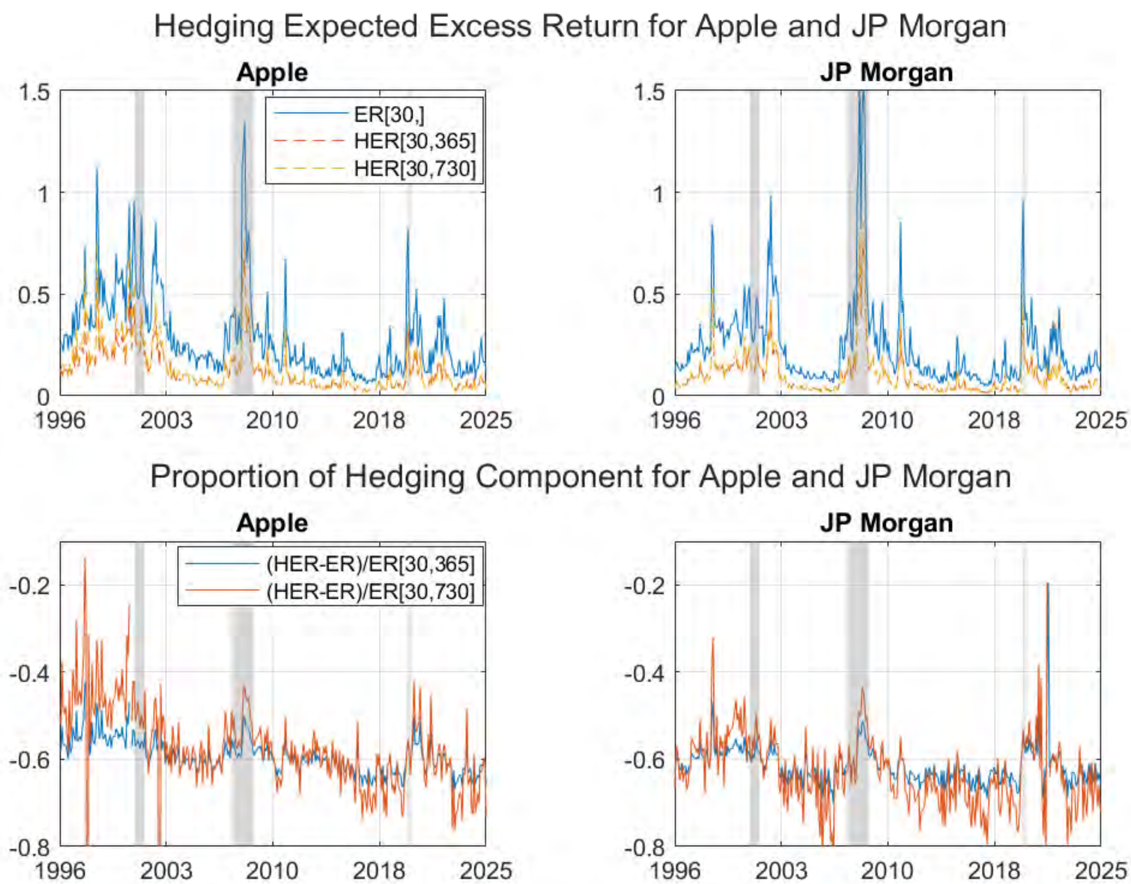

Fig. OA.10: Time Series of Expected Excess Return for AAPL and JPM Under the CRRA Utility (Risk Aversion=4) This figure depicts the time series of expected excess returns (ER) for two stocks, Apple and JP Morgan, with and without hedging, under the case of CRRA utility. In particular, we set the preference parameters with risk aversion equal to 4. The figure also plots time-series proportion of the hedging component, measured as the difference between hedging expected excess return (HER) and ER scaled by ER with $T_1 = 30$ and $T_N = 365/730$. The sample period spans from January 1996 to August 2025. The grey areas indicate the National Bureau of Economic Research (NBER) recession periods.

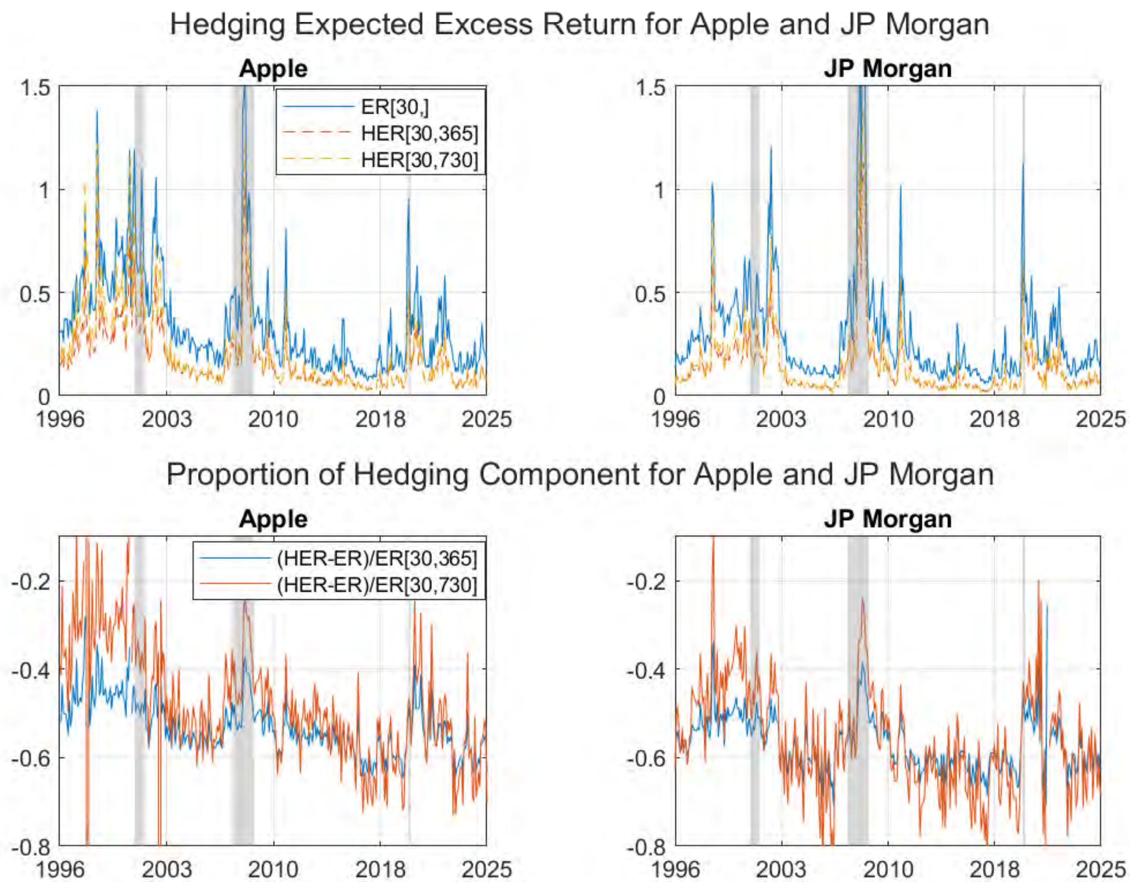

Fig. OA.11: Time Series of Expected Excess Return for AAPL and JPM Under the CRRA Utility (Risk Aversion=5) This figure depicts the time series of expected excess returns (ER) for two stocks, Apple and JP Morgan, with and without hedging, under the case of CRRA utility. In particular, we set the preference parameters with risk aversion equal to 5. The figure also plots time-series proportion of the hedging component, measured as the difference between hedging expected excess return (HER) and ER scaled by ER with $T_1 = 30$ and $T_N = 365/730$. The sample period spans from January 1996 to August 2025. The grey areas indicate the National Bureau of Economic Research (NBER) recession periods.

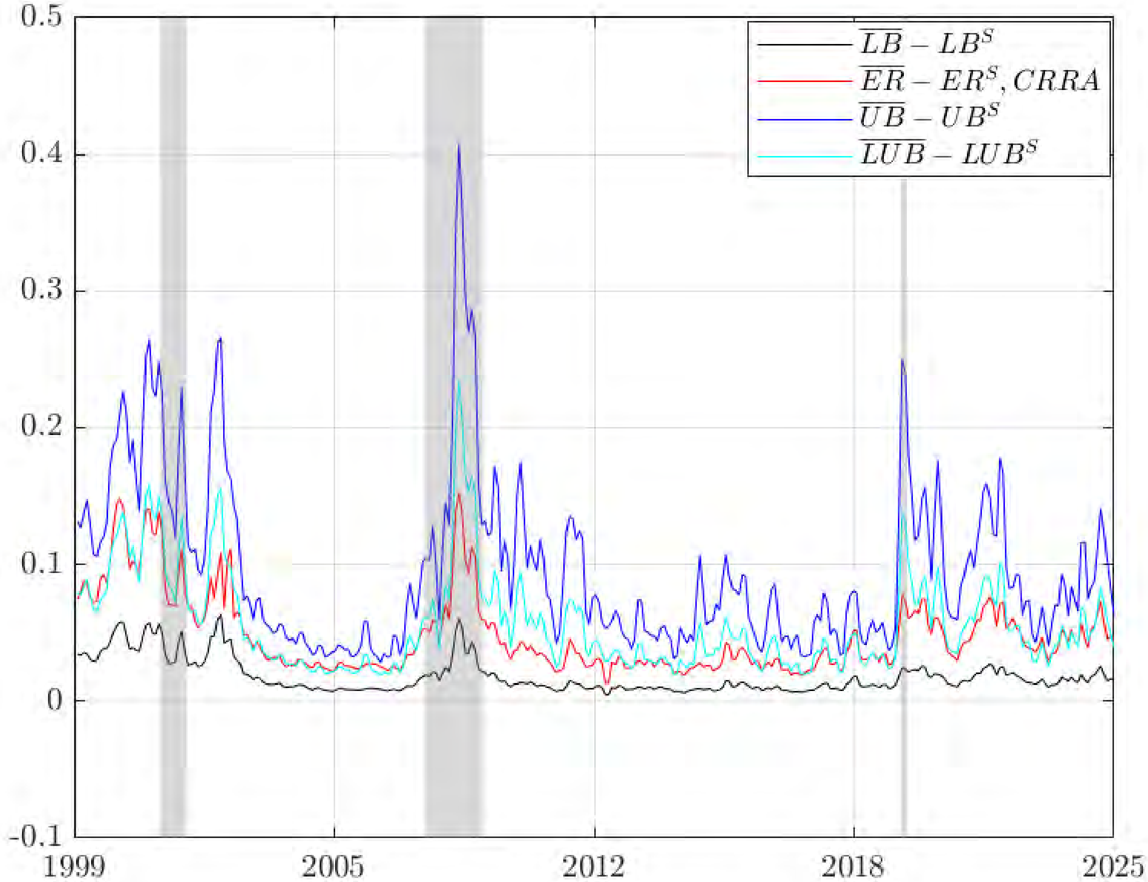

Fig. OA.12: Pricing Consistency of Static Expected Excess Return with CRRA Utility (Risk Aversion=3) This figure displays the average difference in 30-day annualized expected excess return (ER) for nine S&P500-based SPDR ETFs (X^S) and the value-weighted ERs of the ETF components ($\bar{X}$) under the case of CRRA Utility with a risk aversion equal to 3. As a comparison, we also plot the lower and upper bounds (LB/UB), and the average of them ((LB+UB)/2) based on our baseline setting ($[1/\tau, \rho, \kappa, \xi]$=[1, 2, 4, 8]). The series represents monthly averages of annualized daily values, covering the period from the start of option trading in sector ETFs in January 1999 to August 2025 at monthly frequency. The grey areas indicate the National Bureau of Economic Research (NBER) recession periods.

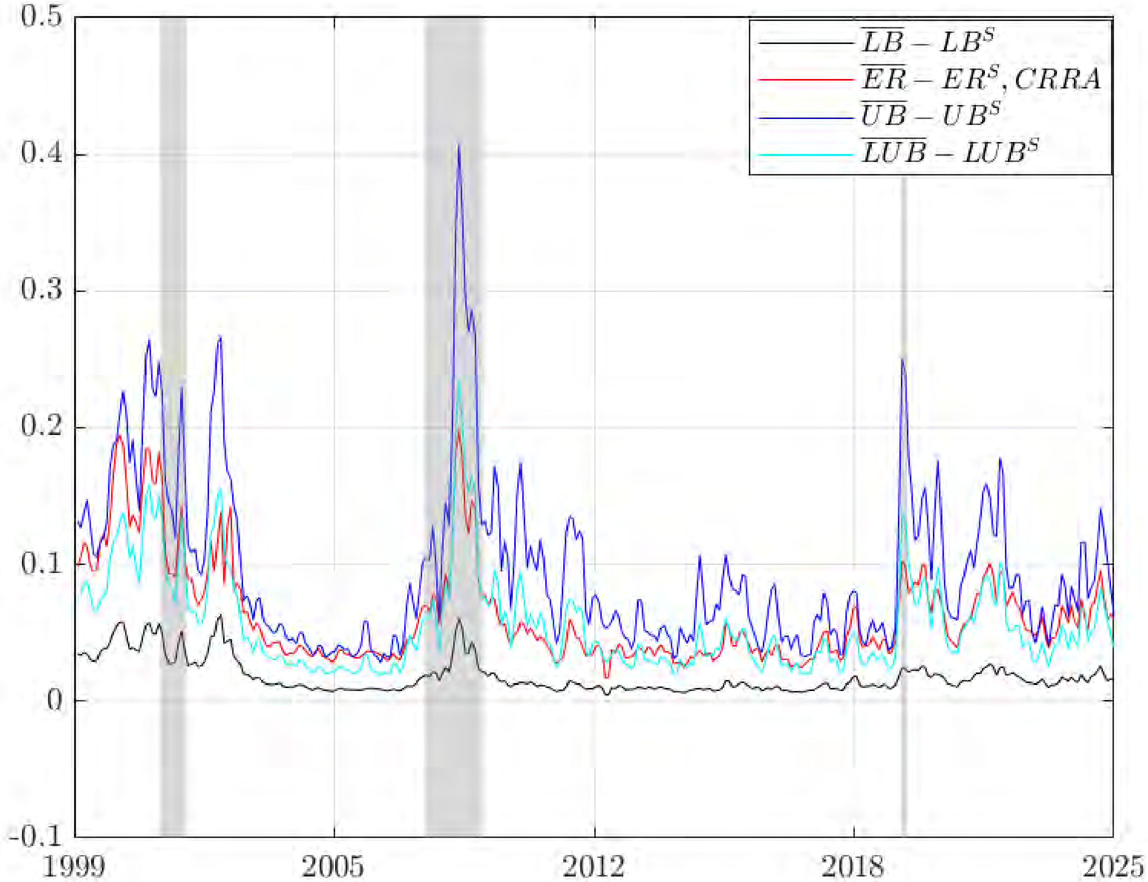

Fig. OA.13: Pricing Consistency of Static Expected Excess Return with CRRA Utility (Risk Aversion=4) This figure displays the average difference in 30-day annualized expected excess return (ER) for nine S&P500-based SPDR ETFs (X^S) and the value-weighted ERs of the ETF components ($\bar{X}$) under the case of CRRA Utility with a risk aversion equal to 4. As a comparison, we also plot the lower and upper bounds (LB/UB), and the average of them ((LB+UB)/2) based on our baseline setting ([$1/\tau, \rho, \kappa, \xi$]=[1, 2, 4, 8]). The series represents monthly averages of annualized daily values, covering the period from the start of option trading in sector ETFs in January 1999 to August 2025 at monthly frequency. The grey areas indicate the National Bureau of Economic Research (NBER) recession periods.

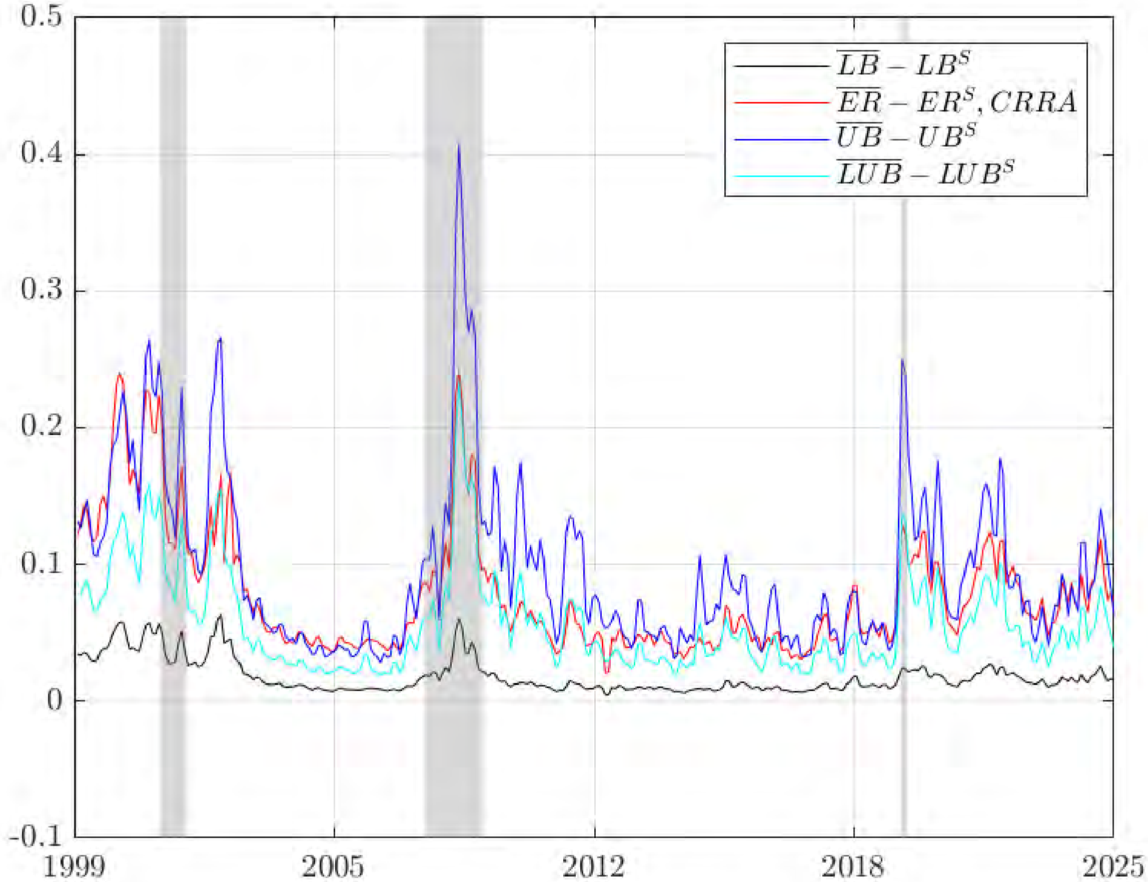

Fig. OA.14: Pricing Consistency of Static Expected Excess Return with CRRA Utility (Risk Aversion=5) This figure displays the average difference in 30-day annualized expected excess return (ER) for nine S&P500-based SPDR ETFs (X^S) and the value-weighted ERs of the ETF components ($\bar{X}$) under the case of CRRA Utility with a risk aversion equal to 5. As a comparison, we also plot the lower and upper bounds (LB/UB), and the average of them ((LB+UB)/2) based on our baseline setting ([$1/\tau, \rho, \kappa, \xi$]=[1, 2, 4, 8]). The series represents monthly averages of annualized daily values, covering the period from the start of option trading in sector ETFs in January 1999 to August 2025 at monthly frequency. The grey areas indicate the National Bureau of Economic Research (NBER) recession periods.

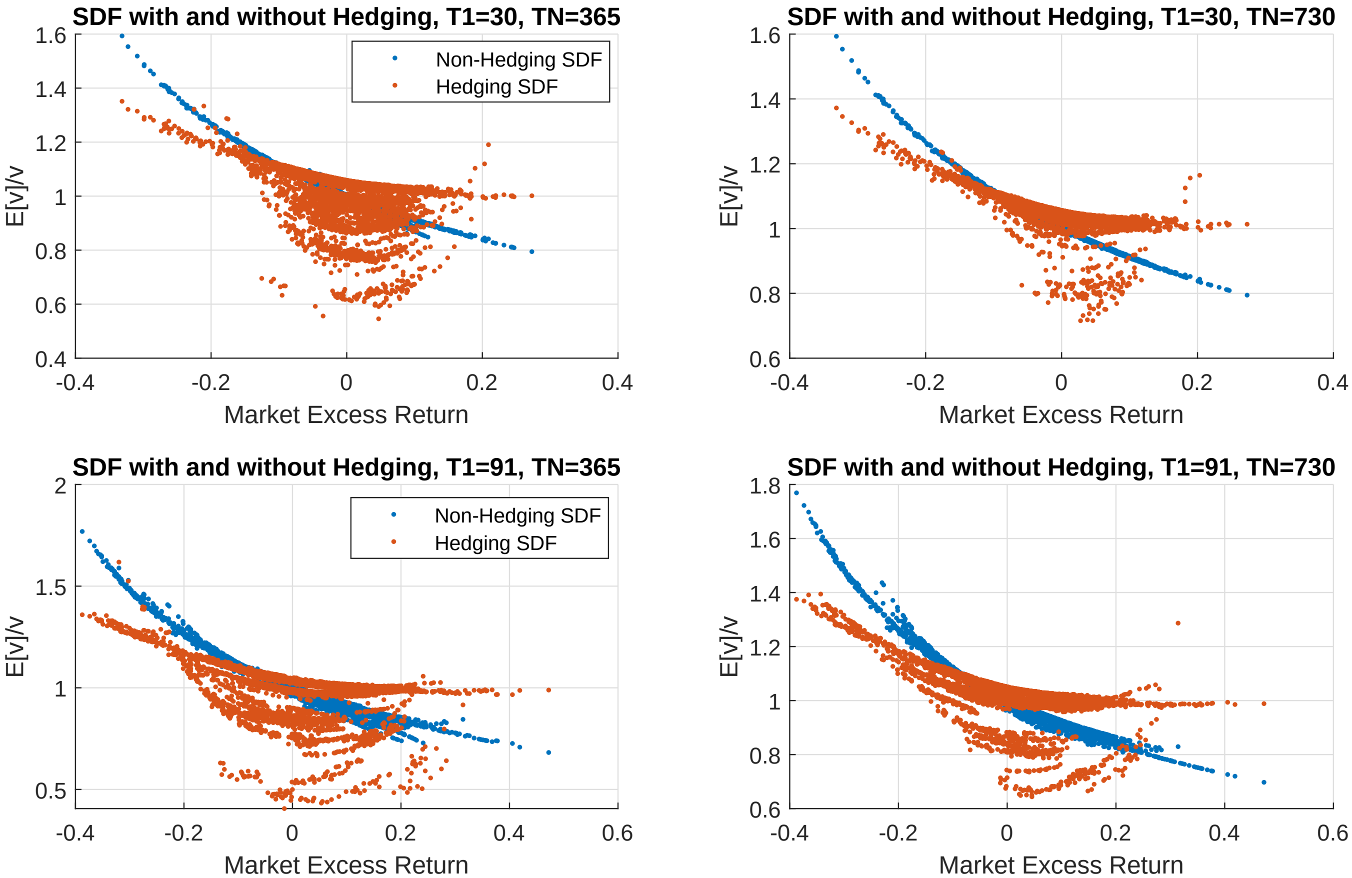

Fig. OA.15: SDF Estimation with and without Intertemporal Hedging Calibrated based on Out-of-sample Performance This figure depicts the estimation of the SDF using our approximation based on realized market excess returns with and without intertemporal hedging. The preference parameters are calibrated at end of each month to maximize out-of-sample forecast accuracy of the midpoint (i.e., (LB+UB)/2 for the non-hedging case and (HLB+HUB)/2 for the hedging case) relative to the default calibration [1, 2, 4, 8] up to each time using an expanding window as specified in Section 3.2.2. The sample periods to estimate SDF spans from January 1996 to August 2025.

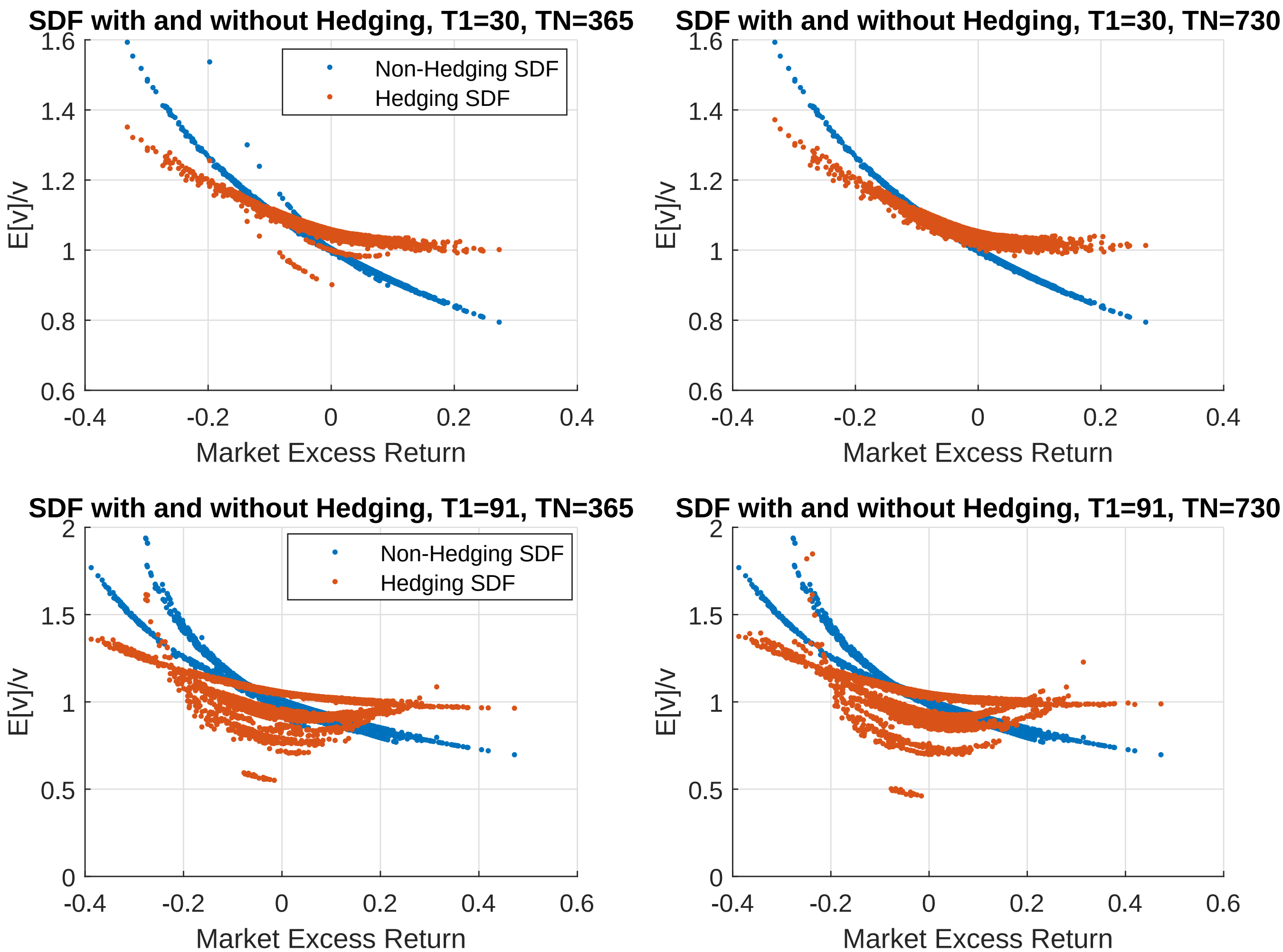

Fig. OA.16: SDF Estimation with and without Intertemporal Hedging Calibrated based on Variance Risk Premium This figure depicts the estimation of the SDF using our approximation based on realized market returns with and without intertemporal hedging. The preference parameters are calibrated at end of each month based on the past daily observations of option prices and variance risk premium using an expanding window as specified in Section 3.2.2. The sample periods to estimate SDF spans from January 1996 to August 2025.

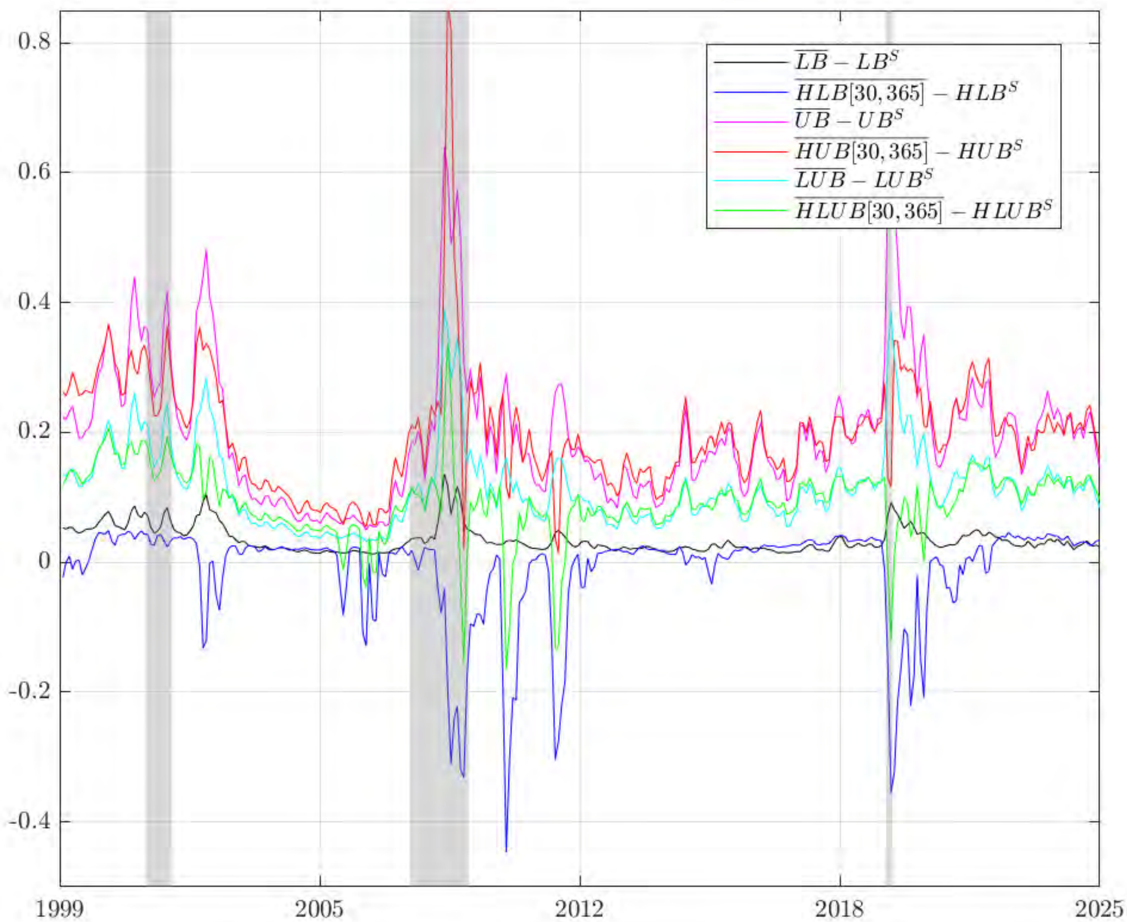

Fig. OA.17: Pricing Consistency: Robustness to an Alternative Specification of Equation (2.47) This figure reports pricing-consistency results using the alternative representation of $\mathbb{E}^*_{T_1} R^l_{M,T_1\to T_N} - R^l_{f,T_1\to T_N}$ in Online Appendix OA.4. This figure reports average differences in 30-day annualized expected excess return bounds between nine S&P500-based SPDR ETFs (X^S) and the value-weighted bounds of their underlying constituents ($\bar{X}$) based on the new approach. The figure includes the static bounds (LB and UB) and midpoint (LUB=(LB+UB)/2), as well as the hedging bounds (HLB and HUB) and midpoint (HLUB=(HLB+HUB)/2). The series are monthly averages of annualized daily values from January 1999 to August 2025. The grey areas indicate NBER recessions.